Global Magnetohydrodynamic Waves in Stably Stratified Rotating Layers

Xiomara Márquez Artavia

Submitted in accordance with the requirements for the degree of Doctor of Philosophy

The University of Leeds

Department of Applied Mathematics

April 2017

The candidate confirms that the work submitted is her own and that appropriate credit has been given where reference has been made to the work of others. This copy has been supplied on the understanding that it is copyright material and that no quotation from the thesis may be published without proper acknowledgement.

Abstract

The 2D shallow water approximation in magnetohydrodynamics is solved, numerically and analytically, for a perfectly conducting fluid on a rotating sphere with a basic state for the toroidal magnetic field: $B_\phi = B_0 \sin\theta$. The results are given in terms of the parameters $\epsilon = 4\Omega_0^2 R_0^2/gH_0$ and $\alpha^2 = v_A^2/4\Omega_0^2 R_0^2$, where Ω_0 is the rotation rate, R_0 is the radius, g is the gravity, H_0 is the height of the layer and v_A is the Alfvén speed. Five types of solution have been found: Magneto-inertial gravity waves (MIG), Kelvin waves, fast and slow magnetic Rossby waves and a slow anomalous mode travelling westward. A comprehensive numerical study describes the modes in a full range of parameters.

As $\alpha \to 0$, the eigenfunctions are the Associated Legendre polynomials, if $\epsilon \to 0$. When $\epsilon \to \infty$ the eigenfunctions describing MIG and Fast magnetic Rossby waves are defined by the parabolic cylinder functions for waves confined to the equator. The slow magnetic Rossby waves are not equatorially trapped.

When $\alpha \geq 0.5$ there is a transition for magnetic Rossby waves. The slow and fast modes coalesce and an unstable mode emerges, but only when the azimuthal wavenumber $m = 1$. After this transition point ($\alpha = 0.5$) the fast magnetic Rossby waves turn into subalfvénic waves and tend to be trapped at the poles.

As $\alpha \to \infty$, the MIG waves become equatorially trapped Alfvén waves. These modes are always stable. The slow and fast magnetic Rossby waves (real and complex) are polar trapped with eigenfunctions described by Laguerre polynomials multiplied by a factor that gives the confinement.

The antisymmetric configuration for the field $B_\phi = B_0 \sin\theta\cos\theta$, produces similar results to the previous case but the main difference is that the slow magnetic Rossby waves are absent. Also, magnetic Rossby waves become unstable for certain values of α and ϵ, then become real again by interacting with another mode and so on, weaving a net. On the other hand, when α is large, there is a critical layer which absorbs the MIG waves.

To my beloved parents Waldo Márquez and Ligia Artavia.

Acknowledgements

I give thanks to God because His hand was with me.

This project was carried out with the sponsorship of the Universidad Nacional of Costa Rica, to whom I thank.

I want to express my gratitude to everyone who supported me throughout this PhD project. Especially to my supervisors Prof.Chris Jones and Prof.Steven Tobias for their constant support and patience.

I would like also to acknowledge Kumiko Hori for her valuable suggestions and comments.

My very special gratitude goes out to the Blenheim Baptist church, for always taking care of students and foreigners. I am grateful to Richard Gunton who helped me with proof reading. Also I express my warm thanks to Mrs.Grace Pang for her kindness and love making me feel at home.

Finally, I must express my very deep gratitude to my husband Jorge Brenes for his companionship and love.

Contents

List of figures

List of tables

Chapter 1

Introduction

Wave motion occurs in a great variety of physical phenomena, such as the study earthquakes, propagation of light and acoustics. The mathematical theory of wave motion is very general, and can be applied in many different physical situations.

There are two important constants for all the waves, the amplitude and the frequency, or equivalently the wavelength (Hecht and Zajac, 1974). The frequency is the number of cycles per unit of time, this quantity is critical to classify the wave. Waves are often described as fast and slow, and we can base this distinction on the magnitudes of the frequency. The relative sign of the frequency and the wavenumber also describes the direction of propagation and the frequency also affects the group velocity, which is the speed at which energy is propagated. It remains constant when the wave is reflected or transmitted in a new media. Also it is related to the period of the wave that is the time elapsed between two consecutive oscillations, by a simple formula.

Knowing how a wave propagates through a medium can give valuable information about the conditions in that media. For example, the microscopic structure of a crystalline material can be deduced by measuring wave properties of the light beams passing through it (Hecht and Zajac, 1974). The measurement of its velocity is associated with the

composition and elastic properties of the medium in which it propagates, for example the velocity of the seismic waves is proportional to the density of the inner Earth (Fowler, 1990). The reflection of sound waves in sonar devices can draw a map of the sea floor (Kinsler et al., 1999). These are classical examples of wave physics. Our main concern is waves in fluids.

The waves in fluid are known as mechanical waves; the perturbation cannot exist without material media. They are in themselves a vast field of study for their behaviours and the physical laws that govern them (Whitham, 2011) but a deep comprehension of them could help us to study the medium in which they develop.

A detailed study of magnetohydrodynamic (MHD) waves in perfectly conducting fluids is presented in this thesis: the complete set of solutions to the system of equations for a thin shell of rotating fluid. Maybe the study of MHD waves in stars and planetary interiors can give an insight about their composition and dynamics: comparing the observations of waves in the stellar tachoclines or inner Earth with our results, we can infer if there are stratified layers or have an estimation of the magnitude of the magnetic field.

1.1 Geophysical and Astrophysical Motivations

The effect of the gravitational force on a fluid produces vertical changes in density, so the density decreases as the height increases (Hines, 1972). This density variation could be present as a continuous transition or it can lead to the formation of layers with different properties like temperature, composition and pressure. Such layers are called stratified layers.

When the structure of a layer is that lower densities are at the top and the higher densities are below, the distribution is said to be stably stratified (e.g. Cushman-Roisin and Beckers, 2011). Stable stratification occurs frequently in nature and creates different

layers, each region having particular properties. For example, the Earth's atmosphere is considered stably stratified except for a thin layer which is in contact with the Earth's surface, (Nappo, 2013). The stratosphere is a stably stratified layer located in heights $15 - 50$ km above the surface. In the ocean, the density stratification defines three layers. A surface layer, a pycnocline layer, sometimes called the thermocline (for low latitudes) and a deep layer (Pinet, 2012). The thermocline is a region of sharp transition between less dense warm water and deeper denser cold water.

Stratification can be measured by a physical parameter called the Brunt-Väisälä frequency or buoyancy frequency (e.g. Melchior, 2013), at which a small element of fluid oscillates when it is perturbed. There is a relation between the Brunt-Väisälä frequency and the adiabatic gradient of temperature. If the temperature gradient is subadiabatic, the layer is stable and there is a Brunt-Väisälä frequency. If the layer is superadiabatic, it is not stably stratified and convection occurs.

Additionally, the rotation of the system can lead to other types of waves (e.g. Lighthill, 2001). In addition to gravity waves, rotation leads to Kelvin waves and Rossby waves, which are related to significant geophysical and astrophysical phenomena. It is also possible for magnetic field to be important in generating new types of waves, for example in the solar interior or the liquid iron core of the Earth. We then expect to find Alfvén waves, which are waves which owe their existence to the presence of the magnetic field.

In atmospheric dynamics, meridional flow fluctuations are associated with mixed Rossby gravity waves (Yanai et al., 1968) and other zonal fluctuations are associated with a Kelvin mode in the equatorial stratosphere (Wallace and Kousky, 1968, Holton and Lindzen, 1968). In addition, these mixed Rossby gravity waves are a potential explanation for the Quasi-Biennal Oscillation, in which the zonal wind alternates direction between eastward and westward propagation, with a period of $\sim 22 - 28$ months, in the equatorial region. Also, the existence of Equatorial Rossby waves has been inferred from the study of the westward propagating "cyclone pairs" (Kiladis et al.,

2009).

There are many representative cases of the influence of these waves in the weather and also climate. Gravity waves in the upper atmosphere are an important part of the dynamics of the system. Mountain waves produced by the perturbation of the horizontal wind flow have been recognized as gravity waves (Hines, 1972).

In addition to these atmospheric and other oceanic applications, waves play an important role in astrophysical and geophysical systems. Our particular interest extends to the stably stratified layer in the Earth at the Core Mantle Boundary (CMB) and the thin layer in the Sun which is called the solar tachocline.

Helioseismic results suggests that there is a thin layer of transition around the radiative zone and the convection region. This layer has a sharp change in the rotation rate; the outer part rotates differentially with the poles rotating slowly and the equator faster, see figure 1.1. The radiative interior has a solid-body rotation rate (Miesch, 2005). According to Charbonneau et al. (1999), the location of the tachocline is $0.693 \pm 0.003 R_\odot$ near the equator and $0.717 \pm 0.003 R_\odot$ at a latitude of 60° (Charbonneau et al., 1999). Their estimations for the width are $0.039 \pm 0.013 R_\odot$ at the equator and $0.042 \pm 0.013 R_\odot$ at a latitude of 60°, where $R_\odot$ is the Sun's radius. These estimates are not very certain and the tachocline might be thinner than this. It has been suggested that the movement of plasma acting in this layer contributes to generating the solar magnetic field.

The solar magnetic field has a complex behaviour but shows some patterns. The sunspot cycle is the most common pattern of solar activity, which emerges at a certain band of latitudes and moves to the equator, then the polarity of the global field reverses and the patterns emerge again to complete a cycle in 22 years. It is known that the solar activity is maximum when there is a greater number of sunspots and minimum when there is less. The solar activity also presents other cycles such as the Gleissberg cycles of $60 \sim 150$ years (Ma, 2009) or for instance, Rieger type periodicities of hundreds of years.

On the largest scales, during solar minimum, the axisymmetric component of the poloidal field is mainly dipolar with a magnitude of $10G$ for the solar photosphere. As the cycle continues the field shows multipolar components and becomes more complicated (Miesch, 2005).

Moving on now to consider the magnetic field in the tachocline, many researchers assume that the amplitude of the toroidal component is large with respect to the poloidal component (Tobias, 2005). According to many authors it could be a purely toroidal magnetic field (Gilman, 2000, Zaqarashvili et al., 2007). Despite the fact that part of the

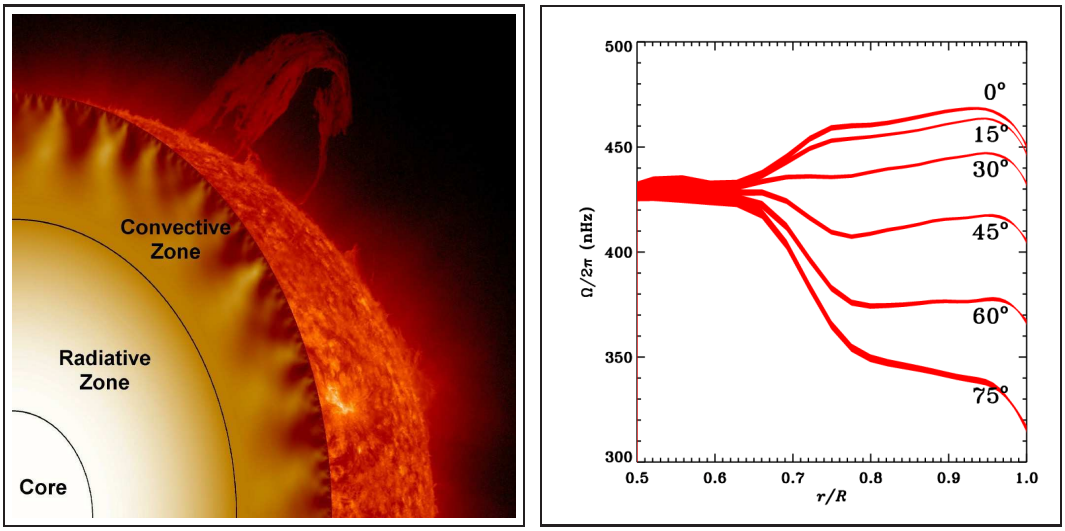

Figure 1.1: At the left, inner structure of the Sun, the tachocline is the transition region separating the radiative zone and the convective region. Courtesy: Marshall Space Flight Centre/NASA. http://solarscience.msfc.nasa.gov. At the right, rotation rate varying with the solar radius, for different latitudes, the tachocline is located about $\sim 0.7R_{\odot}$. National Solar Observatory.http://gong.nso.edu/gallery/disk2k10/data/resource/ torsional/torsional.html.

tachocline experiences differential rotation (Schou et al., 1998), see figure 1.1, for our purpose of studying waves in general, we consider that the layer has constant solid body rotation, with a rotation rate of ~ 27 days (Hughes et al., 2007).

It seems possible that if a spectrum of oscillations arise in the tachocline, these waves

can describe some solar activity (Spiegel, 1994). Observations from satellites of Coronal Bright Points for tracking magnetic activity of the Sun have revealed certain wave patterns with westward phase speeds of $3.25 \pm 2.25 m/s$ and $2.65 \pm 1.60 m/s$ in the north and south hemispheres. These waves have eastward group speeds of $24.4 \pm 15.3 m/s$ in the southern hemisphere and $23.8 \pm 20.8 m/s$ in the northern hemisphere, (McIntosh et al., 2017). It is believed that this is a kind of magnetic Rossby wave arising from the rotation and the toroidal field of the tachocline, see figure 1.2.

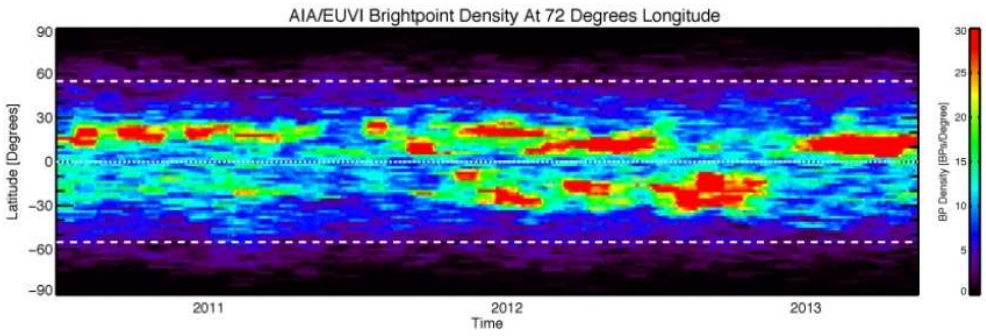

Figure 1.2: Illustration of solar activity: average of coronal bright points density at given longitude of $72°$ (From McIntosh et al. (2017)).

Other solar type stars will have a tachocline as well, and in all of them rotation rate and magnetic strength will differ from that in the Sun (Oláh et al., 2009, Hughes et al., 2007). The study of solar type stars could clarify the relationship between the wave generation in the tachocline and the periodicities of the magnetic field of the sun. It is therefore of interest to consider a wide range of possible parameters for the rotation rate and the magnetic field, not just specific values.

Let us now consider instability. The interest for investigating instability in MHD problems has grown in recent years, due to the discovery of countless relations between unstable modes and certain natural phenomena, for instance bursts of gamma and x-rays

in the sun or neutron stars (Gilman and Dikpati, 2002). Some authors also suggest that reversals of the Earth's magnetic field could be activated by magnetic instabilities. It is also possible that gravitational instability in giant molecular clouds could initiate star formation e.g. Rüdiger and Hollerbach (2006).

Also, there is another motivation for this thesis: to study the stratified layer at the top of the outer core of the Earth. The Earth's core has a liquid exterior and solid interior. The outer core has a smaller density than the inner core and is composed mainly of iron and a few percent of light elements, but the inner core is composed mostly of pure iron (Karato, 2003).

The geomagnetic field is generated in the outer core by a dynamo effect (e.g. Jones 2011). The structure of the field is predominantly dipolar. However, it has been suggested that the magnitude of the toroidal field in the core may be as much as $2 \times 10^{-2}T$, which is considered stronger than the poloidal component of magnitude $4 \times 10^{-4}T$ (Melchior, 2013). The fact that the toroidal field may be stronger than the poloidal field has relevance for this research.

The magnetic field of the Earth undergoes variations. Some changes are due to the interactions between the solar wind and the magnetosphere, which are fast and last seconds. On the other hand, the time elapsed between polarity reversals, which are inversions of the polarity of the field, can take millions of years to occur. Also, there is the secular variation, which occurs over periods of time from years to centuries, like westward drift, geomagnetic jerks, the growth of the South Atlantic anomaly, and the anticyclonic motions of field features in the North pole (Finlay et al., 2010). In figure 1.3, the radial component of the core's field is shown, where intense spots are located near the equator and propagate westward (Finlay et al., 2010).

Braginsky (1998) suggested the existence of a stable stratified layer at the top of the core, see figure 1.4, where many kinds of waves could arise, analogous to those which propagate in the ocean of the Earth. Then, the slow oscillations produced by

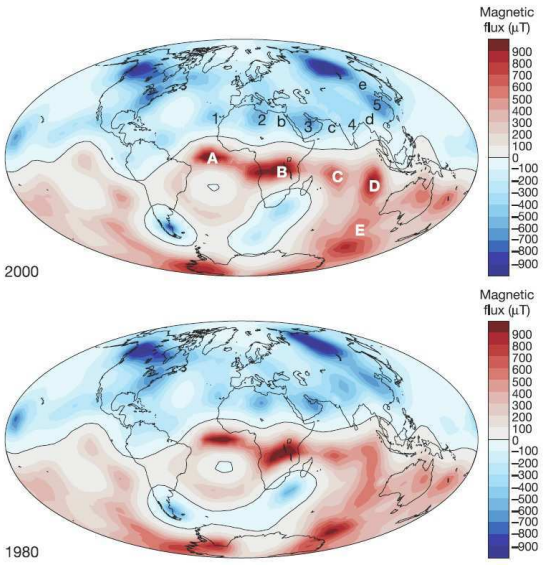

Figure 1.3: Radial component of the core magnetic field. Note how flux spots in the positions A, B, C, D and E are slightly moved toward the west with respect to the 1980's plot. Reproduced from Jackson (2003).

an equilibrium between magnetic, Archimedean and Coriolis forces, called magnetic Rossby waves are considered to be related to short time-scale geomagnetic secular variation, length of day variation and oscillation of the pole position.

Other theoretical models describing the movement of fluids in the Earth's core establish that waves can be responsible for short term secular variation in the geomagnetic field (Finlay et al., 2010, Hori et al., 2015). Bergman (1993) proposed a thin shell model, and solved the Laplace tidal equations modified by the Lorentz force for a dipolar field, using the β-plane approximation. He suggested that solutions with long periods such as magnetic Rossby waves, are a plausible cause for secular variation.

Recently, seismic evidence has shown (Helffrich and Kaneshima, 2010), a reduction in the outer-core wave speeds of 0.3% relative to the expected speed at 60 km into the outer core, which slowly recovers the expected value at a depth of 300 km. These differences reflect the presence of a layer of 300 km in thickness at the top of the core: a stratified

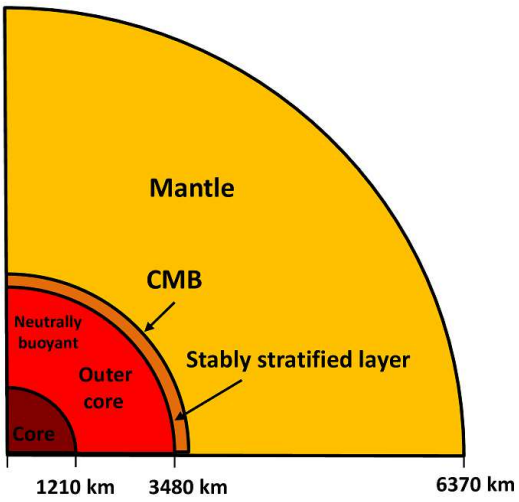

Figure 1.4: Inner structure of the Earth. It has been suggested that there is a stably stratified layer at the top of the core.

layer.

1.2 Modelling Approaches

The aim of this thesis is the study of MHD waves in stably stratified layers, describing the solutions with generality for any physical system. Then, we can analyse more deeply some special cases that could represent the tachocline of the Sun or the stably stratified layer at the top of the Earth's core.

Our analysis starts from the shallow water approximation set of equations, for a fluid with constant density ρ and Ω_0 as the rotation rate of this system where the height of the fluid is much less than the horizontal distances. As a result of this the vertical component of the velocity will be less than the horizontal components, and the same will occur for the vertical component of the magnetic field. In this case radial displacements do not appear explicitly in the governing equations. Despite the simplicity of the shallow water model it can be applied to many cases in oceanic and atmospheric fluids, where it is capable

of describing important phenomena (Pedlosky, 2013). Longuet-Higgins (1968), in the context of geophysical fluids, has solved the problem for the set of equations known as "Laplace Tidal equations".

We follow the MHD shallow water approximation proposed by Gilman (2000). He considered thin layers of conducting fluid immersed in a toroidal magnetic field, and used this model to research the dynamics of the solar tachocline (Gilman, 2000). Since then the MHD shallow water model has been applied to the study of Rossby and gravity waves in the tachocline of the Sun (Zaqarashvili et al., 2007, 2009).

Several studies have provided important information on MHD "shallow water" waves. Schecter et al. (2001) have found two kinds of waves: Alfvén waves and "magneto-gravity" modes in the context the solar tachocline, this MHD shallow water model is developed in Cartesian coordinates for a rotating system with a constant toroidal magnetic field B_0. Other MHD shallow water approximations have taken into account multiple layers (Hunter, 2015), yielding solitary and cnoidal waves.

Our results will be expressed in terms of the normalized frequency of waves: $\lambda = \omega/2\Omega_0$ and some dimensionless parameters, where Ω_0 is the rotation rate of the system. These include the magnetic parameter α, defined by $\alpha^2 = B_0^2/\rho\mu_0 4\Omega_0^2 R_0^2$, and the parameter $\epsilon = 4\Omega_0^2 R_0^2/gH_0$, for definition of symbols see table 1.1. The values of the parameters are uncertain, but the order of magnitude can be calculated for stably stratified layers of the Earth and Sun, using the physical constants in table 1.1.

The physical constants can vary with the position. In the solar tachocline the stratification is high in the radiative zone and lower in the overshoot region. This must be common in stars similar to the sun, with a stably stratified layer between the convection zone and rigid body rotating region. This stably stratified layer changes from adiabatic to subadiabatic gradient of temperature. In the Earth's core a smooth transition is expected from convection to stable stratification, but this is very difficult to determine. For this reason, we give a complete study of the solutions in a very large range for the parameters

α and ϵ. Therefore, these results must be interpreted with caution when they are applied to astrophysical context, because of the uncertainty of the parameters and the simplicity of the model.

For the estimation of the parameters, we choose a constant gravitational acceleration and the highest published values for the magnetic field. The values of density and gravity for the Earth's stratified layer come from PREM model (Dziewonski and Anderson, 1981). Although, in the solar tachocline the value of the gravity is valid for the radiative part of the tachocline and changes abruptly in the overshoot part. Mak et al. (2016) has suggested that the factor $\sqrt{gH_0}$ could be calculated through the Brunt-Väisälä frequency, as the fastest possible gravity wave NH_1/π, where H_1 is the depth of the layer. Taking $N = 8 \times 10^{-4} s^{-1}$ at $0.7R_\odot$, the value of $\sqrt{gH_0}$ is $16000m/s$ with a height equal to $H_1 = 1 \times 10^7 m$. Then the parameter ϵ for the solar tachocline is 0.03, as showed in table 1.1. However, it is important to bear in mind that the value of the buoyancy frequency varies across the tachocline and reduces to zero at the base of the convection zone, (Hughes et al., 2007).

In the same way the velocity can be calculated for the stratified layer of the Earth $\sqrt{gH_0} = 305m/s$, taking $H_1 = 3 \times 10^5 m$ and $N = 0.51mHz$ from Helffrich and Kaneshima (2010), then $\epsilon = 2.7$.

In table 1.1 the values of ϵ in blue color correspond to the calculation using the values of g and H_0 written in this table.

Based on this model and these parameters, we try to find a relation between our solutions for the MHD shallow water system to some geophysical and astrophysical observations. In the next chapter, we explain the mathematical details of the MHD shallow water model.

Another significant aspect of the MHD waves is that instability could be present. In stable equilibrium, a physical system tends to remain close to the original state after a perturbation. In unstable equilibrium, the system has a different response to small

Table 1.1: Estimated values of fundamental parameters for the Earth and Sun. The numbers for the tachocline with* have been taken from Tobias (2005) and ** corresponds to Hughes et al. (2007).

	Symbol	Earth	Sun
Density	ρ	$9.9 \times 10^3 kg/m^3$	$210 kg/m^{3**}$
Rotation rate	Ω_0	$7.29 \times 10^{-5} rad/s$	$2.7 \times 10^{-6**} rad/s$
External radius of the layer	R_0	$3.48 \times 10^6 m$	$5 \times 10^8 m$
Magnetic field	B_0	$2 \times 10^{-2} T$	$10 T^*$
Height of the layer	H_0	$3 \times 10^5 m$	$1 \times 10^{7**} m$
Gravitational acceleration	g	$10.68 m/s^2$	$540 m/s^2 **$
Effective "gH_0"	gH_0	$9.4 \times 10^8 m^2/s^2$	$4.7 \times 10^7 m^2/s^2$
Parameters	α	4×10^{-4}	0.2
	ϵ	0.08-2.7	0.03-0.04

disturbances, moving away from the basic state.

In the present study, the variables of the system, velocities and magnetic field are perturbed about a basic state by a small amount and the governing equations are linearised. Then, we expect that the solutions are proportional to the factor $e^{-i\omega t}$, as will be shown later. If the imaginary part of the frequency $\omega_i > 0$ is greater than zero, the exponential factor tends to grow in amplitude, and the mode is unstable.

Next, we study the solutions in the space of parameters. For example, we have three parameters: wave number (m), rotation rate (ϵ) and magnetic field amplitude (α), and by varying these we try to obtain a critical value which sets the instability (Chandrasekhar, 2013).

Numerous studies have attempted to describe instabilities. Malkus (1967) found instabilities in the problem of a rotating sphere of conductive fluid, in a toroidal magnetic

field $B_0 \sin\theta$ for the azimuthal wave number $m = 1$. He estimated the minimum value of the magnetic parameter equivalent to $\alpha \geq 0.5$ for instability.

A significant analysis and discussion on the subject was presented by Tayler (1973). He obtained conditions for the stability of a non rotating star containing a toroidal magnetic field $B_\phi(r, z)$ and demonstrated that a large class of configurations are unstable and the instability depends on the topology of the field rather than in its strength. The effect of the rotation has been considered in a later publication (Pitts and Tayler, 1985), where instabilities exist for $m = 1$ and other conditions of the problem, see also Spruit (1999).

Gilman and Fox (1997) studied the instability of latitudinal differential rotation and toroidal magnetic field in the form $B_0 \sin\theta$. They found instabilities only for the wave number $m = 1$, for almost any magnitude of the toroidal field, although in this work they suggested that there is no instability when differential rotation is absent.

In a later study, Gilman and Dikpati (2002) studied MHD Shallow Water systems with toroidal fields and differential rotation for the solar tachocline. They found mainly that the mode $m = 1$ is the preference for instabilities; nevertheless for $m = 2$ in the presence of weak fields, unstable modes exist. When the magnetic field is strong and $m = 1$ the growth rates are independent of the "gravity parameter" (we call it ϵ). In their research, they showed that the existence of complex modes implies transport of angular momentum. For the two dimensional problem of an electrically conducting and viscous fluid in a spherical shell, Sharif and Jones (2005) proposed the azimuthal magnetic field $B_0 \sin\theta\cos\theta$, under differential rotation and taking into account diffusion. They found unstable modes for $m = 1$ and $m = 2$, and the modes can also be unstable under solid body rotation. In addition, they found that there is a value of the amplitude of the field ($\alpha = 0.5$) where the curves for the growth rates start having a different behaviour.

A criterion for instabilities was described by Cally (2003) in a 3D Boussinesq thin layer approximation for toroidal fields in the Sun. It establishes unstable waves occur if the Alfvén frequency exceeds the rotational frequency and symmetric growing modes are

confined at the poles for $m = 1$. He also mentioned that including diffusion in the problem does not suppress the instability.

In a later work, Cally et al. (2008), they consider the instability for the axisymmetric mode ($m = 0$) with a 3D Boussinesq model for spherical shell for banded magnetic profiles and differential rotation. Instabilities are found for a high radial wavenumber and also the modes are confined at the poles.

Our starting point in chapter 2 is the description of the set of equations for the thin layer model for a toroidal field with equatorial symmetry: $B_0 \sin\theta$, in spherical geometry. We also present an eigenvalue numerical method for solving the system of equations. As an alternative, ordinary differential equation formulations are also developed in this chapter. Chapter 3 is a summary of the hydrodynamic case, studied previously by other authors (Longuet-Higgins, 1968, Matsuno, 1966). In chapter 4, we solve the MHD Shallow water model numerically. In chapter 5, the asymptotic theory for the different waves is explained in the limiting cases of large and small parameters. Some unstable modes were found, and, these solutions are described extensively in chapter 6. Chapter 7 is related to solutions and considerations for the problem of the antisymmetric field $B_0 \cos\theta \sin\theta$. We discuss the main consequences of this work in chapter 8.

Chapter 2

System of Equations for the Shallow Water Approximation in MHD

2.1 Magnetohydrodynamic "Shallow Water" Approximation

The shallow water approximation is a model extensively applied in the study of fluids in the atmosphere and the ocean. Although, the model is straightforward, it is capable of describing relevant phenomena in geophysics (Pedlosky, 2013). The classical shallow water approximation of geophysical fluid dynamics describes a thin layer of fluid in hydrostatic balance, with a rigid surface in the lower boundary and a free surface in the upper boundary.

In 2000, Gilman introduced a magnetohydrodynamic set of equations for a shallow water system of conductive fluid immersed in a strong toroidal magnetic field (Gilman, 2000). Since then, the applications of the shallow water model have been extended to the inner planets and stars (Zaqarashvili et al., 2010a,b).

In this section we will make a formal derivation of the magnetohydrodynamic shallow

water equations, and establish the parameters and validity of this model.

2.2 Governing Equations

We consider a thin layer of fluid, with constant density ρ and height $H = H_0 + h$, where H_0 is the average height and $h(x, y, t)$ is the deviation independent of z (vertical). The vertical length scale H is much less than the horizontal length scale, L, so it can be expressed by

$$H/L \ll 1.$$

The equation of continuity for an incompressible fluid results in

$$\nabla \cdot \vec{v} = 0, \qquad \Rightarrow \qquad \frac{\partial u}{\partial x} + \frac{\partial v}{\partial y} + \frac{\partial w}{\partial z} = 0.$$

Using the lengths scales of the thin layer, it follows that the vertical velocity is smaller than the horizontal components

$$w \ll u, v.$$

In the same way, the magnetic field's components satisfy the equation $\nabla \cdot \vec{B} = 0$, stating that the vertical component of the field is small compared with the horizontal components

$$b_z \ll b_x, b_y.$$

The solar magnetic field in the tachocline can be considered mainly toroidal (Tobias, 2005). Despite the Earth's magnetic field having a dipolar component in the core, where the stably stratified layer is, the toroidal field component is much stronger (Melchior, 2013).

In addition, the magnetic field and the velocity are also independent of z (Gilman, 2000). Also if the fluid is perfectly conducting, we can neglect the diffusion terms.

We suppose that the fluid above the layer has negligible density ($\rho^{'} \approx 0$) compared to our layer density, as illustrated in figure 2.1 and at the bottom there is a rigid surface. If

we would like to consider a layer of fluid with density ρ_0 on top of our stratified layer, similar to the layers in the Earth's ocean, the governing equations remain the same but this active layer could be taking into account through the concept of "reduced gravity" (Vallis, 2006).

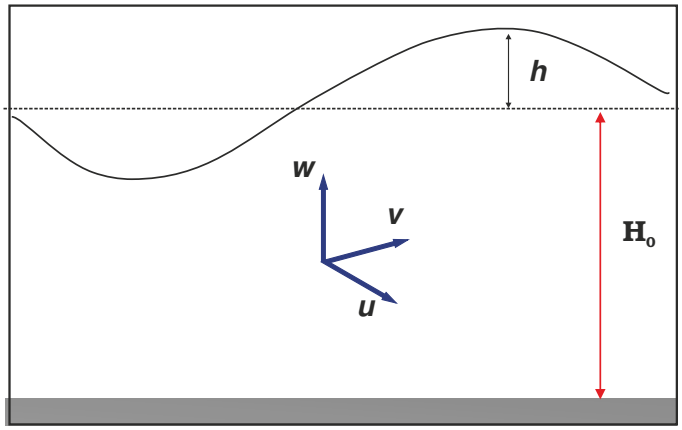

Figure 2.1: Shallow water system: the velocity field is shown, w is the vertical velocity, u and v are the horizontal components. The height of the layer is $H = H_0 + h$, where H_0 is the average height while its deviation is h.

2.2.1 Induction Equation

The induction equation can be derived using Maxwell's equation and Ohm's law (Thompson, 2006). Without considering diffusion and neglecting electrostatic forces, the equation takes the form

$$\frac{\partial \vec{B}}{\partial t} = \nabla \times (\vec{v} \times \vec{B}), \tag{2.1}$$

where $\vec{B} = (B_x, B_y, B_z)$ is the magnetic field. Using the vectorial identity $\nabla \times (\vec{a} \times \vec{b}) = (\vec{b} \cdot \nabla)\vec{a} - \vec{b}(\nabla \cdot \vec{a}) - (\vec{a} \cdot \nabla)\vec{b} + \vec{a}(\nabla \cdot \vec{b})$, we can change the right hand side of the equation

$$\frac{\partial \vec{B}}{\partial t} = (\vec{B} \cdot \nabla)\vec{v} - \vec{B}(\nabla \cdot \vec{v}) - (\vec{v} \cdot \nabla)\vec{B} + \vec{v}(\nabla \cdot \vec{B}). \tag{2.2}$$

Using the Gauss Law for magnetism, $\nabla \cdot \vec{B} = 0$ (Reitz et al., 2008), and the condition for incompressible fluid $\nabla \cdot \vec{v} = 0$, we have

$$\frac{\partial \vec{B}}{\partial t} = (\vec{B} \cdot \nabla)\vec{v} - (\vec{v} \cdot \nabla)\vec{B}. \tag{2.3}$$

The components of the velocity and the magnetic field are independent of z thus the terms $d\vec{v}/dz$ and $d\vec{B}/dz$ are zero, the induction equation for the horizontal components of the velocity and the magnetic field, can be written as

$$\frac{\partial \vec{B}_H}{\partial t} + (\vec{V}_H \cdot \nabla_H)\vec{B}_H = (\vec{B}_H \cdot \nabla_H)\vec{V}_H. \tag{2.4}$$

where $\vec{V}_H$ and $\vec{B}_H$ are the horizontal components of the velocity and the field respectively, likewise, ∇_H is the horizontal gradient.

2.2.2 Momentum Equation

Newton's second law of motion for a conductive fluid can be written as

$$\frac{\partial \vec{v}}{\partial t} + (\vec{v} \cdot \nabla)\vec{v} + 2\vec{\Omega} \times \vec{v} = -\frac{1}{\rho}\nabla P - g\hat{k} + \frac{1}{\rho\mu_0}(\nabla \times \vec{B}) \times \vec{B}. \tag{2.5}$$

The term $2\vec{\Omega} \times \vec{v}$ refers to the Coriolis force, introduced to take into account the effect of the system's rotation. The first term in the right hand side of the equation is the pressure gradient, the second term is the gravity force and the last term is the Lorentz force, diffusion is not considered here. Using vectorial identities, we can rewrite the Lorentz force term, and the equation takes the form

$$\frac{\partial \vec{v}}{\partial t} + (\vec{v} \cdot \nabla)\vec{v} + 2\vec{\Omega} \times \vec{v} = -\frac{1}{\rho}\nabla P - \nabla\left(\frac{B^2}{2\mu_0\rho}\right) + \frac{1}{\rho\mu_0}(\vec{B} \cdot \nabla)\vec{B} - g\hat{k}. \tag{2.6}$$

Rearranging the last equation, we have:

$$\frac{\partial \vec{v}}{\partial t} + (\vec{v} \cdot \nabla)\vec{v} + 2\vec{\Omega} \times \vec{v} = -\nabla\left(\frac{P}{\rho} + \frac{B^2}{2\mu_0\rho}\right) + \frac{1}{\rho\mu_0}(\vec{B} \cdot \nabla)\vec{B} - g\hat{k}. \tag{2.7}$$

We assume that the density is constant, the fluid is incompressible. Analysing the vertical component of the vectorial equation (2.7), we consider the velocity and the magnetic field vertical components negligible. Then, this simplification leads to magnetostrophic balance

$$0 = -\frac{\partial}{\partial z}\left(\frac{P}{\rho} + \frac{B^2}{2\mu_0\rho}\right) - g. \tag{2.8}$$

Solving this differential equation by integration, the result is

$$P + \frac{B^2}{2\mu_0} = -\rho g z + P_0, \tag{2.9}$$

where P_0 is a constant. Gilman (2000) establishes that *"the gas pressure is reduced by the amount of the magnetic pressure there"*, referring to the upper boundary, when $z = H$, the total pressure is $P + \frac{B^2}{2\mu_0} = 0$, hence

$$P_0 = \rho g H.$$

Substituting this result into (2.9), we obtain

$$P + \frac{B^2}{2\mu_0} = \rho g(H - z). \tag{2.10}$$

Hence, the horizontal pressure gradient can be written as

$$\nabla_H\left(P + \frac{B^2}{2\mu_0}\right) = \rho g \nabla_H H. \tag{2.11}$$

Taking the horizontal components of the momentum equation (2.7), the formula for the shallow water approximation in magnetohydrodynamics will be

$$\frac{\partial \vec{V}_H}{\partial t} + (\vec{V}_H \cdot \nabla_H)\vec{V}_H + 2\vec{\Omega} \times \vec{V}_H = \frac{1}{\rho\mu_0}(\vec{B}_H \cdot \nabla_H)\vec{B}_H - g\nabla_H H, \tag{2.12}$$

where $\vec{V}_H$ and $\vec{B}_H$ refer to the horizontal components of the velocity and the magnetic field, respectively.

In case we want to consider that on top of our stratified layer there is another layer of density ρ_0 not negligible then the boundary condition at $z = H$ must be different. Then

the hydrostatic and magnetic pressure equals the hydrostatic pressure of the fluid of the upper layer, as follows

$$P + \frac{B^2}{2\mu_0} = \rho_0 g(H_1 - H), \qquad \text{at} \qquad z = H, \tag{2.13}$$

where H_1 is the height of the upper layer and is a constant. Therefore the horizontal gradient of pressure is represented by

$$\nabla_H \Big(P + \frac{B^2}{2\mu_0} \Big) = \rho g^{'} \nabla_H H.$$

with $g^{'}$ as the reduced gravity defined by

$$g^{'} = \frac{\rho - \rho_0}{\rho}. \tag{2.14}$$

We will take into account this effect through the calculation of the parameter ϵ.

2.2.3 Equation of Conservation of Mass

The mass contained in a fluid column of height H and cross section A is $\int_A \rho H \, dA$. If there is a net flux of fluid across the column, with an increase in the mass in the region, the height of the column increases (Vallis, 2006).

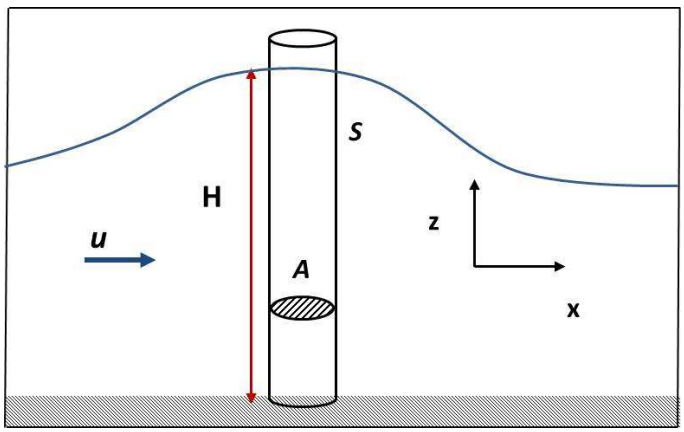

Figure 2.2: Mass flux entering in a column of fluid of cross-sectional area $\vec{A}$ and lateral area $\vec{S}$.

The mass flux entering the column is related to the derivative of the mass in a given volume V

$$F_m = -\int \rho\vec{v}\cdot\ d\vec{S}, \tag{2.15}$$

where $\vec{S}$ is the lateral area of the column. The element of area is $H\hat{n}\ dl$ where $\hat{n}$ is a unit vector perpendicular to the boundary pointing outwards, see figure 2.2 and dl is a line element around the column. Then, the equation (2.15) becomes

$$F_m = -\int \rho H\vec{v}\cdot\hat{n}\ dl.$$

Using the divergence theorem, the last formula simplifies to

$$F_m = -\int_A \nabla\cdot(\rho H\vec{v})\ dA, \tag{2.16}$$

where the integral is over the cross-sectional area of the column of fluid. The increase in the height of the water column is given by

$$F_m = \frac{d}{dt}\int_V \rho\ dV = \frac{d}{dt}\int_A \rho H\ dA = \int_A \rho\frac{\partial H}{\partial t}\ dA. \tag{2.17}$$

Because of the conservation of mass, the equations (2.16) and (2.17) are equivalent, hence

$$\int_A \rho\frac{\partial H}{\partial t}\ dA = -\int_A \nabla\cdot(\rho H\vec{v})\ dA. \tag{2.18}$$

Rearranging the equation for constant density, we obtain

$$\int_A \frac{\partial H}{\partial t} + \nabla\cdot(H\vec{v})\ dA = 0. \tag{2.19}$$

For any arbitrary surface, the expression is

$$\frac{\partial H}{\partial t} + \nabla_H\cdot(H\vec{V_H}) = 0, \tag{2.20}$$

As stated before, there is no dependence on z, then the differential operator simplifies to the horizontal derivatives, ∇_H.

2.2.4 Divergence Free Condition

The following is a brief description of one of the Maxwell's equations, the divergence free condition or Gauss's law for magnetism which establishes a condition for the magnetic field

$$\oint_A \vec{B} \cdot d\vec{S} = 0,$$

which states that the magnetic flux in a closed surface is zero. The surface is depicted in the figure 2.2. Then, the area element $d\vec{S}$ is $H\hat{n}\ dl$ (lateral area), $\hat{n}$ is a unitary vector perpendicular to this surface and dl is a line element circumscribing the column, as shown in the figure 2.2. As a result the integral around a curve C is

$$\int_C H\vec{B} \cdot \hat{n}\ dl = 0. \tag{2.21}$$

Using the divergence theorem

$$\int_C H\vec{B} \cdot \hat{n}\ dl = \int_A \nabla \cdot (H\vec{B})\ dA = 0, \tag{2.22}$$

because H and B_z does not depend on z, we have

$$\int_A \nabla_H \cdot (H\vec{B}_H)\ dA = 0. \tag{2.23}$$

Therefore, the divergence free condition for this model is

$$\nabla_H \cdot (H\vec{B}_H) = 0. \tag{2.24}$$

2.3 The Set of Equations and the Basic State

In summary, the equations for shallow water MHD are

$$\frac{\partial \vec{B}_H}{\partial t} + (\vec{V}_H \cdot \nabla_H)\vec{B}_H = (\vec{B}_H \cdot \nabla_H)\vec{V}_H, \tag{2.25a}$$

$$\frac{\partial \vec{V}_H}{\partial t} + (\vec{V}_H \cdot \nabla_H)\vec{V}_H + 2\Omega \times \vec{V}_H = \frac{1}{\mu_0 \rho}(\vec{B}_H \cdot \nabla_H)\vec{B}_H - g\nabla_H H, \tag{2.25b}$$

$$\frac{\partial H}{\partial t} + \nabla_H \cdot (H\vec{V}_H) = 0, \tag{2.25c}$$

$$\nabla_H \cdot (H\vec{B}_H) = 0. \tag{2.25d}$$

The set of equations will be developed in the following pages for spherical coordinates, where θ is the colatitude and ϕ is the longitude. There is no radial dependence, so the system is $2D$.

The basic state can follow different configurations: the latitudinal dependence of the magnetic field, a height dependent on the latitude, variable effective gravity (Dikpati et al., 2003, Dikpati and Gilman, 2001), mean zonal flows and stresses on the convection regions.

Previous studies have analysed some basic states for waves and instabilities in the shallow water model or the continuously stratified layer. Tayler (1973, 1980) and Pitts and Tayler (1985) have established the conditions for stability for a continuously stratified layer where the gravity and the pressure field depend on the position.

Rashid et al. (2008) have considered as the basic state, a zonal flow dependent of the vertical coordinate that may be maintained by a latitudinal temperature gradient and a radial shear or thermal wind. The condition of magnetohydrostatic balance could be mantained by imposing a zonal jet in the stably stratified layer (Rempel et al., 2000).

There are several options for choosing the basic state in the MHD shallow water approximation, Zaqarashvili et al. (2007) consider an unperturbed toroidal magnetic field

$$\vec{B}_\phi = B_0 \sin\theta \hat{e}_\phi,$$

and its perturbation

$$\vec{B}' = b_\theta \hat{e}_\theta + b_\phi \hat{e}_\phi,$$

where B_0 is a constant.

We note that a toroidal field can be linked to a current, which we suppose closes outside of the thin layer that is being modelled, but we do not discuss the currents here.

The velocity perturbation corresponds to

$$\vec{V}_H = u_\theta \hat{e}_\theta + u_\phi \hat{e}_\phi.$$

The perturbation of the layer thickness is

$$H = H_0 + h(\theta, \phi, t),$$

and the basic state H_0 is constant, for the height field can be constant the magnetic stress term $(\vec{B}_H \cdot \nabla)\vec{B}_H$ in the momentum equation (2.25b) has to balance with an external stress. Then the θ-component of (2.25b) requires the following basic state balance:

$$0 = -\frac{g}{R_0}\frac{dH_0}{d\theta} - \frac{\cot\theta B_\phi^2}{\rho\mu_0 R_0} + F_\theta,$$

where F_θ is an external stress. So constant H_0 implies non-zero F_θ.
Moreover, this basic state leads us to the possibility of finding analytic solutions in certain limits.

2.4 Linearised Equations in Spherical Coordinates

We substitute the basic state of the height, the magnetic field and the velocity into the equations (2.25a)-(2.25d), and linearise the system. Neglecting all the terms considered small, the equations are therefore:

$$\frac{\partial u_\theta}{\partial t} - 2\Omega_0 \cos\theta u_\phi + \frac{g}{R_0}\frac{\partial h}{\partial \theta} - \frac{B_\phi}{\mu_0 \rho R_0 \sin\theta}\frac{\partial b_\theta}{\partial \phi} + 2\frac{B_\phi}{\mu_0 \rho R_0}\frac{\cos\theta}{\sin\theta} b_\phi = 0, \tag{2.26a}$$

$$\frac{\partial u_\phi}{\partial t} + 2\Omega_0 \cos\theta u_\theta + \frac{g}{R_0 \sin\theta}\frac{\partial h}{\partial \phi} - \frac{b_\theta}{\mu_0 \rho R_0}\frac{\partial B_\phi}{\partial \theta} - \frac{B_\phi}{\mu_0 \rho R_0 \sin\theta}\frac{\partial b_\phi}{\partial \phi} - \frac{B_\phi}{\mu_0 \rho R_0}\frac{\cos\theta}{\sin\theta} b_\theta = 0, \tag{2.26b}$$

$$\frac{\partial h}{\partial t} + \frac{H_0}{R_0 \sin\theta}\frac{\partial}{\partial \theta}(\sin\theta u_\theta) + \frac{H_0}{R_0 \sin\theta}\frac{\partial u_\phi}{\partial \phi} = 0, \tag{2.26c}$$

$$\frac{\partial b_\theta}{\partial t} - \frac{B_\phi}{R_0 \sin\theta}\frac{\partial u_\theta}{\partial \phi} = 0, \tag{2.26d}$$

$$\frac{\partial b_\phi}{\partial t} + \frac{1}{R_0}\frac{\partial}{\partial \theta}(u_\theta B_\phi) = \frac{B_\phi}{R_0 \sin\theta}\left\{\frac{\partial}{\partial \theta}(u_\theta \sin\theta) + \frac{\partial u_\phi}{\partial \phi}\right\}. \tag{2.26e}$$

We propose solutions of the form $e^{im\phi - i\omega t}$, t is the time, ω is the frequency of the oscillation and m is the azimuthal wave number. It leads to a set of five coupled ordinary differential equations with θ as the independent variable:

$$-i\omega\hat{u}_\theta - 2\Omega_0 \cos\theta \hat{u}_\phi + \frac{g}{R_0}\sin\theta\frac{\partial h}{\partial \theta} - \frac{imB_0}{\mu_0 \rho R_o}\hat{b}_\theta + \frac{2B_0}{\mu_0 \rho R_o}\cos\theta \hat{b}_\phi = 0, \tag{2.27a}$$

$$-i\omega\hat{u}_\phi + 2\Omega_0 \cos\theta \hat{u}_\theta + im\frac{g}{R_0}h - \frac{imB_0}{\mu_0 \rho R_o}\hat{b}_\phi - \frac{2B_0}{\mu_0 \rho R_o}\cos\theta \hat{b}_\theta = 0, \tag{2.27b}$$

$$-i\omega \sin^2\theta h + \frac{H_0}{R_0}\sin\theta\frac{\partial \hat{u}_\theta}{\partial \theta} + im\frac{H_0}{R_o}\hat{u}_\phi = 0, \tag{2.27c}$$

$$i\omega\hat{b}_\theta + im\frac{B_0}{R_0}\hat{u}_\theta = 0, \tag{2.27d}$$

$$i\omega\hat{b}_\phi + im\frac{B_0}{R_0}\hat{u}_\phi = 0, \tag{2.27e}$$

where $\hat{u}_\theta$, $\hat{u}_\phi$, h, $\hat{b}_\theta$ and $\hat{b}_\phi$ are the corresponding amplitudes of these new variables:

$$\hat{u}_\theta = \sin\theta u_\theta, \qquad \hat{u}_\phi = \sin\theta u_\phi,$$

$$\hat{b}_\theta = \sin\theta b_\theta \qquad \text{and} \qquad \hat{b}_\phi = \sin\theta b_\phi.$$

We now change the variable θ to $\mu = \cos\theta$ and introduce the differential operator $D = -\sin\theta\partial/\partial\theta = (1-\mu^2)\partial/\partial\mu$.

We also define the Alfvén velocity v_A through $v_A^2 = B_0^2/\mu_0\rho$.

Our results will be given in terms of the dimensionless parameters

$$\epsilon = \frac{4\Omega_0^2 R_0^2}{gH_0}, \qquad \text{and} \qquad \alpha^2 = \frac{v_A^2}{4\Omega_0^2 R_0^2},$$

and a dimensionless frequency via $\lambda = \omega/2\Omega_0$. Additionally, the dimensionless variables are

$$\tilde{u}_\theta = \frac{i\hat{u}_\theta}{2\Omega_0 R_0}, \qquad \tilde{u}_\phi = \frac{\hat{u}_\phi}{2\Omega_0 R_0}, \tag{2.28}$$

$$\eta = \frac{gh}{4\Omega_0^2 R_0^2}, \qquad \hat{b}_\theta = iB_0\tilde{b}_\theta, \qquad \hat{b}_\phi = B_0\tilde{b}_\phi.$$

Then, the equations take the form

$$\lambda\tilde{u}_\theta + \mu\tilde{u}_\phi + D\eta + m\alpha^2\tilde{b}_\theta - 2\alpha^2\mu\tilde{b}_\phi = 0, \tag{2.29a}$$

$$\lambda\tilde{u}_\phi + \mu\tilde{u}_\theta - m\eta + m\alpha^2\tilde{b}_\phi - 2\alpha^2\mu\tilde{b}_\theta = 0, \tag{2.29b}$$

$$\lambda\epsilon(1-\mu^2)\eta - D\tilde{u}_\theta - m\tilde{u}_\phi = 0, \tag{2.29c}$$

$$\lambda\tilde{b}_\theta + m\tilde{u}_\theta = 0, \tag{2.29d}$$

$$\lambda\tilde{b}_\phi + m\tilde{u}_\phi = 0. \tag{2.29e}$$

Equation (2.25d) for the divergence free condition can be useful, the linearised form is

$$m\epsilon(1-\mu^2)\eta - (1-\mu^2)\frac{\partial\tilde{b}_\theta}{\partial\mu} + m\tilde{b}_\phi = 0. \tag{2.30}$$

In order to solve we now expand each of the dependent variables as a sum of associated Legendre Polynomials, remembering that each expansion must have $n \geq m$ because the polynomials are not defined for $n < m$,

$$\tilde{u}_\theta = \sum_{n=m}^{\infty} A_n^m P_n^m(\mu), \qquad \tilde{b}_\theta = \sum_{n=m}^{\infty} B_n^m P_n^m(\mu),$$

$$\tilde{u}_\phi = \sum_{n=m}^{\infty} C_n^m P_n^m(\mu), \qquad \tilde{b}_\phi = \sum_{n=m}^{\infty} D_n^m P_n^m(\mu), \qquad \eta = \sum_{n=m}^{\infty} E_n^m P_n^m(\mu).$$

Even though these are infinite expansions, for the purposes of the numerical calculations expansions will be truncated at $n = N$ for all m, where N is the truncation number and for our purposes N is large compared to m. We will make use of two properties of associated Legendre polynomials

$$\mu P_n^m = \frac{(n+m)}{(2n+1)}P_{n-1}^m + \frac{(n-m+1)}{(2n+1)}P_{n+1}^m,$$

$$DP_n^m = \frac{(n+1)(n+m)}{(2n+1)}P_{n-1}^m - \frac{n(n-m+1)}{(2n+1)}P_{n+1}^m.$$

Substituting the expansions of the dependent variables into the equations (2.29a), (2.29b), (2.29c), (2.29d) and (2.29e), and then using the properties of the associated Legendre

Polynomials, we obtain a set of algebraic equations. In each equation we must set the coefficient of $P_n^m(\mu)$ to zero, and we then obtain the following equations for the coefficients in our expansion, A_n^m, B_n^m, C_n^m, D_n^m, E_n^m :

$$\begin{aligned} -\lambda A_n^m &= m\alpha^2 B_n^m - q_{n-1}C_{n-1}^m + 2\alpha^2 q_{n-1}D_{n-1}^m + (n-1)q_{n-1}E_{n-1}^m \\ &- p_{n+1}C_{n+1}^m + 2\alpha^2 p_{n+1}D_{n+1}^m - (n+2)p_{n+1}E_{n+1}^m, \end{aligned} \tag{2.31a}$$

$$\begin{aligned} \lambda C_n^m &= sE_n^m - m\alpha^2 D_n^m + q_{n-1}A_{n-1}^m \\ &- 2\alpha^2 q_{n-1}B_{n-1}^m - 2\alpha^2 p_{n+1}B_{n+1}^m + p_{n+1}A_{n+1}^m, \end{aligned} \tag{2.31b}$$

$$\begin{aligned} &\lambda\{\epsilon(1-p_n q_{n-1} - q_n p_{n+1})E_n^m - \epsilon p_{n+2}p_{n+1}E_{n+2}^m - \epsilon q_{n-1}q_{n-2}E_{n-2}^m\} \\ &\qquad = sC_n^s - (n+2)p_{n+1}A_{n+1}^m + (n-1)q_{n-1}A_{n-1}^m, \end{aligned} \tag{2.31c}$$

$$\lambda B_n^m = -mA_n^m, \tag{2.31d}$$

$$\lambda D_n^m = -mC_n^m, \tag{2.31e}$$

where, $q_n = (n-m+1)/(2n+1)$ and $p_n = (n+m)/(2n+1)$. Because the associated Legendre polynomials are symmetric about the equator if $n-m$ is even, and antisymmetric if $n-m$ is odd, there are two independent set of equations of different parity. The coefficients A_m, B_m, C_{m+1}, D_{m+1}, E_{m+1}, A_{m+2}, B_{m+2}, C_{m+3}, D_{m+3}, E_{m+3}, A_{m+4}, B_{m+4}, C_{m+5}, D_{m+5}, E_{m+5}.... are related to each other, while the others A_{m+1}, B_{m+1}, C_m, D_m, E_m, A_{m+3}, B_{m+3}, C_{m+2}, D_{m+2}, E_{m+2}, A_{m+5}, B_{m+5}, C_{m+4}, D_{m+4}, E_{m+4}.... form another independent set of equations. We solve each set separately using a Matlab eigenvalue and eigenvector solver, designed to solve the system of equations $\boldsymbol{A}\vec{v} = \lambda\boldsymbol{B}\vec{v}$, with a QZ method for the computation of the generalized eigenvalues.

The algorithm for the QZ method is based on the theorem that establishes that there are unitary matrices $\boldsymbol{Q}$ and $\boldsymbol{Z}$ where $\boldsymbol{QAZ}$ and $\boldsymbol{QBZ}$ are both upper triangular. The eigenvalue problems $\boldsymbol{QAZ}\vec{y} = \lambda\boldsymbol{QBZ}\vec{y}$ and $\boldsymbol{A}\vec{v} = \lambda\boldsymbol{B}\vec{v}$ are unitary equivalent. The

eigenvalues are the same for both problems and the eigenvectors are related by $\vec{v} = \boldsymbol{Z}\vec{y}$ (Moler and Stewart, 1973).
The method has four steps, briefly described as follows (Kaufman, 1977):

1. The matrix $\boldsymbol{A}$ is reduced to upper Hessenberg form ($a_{ij} = 0$ for $i > j + 1$) and $\boldsymbol{B}$ is reduced to upper triangular form ($b_{ij} = 0$ for $i > j$) simultaneously.

2. The matrix $\boldsymbol{A}$ is reduced to a quasi-triangular form but maintaining $\boldsymbol{B}$ triangular.

3. The quasitriangular matrix $\boldsymbol{A}$ is reduced to a triangular matrix and the eigenvalues are extracted, using the fact that the eigenvalues of a triangular matrix are the elements of the diagonal.

4. Determining the eigenvector of the triangular matrices and return to the original system.

The eigenvalues of the original problem are calculated dividing α_i and β_i, the diagonal elements of the triangular matrices $\boldsymbol{QAZ}$ and $\boldsymbol{QBZ}$ with $\lambda_i = \alpha_i/\beta_i$. With this algorithm is not necessary to invert the matrix $\boldsymbol{B}$.

2.4.1 First System of Equations

The first system of equation is obtained on rearranging the equations for the A_m, B_m, C_{m+1}, D_{m+1}, E_{m+1} ..., coefficients. In this set, the solutions for $\tilde{u}_\theta$ and $\tilde{b}_\theta$ are symmetric with respect to the equator but the eigenfunctions for $\tilde{u}_\phi$, $\tilde{b}_\phi$ and η are antisymmetric. These modes are known as sinuous or kink modes since fluid will flow northwards at the equator in some locations and southward in others. Then the equations (2.31) are rewritten as

$$\lambda B_n^m = -mA_n^m, \tag{2.32a}$$

$$\lambda D_{n+1}^m = -mC_{n+1}^m, \tag{2.32b}$$

$$
\begin{aligned}
-\lambda A_n^m &= m\alpha^2 B_n^m - q_{n-1}C_{n-1}^m + 2\alpha^2 q_{n-1}D_{n-1}^m + (n-1)q_{n-1}E_{n-1}^m \\
&- p_{n+1}C_{n+1}^m + 2\alpha^2 p_{n+1}D_{n+1}^m - (n+2)p_{n+1}E_{n+1}^m, \qquad (2.32c)
\end{aligned}
$$

$$
\begin{aligned}
\lambda C_{n+1}^m &= sE_{n+1}^m - m\alpha^2 D_{n+1}^m + q_n A_n^m \\
&- 2\alpha^2 q_n B_n^m - 2\alpha^2 p_{n+2}B_{n+2}^m + p_{n+2}A_{n+2}^m, \qquad (2.32d)
\end{aligned}
$$

$$
\begin{aligned}
&\lambda\{\epsilon(1 - p_{n+1}q_n - q_{n+1}p_{n+2})E_{n+1}^m - \epsilon p_{n+3}p_{n+2}E_{n+3}^m - \epsilon q_n q_{n-1}E_{n-1}^m\} \\
&\qquad = sC_{n+1}^m - (n+3)p_{n+2}A_{n+2}^m + (n)q_n A_n^m, \qquad (2.32e)
\end{aligned}
$$

where $n = m, m+2, m+4, m+6, ...$

2.4.2 Second System of Equations

On the other hand, the second system of equation is obtained when we rearrange the equations for the other parity, A_{m+1}, B_{m+1}, C_m, D_m, E_m.... In this case the eigenfunctions for $\tilde{u}_\theta$ and $\tilde{b}_\theta$ are antisymmetric and $\tilde{u}_\phi$, $\tilde{b}_\phi$ and η are symmetric with respect to the equator. These modes are called varicose or sausage modes. Then the equations (2.31) are rewritten as

$$\lambda B_{n+1}^m = -mA_{n+1}^m, \qquad (2.33a)$$

$$\lambda D_n^m = -mC_n^m, \qquad (2.33b)$$

$$
\begin{aligned}
-\lambda A_{n+1}^m &= m\alpha^2 B_{n+1}^m - q_n C_n^m + 2\alpha^2 q_n D_n^m + (n)q_n E_n^m \\
&- p_{n+2}C_{n+2}^m + 2\alpha^2 p_{n+2}D_{n+2}^m - (n+3)p_{n+2}E_{n+2}^m, \qquad (2.33c)
\end{aligned}
$$

$$
\begin{aligned}
\lambda C_n^m &= sE_n^m - m\alpha^2 D_n^m + q_{n-1}A_{n-1}^m \\
&- 2\alpha^2 q_{n-1}B_{n-1}^m - 2\alpha^2 p_{n+1}B_{n+1}^m + p_{n+1}A_{n+1}^m, \qquad (2.33d)
\end{aligned}
$$

$$\lambda\{\epsilon(1-p_n q_{n-1}-q_n p_{n+1})E_n^m-\epsilon p_{n+2}p_{n+1}E_{n+2}^m-\epsilon q_{n-1}q_{n-2}E_{n-2}^m\}$$

$$=mC_n^m-(n+2)p_{n+1}A_{n+1}^m+(n-1)q_{n-1}A_{n-1}^m, \qquad (2.33e)$$

where $n=m,m+2,m+4,m+6,.....$

With regard to the validity of the solutions, we perform a test to ensure that only lower degree eigenfunctions will be chosen. This means that the expansions of the Associated Legendre Polynomials will not be affected by the truncation number N, because the coefficients of high degree are smaller than those of lower degree. We measure the ratio between the sum of the first half of the square of the coefficients and the second half

$$Ratio=\frac{\sum_{n=m}^{N/2}(A_n^m)^2}{\sum_{n=N/2+1}^{N}(A_n^m)^2}. \qquad (2.34)$$

For a given eigenvalue, if the ratio is large, it means that the solution has a lower degree and it is valid. If the ratio is small ($<10^3$), the solution is discarded.

2.5 The Normalization Constant

A detailed description of the conservation of energy for the set of equations is given in the following section. First, we analyse the general conservation law for the special magnetic field configuration $B_\phi=B_0\sin\theta$. Then we substitute the solutions, which are associated Legendre Polynomial expansions multiplied by a constant into the energy expression, and try to find a value of the constant for a special definition of energy. This value of the constant is our normalization quantity.

The purpose of normalization is to make the total energy equal to a constant and from the expression of energy we can infer if instability is present.

Let us now multiply the equation (2.26a) by u_θ.

$$u_\theta\frac{\partial u_\theta}{\partial t}-2\Omega_0\cos\theta u_\theta u_\phi+\frac{g}{R_o}u_\theta\frac{\partial h}{\partial\theta}-\frac{B_0}{\mu_0\rho R_o}u_\theta\frac{\partial b_\theta}{\partial\phi}+\frac{2B_0}{\mu_0\rho R_o}\cos\theta u_\theta b_\phi=0. \qquad (2.35)$$

In addition, we multiply the equation (2.26b) by u_ϕ

$$u_\phi\frac{\partial u_\phi}{\partial t}+2\Omega_0\cos\theta u_\phi u_\theta+\frac{g}{R_o\sin\theta}u_\phi\frac{\partial h}{\partial\phi}-\frac{B_0}{\mu_0\rho R_o}u_\phi\frac{\partial b_\phi}{\partial\phi}-\frac{2B_0}{\mu_0\rho R_o}\cos\theta u_\phi b_\theta=0. \quad (2.36)$$

Adding these two equations gives

$$\frac{1}{2}\frac{\partial}{\partial t}(u_\theta^2+u_\phi^2)+\frac{g}{R_o}u_\theta\frac{\partial h}{\partial\theta}+\frac{g}{R_o\sin\theta}u_\phi\frac{\partial h}{\partial\phi}-\frac{B_0}{\mu_0\rho R_o}u_\theta\frac{\partial b_\theta}{\partial\phi}-\frac{B_0}{\mu_0\rho R_o}u_\phi\frac{\partial b_\phi}{\partial\phi}$$
$$-\frac{2B_0}{\mu_0\rho R_o}\cos\theta u_\phi b_\theta+\frac{2B_0}{\mu_0\rho R_o}\cos\theta u_\theta b_\phi=0. \quad (2.37)$$

Multiply the equations (2.26d) and (2.26e) by $b_\theta/\mu_0\rho$ and $b_\phi/\mu_0\rho$ respectively

$$\frac{1}{\mu_0\rho}\frac{\partial}{\partial t}\frac{b_\theta^2}{2}-\frac{B_0}{\mu_0\rho R_o}b_\theta\frac{\partial u_\theta}{\partial\phi}=0, \quad (2.38)$$

$$\frac{1}{\mu_0\rho}\frac{\partial}{\partial t}\frac{b_\phi^2}{2}-\frac{B_0}{\mu_0\rho R_o}b_\phi\frac{\partial u_\phi}{\partial\phi}=0. \quad (2.39)$$

Adding equations (2.37), (2.38) and (2.39), we obtain

$$\frac{1}{2}\frac{\partial}{\partial t}(u_\theta^2+u_\phi^2+\frac{b_\phi^2}{\mu_0\rho}+\frac{b_\theta^2}{\mu_0\rho})+\frac{g}{R_o}u_\theta\frac{\partial h}{\partial\theta}+\frac{g}{R_o\sin\theta}u_\phi\frac{\partial h}{\partial\phi}$$
$$-\frac{B_0}{\mu_0\rho R_o}\frac{\partial}{\partial\phi}(u_\theta b_\theta)-\frac{B_0}{\mu_0\rho R_o}\frac{\partial}{\partial\phi}(u_\phi b_\phi)+\frac{2B_0}{\mu_0\rho R_o}\cos\theta(u_\theta b_\phi-u_\phi b_\theta)=0. \quad (2.40)$$

Multiplying the equation (2.40) by H_0 yields

$$\frac{H_0}{2}\frac{\partial}{\partial t}(u_\theta^2+u_\phi^2+\frac{b_\phi^2}{\mu_0\rho}+\frac{b_\theta^2}{\mu_0\rho})+\frac{gH_0}{R_o}u_\theta\frac{\partial h}{\partial\theta}+\frac{gH_0}{R_o\sin\theta}u_\phi\frac{\partial h}{\partial\phi}$$
$$-\frac{B_0H_0}{\mu_0\rho R_o}\frac{\partial}{\partial\phi}(u_\theta b_\theta)-\frac{B_0H_0}{\mu_0\rho R_o}\frac{\partial}{\partial\phi}(u_\phi b_\phi)+\frac{2B_0H_0}{\mu_0\rho R_o}\cos\theta(u_\theta b_\phi-u_\phi b_\theta)=0. \quad (2.41)$$

Multiplying the equation (2.26c) by gh

$$\frac{g}{2}\frac{\partial h^2}{\partial t}+\frac{gH_0}{R_o\sin\theta}h\frac{\partial(\sin\theta u_\theta)}{\partial\theta}+\frac{gH_0}{R_o\sin\theta}h\frac{\partial u_\phi}{\partial\phi}=0. \quad (2.42)$$

Adding equations (2.41) and (2.42), we obtain

$$\frac{\partial}{\partial t}\left\{\frac{H_0}{2}(u_\theta^2+u_\phi^2+\frac{b_\phi^2}{\mu_0\rho}+\frac{b_\theta^2}{\mu_0\rho})+\frac{g}{2}h^2\right\}+\frac{gH_0}{R_o\sin\theta}\frac{\partial}{\partial\theta}(\sin\theta u_\theta h)+\frac{gH_0}{R_o\sin\theta}\frac{\partial}{\partial\phi}(u_\phi h)$$
$$-\frac{B_0H_0}{\mu_0\rho R_o}\frac{\partial}{\partial\phi}(u_\theta b_\theta)-\frac{B_0H_0}{\mu_0\rho R_o}\frac{\partial}{\partial\phi}(u_\phi b_\phi)+\frac{2B_0H_0}{\mu_0\rho R_o}\cos\theta(u_\theta b_\phi-u_\phi b_\theta)=0.$$

The terms with velocity and height can be arranged in a divergence

$$\frac{\partial}{\partial t}\left\{\frac{H_0}{2}(u_\theta^2+u_\phi^2+\frac{b_\phi^2}{\mu_0\rho}+\frac{b_\theta^2}{\mu_0\rho})+\frac{g}{2}h^2\right\}+gH_0\nabla\cdot(\vec{u}h)$$

$$-\frac{B_0H_0}{\mu_0\rho R_o}\frac{\partial}{\partial\phi}(u_\theta b_\theta)-\frac{B_0H_0}{\mu_0\rho R_o}\frac{\partial}{\partial\phi}(u_\phi b_\phi)+\frac{2B_0H_0}{\mu_0\rho R_o}\cos\theta(u_\theta b_\phi-u_\phi b_\theta)=0. \quad (2.43)$$

With respect to the above equations, they are related to the energy per mass unit. Let now us consider the total energy which could be calculated by multiplying the last equation by the constant density ρ and integrating over ϕ and θ:

$$\int\int\frac{\partial}{\partial t}\{\frac{\rho H_0}{2}(u_\theta^2+u_\phi^2+\frac{b_\phi^2}{\mu_0\rho}+\frac{b_\theta^2}{\mu_0\rho})+\frac{\rho g}{2}h^2\}\quad dS+\int\int\rho gH_0\nabla\cdot(\vec{u}h)\quad dS$$

$$-\int\int\frac{B_0H_0}{\mu_0R_o}\frac{\partial}{\partial\phi}(\vec{u}\cdot\vec{b})dS+\int\int\frac{2B_0H_0}{\mu_0R_o}\cos\theta(u_\theta b_\phi-u_\phi b_\theta)\quad dS=0. \quad (2.44)$$

The second integral is equal to zero, when integrating over ϕ because of the periodicity and also over θ because of the boundary conditions at the poles

$$\int\int\rho gH_0\nabla\cdot(\vec{u}h)\quad dS=\frac{\rho gH_0}{R_0}\int_0^{2\pi}\int_0^{\pi}\frac{\partial}{\partial\theta}(\sin\theta hu_\theta)+\frac{\partial hu_\phi}{\partial\phi}d\theta d\phi=0$$

The third one vanishes too when it is integrated over ϕ, because of the periodicity of the solutions

$$\int_0^{2\pi}\int_0^{\pi}\frac{\partial}{\partial\phi}(\vec{u}\cdot\vec{b})\sin\theta\quad d\theta d\phi=\int_0^{\pi}\{[\vec{u}\cdot\vec{b}]_{\phi=2\pi}-[\vec{u}\cdot\vec{b}]_{\phi=0}\}\sin\theta\quad d\theta=0.$$

Then, the equation (2.44) becomes

$$\int\int\frac{\partial}{\partial t}\{\frac{\rho H_0}{2}(u_\theta^2+u_\phi^2+\frac{b_\phi^2}{\mu_0\rho}+\frac{b_\theta^2}{\mu_0\rho})+\frac{\rho g}{2}h^2\}\quad dS$$

$$+\int\int\frac{2B_0H_0}{\mu_0R_o}\cos\theta(u_\theta b_\phi-u_\phi b_\theta)\quad dS=0. \quad (2.45)$$

Performing a Fourier analysis for the equations (2.26d) and (2.26e), taking $\vec{b}$ and $\vec{u}$ proportional to $e^{im\phi-i\omega t}$ with ω real, the case when ω is complex will be explained in the section 2.5.1. Then we get:

$$b_\theta=-\frac{mB_0}{R_o\omega}u_\theta\qquad and\qquad b_\phi=-\frac{mB_0}{R_o\omega}u_\phi,$$

also, we substitute into the fourth integral,and realise that the term $(u_\theta b_\phi - u_\phi b_\theta)$ is zero. The final equation represents the variation of the energy respect to time

$$\int\int \frac{\partial}{\partial t}\{\frac{\rho H_0}{2}(u_\theta^2 + u_\phi^2 + \frac{b_\phi^2}{\mu_0\rho} + \frac{b_\theta^2}{\mu_0\rho}) + \frac{\rho g}{2}h^2\} \quad dS = 0. \tag{2.46}$$

This is a conservation law, for the system, therefore the total energy, is defined by

$$E = \int\int \left\{\frac{\rho H_0}{2}(u_\theta^2 + u_\phi^2 + \frac{b_\phi^2}{\mu_0\rho} + \frac{b_\theta^2}{\mu_0\rho}) + \frac{\rho g}{2}h^2\right\} \quad dS. \tag{2.47}$$

Turning now to the numerical calculation of the normalization function for the equations, we return to the original variables (2.28) by

$$u_\theta = -\frac{2i\Omega_0 R_0 \tilde{u}_\theta}{\sin\theta}, \qquad u_\phi = \frac{2\Omega_0 R_0 \tilde{u}_\phi}{\sin\theta},$$

$$b_\theta = \frac{iB_0\tilde{b}_\theta}{\sin\theta}, \qquad b_\phi = \frac{B_0\tilde{b}_\phi}{\sin\theta}, \qquad h = \frac{4\Omega_0^2 R_0^2 \eta}{g}.$$

Alternatively the energy takes the form

$$\int\int \left\{\frac{\rho H_0 4\Omega_0^2 R_o^2}{2\sin^2\theta}(\tilde{u}_\theta^2 + \tilde{u}_\phi^2) + \frac{\rho H_0 B_0^2}{2\mu_0\rho\sin^2\theta}(\tilde{b}_\phi^2 + \tilde{b}_\theta^2) + \frac{8\rho\Omega_0^4 R_o^4}{g}\eta^2\right\} \quad dS = E. \tag{2.48}$$

Substituting the parameters $\epsilon = 4\Omega_0^2 R_0^2/gH_0$ and $\alpha^2 = v_A^2/4\Omega_0^2 R_0^2$ for $v_A^2 = B_0^2/\mu_0\rho$, we have a final equation

$$\int\int \rho H_0 2\Omega_0^2 R_o^2 \left\{\frac{1}{\sin^2\theta}(\tilde{u}_\theta^2 + \tilde{u}_\phi^2) + \frac{\alpha^2}{\sin^2\theta}(\tilde{b}_\phi^2 + \tilde{b}_\theta^2) + \epsilon\eta^2\right\} \quad dS = E. \tag{2.49}$$

Analogous to Longuet-Higgins (1968), we set the total energy

$$E \equiv 4\pi\rho H_o \Omega_0^2 R_0^4.$$

Substituting the definition into the equation (2.49) and integrating with respect to ϕ, we have

$$\int_0^\pi \left\{\frac{1}{\sin^2\theta}(\tilde{u}_\theta^2 + \tilde{u}_\phi^2) + \frac{\alpha^2}{\sin^2\theta}(\tilde{b}_\phi^2 + \tilde{b}_\theta^2) + \epsilon\eta^2\right\} \quad \sin\theta d\theta = 1. \tag{2.50}$$

Next, we substitute into the equation (2.50) the Legendre expansion solutions multiplied by a normalization constant, γ

$$\tilde{u}_\theta = \gamma\sum_{n=m}^{\infty} A_n^m P_n^m(\mu) \quad e^{im\phi - i\omega t}, \qquad \tilde{b}_\theta = \gamma\sum_{n=m}^{\infty} B_n^m P_n^m(\mu) \quad e^{im\phi - i\omega t},$$

$$\tilde{u}_\phi = \gamma \sum_{n=m}^{\infty} C_n^m P_n^m(\mu) \quad e^{im\phi - i\omega t}, \qquad \tilde{b}_\phi = \gamma \sum_{n=m}^{\infty} D_n^m P_n^m(\mu) \quad e^{im\phi - i\omega t},$$

$$\eta = \gamma \sum_{n=m}^{\infty} E_n^m P_n^m(\mu) \quad e^{im\phi - i\omega t}.$$

We use again this important result

$$u_\theta u_\theta^* = \frac{\gamma^2}{2} \sum_{n=m}^{N} \sum_{k=m}^{N} A_n^m A_k^{m*} P_n^m(\mu) P_k^m(\mu).$$

where the star means the complex conjugate quantity. After some algebra steps the equation obtained is

$$\int_{-1}^{1} \frac{\gamma^2}{2} \left\{ \sum_{n=m}^{\infty} \sum_{k=m}^{\infty} \frac{(A_n^m A_k^{m*} + C_n^m C_k^{m*})}{(1-\mu^2)} + \frac{\alpha^2 (B_n^m B_k^{m*} + D_n^m D_k^{m*})}{(1-\mu^2)} + \epsilon E_n^m E_k^{m*} \right\} P_n^m(\mu) P_k^m(\mu) \quad d\mu = 1. \tag{2.51}$$

There are some integrals to be evaluated in this equation

$$\frac{\gamma^2}{2} \left\{ \sum_{n=m}^{\infty} \sum_{k=m}^{\infty} (A_n^m A_k^{m*} + C_n^m C_k^{s*}) + \alpha^2 (B_n^m B_k^{m*} + D_n^m D_k^{m*}) \right\} \int_{-1}^{1} \frac{P_n^m(\mu) P_k^m(\mu)}{(1-\mu^2)} \quad d\mu$$

$$+ \frac{\gamma^2}{2} \epsilon E_n^m E_k^{m*} \int_{-1}^{1} P_n^m(\mu) P_k^m(\mu) \quad d\mu = 1.$$

The last integral has been calculated by Abramowitz and Stegun (1964)

$$\int_{-1}^{1} P_n^m(\mu) P_k^m(\mu) d\mu = \frac{2(n+m)\,!}{(2n+1)(n-m)\,!} \delta_{nk}.$$

Therefore

$$\frac{1}{\gamma^2} = \sum_{n=m}^{N} \sum_{k=m}^{N} [(C_n^m C_n^{m*} + A_n^m A_n^{m*}) + \alpha^2 (D_n^m D_n^{m*} + B_n^m B_n^{m*})] \quad \int_{-1}^{1} \frac{P_n^m(\mu) P_k^m(\mu)}{(1-\mu^2)} \quad d\mu$$

$$+ \sum_{n=m}^{N} \epsilon E_n^m E_n^{m*} \frac{2(n+m)\,!}{(2n+1)(n-m)\,!}. \tag{2.52}$$

We are therefore able to calculate the value of the normalization constant γ

$$\gamma = \frac{1}{\sqrt{E'}}$$

where E' is given by

$$E' = \sum_{n=m}^{N}\sum_{k=m}^{N}[(C_n^m C_n^{m*} + A_n^m A_n^{m*}) + \alpha^2(D_n^m D_n^{m*} + B_n^m B_n^{m*})] \quad \int_{-1}^{1} \frac{P_n^m(\mu)P_k^m(\mu)}{(1-\mu^2)} \quad d\mu$$
$$+ \sum_{n=m}^{N} \epsilon E_n^m E_n^{m*} \frac{2(n+m)\,!}{(2n+1)(n-m)\,!}. \tag{2.53}$$

Rearranging the expression

$$E' = \sum_{n=m}^{N}\sum_{k=m}^{N}[(C_n^m C_n^{m*} + A_n^m A_n^{m*}) + \alpha^2(D_n^m D_n^{m*} + B_n^m B_n^{m*})]I_{nk}^m$$
$$+ \sum_{n=m}^{N} \epsilon E_n^m E_n^{m*} \frac{2(n+m)\,!}{(2n+1)(n-m)\,!,} \tag{2.54}$$

where the index runs different for some coefficients than others. For first parity problem, the value of n for the coefficients A_n^m and B_n^m are $n = m, m+2, m+4, ...$, also for C_n^m, D_n^m and E_n^m are $n = m+1, m+3, m+5, ...$ For the other parity solution, the index runs in the opposite way. The integral I_{nk}, has the following result

$$I_{nk}^m = \begin{cases} 0 & \text{if} \quad n \quad \text{and } k \quad \text{have different parity,} \\ \frac{(n+m)\,!}{m(n-m)\,!} & \text{if} \quad n < k, \quad \text{for} \quad n,k \quad \text{same parity,} \\ \frac{(k+m)\,!}{m(k-m)\,!} & \text{if} \quad k < n, \quad \text{for} \quad n,k \quad \text{same parity,} \end{cases} \tag{2.55}$$

2.5.1 Energy Equation for Complex Eigenvalues

When the eigenvalues are complex, the term $(u_\theta b_\phi - u_\phi b_\theta)$ in the equation (2.45) is not zero, then we have to evaluate this expression. In general, the eigenfunction for the

velocity, can be expressed by

$$\tilde{u}_\theta = \frac{1}{2}\left[\bar{u}_\theta e^{i(m\phi-\omega t)} + \bar{u}^*_\theta e^{-i(m\phi-\omega^* t)}\right].$$

As a consequence of the complex form of the eigenvalues $\omega = \omega_r + i\omega_i$, and the eigenfunctions, the integrals over ϕ are

$$\int_0^{2\pi} |u_\theta|^2 \quad d\phi = \pi \bar{u}^*_\theta \bar{u}_\theta e^{2\omega_i t},$$

and

$$\int_0^{2\pi} u_\theta b_\phi \quad d\phi = \frac{\pi}{2}(\bar{u}^*_\theta \bar{b}_\phi + \bar{u}_\theta \bar{b}^*_\phi) e^{2\omega_i t}.$$

Then, the integral (2.45) takes the expression, for $m = 1$

$$\sigma \int_0^\pi \left\{ \frac{|\tilde{u}_\theta|^2 + |\tilde{u}_\phi|^2}{\sin^2\theta} + \alpha^2 \frac{|\tilde{b}_\phi|^2 + |\tilde{b}_\theta|^2}{\sin^2\theta} + \epsilon|\eta|^2 + \alpha^2 \frac{\cos\theta}{\sin^2\theta}(\tilde{b}^*_\theta \tilde{b}_\phi + \tilde{b}^*_\phi \tilde{b}_\theta) \right\} \sin\theta d\theta = 0, \tag{2.56}$$

where σ is the growth rate, defined by $\sigma = \omega_i / 2\Omega_0$. For growing modes the last term must be negative to compensate the other positive definite terms of the energy equation (2.56).

2.6 Second Order Differential Equation Formulation

The original system of equations for a shallow water model can be simplified to a second order differential equation for $\tilde{u_\theta}$ and for η as follows. Substituting the components of the magnetic fields from (2.29d)-(2.29e) into (2.29a) and (2.29b). Then, the equations are

$$(\lambda^2 - m^2\alpha^2)\tilde{u}_\theta + (\lambda + 2m\alpha^2)\mu\tilde{u}_\phi + \lambda(1-\mu^2)\frac{\partial \eta}{\partial \mu} = 0, \tag{2.57a}$$

$$(\lambda^2 - m^2\alpha^2)\tilde{u}_\phi + (\lambda + 2m\alpha^2)\mu\tilde{u}_\theta - \lambda m\eta = 0, \tag{2.57b}$$

$$\epsilon\lambda(1-\mu^2)\eta - (1-\mu^2)\frac{\partial \tilde{u}_\theta}{\partial \mu} - m\tilde{u}_\phi = 0. \tag{2.57c}$$

2.6.1 Differential Equation for $\tilde{u}_\theta$

From equation (2.57c)

$$\tilde{u}_\phi = \frac{1}{m}\Big[- D\tilde{u}_\theta + \epsilon\lambda(1-\mu^2)\eta\Big]. \tag{2.58}$$

After substituting $\hat{u}_\phi$ into (2.57a) and (2.57b), we obtain

$$m(\lambda^2 - m^2\alpha^2)\tilde{u}_\theta + \epsilon\lambda(\lambda + 2m\alpha^2)\mu(1-\mu^2)\eta - (\lambda + 2m\alpha^2)\mu D\tilde{u}_\theta + \lambda m D\eta = 0, \tag{2.59}$$

$$-(\lambda^2 - m^2\alpha^2)D\tilde{u}_\theta + [(\lambda^2 - m^2\alpha^2)\epsilon(1-\mu^2) - m^2]\lambda\eta + m(\lambda + 2m\alpha^2)\mu\tilde{u}_\theta = 0. \tag{2.60}$$

From equation (2.60)

$$\lambda\eta = \frac{1}{[(\lambda^2 - m^2\alpha^2)\epsilon(1-\mu^2) - m^2]}\big\{(\lambda^2 - m^2\alpha^2)D\tilde{u}_\theta - m(\lambda + 2m\alpha^2)\mu\tilde{u}_\theta\big\}. \tag{2.61}$$

From equation (2.59)

$$\lambda\frac{\partial\tilde{\eta}}{\partial\mu} = \frac{(\lambda + 2m\alpha^2)}{m}\mu\frac{\partial\tilde{u}_\theta}{\partial\mu} - \frac{\epsilon\lambda}{m}(\lambda + 2m\alpha^2)\mu\eta - \frac{(\lambda^2 - m^2\alpha^2)}{(1-\mu^2)}\tilde{u}_\theta. \tag{2.62}$$

Taking the derivative of equation (2.60) yields

$$\begin{aligned} -(\lambda^2 w - m^2\alpha^2)(1-\mu^2)\frac{\partial^2\tilde{u}_\theta}{\partial\mu^2} + \lambda(m+2\lambda)\mu\frac{\partial\tilde{u}_\theta}{\partial\mu} + m(\lambda + 2m\alpha^2)\tilde{u}_\theta + \\ \lambda[(\lambda^2 - m^2\alpha^2)\epsilon(1-\mu^2) - m^2]\frac{\partial\eta}{\partial\mu} - 2\epsilon\lambda(\lambda^2 - m^2\alpha^2)\mu\eta = 0. \end{aligned} \tag{2.63}$$

Substituting η and $\frac{\partial\eta}{\partial\mu}$ into equation (2.63), and simplifying the expression, we have

$$\begin{aligned} (1-\mu^2)\frac{\partial^2\tilde{u}_\theta}{\partial\mu^2} + \frac{2m^2}{[(\lambda^2 - m^2\alpha^2)\epsilon(1-\mu^2) - m^2]}\mu\frac{\partial\tilde{u}_\theta}{\partial\mu} + \\ \Big\{\epsilon(\lambda^2 - m^2\alpha^2) - \frac{m(\lambda + 2m\alpha^2)}{(\lambda^2 - m^2\alpha^2)} - \frac{\epsilon(\lambda + 2m\alpha^2)^2\mu^2}{(\lambda^2 - m^2\alpha^2)} - \frac{m^2}{(1-\mu^2)} \\ - \frac{2\epsilon m(\lambda + 2m\alpha^2)\mu^2}{[(\lambda^2 - m^2\alpha^2)\epsilon(1-\mu^2) - m^2]}\Big\}\tilde{u}_\theta = 0. \end{aligned} \tag{2.64}$$

This is a complicated second order differential equation for the variable $\tilde{u}_\theta$, we solve it numerically or asymptotically in certain limits.

We may also analyse the limit, when ϵ tends to zero. Then, if $\epsilon \ll 1$, the equation (2.64) reduces to

$$(1-\mu^2)\frac{\partial^2 \tilde{u}_\theta}{\partial \mu^2} - 2\mu\frac{\partial \tilde{u}_\theta}{\partial \mu} + \Big\{-\frac{(\lambda + 2m\alpha^2)m}{(\lambda^2 - m^2\alpha^2)} - \frac{m^2}{(1-\mu^2)}\Big\}\tilde{u}_\theta = 0. \tag{2.65}$$

This is the Legendre differential equation, a second-order ordinary differential equation, it occurs in numerous physical problems, specially in situations with axial symmetry (Riley et al., 2006), which can be written

$$(1-\mu^2)\frac{\partial^2 y}{\partial \mu^2} - 2\mu\frac{\partial y}{\partial \mu} + \{n(n+1) - \frac{m^2}{(1-\mu^2)}\}y = 0, \tag{2.66}$$

where the parameter n is a given integer number, in this way our solutions are finite and then physically relevant. The solution is known as the Associated Legendre Polynomials

$$\tilde{u}_\theta = P_n^m(\mu),$$

where m is the azimuthal wave-number, and n is the poloidal wave-number. Therefore the dispersion relation will be

$$n(n+1) = -\frac{(\lambda + 2m\alpha^2)m}{(\lambda^2 - m^2\alpha^2)}. \tag{2.67}$$

We have the following formula, for different values of n

$$n(n+1)\lambda^2 + m\lambda + m^2\alpha^2[2 - n(n+1)] = 0. \tag{2.68}$$

This expression corresponds to the (44) equation in the article Zaqarashvili et al. (2007). Solving the quadratic equation for λ

$$\lambda = \frac{-m - \sqrt{m^2 - 4n(n+1)m^2\alpha^2[2 - n(n+1)]}}{2n(n+1)}, \tag{2.69}$$

and

$$\lambda = \frac{-m + \sqrt{m^2 - 4n(n+1)m^2\alpha^2[2 - n(n+1)]}}{2n(n+1)}, \tag{2.70}$$

where $\lambda = \frac{\omega}{2\Omega_0}$.

These equations correspond to dispersion relation of magnetic Rossby waves. The first

one is referred as fast magnetic Rossby waves and the second one is referred as slow magnetic Rossby waves. For α small these fast waves become the ordinary Rossby waves travelling to the west

$$\lambda = \frac{-m}{n(n+1)}, \tag{2.71}$$

and the frequency of the slow modes is given by

$$\lambda = m\alpha^2[n(n+1) - 2]. \tag{2.72}$$

These results are corresponding to the formulas (47) and (48) in Zaqarashvili et al. (2007). This discussion is concerned about oscillatory solutions that represent a train of waves. Their dispersion relation relates the frequency ω (or λ) to a function $f(k)$ of the wave number k

$$\omega = f(k).$$

In this case the wave numbers are represented by m and n, the azimuthal (longitude) and the poloidal (latitudinal) wave number respectively. From this relation we can deduce the phase speed v_{ph} and the group speed of the waves v_g:

$$v_{ph} = \frac{\omega}{k}, \qquad \text{and} \qquad v_g = \frac{\partial\omega}{\partial k}.$$

The group velocity is the speed in which the energy and information travels (Vallis, 2006). The phase speed and the group speed for the magnetic Rossby modes in the azimuthal direction is:

$$v_{ph} = v_g = \frac{-2\Omega_0 R_0}{n(n+1)}, \qquad \text{Fast magnetic Rossby mode} \tag{2.73}$$

$$v_{ph} = v_g = 2\Omega_0 R_0 \alpha^2[n(n+1) - 2]. \qquad \text{Slow magnetic Rossby mode} \tag{2.74}$$

We note that the group speed and the phase speed are equal for both modes.

2.6.2 Differential Equation for η

From the equation (2.57b)

$$\tilde{u}_\theta = \frac{1}{(\lambda + 2m\alpha^2)\mu}\{\lambda m\eta - (\lambda^2 - m^2\alpha^2)\tilde{u}_\phi\}. \tag{2.75}$$

Differentiating $\tilde{u}_\theta$, we obtain

$$\frac{\partial \tilde{u}_\theta}{\partial \mu} = -\frac{\tilde{u}_\theta}{\mu} + \frac{1}{(\lambda + 2m\alpha^2)\mu}\left[\lambda m \frac{\partial \eta}{\partial \mu} - (\lambda^2 - m^2\alpha^2)\frac{\partial \tilde{u}_\phi}{\partial \mu}\right]. \tag{2.76}$$

Substituting $\frac{\partial \tilde{u}_\theta}{\partial \mu}$ into (2.57c), we have

$$\epsilon\lambda(\lambda + 2m\alpha^2)(1-\mu^2)\mu\eta + (\lambda + 2m\alpha^2)(1-\mu^2)\tilde{u}_\theta - \lambda m(1-\mu^2)\frac{\partial \eta}{\partial \mu}$$
$$+(\lambda^2 - m^2\alpha^2)(1-\mu^2)\frac{\partial \tilde{u}_\phi}{\partial \mu} - m(\lambda + 2m\alpha^2)\mu\tilde{u}_\phi = 0. \tag{2.77}$$

We substitute $\tilde{u}_\theta$ into the last equation

$$-\left[(\lambda^2 - m^2\alpha^2)(1-\mu^2) + m(\lambda + 2m\alpha^2)\mu^2\right]\tilde{u}_\phi + (\lambda^2 - m^2\alpha^2)(1-\mu^2)\mu\frac{\partial \tilde{u}_\phi}{\partial \mu}$$
$$\lambda\left[m + \epsilon(\lambda + 2m\alpha^2)\mu^2\right](1-\mu^2)\eta - \lambda m(1-\mu^2)\mu\frac{\partial \eta}{\partial \mu} = 0. \tag{2.78}$$

On the other hand, we substitute $\tilde{u}_\theta$ into (2.57a) and the result is

$$\lambda m(\lambda^2 - m^2\alpha^2)\eta + \left[(\lambda + 2m\alpha^2)^2\mu^2 - (\lambda^2 - m^2\alpha^2)^2\right]\tilde{u}_\phi$$
$$+\lambda(\lambda + 2m\alpha^2)(1-\mu^2)\mu\frac{\partial \eta}{\partial \mu} = 0. \tag{2.79}$$

From this equation, we can find an expression for $\tilde{u}_\phi$, then

$$\tilde{u}_\phi = \frac{\lambda}{[(\lambda^2 - m^2\alpha^2)^2 - (\lambda + 2m\alpha^2)^2\mu^2]}$$
$$\left[m(\lambda^2 - m^2\alpha^2)\eta + (\lambda + 2m\alpha^2)(1-\mu^2)\mu\frac{\partial \eta}{\partial \mu}\right]. \tag{2.80}$$

Differentiating $\tilde{u}_\phi$ from the last equation, we found an expression for $\frac{\partial \tilde{u}_\phi}{\partial \mu}$

$$\frac{\partial \tilde{u}_\phi}{\partial \mu} = \frac{1}{[(\lambda^2 - m^2\alpha^2)^2 - (\lambda + 2m\alpha^2)^2\mu^2]}$$
$$\Big\{2(\lambda + 2m\alpha^2)\mu\tilde{u}_\phi + [m\lambda(\lambda^2 - m^2\alpha^2) + \lambda(\lambda + 2m\alpha^2)(1 - 3\mu^2)]\frac{\partial \eta}{\partial \mu}$$
$$+\lambda(\lambda + 2m\alpha^2)(1-\mu^2)\mu\frac{\partial^2 \eta}{\partial \mu^2}\Big\}. \tag{2.81}$$

Then, we substitute, $\frac{\partial \tilde{u}_\phi}{\partial \mu}$ into the equation (2.78), rearrange the terms and obtain

$$\Big\{\frac{2(\lambda+2m\alpha^2)^2(\lambda^2-m^2\alpha^2)(1-\mu^2)\mu^2}{[(\lambda^2-m^2\alpha^2)^2-(\lambda+2m\alpha^2)^2\mu^2]}$$

$$-\left[(\lambda^2-m^2\alpha^2)(1-\mu^2)+m(\lambda+2m\alpha^2)\mu^2\right]\Big\}\tilde{u}_\phi$$

$$+\lambda\frac{(\lambda+2m\alpha^2)(\lambda^2-m^2\alpha^2)(1-\mu^2)^2\mu^2}{[(\lambda^2-m^2\alpha^2)^2-(\lambda+2m\alpha^2)^2\mu^2]}\frac{\partial^2\eta}{\partial\mu^2}+\lambda\left[m+\epsilon(\lambda+2m\alpha^2)\mu^2\right](1-\mu^2)\eta$$

$$+\lambda\Big\{-m+(\lambda^2-m^2\alpha^2)\frac{[m(\lambda^2-m^2\alpha^2)+(\lambda+2m\alpha^2)(1-3\mu^2)]}{[(\lambda^2-m^2\alpha^2)^2-(\lambda+2m\alpha^2)^2\mu^2]}\Big\}(1-\mu^2)\mu\frac{\partial\eta}{\partial\mu}=0. \tag{2.82}$$

We obtain the final equation when substitute the expression for $\tilde{u}_\phi$ from equation (2.80) into the equation (2.82)

$$(\lambda^2-m^2\alpha^2)(1-\mu^2)\frac{\partial^2\eta}{\partial\mu^2}+2(\lambda^2-m^2\alpha^2)\left[\frac{(\lambda+2m\alpha^2)^2(1-\mu^2)}{[(\lambda^2-m^2\alpha^2)^2-(\lambda+2m\alpha^2)^2\mu^2]}-1\right]\mu\frac{\partial\eta}{\partial\mu}$$

$$+\Big\{-m(\lambda+2m\alpha^2)-\frac{m^2(\lambda^2-m^2\alpha^2)}{(1-\mu^2)}+\epsilon[(\lambda^2-m^2\alpha^2)^2-(\lambda+2m\alpha^2)^2\mu^2]$$

$$+\frac{2m(\lambda+2m\alpha^2)(\lambda^2-m^2\alpha^2)^2}{[(\lambda^2-m^2\alpha^2)^2-(\lambda+2m\alpha^2)^2\mu^2]}\Big\}\eta=0. \tag{2.83}$$

This equation could be written in the form

$$(1-\mu^2)\frac{\partial^2\eta}{\partial\mu^2}+2\Big\{\frac{(\lambda+2m\alpha^2)^2(1-\mu^2)}{[(\lambda^2-m^2\alpha^2)^2-(\lambda+2m\alpha^2)^2\mu^2]}-1\Big\}\mu\frac{\partial\eta}{\partial\mu}$$

$$+\Big\{\frac{-m(\lambda+2m\alpha^2)}{(\lambda^2-m^2\alpha^2)}-\frac{m^2}{(1-\mu^2)}+\frac{\epsilon}{(\lambda^2-m^2\alpha^2)}[(\lambda^2-m^2\alpha^2)^2-(\lambda+2m\alpha^2)^2\mu^2]$$

$$+\frac{2m(\lambda+2m\alpha^2)(\lambda^2-m^2\alpha^2)}{[(\lambda^2-m^2\alpha^2)^2-(\lambda+2m\alpha^2)^2\mu^2]}\Big\}\eta=0. \tag{2.84}$$

This is a complicated second order differential equation for the variable η, we will need it for solving analytically in some special cases.

In summary, in this chapter we developed the numerical method for solving the MHD shallow water system and the ordinary differential equation formulation that will be important to find asymptotic solutions.

Chapter 3

Hydrodynamic Shallow Water System

3.1 Solving the System of Equations for the Non-magnetic Case

In the absence of magnetic field, $B_0 = 0$, the set of five equations (2.26a)- (2.26e) reduces to three equations, known as Laplace tidal equations, which have been solved by Longuet-Higgins (1968). The following chapter of this thesis moves on to describe in detail the solutions of the shallow water system. A summary of the derivation of Longuet-Higgins (1968), for the dispersion relation for different kind of waves is presented here. In the last section, we will present our numerical calculations and compare with Longuet-Higgins results.

Let us now consider the Laplace tidal equations

$$\frac{\partial u_\theta}{\partial t} - 2\Omega_0 \cos\theta u_\phi + \frac{g}{R_o}\frac{\partial h}{\partial \theta} = 0, \tag{3.1a}$$

$$\frac{\partial u_\phi}{\partial t} + 2\Omega_0 \cos\theta u_\theta + \frac{g}{R_o \sin\theta}\frac{\partial h}{\partial \phi} = 0, \tag{3.1b}$$

$$\frac{\partial h}{\partial t} + \frac{H_0}{R_o \sin\theta}\frac{\partial(\sin\theta u_\theta)}{\partial \theta} + \frac{H_0}{R_o \sin\theta}\frac{\partial u_\phi}{\partial \phi} = 0. \tag{3.1c}$$

For this problem, Longuet-Higgins (1968) has found two regimes: large and small $\epsilon = 4\Omega_0^2 R_0^2/gH_0$ and the behaviour of the oscillations changes depending on this parameter. In general, there are three types of waves: gravity waves, Rossby or planetary waves and Kelvin waves.

3.1.1 Case for Small Values of ϵ

First Class Waves: Gravity Waves

This kind of waves is produced by the action of gravity as the restoring force in the system. They are common in stably stratified layers of fluid, they can propagate in the vertical or horizontal direction (Gill, 1982), and either eastward or westward in this case. Gravity waves propagate as pressure gradients and horizontal divergence, caused by the gravitational field, (Hines, 1972), see figure 3.1. If the fluid moves from the position in blue to the position in red, this oscillation produces a positive change in pressure.

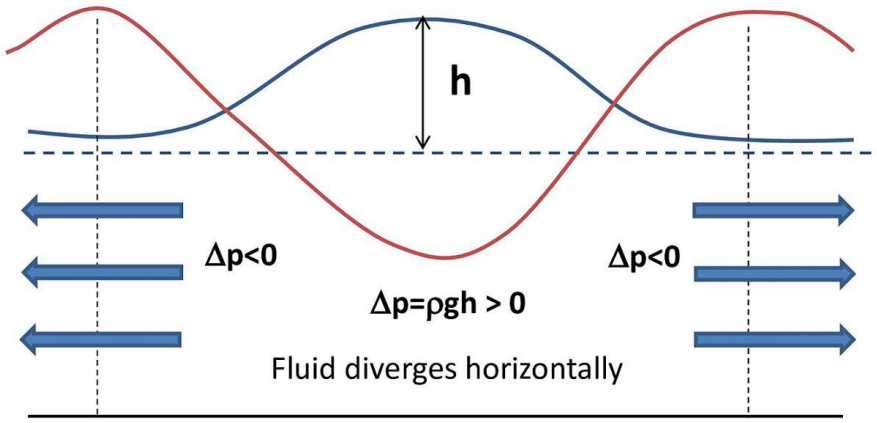

Figure 3.1: Gravity waves in a fluid are produced by the gravity force as restoring force and propagate as pressure gradients and horizontal divergences.

Beginning with the equation (2.84) for the magnetic parameter $\alpha = 0$, we will derive the

dispersion relation and the eigenfunction for the height of fluid in gravity waves

$$(1-\mu^2)\frac{\partial^2\eta}{\partial\mu^2}+2\left[\frac{(1-\mu^2)}{(\lambda^2-\mu^2)}-1\right]\mu\frac{\partial\eta}{\partial\mu}+\left[\epsilon(\lambda^2-\mu^2)-\frac{m^2}{(1-\mu^2)}+\frac{m(\lambda^2+\mu^2)}{\lambda(\lambda^2-\mu^2)}\right]\eta=0. \tag{3.2}$$

The numerical evidence shows that the gravity waves correspond to the highest frequency oscillation. Then, we consider in this part the case when the frequency is high $\lambda^2 \gg 1$ and $\epsilon \ll 1$, hence, the factors $(\lambda^2+\mu^2)$ and $(\lambda^2-\mu^2)$ reduce to $\sim \lambda^2$. For the first order derivative of this differential equation, we neglect terms of order $\mathcal{O}(\lambda^{-2})$ and for the factor proportional to η only the terms of order $\mathcal{O}(\lambda^2)$ will be taken into account. As a result of this simplification the expression reduces to the Legendre Differential Equation

$$(1-\mu^2)\frac{\partial^2\eta}{\partial\mu^2}-2\mu\frac{\partial\eta}{\partial\mu}+\lambda^2\epsilon\eta=0. \tag{3.3}$$

The solution for this differential equation is $\eta = P_n(\cos\theta)$, and $\lambda^2\epsilon = n(n+1)$, where n is an integer, $n = 1, 2, 3, ...$

Consequently, the dispersion relation will be

$$\lambda=\pm\sqrt{\frac{n(n+1)}{\epsilon}} \qquad \text{and so} \qquad \omega=\pm\frac{\sqrt{n(n+1)gH_0}}{R_0}. \tag{3.4}$$

These waves are also called First class waves and correspond to the formulas (4.4) and (4.5) in the article of Longuet-Higgins (1968), and their dispersion relation is plotted in the figure 3.2. This reflects that when ϵ is small, the frequency is large and decreases when the rotation parameter increases.

Interestingly, $u_\theta \sim 1/\lambda$ and $u_\phi \sim 1/\lambda$, so when λ is large the amplitude of η is larger compared to the amplitude of the velocities. Then, the potential energy is the major contribution to the mechanical energy, because the amplitude of η is the highest.

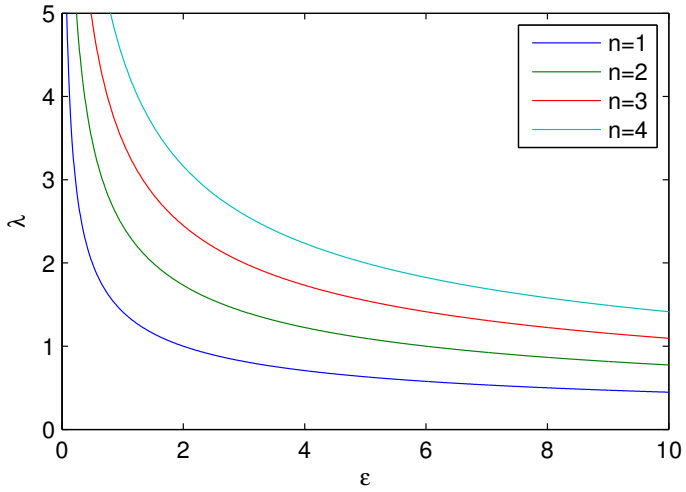

Figure 3.2: Dispersion relation for gravity waves.

We will find First class waves or gravity waves for small values of ϵ numerically in section 4.1 where λ^2 is proportional to $1/\epsilon$ and the eigenfunctions are the Legendre Polynomials.

Second Class Waves: Rossby Waves

Rossby waves are produced by the effect of the rotation of the system on the fluid (Tritton, 2012). In the Earth, they arise from the latitudinal variation of the Coriolis force $2\vec{\Omega} \times \vec{v}$, and the conservation of the potential vorticity ζ as $\hat{\omega} + f$ with $\hat{\omega}$ as the vorticity of the fluid (Vallis, 2006). In the northern hemisphere $f = 2\Omega_0 \sin\Theta$ increases with the latitude $\Theta = 90 - \theta$. If fluid is displaced northward, since f increases, so ω must decrease, see figure 3.3. If fluid is displaced southward, ω has to increase. In this way a westward propagating wave is generated.

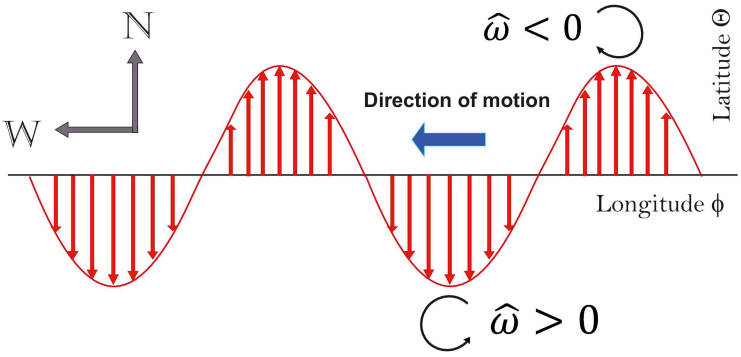

Figure 3.3: Rossby or planetary waves are produced by the conservation of the potential vorticity $\zeta = \hat{\omega} + f$, where $f = 2\Omega_0 \sin\Theta$, the resulting effect is a shift to the west of the fluid.

In this section, we will derive the dispersion relation for Rossby waves. We start from the equations of the shallow water model without magnetic field, multiplying the equation (3.1b) by $\sin\theta$

$$\frac{\partial}{\partial t}(\sin\theta u_\phi) + 2\Omega_0 \cos\theta \sin\theta u_\theta + \frac{g}{R_0}\frac{\partial h}{\partial \phi} = 0. \tag{3.5}$$

We differentiate the last equation with respect to θ

$$\frac{\partial}{\partial t}\frac{\partial}{\partial \theta}(\sin\theta u_\phi) + \frac{\partial}{\partial \theta}[2\Omega_0 \cos\theta \sin\theta u_\theta] + \frac{g}{R_0}\frac{\partial^2 h}{\partial\phi\partial\theta} = 0. \tag{3.6}$$

Rearranging this equation, we obtain

$$\frac{\partial}{\partial t}\frac{\partial}{\partial \theta}(\sin\theta u_\phi) + 2\Omega_0 \cos\theta \frac{\partial}{\partial\theta}[\sin\theta u_\theta] - 2\Omega_0 \sin^2\theta \quad u_\theta + \frac{g}{R_0}\frac{\partial^2 h}{\partial\phi\partial\theta} = 0. \tag{3.7}$$

Differentiating the equation (3.1a) with respect to ϕ

$$\frac{\partial}{\partial t}\frac{\partial u_\theta}{\partial \phi} - 2\Omega_0 \cos\theta \frac{\partial u_\phi}{\partial\phi} + \frac{g}{R_0}\frac{\partial^2 h}{\partial\theta\partial\phi} = 0. \tag{3.8}$$

We subtract the equations (3.7) and (3.8), the result being

$$\frac{\partial}{\partial t}\left[\frac{\partial}{\partial\theta}(\sin\theta u_\phi)-\frac{\partial u_\theta}{\partial\phi}\right]+2\Omega_0\cos\theta\left[\frac{\partial}{\partial\theta}[\sin\theta u_\theta]+\frac{\partial u_\phi}{\partial\phi}\right]-2\Omega_0\sin^2\theta u_\theta=0. \quad (3.9)$$

Taking the equation (3.1c) and rearranging it, the formula is

$$\frac{R_0\sin\theta}{H_0}\frac{\partial h}{\partial t}+\frac{\partial}{\partial\theta}(\sin\theta u_\theta)+\frac{\partial u_\phi}{\partial\phi}=0. \quad (3.10)$$

The parameter $\epsilon = 4\Omega_0^2R_0^2/gH_0$ and the variable $\eta = gh/2\Omega_0R_0$ will be introduced in the above equation

$$\frac{\epsilon}{2\Omega_0}\frac{\partial\eta}{\partial t}+\frac{\partial}{\partial\theta}(\sin\theta u_\theta)+\frac{\partial u_\phi}{\partial\phi}=0. \quad (3.11)$$

We study the limit case when ϵ tends to zero, we can say that ϵ is small, and the equation (3.11) becomes

$$\frac{\partial}{\partial\theta}(\sin\theta u_\theta)+\frac{\partial u_\phi}{\partial\phi}=0. \quad (3.12)$$

Returning to the equation (3.9) and using the result (3.12), the second term of (3.9) is zero

$$\frac{\partial}{\partial t}\left[\frac{\partial}{\partial\theta}(\sin\theta u_\phi)-\frac{\partial u_\theta}{\partial\phi}\right]-2\Omega_0\sin^2\theta u_\theta=0. \quad (3.13)$$

The stream function Ψ, related to the trajectories of the particles, is defined by

$$\mathbf{u}=\nabla\times\left(\Psi(\theta,\phi,t)\mathbf{e}_r\right).$$

The components of the velocity can be written as

$$u_\theta=\frac{1}{R_0\sin\theta}\frac{\partial\Psi}{\partial\phi}\qquad\text{and}\qquad u_\phi=-\frac{1}{R_0}\frac{\partial\Psi}{\partial\theta}.$$

Hence, if Ψ does not have radial dependence

$$\frac{1}{R_0\sin\theta}\left[\frac{\partial}{\partial\theta}(\sin\theta u_\phi)-\frac{\partial u_\theta}{\partial\phi}\right]=-\frac{1}{R_0^2\sin\theta}\frac{\partial}{\partial\theta}\left(\sin\theta\frac{\partial\Psi}{\partial\theta}\right)-\frac{1}{R_0^2\sin^2\theta}\frac{\partial^2\Psi}{\partial\phi^2}=-\nabla^2\Psi.$$

Dividing the equation (3.13) by $R_0\sin\theta$

$$\frac{\partial}{\partial t}\frac{1}{R_0\sin\theta}\left[\frac{\partial}{\partial\theta}(\sin\theta u_\phi)-\frac{\partial u_\theta}{\partial\phi}\right]-\frac{2\Omega_0}{R_0}\sin\theta u_\theta=0. \quad (3.14)$$

We change the variable of the above equation to Ψ giving

$$-\frac{\partial}{\partial t}\nabla^2\Psi - \frac{2\Omega_0}{R_0^2}\frac{\partial\Psi}{\partial\phi} = 0. \tag{3.15}$$

This equation has solutions of the form $\Psi = P_n^m(\cos\theta)e^{i(m\phi-\omega t)}$, where P_n^m are the associated Legendre polynomials. Therefore, when we substitute in the equation (3.15), the result is

$$\omega\nabla^2\Psi - \frac{2\Omega_0 m}{R_0^2}\Psi = 0. \tag{3.16}$$

We applied the properties of the associated Legendre differential equation to evaluate this derivative: $\nabla^2\Psi = -n(n+1)/R_0^2\Psi$. The dispersion relation of these waves is

$$\omega = -\frac{2\Omega_0 m}{n(n+1)}. \tag{3.17}$$

These are called Rossby waves and from the minus sign of the equation it is clear that the waves travel to the west, this is due to the vorticity which induces westward motion.With respect to the dependence with ϵ, it shows that the frequency does not depend on ϵ.

$$\lambda = -\frac{m}{n(n+1)}. \tag{3.18}$$

In this derivation, we have found an expression for the dispersion relation of Rossby waves for small values of ϵ, these formulas correspond to the expresion (4.8) and (4.9) in the article of Longuet-Higgins (1968).

3.1.2 Case of large Values of ϵ

Type 1 and Type 2

Starting from the ordinary differential equation (2.64) for the equations of MHD shallow water system, a complicated second order differential equation for the variable $\tilde{u}_\theta$, we will solve it in asymptotic form.

In this case, when $\alpha = 0$ the equation (2.64) becomes

$$(1-\mu^2)\frac{\partial^2\tilde{u}_\theta}{\partial\mu^2} + \frac{2m^2}{[\lambda^2\epsilon(1-\mu^2)-m^2]}\mu\frac{\partial\tilde{u}_\theta}{\partial\mu}$$
$$-\Big\{\frac{m}{\lambda}+\epsilon\mu^2-\frac{1}{(1-\mu^2)}[\lambda^2\epsilon(1-\mu^2)-m^2]+\frac{2\epsilon m\lambda\mu^2}{[\lambda^2\epsilon(1-\mu^2)-m^2]}\Big\}\tilde{u}_\theta = 0. \quad (3.19)$$

We will take the limit case when ϵ is large, then, the factor $[\lambda^2\epsilon(1-\mu^2)-m^2]$ can be approximated to $\approx \lambda^2\epsilon(1-\mu^2)$

$$(1-\mu^2)\frac{\partial^2\tilde{u}_\theta}{\partial\mu^2} + \frac{2m^2}{\lambda^2\epsilon(1-\mu^2)}\mu\frac{\partial\tilde{u}_\theta}{\partial\mu} - \Big\{\frac{m}{\lambda}+\epsilon\mu^2-\lambda^2\epsilon+\frac{2m\mu^2}{\lambda(1-\mu^2)}\Big\}\tilde{u}_\theta = 0. \quad (3.20)$$

We confined the solution to the neighbourhood of the equator (Longuet-Higgins, 1968), taking the limit $\mu^2 \ll 1$, then $1-\mu^2 \approx 1$, therefore the equation is determined by

$$\frac{\partial^2\tilde{u}_\theta}{\partial\mu^2} + \frac{2m^2}{\lambda^2\epsilon}\mu\frac{\partial\tilde{u}_\theta}{\partial\mu} - \Big\{\frac{m}{\lambda}+\epsilon\mu^2-\lambda^2\epsilon+\frac{2m\mu^2}{\lambda}\Big\}\tilde{u}_\theta = 0. \quad (3.21)$$

Analysing the last term in the equation (3.21), if ϵ is large but λ is small and its order is $\lambda \sim \mathrm{O}\big(\epsilon^{-1/4}\big)$, then $\epsilon\lambda^4$ is order one, $\mathrm{O}\big(1\big)$. From this result, $\lambda^2 \sim \mathrm{O}\big(\epsilon^{-1/2}\big)$. Therefore, $\epsilon\lambda^2 \sim \mathrm{O}\big(\epsilon^{1/2}\big) \gg 1$, in addition, $1/\lambda \sim \mathrm{O}\big(\epsilon^{1/4}\big)$. With this consideration, the term $\frac{m}{\lambda}$ is order $\sim \mathrm{O}\big(\epsilon^{1/4}\big)$, the next $\epsilon\mu^2$ goes $\sim \mathrm{O}\big(\epsilon\big)$, the term $\epsilon\lambda^2$ is $\sim \mathrm{O}\big(\epsilon^{1/2}\big)$ and the last term $\frac{2m\mu^2}{\lambda} \sim \mu^2\epsilon^{1/4}$. This term is the smallest in the equation and it can be neglected, since $\mu^2 \ll 1$. Hence, we have

$$\frac{\partial^2\tilde{u}_\theta}{\partial\mu^2} + \Big\{-\frac{m}{\lambda}+\lambda^2\epsilon-\epsilon\mu^2\Big\}\tilde{u}_\theta = 0. \quad (3.22)$$

We introduce a change of variable

$$\xi = \epsilon^{\frac{1}{4}}\mu \qquad \text{and} \qquad A = -\frac{m}{\lambda}+\lambda^2\epsilon,$$

after these substitutions, the equation (3.22) becomes

$$\frac{\partial^2\tilde{u}_\theta}{\partial\xi^2} + \Big\{\frac{A}{\epsilon^{1/2}}-\xi^2\Big\}\tilde{u}_\theta = 0. \quad (3.23)$$

This Differential Equation is called Weber's equation and the solutions are parabolic cylinder functions. Let

$$A = \epsilon^{1/2}(2\nu + 1) \qquad \nu = 0, 1, 2, ... \tag{3.24}$$

The differential equation becomes

$$\frac{\partial^2 \tilde{u}_\theta}{\partial \xi^2} + \{(2\nu + 1) - \xi^2\}\tilde{u}_\theta = 0, \tag{3.25}$$

whose solutions are in the form

$$\tilde{u}_\theta = Ce^{-\frac{1}{2}\xi^2} H_\nu(\xi) = Ce^{-\frac{1}{2}\epsilon^{1/2}\mu^2} H_\nu(\epsilon^{1/4}\mu),$$

where C is a constant and $H_\nu(\xi)$ is the Hermite polynomial of order ν. The first solutions are plotted in the figure 3.4 for two different values of ϵ. We note that as ϵ increases the waves become confined to the equator. As a result of the equation (3.24), the dispersion

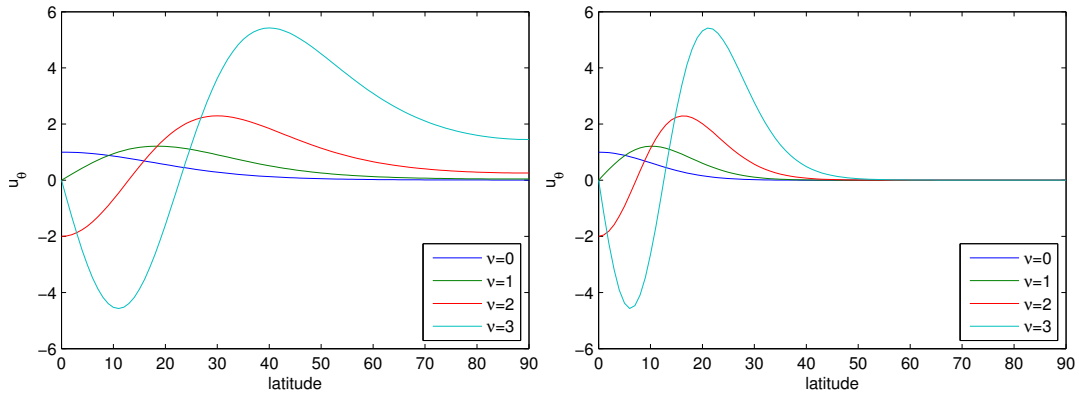

Figure 3.4: Solutions for the velocity $\tilde{u_\theta}$ for $\nu = 0, 1, 2, 3$ .The first panel shows the solutions for $\epsilon = 100$, the second panel for $\epsilon = 1000$.

relation of the waves is

$$\epsilon\lambda^2 - \frac{m}{\lambda} = \epsilon^{1/2}(2\nu + 1). \tag{3.26}$$

This is a cubic equation for λ

$$\lambda^3 - \frac{(2\nu + 1)}{\epsilon^{1/2}}\lambda - \frac{m}{\epsilon} = 0. \tag{3.27}$$

We will find an approximate solution. For the first approximation we neglect the term m/ϵ, then, equation (3.27) becomes

$$\lambda^2 - \frac{(2\nu+1)}{\epsilon^{1/2}} = 0, \qquad \text{and} \qquad \lambda = 0. \tag{3.28}$$

The solution for the first equation is

$$\lambda = \pm\frac{(2\nu+1)^{1/2}}{\epsilon^{1/4}}. \tag{3.29}$$

We add more terms to this approximation

$$\lambda = \pm\frac{(2\nu+1)^{1/2}}{\epsilon^{1/4}} + \delta. \tag{3.30}$$

Substituting this approximation into the equation (3.27), hence

$$\left[\pm\frac{(2\nu+1)^{1/2}}{\epsilon^{1/4}} + \delta\right]^3 - \frac{(2\nu+1)}{\epsilon^{1/2}}\left[\pm\frac{(2\nu+1)^{1/2}}{\epsilon^{1/4}} + \delta\right] - \frac{m}{\epsilon} = 0, \tag{3.31}$$

in order to find an expression for δ, we neglect terms with order δ^2 and superior and obtain

$$\delta = \frac{m}{\epsilon^{1/2}(4\nu+2)}. \tag{3.32}$$

The first two solutions are approximated by

$$\lambda = \pm\frac{(2\nu+1)^{1/2}}{\epsilon^{1/4}} + \frac{m}{\epsilon^{1/2}(4\nu+2)}. \tag{3.33}$$

They are called Type 1 waves and the equation (3.33) is the formula (8.9) in the article of Longuet-Higgins (1968), and correspond to gravity waves travelling eastward and westward. The third solution is approximated by the equation

$$\delta^3 - \frac{(2\nu+1)}{\epsilon^{1/2}}\delta - \frac{m}{\epsilon} = 0. \tag{3.34}$$

We neglect the term with δ^3

$$\delta = -\frac{m}{\epsilon^{1/2}(2\nu+1)}. \tag{3.35}$$

Therefore, the solution will be

$$\lambda = -\frac{m}{\epsilon^{1/2}(2\nu+1)}. \tag{3.36}$$

These solutions are called Type 2 waves and are plotted in the figure 3.5, and describe the Rossby waves travelling to the west, when the parameter ϵ is large. The formula (8.33) of (Longuet-Higgins, 1968) is our (3.36). The theory for waves trapped at the equator was developed by Longuet-Higgins (1968) in section 8.

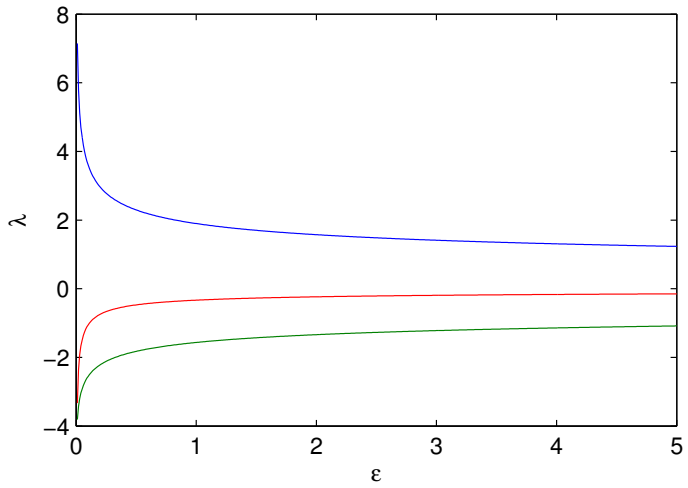

Figure 3.5: Dispersion relation for $\nu = 1$ and $m = 1$. The blue and green lines correspond to the positive and negative values, equation (3.33), (Gravity waves travelling eastward and westward), the red line is related to the equation (3.36) for Rossby waves travelling to the west.

The equatorial trapping of the waves is shown by the results of this method. When the parameter ϵ is large the waves become concentrated at the equator, because of the factor $e^{-\frac{1}{2}\epsilon^{1/2}\mu^2}$ in the solutions, so when ϵ is large the equatorial trapping increases.
The solutions for ϵ small for a given n (poloidal wavenumber) are associated with the large ϵ theory waves with ν wavenumber, in this form

$$\nu = n - m + 1, \qquad \text{Westward propagating gravity waves,}$$

$$\nu = n - m - 1, \qquad \text{Eastward propagating gravity waves.}$$

As shown in the article of Longuet-Higgins (1968), the numerical results show which solutions in the low ϵ limit match with large ϵ waves. The number of nodes of a solution

for ϵ small is expected to be the same than the corresponding solution in the case for ϵ large, but this is not always true, especially if ϵ is very large.

Although, for waves travelling to the east, the mode $n - m = 0$ always corresponds to the Kelvin mode in the large ϵ theory. Rossby modes are related by $\nu = n - m$. However there is a **mixed Rossby-gravity** wave travelling westward which for large ϵ corresponds to the $\nu = 0$ gravity wave in the formula (3.33) with the minus sign.

Type 3: Kelvin waves

A Kelvin wave is a kind of non-dispersive gravity wave where the Coriolis force balances against a topographic boundary (Gill, 1982). In this case the equator acts a wave guide. We will start the analysis from the equations (3.1a), (3.1b) and (3.1c) and derive the dispersion relation for the Kelvin waves. As a result of the existence of a boundary, we set the velocity $u_\theta = 0$. This assumption can lead to the next set of equations

$$2\Omega_0 \cos\theta u_\phi = \frac{g}{R_0}\frac{\partial h}{\partial \theta}, \tag{3.37}$$

$$\frac{\partial u_\phi}{\partial t} = -\frac{g}{R_0 \sin\theta}\frac{\partial h}{\partial \phi}, \tag{3.38}$$

$$\frac{\partial h}{\partial t} + \frac{H_0}{R_0 \sin\theta}\frac{\partial u_\phi}{\partial \phi} = 0. \tag{3.39}$$

We perform a Fourier analysis in the form $e^{i(m\phi - \omega t)}$. Hence the equations (3.38) and (3.39) change to

$$\omega u_\phi = \frac{gm}{R_0 \sin\theta} h, \tag{3.40}$$

$$\omega h = \frac{mH_0}{R_0 \sin\theta} u_\phi. \tag{3.41}$$

We deduce from the equation (3.41) that $u_\phi = \frac{gm}{\omega R_0} h$ and substitute it into the equation (3.40), obtain a result for the frequency

$$\omega = \pm\frac{\sqrt{gH_0}m}{R_0}, \qquad \text{or} \qquad \lambda = \pm\frac{m}{\sqrt{\epsilon}}. \tag{3.42}$$

The negative value of λ must be discarded, in order to have finite solutions. The colatitude θ is related to the latitude through this expression: $\Theta = \pi/2 - \theta$. We consider latitudes near the equator, then Θ the latitude is small, near zero. Therefore, the quantity $\cos\theta = \sin\Theta$, can be approximated by $\sim \Theta$, also $\sin\theta = \cos\Theta \sim 1$. Making these approximations in the equations (3.37) and (3.41) and substituting $u_\phi = \frac{\sqrt{g}}{\sqrt{H_0}}h$ into (3.37) we obtain

$$\frac{\partial h}{\partial \Theta} = -\frac{2\Omega_0 R_0}{gH_0}\Theta h. \tag{3.43}$$

In terms of the parameter ϵ and the latitude Θ, the equation for the height becomes

$$\frac{\partial h}{\partial \Theta} = -\sqrt{\epsilon}\Theta h, \tag{3.44}$$

The solution for this differential equation is

$$h = h_0 e^{-\sqrt{\epsilon}\frac{\Theta^2}{2}}, \tag{3.45}$$

where h_0 is a constant. The solution gives equatorially trapped waves depending on the value of ϵ and a balance between the buoyancy and the Coriolis force in the north-south direction is produced.

3.2 Our numerical results

In the complete range of values of ϵ, we can reproduce the plots of Longuet-Higgins (1968), for λ against ϵ with the numerical method developed in section 2.4. These results are shown in the figure 3.6, the left panel shows some gravity modes travelling to the east, the mode $n - m = 0$ is the Kelvin mode for large values of ϵ. The right panel presents westward propagating waves, the modes in the upper part are gravity waves , the green line is the **mixed Rossby-gravity mode** and the lower modes are the Rossby waves.

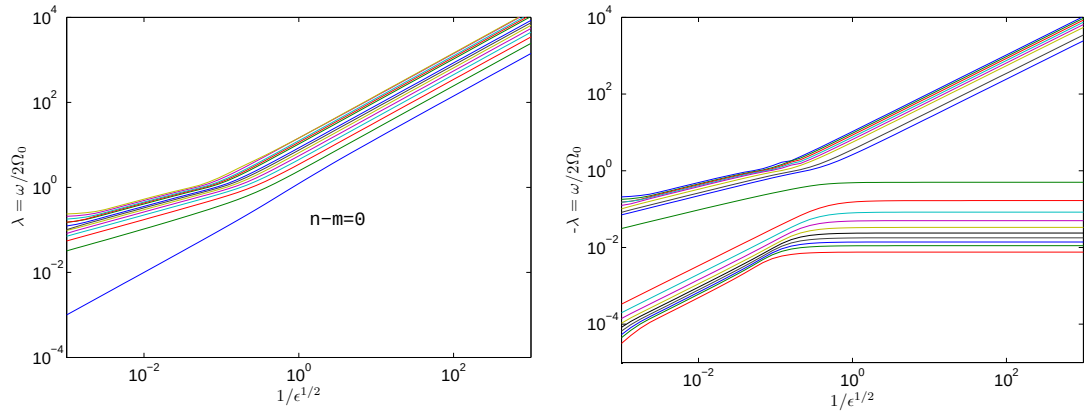

Figure 3.6: Plot for λ against ϵ, $m = 1$ and $\alpha^2 = 0$. Modes travelling eastward at the left side, the mode $n - m = 0$ is the Kelvin wave. At the right the waves propagate westward.

Our numerical results are summarized in the tables 3.1 and 3.2. Negative frequencies correspond to waves propagating westward (table 3.1), especially the first Rossby mode, while positive frequencies correspond to modes propagating eastward (table 3.2), this example is the first gravity wave for $n = 1$. Our expansions are truncated at $n = N$. Since the expansions should ideally extend to infinity, we expect that more accurate results will be obtained with larger N.

Table 3.1: Comparison between the eigenvalues obtained and the results of Longuet-Higgins, for $m = 1$ and westward modes. First Rossby mode, taking $N = 10$, $N = 40$ and $N = 85$ with $\alpha^2 = 0$

ϵ	λ_{LH}	λ_{10}	λ_{40}	λ_{85}
0.0886	-0.498896	-0.4989	-0.4989	-0.4989
0.1254	-0.498440	-0.4984	-0.4984	-0.4984
0.1776	-0.497795	-0.4978	-0.4979	-0.4980
0.2516	-0.496885	-0.4969	-0.4969	-0.4969
0.3567	-0.495602	-0.4956	-0.4956	-0.4956
0.5063	-0.493793	-0.4938	-0.4938	-0.4938
0.7197	-0.491248	-0.4912	-0.4912	-0.4912
1.0253	-0.487679	-0.4877	-0.4877	-0.4877
1.4649	-0.482695	-0.4827	-0.4827	-0.4827
2.1018	-0.475784	-0.4758	-0.4758	-0.4758
3.0328	-0.466312	-0.4663	-0.4663	-0.4663
4.4094	-0.453575	-0.4536	-0.4536	-0.4536
6.4730	-0.436961	-0.4370	-0.4370	0.4370
9.6096	-0.416252	-0.4163	-0.4163	-0.4163
14.4326	-0.391949	-0.3919	-0.3919	-0.3919
21.9011	-0.365279	-0.3653	-0.3653	-0.3653
33.5008	-0.337715	-0.3377	-0.3377	-0.3377
51.5424	-0.310424	-0.3104	-0.3104	-0.3104
79.6418	-0.284115	-0.2841	-0.2841	-0.2841
123.4763	-0.259159	-0.2592	-0.2592	-0.2592
191.9701	-0.235739	-0.2357	-0.2357	-0.2357
299.1591	-0.213933	-0.2139	-0.2139	-0.2139
467.1419	-0.193752	-0.1938	-0.1938	-0.1938
730.7396	-0.175165	-0.1752	-0.1752	-0.1752
1144.9	-0.158115	-0.1581	-0.1581	-0.1581
1796.1	-0.142529	-0.1425	-0.1425	-0.1425

Table 3.2: Comparison between the eigenvalues obtained and the results of Longuet-Higgins, for $m = 1$ and eastward modes. First gravity mode, taking $N = 10$, $N = 30$ and $N = 85$ with $\alpha^2 = 0$

ϵ	λ_{LH}	λ_{10}	λ_{30}	λ_{85}
9.87×10^{-4}	44.7582	44.7673	44.767	44.7673
0.0020	31.5047	31.3761	31.37	31.3761
0.0040	22.1341	22.1154	22.115	22.1154
0.0081	15.5096	15.4702	15.47	15.4702
0.0163	10.8274	10.8365	10.836	10.8365
0.0332	7.51950	7.5250	7.525	7.5250
0.0682	5.18485	5.1844	5.1844	5.1844
0.1412	3.54036	3.5407	3.5407	3.5407
0.2963	2.38685	2.3866	2.3866	2.3866
0.6310	1.58471	1.5848	1.5848	1.5848
1.3648	1.03619	1.0362	1.0362	1.0362
2.9785	0.671475	0.6715	0.6715	0.6715
6.4724	0.436995	0.4370	0.4370	0.4370
13.8319	0.289186	0.2892	0.2892	0.2892
28.9844	0.195169	0.1952	0.1952	0.1952
59.8086	0.133760	0.1338	0.1338	0.1338
122.1518	0.0926201	0.0926	0.0926	0.0926
247.8092	0.0645658	0.0646	0.0646	0.0646
500.4958	0.0452100	0.0452	0.0452	0.0452
1007.8	0.0317520	0.0318	0.0318	0.0318
2025.2	0.0223460	0.0223	0.0223	0.0223
4063.9	0.0157488	0.0157	0.0157	0.0157
8146.5	0.0111102	0.0111	0.0111	0.0111
16320	0.00784323	0.0077	0.0078	0.0078

Looking at these results, we notice that there is no difference between the $N = 40$ or even $N = 30$ results and the $N = 85$, indicating that a truncation level of $N = 40$ is adequate in all cases. Generally, there is good agreement between our results and those of Longuet-Higgins (1968), but significant differences are seen at large ϵ values. Longuet-Higgins did not report his truncation level, but large ϵ requires larger truncation level and we conjecture that the slight differences between our results and Longuet-Higgins at large ϵ arise because he did not have sufficient resolution in the large ϵ cases.

We compare the Longuet-Higgins (1968) eigenfunctions with our results, we notice that the relation between their variables and ours is $Z = \sqrt{\epsilon}\eta$, $V = \tilde{u}_\theta / \sin\theta$ and $U = \tilde{u}_\phi / \sin\theta$.

In the figure 3.7, the first column corresponds to the Kelvin mode $n - m = 0$, which is trapped at the equator for $\epsilon \geq 100$. The second column corresponds to the first gravity wave and is equatorially trapped when $\epsilon \geq 10$.

These figures 3.8 are gravity waves of higher order, as we increase the value of $n - m$, the number of nodes in latitude increases too.

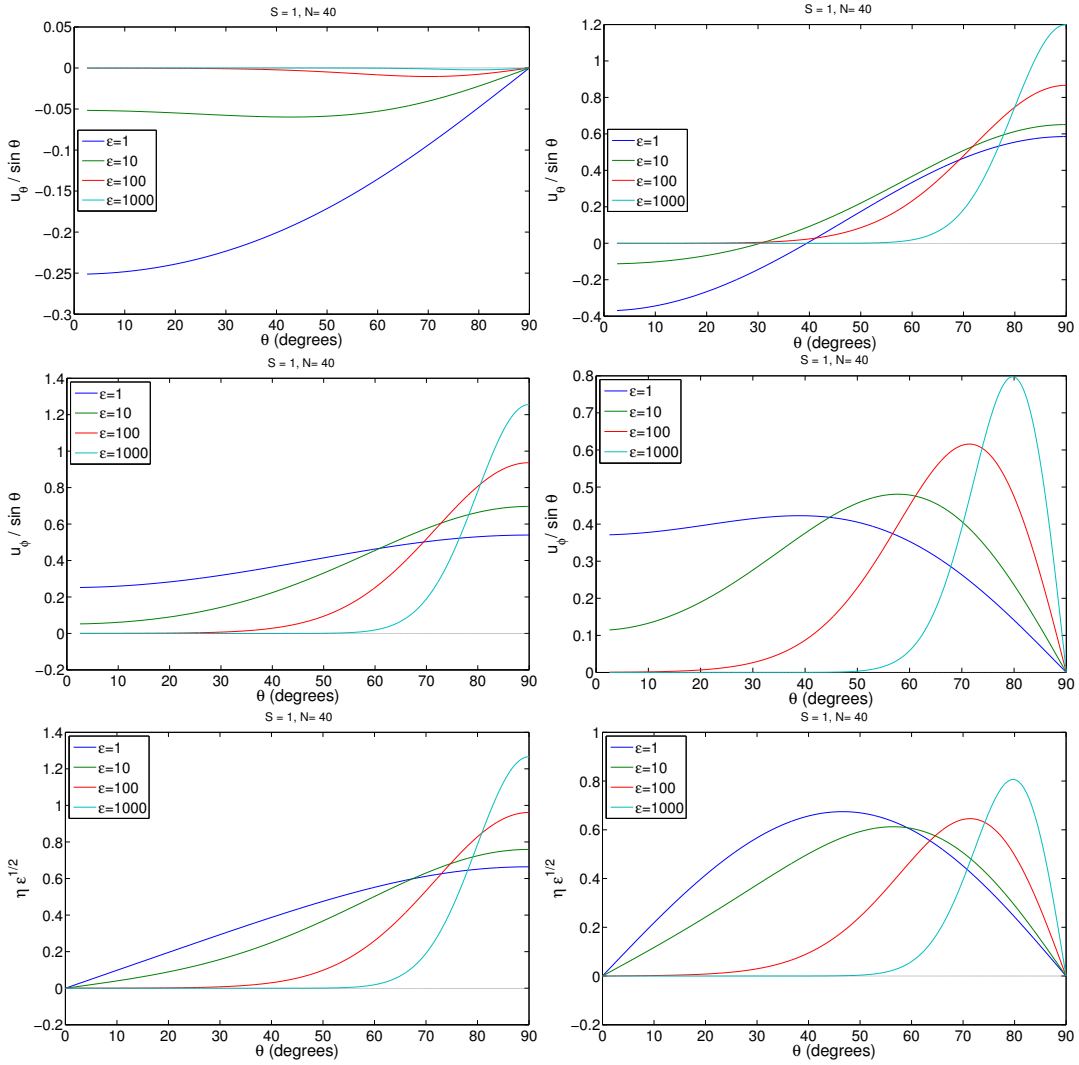

Figure 3.7: Numerical solution for different values of ϵ in eastward modes with $N = 40$, $m = 1$, and $n - m = 0$ for the first column and $n - m = 1$ for the second one.

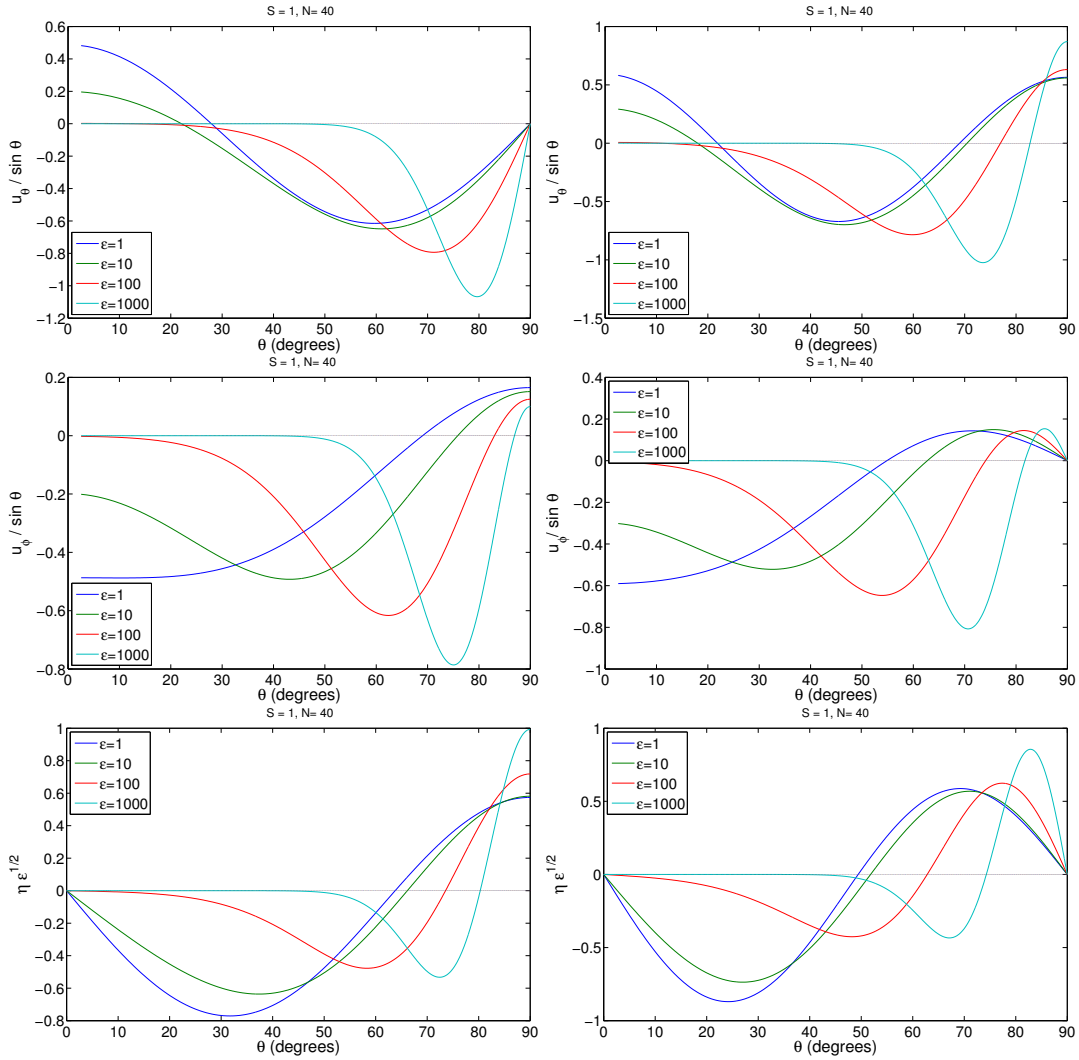

Figure 3.8: Numerical solution for different values of ϵ in eastward modes with $N = 40$, $m = 1$, and $n - m = 2$ for the first column and $n - m = 3$ for the second one.

3.2.1 Modes Travelling Westwards, Class 2, $m = 1$

This figure 3.9 plots the eigenfunctions for Rossby waves, travelling westward. The two first modes $n-m = 0$ and $n-m = 1$ are represented in the left column and right column respectively. It is shown in the pictures that waves are trapped to the Equator when the

rotation parameter increases.

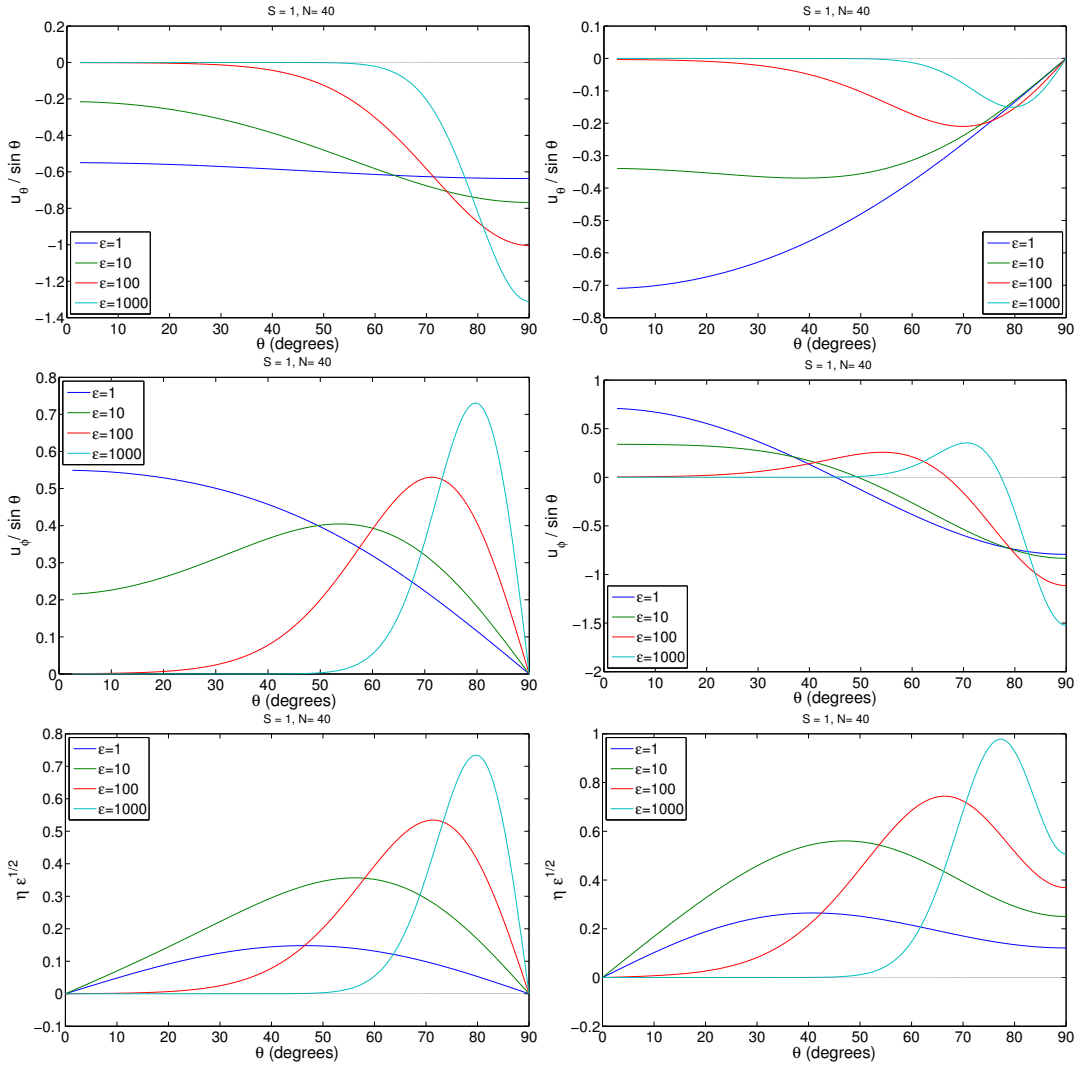

Figure 3.9: Numerical solution for different values of ϵ in westward modes with $N = 40$, $m = 1$, $n - m = 0$ for the first column and $n - m = 1$ for the second one.

Generally, there is good agreement between our numerical results and those of Longuet-Higgins (1968). The figures can be reproduced with fidelity, and the solutions converge when the expansions are truncated at $N = 40$.

Chapter 4

Magnetohydrodynamics: Numerical results

This chapter describes the numerical results for the magnetohydrodynamic system. This problem has been solved by Zaqarashvili et al. (2007) for the limit when ϵ and α are small. The eigenvalue numerical method, developed in section 2.4 is used for identifying and characterising the solutions to the mathematical problem in the all range of ϵ and α in detail. We perform a complete survey of MHD waves in this shallow water system which exceeds previous works.

Moving on now to consider the effect of the toroidal by varying the parameter α. As a result of the presence of the magnetic field, the Rossby waves split in two modes: slow and fast magnetic Rossby waves as shown is section 4.2. Moreover a new anomalous slow mode arises. The gravity waves turn into Magneto Inertial Gravity (MIG) waves, influenced by Coriolis, gravity and Lorentz forces. Furthermore the Kelvin modes are also present, their main features are enhanced by the field and a new Kelvin wave traveling to the west is excited by the field. In addition to the presence of the waves, the magnetic field can drive instabilities, but we will discuss this in detail in chapter 6.

In figure 4.1(a) which shows scaled frequency as a function of $\epsilon^{-1/2}$, the red lines are

two magneto-inertial gravity modes, the green line is the Kelvin mode and the blue ones are the slow magnetic Rossby waves, these waves all travel to the east. The dispersion relation has been modified by a fixed moderate magnetic field ($\alpha = 0.1$). In the next panel, 4.1(b), the red curves are the magneto-inertial gravity waves travelling to the west and the black lines are the fast magnetic Rossby modes.

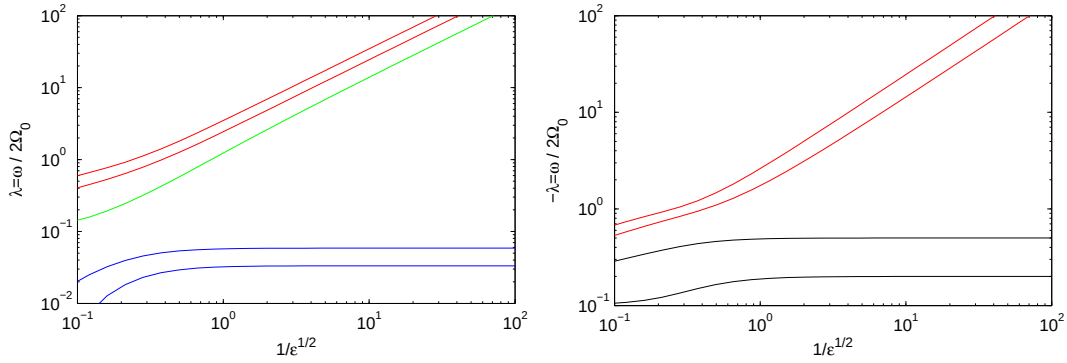

(a) Eastward propagation (b) Westward propagation

Figure 4.1: Dispersion relation λ as a function of $1/\epsilon^{1/2}$, for $\alpha = 0.1$ and $m = 1$. Note that large $1/\epsilon^{1/2}$ corresponds to slow rotation. (a) Eastward propagation: Magneto-inertial gravity modes (red), the Kelvin mode (green) and slow magnetic Rossby waves (blue), (b) Westwards propagation: Magneto-inertial gravity waves in red and the black lines are the fast magnetic Rossby modes.

The magneto-inertial gravity waves have the highest frequencies and their solutions are a sequence of eigenfunctions in which the frequency increases with the number of nodes in latitude, alternating between symmetric and antisymmetric functions with respect to the equator. The perturbation can travel eastward or westward. Note that as $\epsilon^{-1/2}$ is getting large, λ becomes linear with $1/\epsilon^{1/2}$, so $\omega/2\Omega_0 \sim \sqrt{gH_0}/2\Omega_0 R_0$ which means the frequency becomes independent of rotation in this limit as $\Omega_0 \to 0$. This shows that in this limit the waves do become gravity waves, which have a phase speed of $\sqrt{gH_0}$. On the other hand, for the slow magnetic Rossby waves, λ tends to a constant as $\epsilon \to 0$,

showing that $\omega \sim \Omega_0$ for these waves. Similar behaviour is found in figure 4.1(b) for the westward waves.

Figure 4.2 (a) shows the northward velocity for the first three MIG modes, the lowest (symmetric) in blue has two nodes, the next one (antisymmetric) in green has three nodes and the highest (symmetric) in red has four nodes. The Kelvin mode travelling to the east is represented in graph 4.2(b), it has been plotted for $\epsilon = 1$, where this wave has the properties of the first gravity mode. Note that it has only one node and is antisymmetric. The behaviour of the Kelvin wave changes with ϵ; at small ϵ, it has the nature of a gravity wave, but at large ϵ it becomes equatorially trapped and has a velocity which is almost purely azimuthal. This is discussed further in section 4.4 below. These plots were made for $\alpha = 0.1$, $\epsilon = 1$, $m = 1$ and $N = 50$.

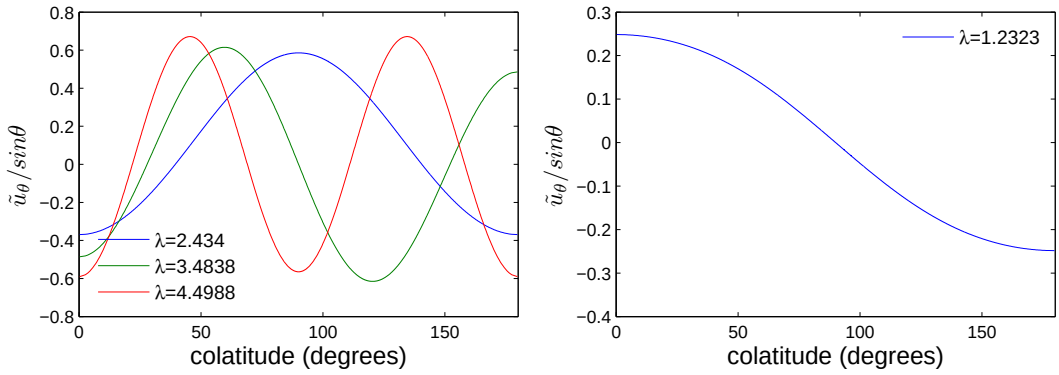

(a) MIG waves (b) Kelvin wave

Figure 4.2: Northward velocity $\tilde{u}_\theta$ for $\alpha = 0.1$, $\epsilon = 1$, $m = 1$ and $N = 50$. (a) Magneto Inertial Gravity Waves travelling eastward, the lowest (symmetric) with two nodes in blue, the next one (antisymmetric) in green with three nodes and the highest (symmetric) in red with 4 nodes. (b) The Kelvin mode travelling eastward, in this regime $\epsilon = 1$, it behaves like the first antisymmetric gravity wave with one node.

Some magnetic Rossby waves are plotted in figure 4.3. In panel (a), the fast mode is travelling to the west, the first symmetric mode is represented in blue and has no nodes,

the next one in green, is an antisymmetric wave with one latitudinal node and the lowest of frequency this example corresponds to a symmetric mode with two nodes. In this case, when the frequency decreases, the number of nodes increases. The lowest frequencies are in panel (b), as slow magnetic Rossby waves travelling to the east, except for the first mode which is anomalous and travels to the west as a symmetric mode. The blue curve has the lowest frequency for an antisymmetric mode with one node, the next highest frequency (green curve) is symmetric mode with two nodes, and the red one is the highest frequency of this sequence, and represents an antisymmetric behaviour and has three nodes. For the slow modes as the frequency increases the number of latitudinal nodes increases too.

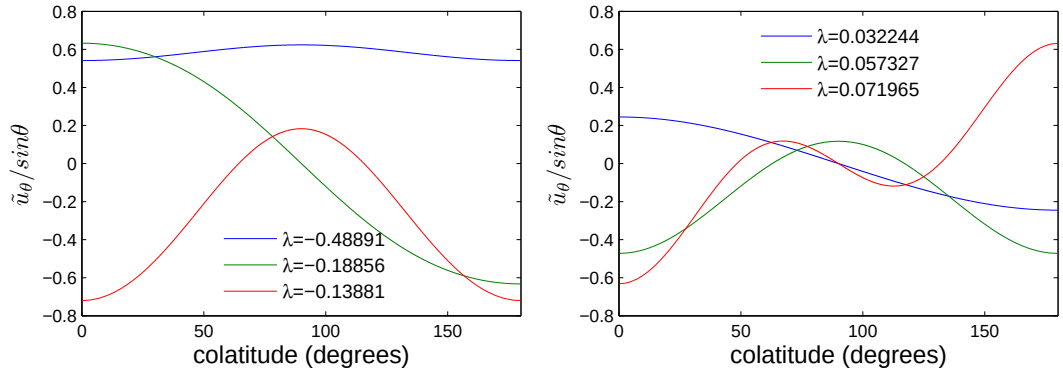

(a) Fast magnetic Rossby waves (b) Slow magnetic Rossby waves

Figure 4.3: Northward velocity $\tilde{u}_\theta$ for $\alpha = 0.1$, $\epsilon = 1$, $m = 1$ and $N = 50$. (a) Fast magnetic Rossby waves travelling westwards, in blue the highest frequency and symmetric without nodes, the green curve represents the following antisymmetric mode with one node and the red curve is the lowest frequency and symmetric wave with two nodes. (b) Slow magnetic Rossby waves travelling eastwards, the blue line corresponds to the first antisymmetric mode with one node, the green curve is the second symmetric mode with two nodes and the red curve is the antisymmetric wave with three nodes and highest frequency.

4.1 Magneto Inertial Gravity Waves

A noted above the highest frequencies correspond to magneto-inertial gravity waves. These waves are essentially Class 1 waves, (Longuet-Higgins, 1968), interfacial gravity waves, modified by the magnetic field. In the limit of a strong magnetic field, large α, the frequency increases and the waves become trapped at the equator as Alfvén waves, quite independent of rotation ϵ as seen in tables 4.1-4.6.

Alfvén waves are magnetic tension oscillations that propagate along magnetic field lines, as waves they transport energy and momentum. These are transversal and non dispersive waves (Gubbins and Herrero-Bervera, 2007).

We choose the modes $n = 1$ and $n = 2$ for $m = 1$ and vary the magnetic parameter α. The results are in tables 4.1 (westward) and 4.2 (eastward) for $n = 1$. Tables 4.3 (eastward) and 4.4 (westward) are for $n = 2$. The mode $n = 3$ for $m = 2$ is shown in table 4.5 (eastward) and 4.6 (westward).

Owing to limited resolution, it is possible that the code cannot calculate the eigenvalues or eigenfunctions with accuracy when some waves undergo equatorial or polar trapping. These sharp and extremely localized functions need a large number of modes in the expansion to be calculated. For this reason, when α or ϵ are large, we write **** in the tables for λ when the value is not certain.

The numerical results for the first MIG mode are summarized in tables 4.1 for the westward wave. When ϵ and α are small, the frequency can be calculated with the hydrodynamic formula (3.4)

$$\lambda = \pm\sqrt{\frac{n(n+1)}{\epsilon}} \qquad \text{and so} \qquad \omega = \pm\frac{\sqrt{n(n+1)gH_0}}{R_0}, \tag{4.1}$$

with $n = 1$, (Longuet-Higgins, 1968). For large ϵ and small α, the frequencies can be computed by the hydrodynamic equation (3.33)

$$\lambda = \pm\frac{(2\nu+1)^{1/2}}{\epsilon^{1/4}} + \frac{m}{\epsilon^{1/2}(4\nu+2)}, \tag{4.2}$$

for $\nu = 1$. For large α, the wave speed tends to the Alfvén speed with frequencies $\lambda = \pm m\alpha$. It is clear that the MIG waves always remain in the superalfvénic regime ($|\lambda| > m\alpha$) and are stable.

Table 4.1: Eigenvalues λ for different values of α and ϵ, Magneto Inertial Gravity Waves travelling westward for $n = 1$, $m = 1$, $N = 80$.

α	10^{-3}	10^{-2}	10^{-1}	1	10^{1}	10^{2}	10^{3}
$\epsilon = 0.01$	-14.400	-14.400	-14.400	-14.398	-16.397	-100.5	****
$\epsilon = 0.1$	-4.7464	-4.7464	-4.7463	-4.7351	-10.501	****	*****
$\epsilon = 1$	-1.7415	-1.7415	-1.7404	-1.6888	-10.050	****	****
$\epsilon = 10$	-0.88188	-0.88185	-0.87935	-1.0516	-10.005	****	****
$\epsilon = 100$	-0.52836	-0.52840	-0.53222	-1.0050	****	****	****

Table 4.2 shows the eigenvalues for waves travelling to the east, comparing with the westward mode. There is no important difference between westward and eastward frequencies, except when α is small. The theory of Longuet-Higgins (1968) establishes that for small ϵ westward and eastward frequencies are equal, see equation 4.1, however there is a difference in our numerical results in favour of westward waves making the frequency slightly larger in magnitude.

In the case of MIG waves travelling eastward for $n = 1$, $m = 1$, this oscillation has been identified as the Kelvin wave for large values of ϵ where the eigenfunctions are equatorially trapped and $\lambda = m\epsilon^{-1/2}$. A more detailed account of Kelvin waves is given in the section 4.4.

Table 4.2: Eigenvalues λ for different values of α and ϵ, Magneto Inertial Gravity Waves travelling eastward for $n = 1$, $m = 1$, $N = 80$.

α	10^{-3}	10^{-2}	10^{-1}	1	10^{1}	10^{2}	10^{3}
$\epsilon = 0.01$	13.9	13.9	13.9	13.9012	15.2263	100.5000	****
$\epsilon = 0.1$	4.2452	4.2452	4.2453	4.2649	10.4999	100.0500	****
$\epsilon = 1$	1.2307	1.2307	1.2323	1.4782	10.0050	****	****
$\epsilon = 10$	0.34457	0.34468	0.35618	1.0496	10.0050	****	****
$\epsilon = 100$	0.10263	0.10309	0.14257	1.005	****	****	****

In general for the westward MIG waves the $n - m + 1$ mode for small ϵ connects to the ν mode in large ϵ theory, see section 3.1.2 and Longuet-Higgins (1968). With regard to eastward propagating waves, the MIG first mode $n - m = 0$, turns into the Kelvin mode, and for the rest of the sequence the mode $n - m - 1$ connects to ν in the large ϵ theory. Table 4.3 summarizes the normalized frequency for $n = 2$ and $m = 1$, for waves travelling eastwards. For small α, the eigenvalue λ can be predicted by the formula (4.1) with $n = 2$, for ϵ small, when ϵ is large the values correspond to the expression (4.2) with $\nu = 0$. For large α, λ tends to $m\alpha$ plus a small variation. This small variation increases for ϵ small.

Table 4.3: Eigenvalues λ for different values of α and ϵ, Magneto Inertial Gravity Waves travelling eastward for $n = 2$, $m = 1$, $N = 80$. Note that **** denotes eigenvalues which could not be computed accurately for numerical reasons.

α	10^{-3}	10^{-2}	10^{-1}	1	10^{1}	10^{2}	10^{3}
$\epsilon = 0.01$	24.419	24.419	24.419	24.434	26.269	117.86	1037.1
$\epsilon = 0.1$	7.6851	7.6851	7.6856	7.7409	14.357	108.09	1018.9
$\epsilon = 1$	2.4316	2.4316	2.434	2.6913	11.839	103.72	****
$\epsilon = 10$	0.8459	0.84601	0.85661	1.5451	10.833	****	****
$\epsilon = 100$	0.37963	0.37989	0.40424	1.2342	10.383	****	****

Figure 4.4 shows the solutions for the velocity field against colatitude: The northward velocity, $\tilde{u}_\theta/\sin\theta$, is plotted in the upper part and the azimuthal velocity, $\tilde{u}_\phi/\sin\theta$ is at the bottom. The first column is for $\alpha = 10^{-3}$, for small ϵ where the eigenfunctions are the Associated Legendre polynomials. When ϵ increases the solutions become confined to the equatorial region. For a strong field ($\alpha = 5$) the eigenfunctions for weak rotation have changed slightly and for strong rotation the equatorial trapping is enhanced. Zaqarashvili et al. (2009) found equatorially trapped waves, considering an antisymmetric basic state field with zero toroidal field at the equator. They established that the variation of the magnetic field across the equator is associated with the trapping rather than the asymptotic nature of the parameters.

The magnetic field perturbation shows the same behaviour as the velocity, for α large and ϵ large: the waves become equatorially trapped. The behaviour of the magnetic field is essentially identical to that of the velocities functions, because the magnetic field perturbation is directly proportional to the velocity, see figure 4.5.

Figure 4.6 is a good illustration of the effect of magnetic field on MIG waves. In the case of $\epsilon = 0.01$ in the upper panels, the solutions correspond to Legendre polynomials and remain similar for α large. Then, when the rotation parameter is increased, the waves

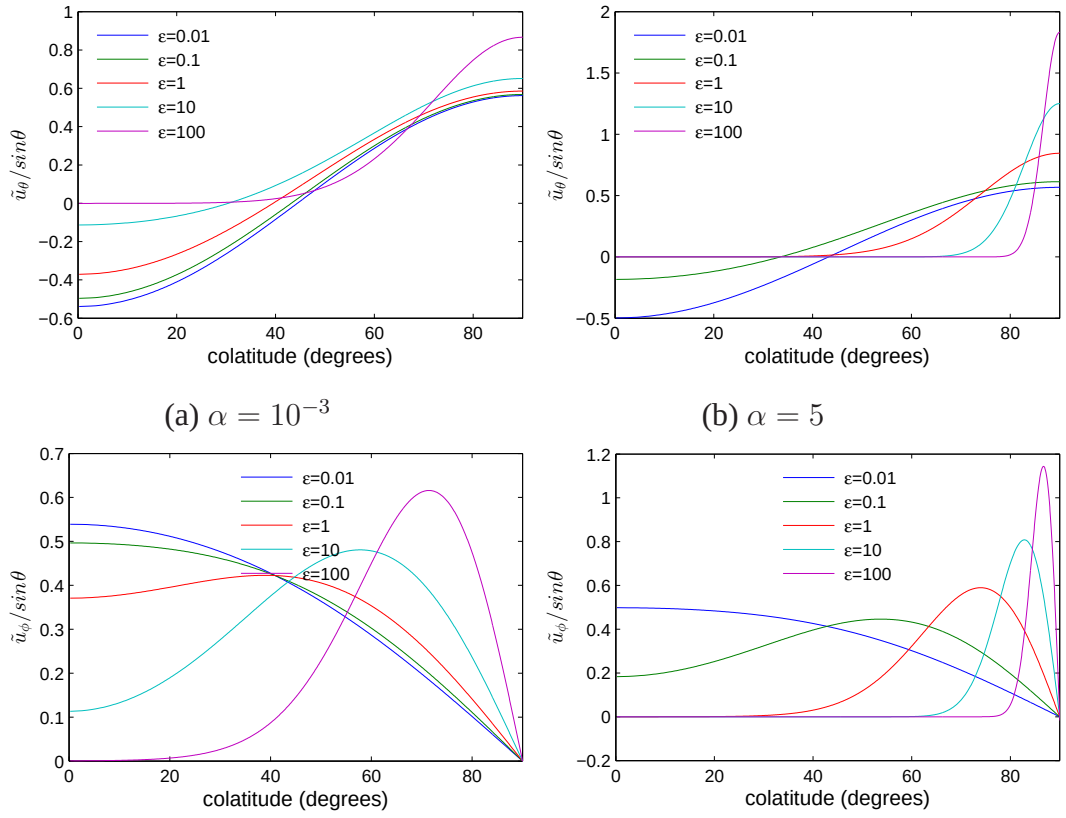

(a) $\alpha = 10^{-3}$ (b) $\alpha = 5$

(c) $\alpha = 10^{-3}$ (d) $\alpha = 5$

Figure 4.4: Numerical solution for the velocity for different values of ϵ in the magneto-inertial gravity wave travelling eastward for the second mode ($n = 2$) with $N = 50$, $m = 1$. The first column corresponds to $\alpha = 10^{-3}$ and $\alpha = 5$ for the second one.

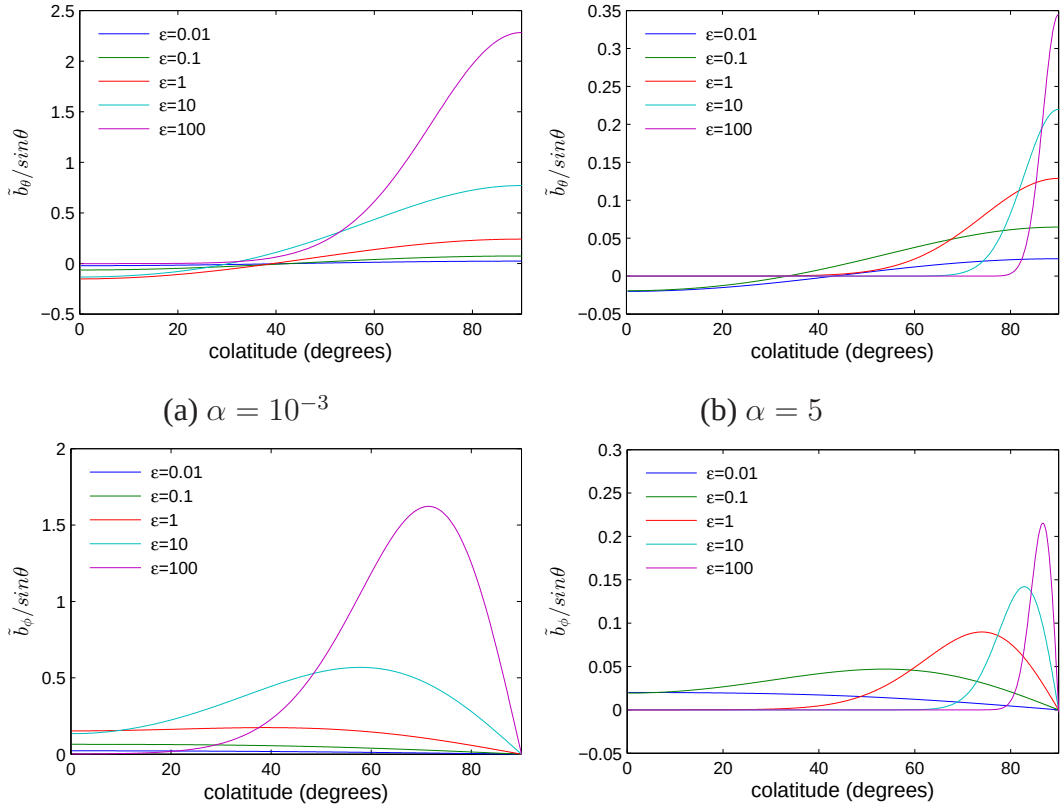

(a) $\alpha = 10^{-3}$ (b) $\alpha = 5$

(c) $\alpha = 10^{-3}$ (d) $\alpha = 5$

Figure 4.5: Numerical solution for the magnetic field perturbation for different values of ϵ in the magneto-inertial gravity wave travelling eastward for the second mode ($n = 2$) with $N = 50$, $m = 1$. The first column corresponds to $\alpha = 10^{-3}$ and $\alpha = 5$ for the second one.

becomes trapped at the equator. It is evident that increasing α produces more equatorial trapping.

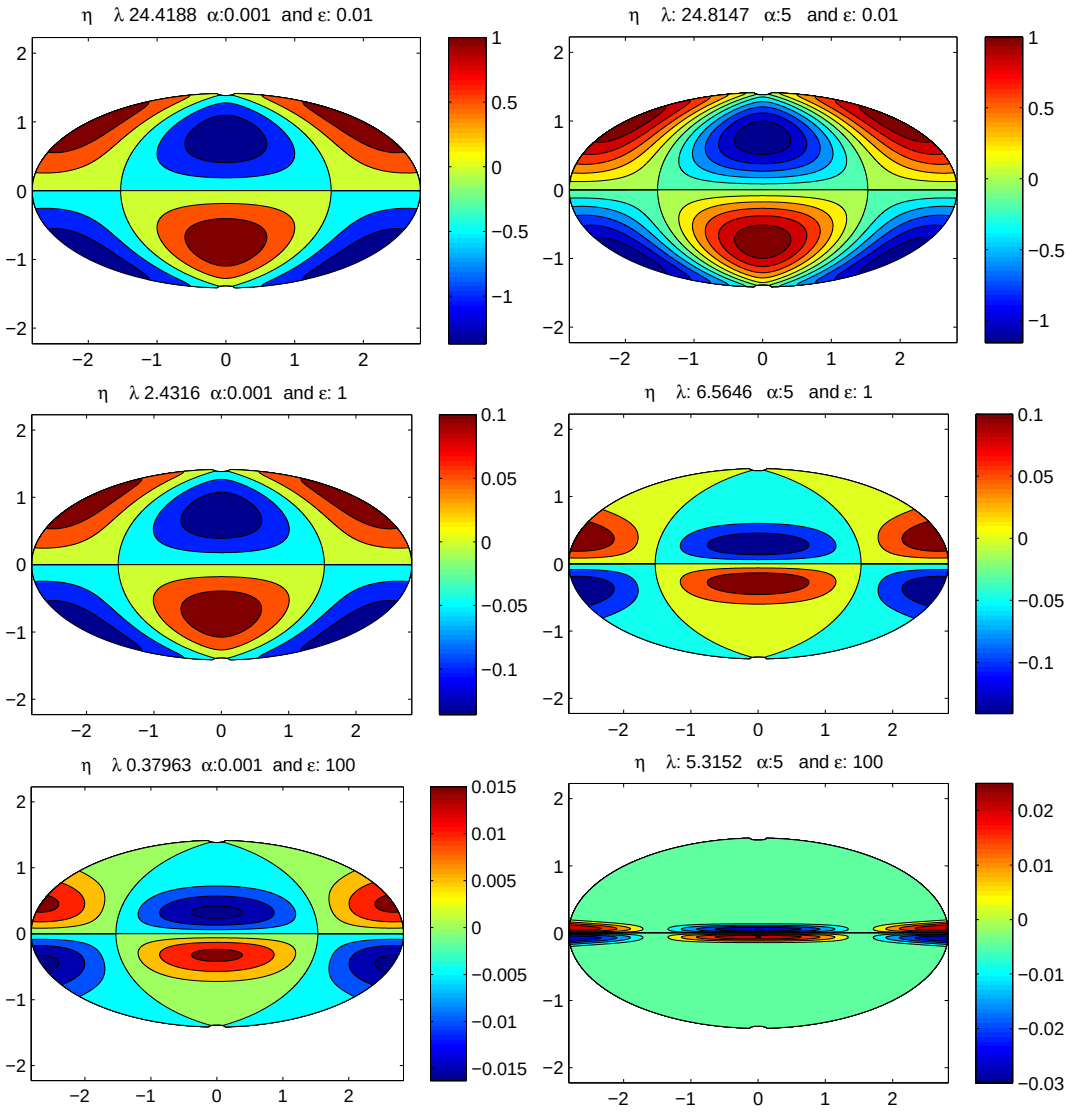

Figure 4.6: Contour plots of the scaled height η, for increasing ϵ (0.01, 1 and 100). Numerical solution for different values of ϵ in the magneto-inertial gravity wave travelling eastward for the second mode and $m = 1$. The first column corresponds to $\alpha = 10^{-3}$ with $N = 50$ and $\alpha = 5$ with $N = 70$ for the second one.

The eigenvalues for the westward propagating MIG wave, $n = 2$ and $m = 1$, are reported in the table 4.4. It is expected that for small values of α, when the field is weak, the frequency can be calculated with the formula (4.1) for $n = 2$ for ϵ small and with the equation (4.2) and $\nu = 2$ for large ϵ.

Table 4.4: Eigenvalues λ for different values of α and ϵ, Magneto Inertial Gravity Waves travelling westward for $n = 2$, $m = 1$, $N = 50$.

α	10^{-3}	10^{-2}	10^{-1}	1	10^{1}	10^{2}	10^{3}
$\epsilon = 0.01$	-24.586	-24.586	-24.586	-24.598	-26.227	-117.74	-1037.1
$\epsilon = 0.1$	-7.8533	-7.8533	-7.8536	-7.8858	-14.102	-108.03	-1018.8
$\epsilon = 1$	-2.6129	-2.6129	-2.6131	-2.6718	-11.719	-103.7	****
$\epsilon = 10$	-1.1119	-1.1118	-1.1088	-1.2956	-10.779	****	****
$\epsilon = 100$	-0.67845	-0.67845	-0.67891	-1.1118	-10.358	****	****

For the mode $n = 2$, eastward and westward eigenfunctions correspond to the same Legendre polynomial: P_2^1, when ϵ is small. However, for large ϵ the eigenfunctions for eastward and westward waves are expected to be different, as it is confirmed in the figure 4.7, because when ϵ is large the westward eigenfunctions evolve toward a $\nu = 2$ mode, unlike the wave propagating eastward which evolves towards the mode $\nu = 1$. For small α values, in the first column, the solutions are the Legendre functions for ϵ small. When the rotation parameter increases the waves become equatorially trapped. When α increases to 5 the wave becomes more trapped at the equator without any difference between west and east modes. It is clear that the magnetic field enhances the equatorial trapping.

As expected, the magnetic field perturbation shows, in figure 4.8, the same behaviour as the velocity. For α large and ϵ large, the waves become equatorially trapped.

Figure 4.9 shows the scaled height of the layer of fluid for waves travelling westward. Here, the equatorial trapping is evident, when ϵ is large and/or α is large. The main

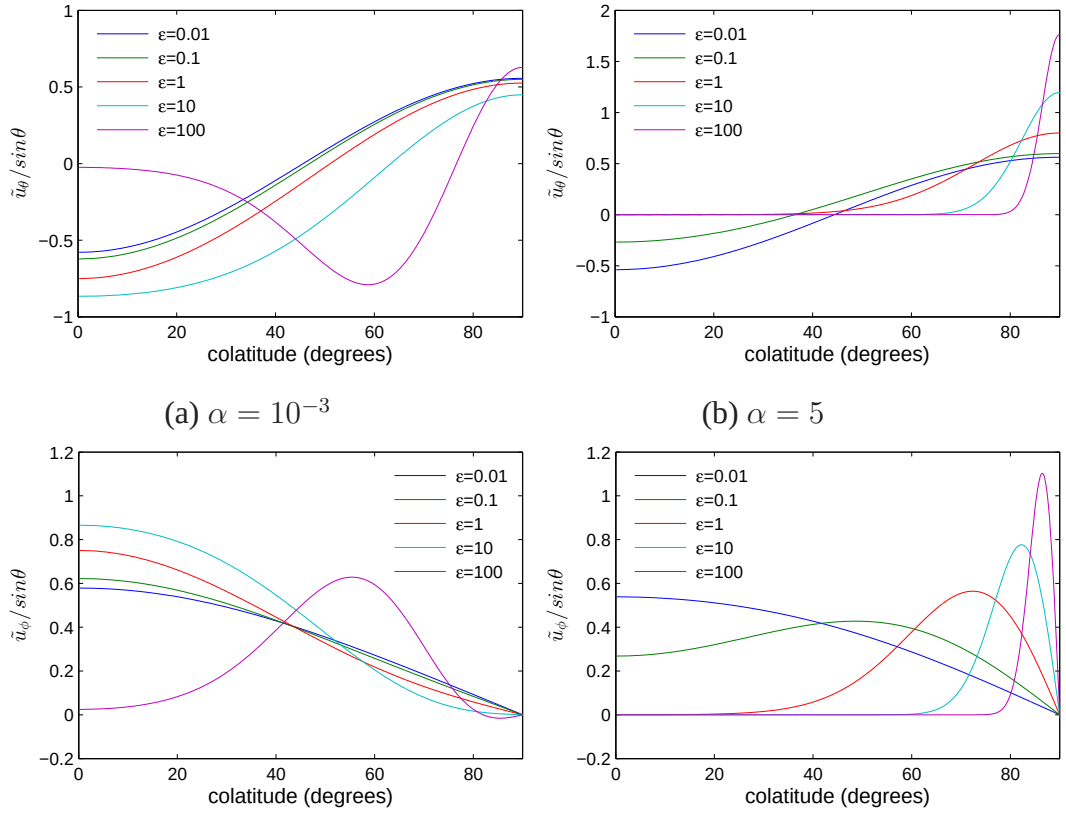

(a) $\alpha = 10^{-3}$ (b) $\alpha = 5$

(c) $\alpha = 10^{-3}$ (d) $\alpha = 5$

Figure 4.7: Numerical solution for the velocity with different values of ϵ in the magneto-inertial gravity waves travelling westward for the second mode $n = 2$ and $m = 1$. The first column corresponds to $\alpha = 10^{-3}$ with $N = 50$ and $\alpha = 5$ with $N = 70$ for the second one.

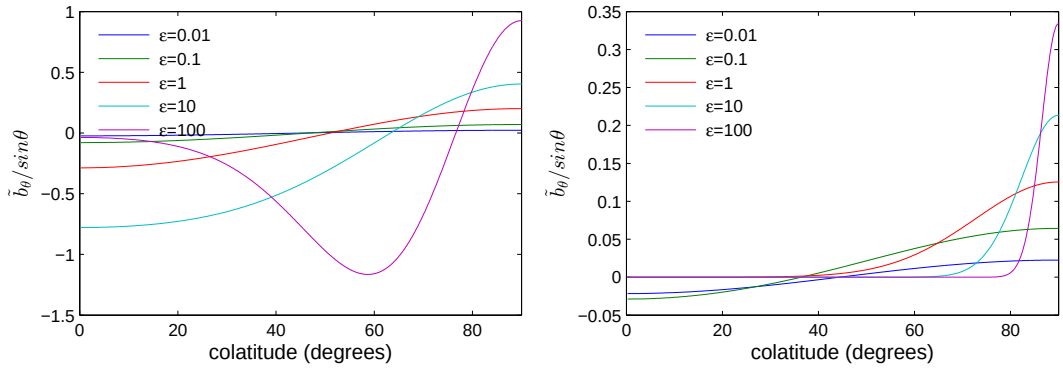

(a) $\alpha = 10^{-3}$ (b) $\alpha = 5$

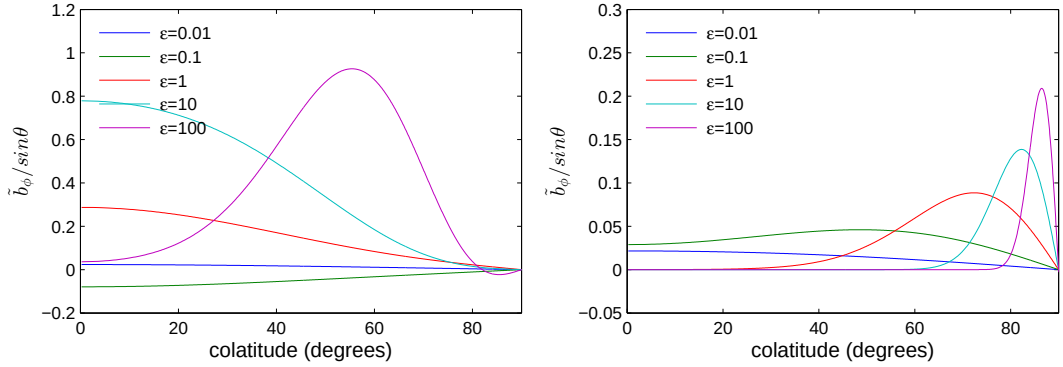

(c) $\alpha = 10^{-3}$ (d) $\alpha = 5$

Figure 4.8: Numerical solution for the magnetic field perturbation for different values of ϵ in the magneto-inertial gravity wave travelling westward for the second mode $n = 2$ with $N = 50$ and $m = 1$. The first column corresponds to $\alpha = 10^{-3}$ and $\alpha = 5$ for the second one.

difference is, as we mention before, that the westward MIG wave in a weak field ($\alpha = 10^{-3}$), turns into a higher mode for strong rotation, as we can see in figure 4.9. In this case, there are more latitudinal nodes.

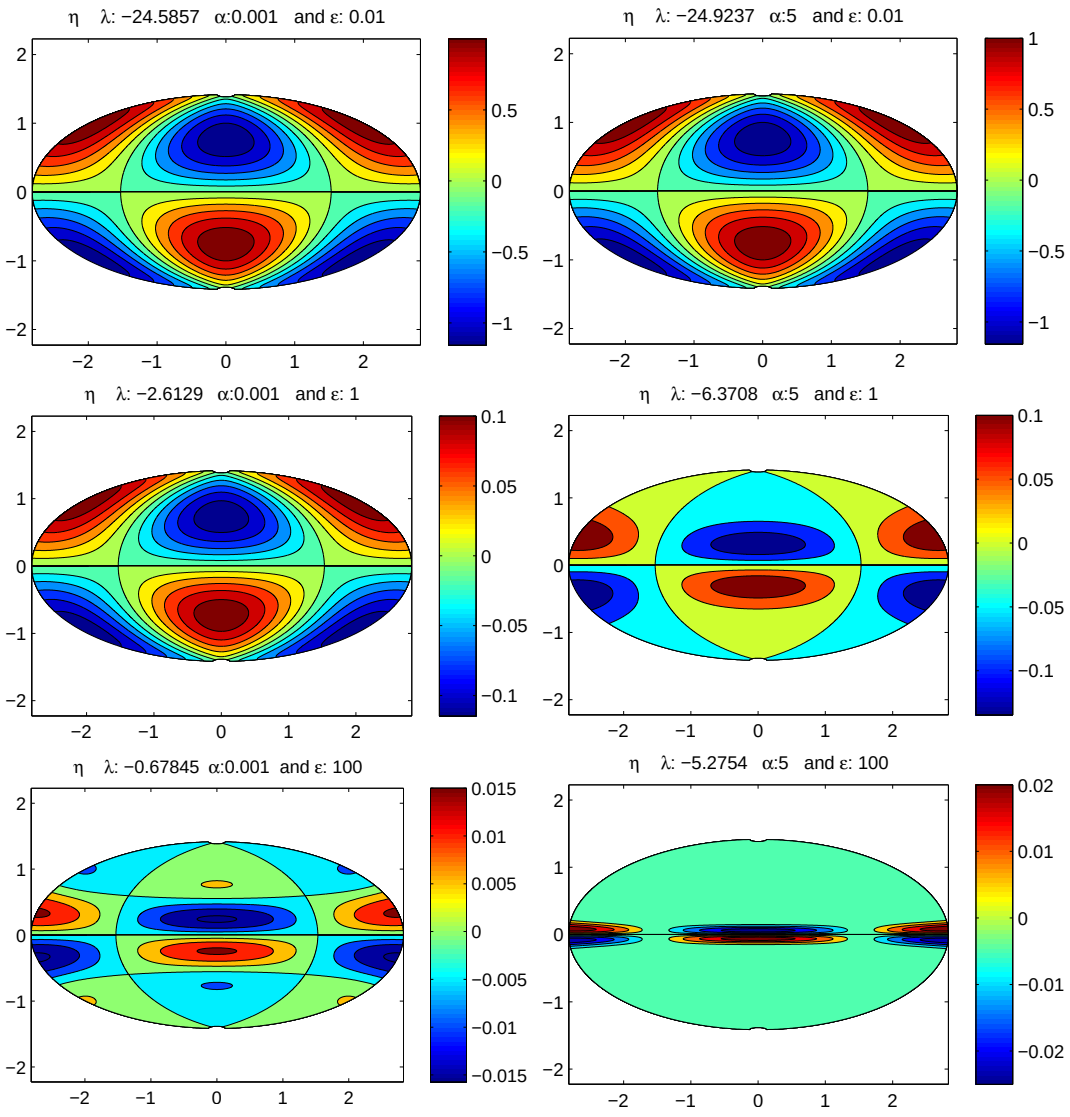

Figure 4.9: Contour plots of the scaled height η for increasing ϵ (0.01, 1 and 100) in the magneto-inertial gravity waves travelling westward for the second mode $n = 2$ and $m = 1$. The first column corresponds to $\alpha = 10^{-3}$ with $N = 50$ and $\alpha = 5$ with $N = 70$ for the second one.

As was pointed out before, the main differences between waves travelling eastward and westward are:

- Small ϵ: the eigenvalues for the westward waves have slightly larger frequencies than the eastward ones. In addition, the solutions for the northward velocity correspond to the Legendre polynomial P_2^1 with different amplitudes. The amplitude of the waves travelling eastward decreases when ϵ increases, for the MIG waves travelling westward the amplitude increases when ϵ increases. This is due to the fact that eastward mode $n-m=1$ has less kinetic energy than westward modes, in this regime. The potential energy has a major contribution for the total energy in the eastward propagating mode, then, when ϵ increases the normalization constant diminishes significantly, reducing the amplitude of the velocity, Longuet-Higgins (1968).

- Large ϵ: the MIG waves travelling westward become an degree larger ($n-m+1$) than its analogous wave travelling eastward ($n-m-1$).

However, when both α and ϵ are large, there is little difference between west and east movements.

Let us now consider one example of $m=2$ MIG waves. In table 4.5 the normalized frequency for the eastward $n=3$ mode is reported. For α small, the values correspond to the formula (4.1) with $n=3$ when ϵ is small, and the large ϵ values correspond to the formula (4.2) with $\nu=0$. For α large the frequency is expected to tend to the Alfvén speed $\lambda=m\alpha$.

Table 4.5: Eigenvalues λ for different values of α and ϵ, $n = 3$, $m = 2$ and $N = 50$ and . Magneto Inertial Gravity Waves: Waves travelling eastward.

α	10^{-3}	10^{-2}	10^{-1}	1	10^{1}	10^{2}	10^{3}
$\epsilon = 0.01$	34.562	34.562	34.563	34.611	39.663	215.92	2030.2
$\epsilon = 0.1$	10.885	10.885	10.887	11.048	24.396	206.78	2017.2
$\epsilon = 1$	3.423	3.423	3.4288	4.0077	21.636	203.03	2015.5
$\epsilon = 10$	1.1224	1.1227	1.1454	2.53	20.697	201.72	2015.3
$\epsilon = 100$	0.44709	0.44778	0.51054	2.2044	20.312	201.55	2015.3

The velocity field illustrated in figure 4.10 shows that the first mode $n = 3$ is symmetric (for $\tilde{u}_\theta$) with respect to the equator. Then, for a weak magnetic field ($\alpha = 10^{-3}$) in the first column the solutions correspond to the Legendre functions, but the large ϵ waves are equatorially trapped, as shown in the purple curves of the left panels for α large.

The magnetic perturbations for the mode $n = 3$ and $m = 2$, illustrated in figure 4.11, show larger amplitudes than the velocity plots and the equatorial trapping is evident for large α and large ϵ.

Figure 4.12, for $n = 3$ mode, shows more longitudinal nodes than the previous results because of the $m = 2$ wave number. Here, the rotation tends to trap the waves at the equator, and the magnetic field enhances the equatorial trapping. For $\alpha = 5$ and $\epsilon = 100$ (lower right panel), the oscillation is hard to resolve numerically, therefore, in order to have more clear graphs , we do not consider values of α greater than 5.

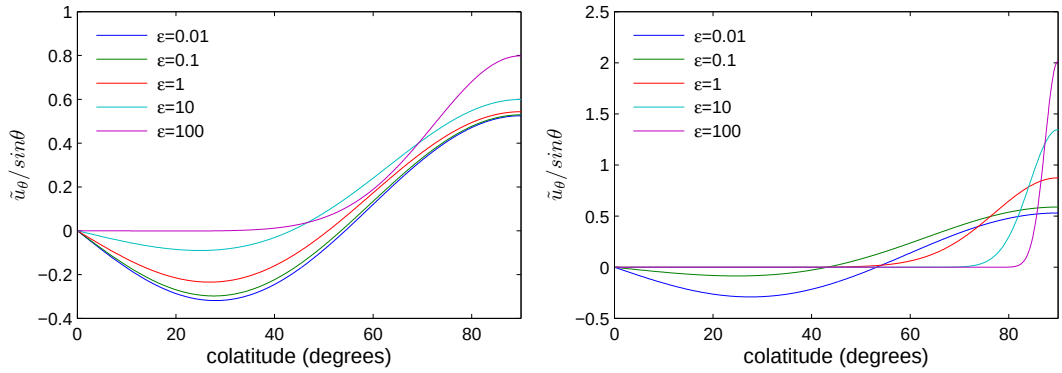

(a) $\alpha = 10^{-3}$ (b) $\alpha = 5$

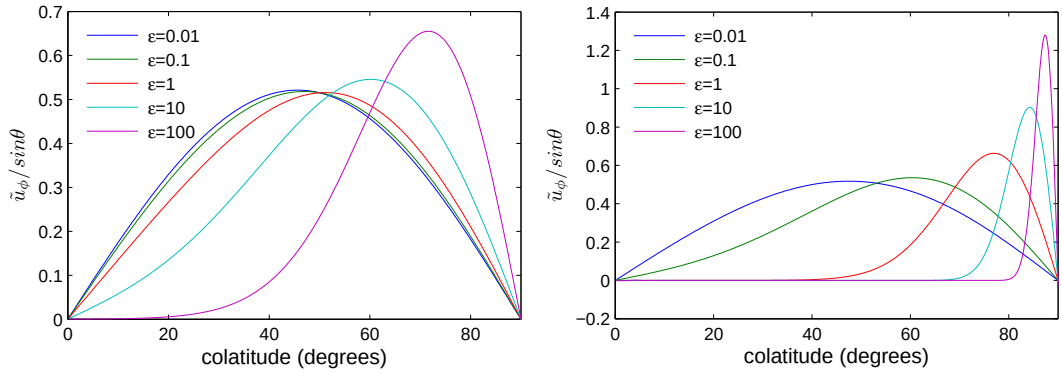

(a) $\alpha = 10^{-3}$ (a) $\alpha = 5$

Figure 4.10: Numerical solution for the velocity for different values of ϵ in the magneto-inertial gravity wave travelling eastward for the first mode $n = 3$, $m = 2$ and $N = 50$. The first column corresponds to $\alpha = 10^{-3}$ and $\alpha = 5$ for the second one.

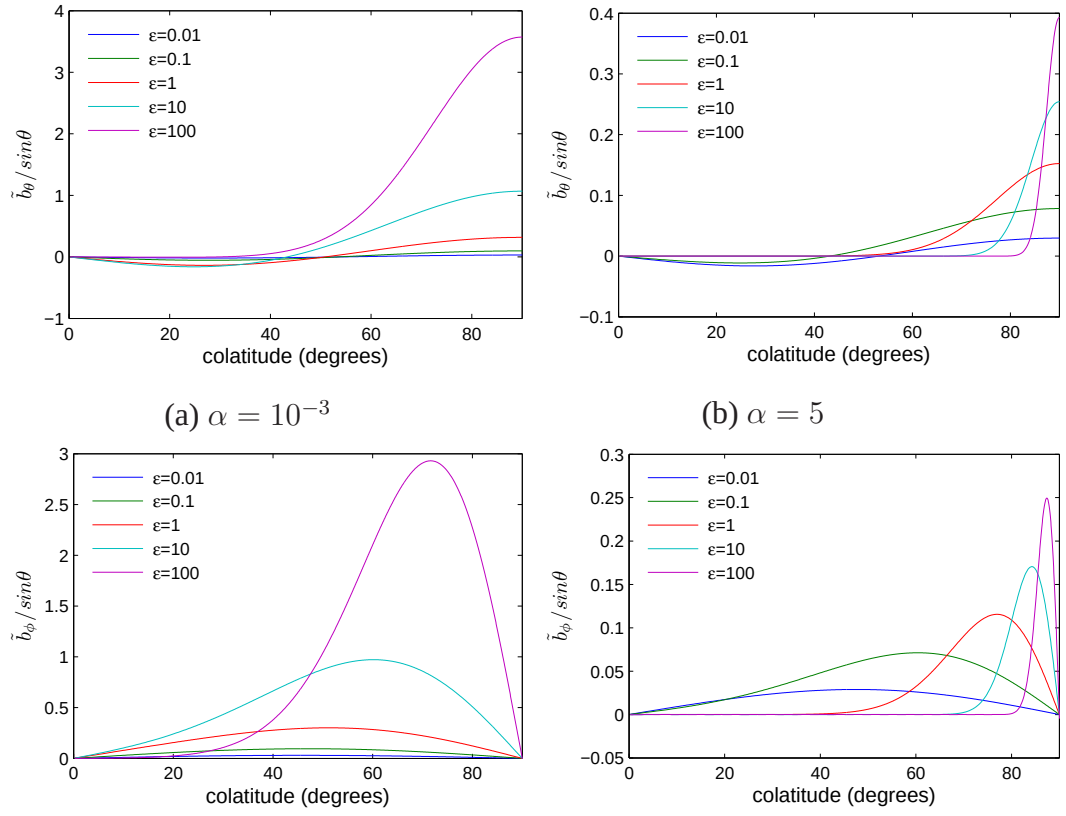

(a) $\alpha = 10^{-3}$ (b) $\alpha = 5$

(c) $\alpha = 10^{-3}$ (d) $\alpha = 5$

Figure 4.11: Numerical solution for the magnetic field perturbation for different values of ϵ in the magneto-inertial gravity wave travelling eastward for the first mode $n = 3$, $m = 2$ and $N = 50$. The first column corresponds to $\alpha = 10^{-3}$ and $\alpha = 5$ for the second one.

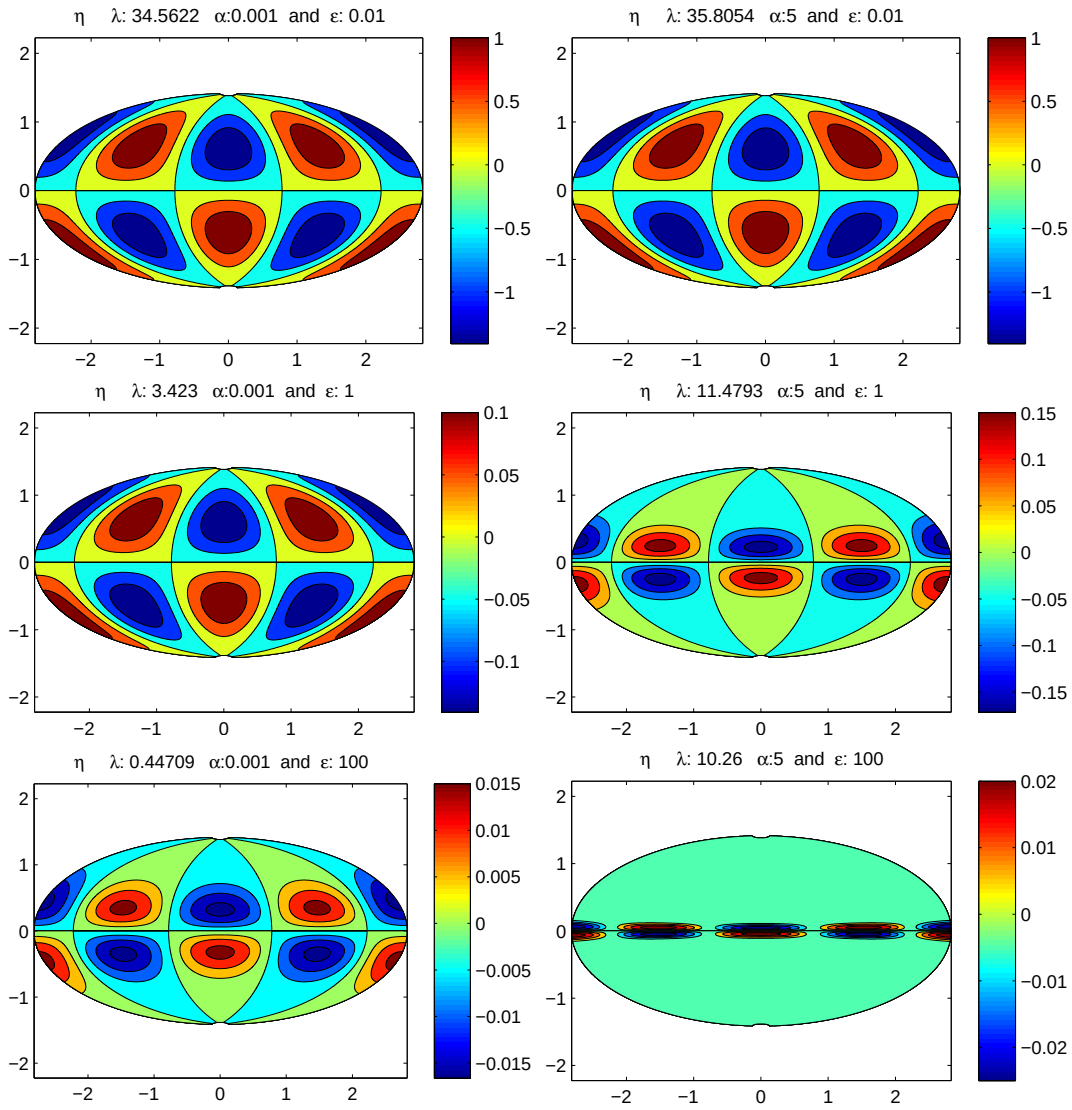

Figure 4.12: Contour plots of the scaled height η for increasing ϵ (0.01, 1 and 100). Numerical solution for different values of ϵ in the magneto-inertial gravity wave travelling eastward for the first mode $n = 3$, $m = 2$ and $N = 50$. The first column corresponds to $\alpha = 10^{-3}$ and $\alpha = 5$ with for the second column.

Regarding the differences between eastward and westward propagating waves, we report the westward MIG wave for $n = 3$, $m = 2$ in the table 4.6. The frequencies for small

α can be computed with the formula (4.1) for $n = 3$ when ϵ is small and equation (4.2) gives the frequencies for large ϵ when $\nu = 2$. As was mentioned earlier, when α is large λ tends to the Alfvén speed, $-m\alpha$, plus a small variation which depends on ϵ.

Table 4.6: Eigenvalues λ for different values of α and ϵ, $n = 3$, $m = 2$ and $N = 50$. Magneto Inertial Gravity waves. Waves travelling westward.

α	10^{-3}	10^{-2}	10^{-1}	1	10^{1}	10^{2}	10^{3}
$\epsilon = 0.01$	-34.729	-34.729	-34.729	-34.776	-39.644	-215.82	-2030.2
$\epsilon = 0.1$	-11.052	-11.052	-11.054	-11.195	-24.183	-206.73	-2017.1
$\epsilon = 1$	-3.5945	-3.5946	-3.5984	-4	-21.537	-203.01	-2015.4
$\epsilon = 10$	-1.3265	-1.3266	-1.3348	-2.319	-20.654	-201.71	-2015.4
$\epsilon = 100$	-0.69022	-0.69045	-0.71298	-2.104	-20.292	-201.54	-2015.3

The velocities $\tilde{u}_\theta$ and $\tilde{u}_\phi$ are plotted in figure 4.13. When ϵ increases the waves move toward the equator, and for large α the equatorial trapping increases. As indicated previously, if α is very large, the field dominates and the eastward and westward motions present no difference and the equatorial trapping is located in a small region of $\sim 15^\circ$ near the equator ($\epsilon = 10$ or 100).

The magnetic field components are plotted in figure 4.14 for the MIG mode $n = 3$, $m = 2$. When α is small the solutions correspond to the Legendre polynomials but if ϵ is large the waves are equatorially trapped. In the large α regime, when ϵ increases the eigenfunctions are shifted towards the equator. In terms of the amplitude of the perturbation, for this mode, the amplitude is higher than the velocity amplitudes.

Figure 4.15 shows more longitudinal nodes, because $m = 2$ in this case, and the equatorial trapping is evident when α or ϵ is large. But in the presence of a strong field, in second column of the figure, the equatorial trapping has been accentuated, particularly for $\alpha = 5$ and $\epsilon = 100$ where the oscillation is confined to a narrow band at the equator.

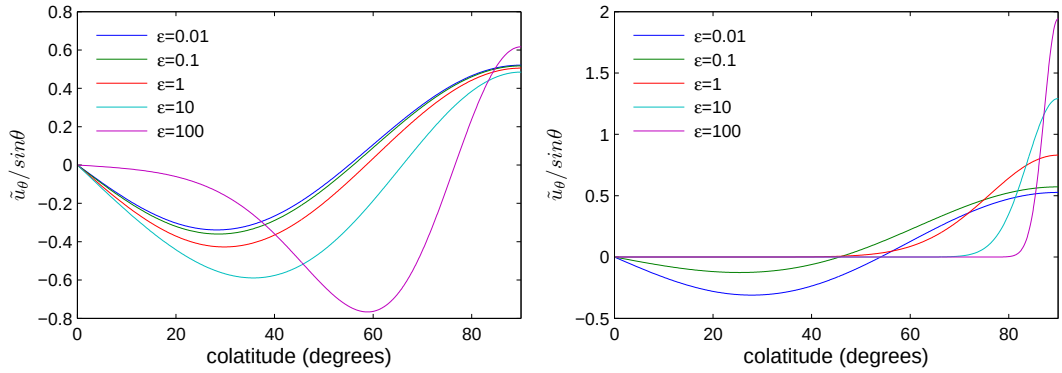

(a) $\alpha = 10^{-3}$ (b) $\alpha = 5$

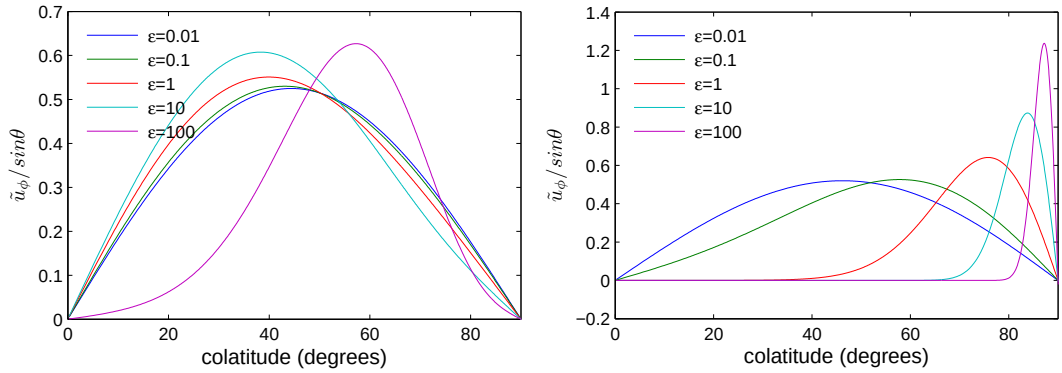

(c) $\alpha = 10^{-3}$ (d) $\alpha = 5$

Figure 4.13: Numerical solution for the velocity for different values of ϵ in the magneto-inertial gravity wave travelling westward for the first mode $n = 3$, $m = 2$ and $N = 50$. The first column corresponds to $\alpha = 10^{-3}$ and $\alpha = 5$ the second column.

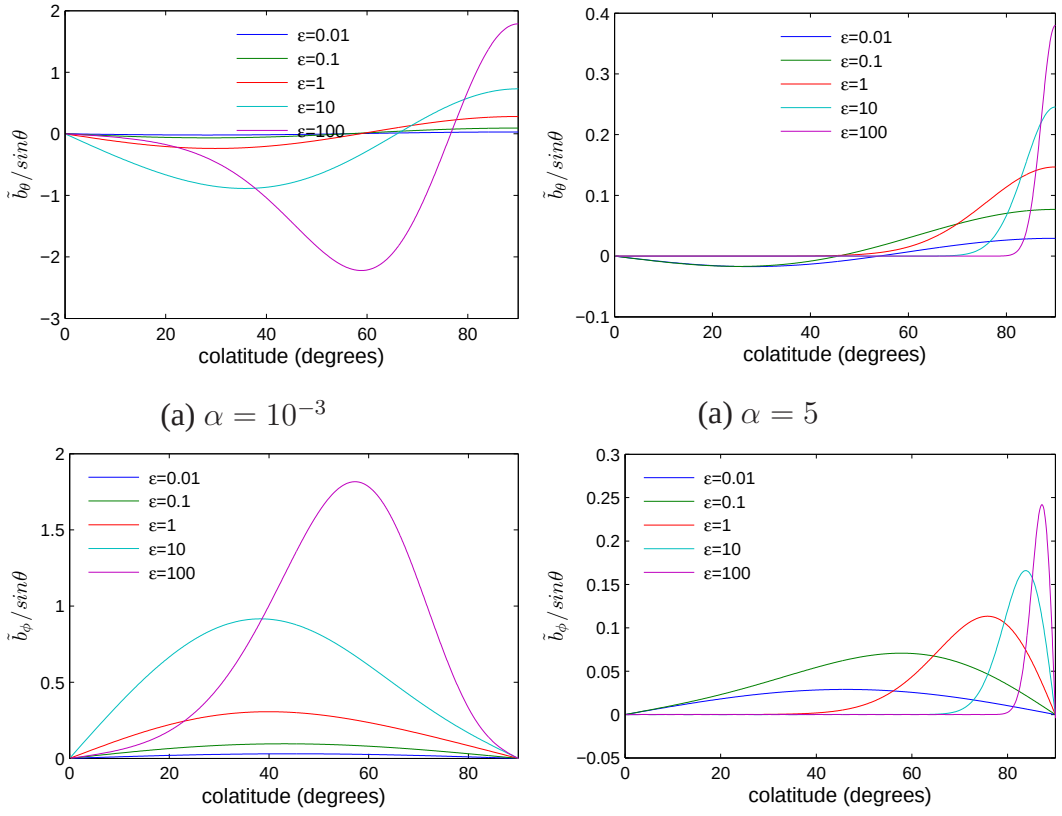

(a) $\alpha = 10^{-3}$ (a) $\alpha = 5$

(d) $\alpha = 10^{-3}$ (a) $\alpha = 5$

Figure 4.14: Numerical solution for the magnetic field perturbation for different values of ϵ in the magneto-inertial gravity wave travelling eastward for the first mode $n = 3$, $m = 2$ and $N = 50$. The first column corresponds to $\alpha = 10^{-3}$ and $\alpha = 5$ for the second one.

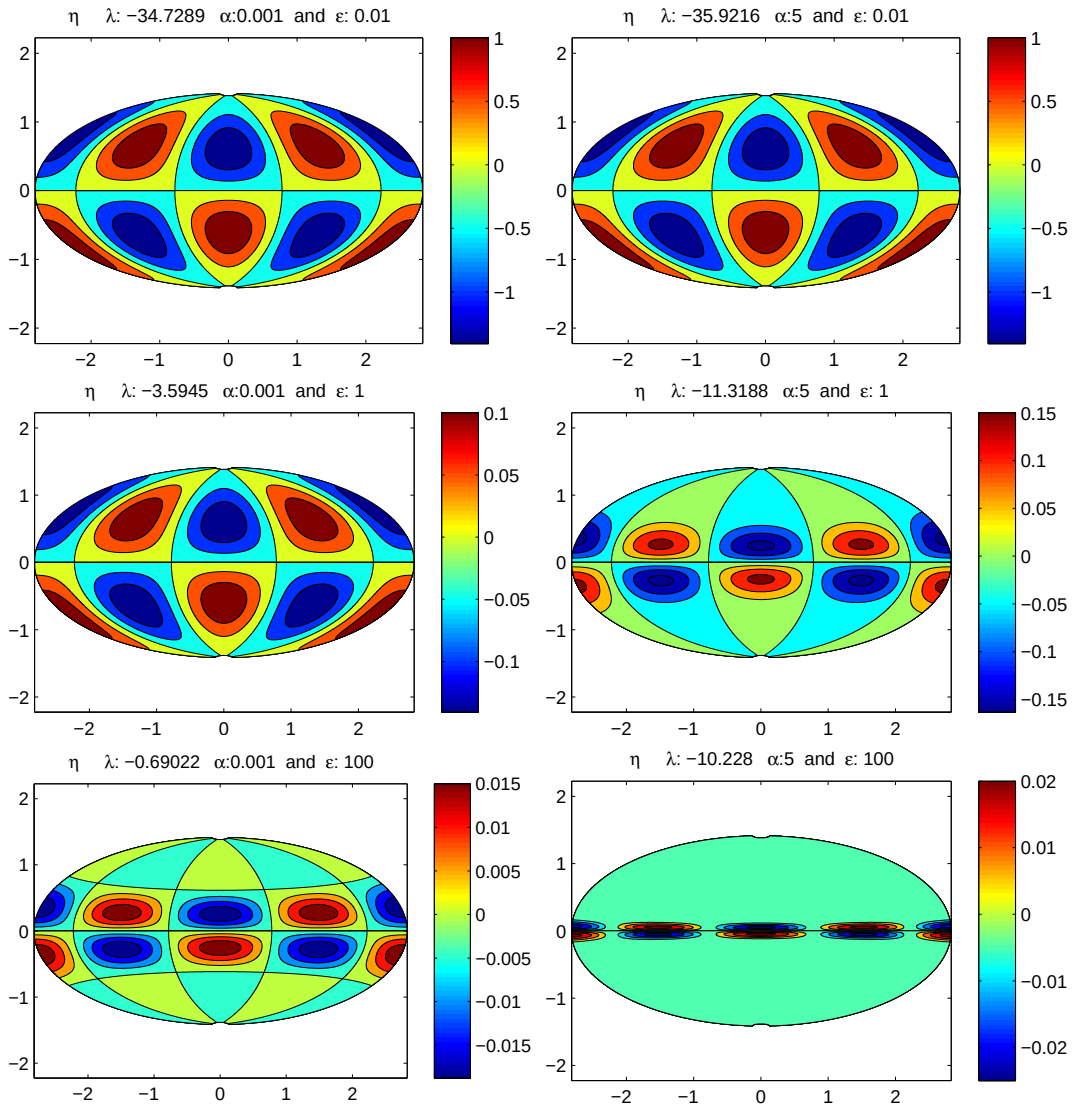

Figure 4.15: Contour plots of the scaled height η for increasing ϵ (0.01, 1 and 100) in the magneto-inertial gravity wave travelling eastward for the first mode $n = 3$, $m = 2$ and $N = 50$. The first column corresponds to $\alpha = 10^{-3}$ with $N = 50$ and $\alpha = 5$ with $N = 70$ for the second one.

4.2 Magnetic Rossby Waves

Rossby waves or planetary waves are an effect of the conservation of the potential vorticity, travelling to the west as a consequence of the rotation of the system. In the presence of a toroidal field this mode splits into two: Fast Magnetic Rossby waves travelling to the west and Slow Magnetic Rossby waves travelling to the east. In this section, we describe analytically and numerically the physical properties of these waves, and in the chapter 6 we will discuss the instability of these modes.

Consider the Magnetic Rossby Modes in a case when the parameter ϵ is very small, (Zaqarashvili et al., 2007). Let us return to equation (2.64), the general differential equation for $\tilde{u}_\theta$ and evaluate it in this limit, the equation (2.64) can be reduced to the Legendre differential equation, a second-order ordinary differential equation whose solutions are the Associated Legendre Polynomials, $\tilde{u}_\theta = P_n^m(\cos\theta)$, see section 2.6.1 and the dispersion relation of these waves is given by the formulas (2.69) and (2.70)

$$\lambda = \frac{-m \pm m\sqrt{1 - 4\alpha^2 n(n+1)[2 - n(n+1)]}}{2n(n+1)}, \tag{4.3}$$

where the expression with the positive sign corresponds to slow magnetic Rossby waves which travel eastward and the negative normalized frequencies are fast magnetic Rossby waves travelling westward. In the case when $\alpha = 0$, the equation for fast Rossby modes reduces to $\lambda = -m/n(n+1)$ which are the hydrodynamic Rossby waves, (Longuet-Higgins, 1968). Note from expression (4.3) that λ decreases with n.

4.2.1 Fast Magnetic Rossby Waves

Some numerical calculations present frequencies which corresponds to fast magnetic Rossby waves. Moreover, the eigenvalues have been reported and the corresponding eigenfunctions have been plotted. When the magnetic field and the rotation are weak, the solutions correspond to pure Rossby Waves and the solutions are the associated

Legendre polynomials, see Zaqarashvili et al. (2010a) and shown above.

The first fast magnetic Rossby mode ($n = 1$) corresponds to the **magneto mixed Rossby-gravity mode**, Matsuno (1966), and this is the highest value for λ of the Rossby waves. The values of the normalized frequency λ are registered in table 4.7. In the first columns where α is small, when ϵ is small the frequency satisfies the formula (4.3), when ϵ is large λ follows (4.2) with negative sign and for $\nu = 0$.

The second and pure fast magnetic Rossby mode is shown in the table 4.8. For α and ϵ small the values agree with the formula (4.3) for $n = 2$ and for large ϵ, λ coincides with equation (3.36) for $\nu = 1$,

$$\lambda = -\frac{m}{\epsilon^{1/2}(2\nu + 1)}. \tag{4.4}$$

In general, fast magnetic Rossby modes corresponding to n and m at small ϵ turn into modes with $\nu = n - m$ at large ϵ.

When $\alpha > 0.5$ the fast magnetic Rossby waves enters a new regime, and they start to coalesce with the slow magnetic Rossby modes and the frequency becomes complex: the instability begins. This will be discussed further in chapter 6.

This unstable behaviour is described for fast and slow magnetic Rossby waves, as well as, the existence of a new regime after $\alpha = 0.5$, when the fast wave becomes subalfvénic $|\lambda| < m\alpha$. It can be seen in table 4.7 for $n = 1$ with $m = 1$, and in table 4.8 for $n = 2$ with $m = 1$.

When α, the magnetic field parameter, increases an instability occurs. The first fast mode, $n = 1$, collides with the anomalous slow magnetic Rossby mode, and becomes complex. The second mode, $n = 2$, collides with the $n = 2$ slow magnetic Rossby mode and so on. However, unstable modes just appear when $m = 1$.

Table 4.7: Eigenvalues λ for different values of α and ϵ, $N = 50$ and $m = 1$. Magneto mixed Rossby-gravity mode $n = 1$: Waves travelling westward.

α	10^{-3}	10^{-2}	10^{-1}	1	10^{1}	10^{2}	10^{3}
$\epsilon = 0.01$	-0.4999	-0.4999	-0.4999	-0.4989	-0.301- 3.2i	-0.482 - 92.7i	-0.498- 992.9i
$\epsilon = 0.1$	-0.4988	-0.4988	-0.4989	-0.4883	-0.442 -7.5i	-0.494 - 97.7i	-0.499- 997.8i
$\epsilon = 1$	-0.4880	-0.4880	-0.4889	-0.294 - 0.1i	-0.482 - 9.3i	-0.498 - 99.3i	-0.500 - 999.1i
$\epsilon = 10$	-0.4140	-0.4141	-0.4202	-0.435-0.6i	-0.494 - 9.8i	-0.499 - 99.8i	-0.480 - 0.8i
$\epsilon = 100$	-0.2710	-0.2711	-0.2877	-0.500 - 99.9i	-0.498 - 9.9i	-0.500 - 99.9i	-0.500- 999.3i

Table 4.8: Eigenvalues λ for different values of α and ϵ, $N = 50$ and $m = 1$. Fast magnetic Rossby Mode $n = 2$: Waves travelling westward.

α	10^{-3}	10^{-2}	10^{-1}	1	10^{1}	10^{2}	10^{3}
$\epsilon = 0.01$	-0.1665	-0.1669	-0.1999	-0.9034	-5.297	-0.482-92.7i	-0.498-992.9i
$\epsilon = 0.1$	-0.1652	-0.1656	-0.1987	-0.8971	-0.443- 7.5i	-0.494 -97.7i	-0.499-997.8i
$\epsilon = 1$	-0.1530	-0.1534	-0.1886	-0.8086	-0.482-9.3i	-0.498-99.3i	-0.500 - 999.1i
$\epsilon = 10$	-0.0950	-0.0956	-0.1408	-0.437-0.600i	-0.494-9.8i	-0.499 - 99.8i	-0.500 - 999.3i
$\epsilon = 100$	-0.033	-0.0346	-0.1054	-0.480 - 0.8i	-0.498 - 9.9i	-0.500 - 99.9i	-0.500 - 999.4i
$\epsilon = 1000$	-0.0106	-0.0145	-0.1006	-0.494 - 0.8i	-0.499-10.0i	-0.500 - 99.9i	-0.500 - 999.3i

Figure 4.16 shows the velocity field. It is clear that the **magneto mixed Rossby-gravity mode** undergoes equatorial trapping for ϵ large, even when the magnetic field is weak. Also, the main difference between the first column ($\alpha = 10^{-3}$) and the second one ($\alpha = 10^{-1}$) is that there is a slightly decreasing in the amplitude of the velocities, even when α increases in two orders of magnitude. In this regime the waves are more influenced by the rotation.

Notice by comparison between panels 4.16(a) and 4.16(c), that while $\tilde{u}_\theta$ is symmetric, $\tilde{u}_\phi$ is antisymmetric. The energy for this **magneto mixed Rossby-gravity mode** is mostly kinetic when ϵ tends to zero and the wave behaves like a Rossby mode. When ϵ is large the wave is a gravity wave and the ratio of the kinetic energy to the total energy is greater than 0.75 for the hydrodynamic case, according to Longuet-Higgins (1968).

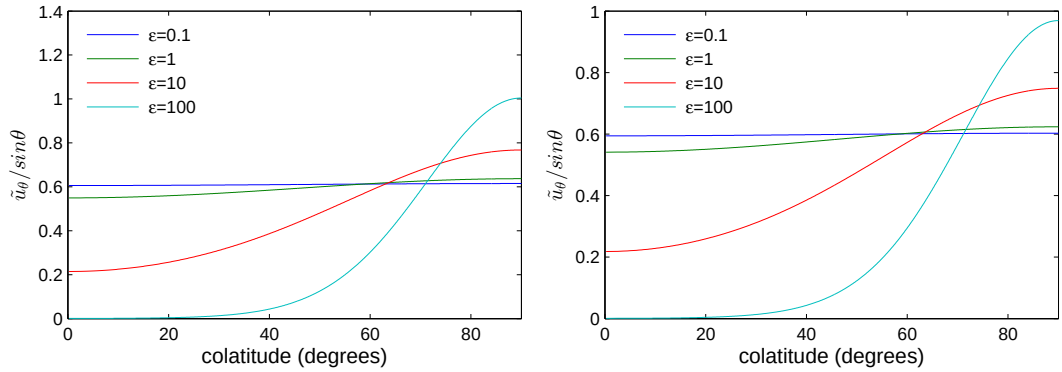

(a) $\alpha = 10^{-3}$ (b) $\alpha = 10^{-1}$

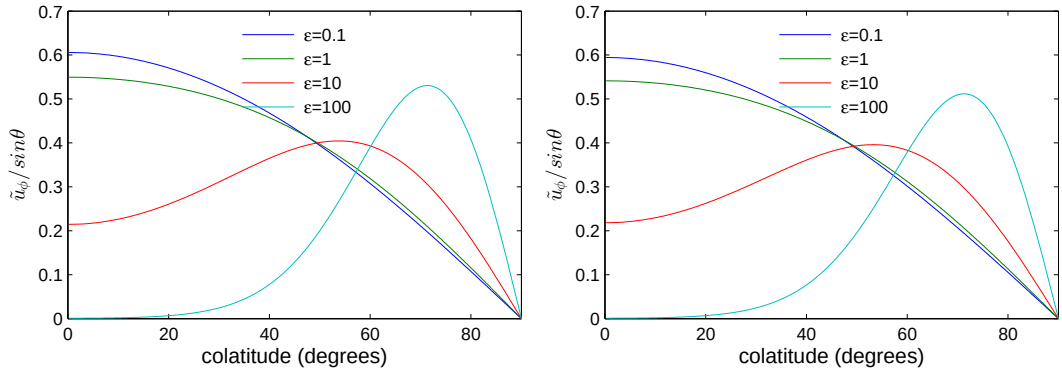

(c) $\alpha = 10^{-3}$ (d) $\alpha = 10^{-1}$

Figure 4.16: Numerical solution of the velocity for different values of ϵ in the fast magnetic Rossby mode for $n = 1$, $m = 1$ and $N = 50$.

The perturbation in the magnetic field has the same behaviour but a high amplitude with respect to the velocity, see figure 4.17, because as shown in equations (2.29d) and (2.29e), the field is proportional to the velocity but inverse to the normalized frequency. Since these frequencies are smaller than 1, the amplitudes for these fields must be intense.

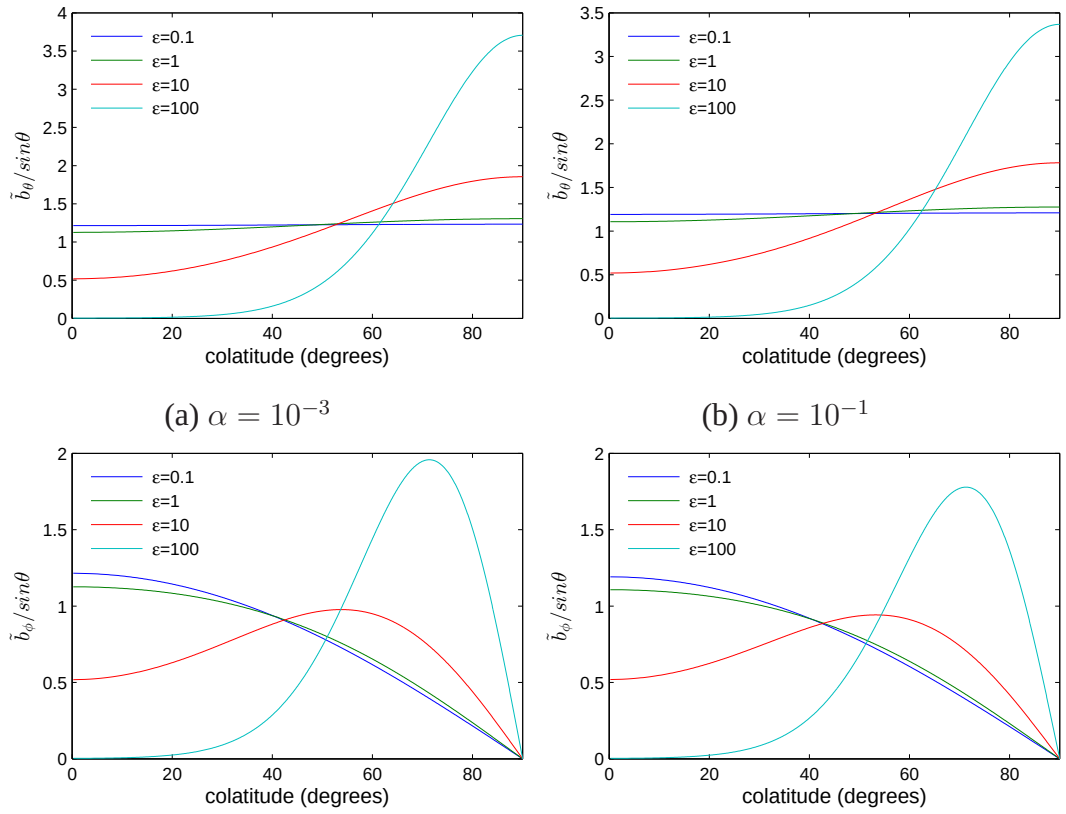

(a) $\alpha = 10^{-3}$ (b) $\alpha = 10^{-1}$

(c) $\alpha = 10^{-3}$ (d) $\alpha = 10^{-1}$

Figure 4.17: Numerical solution of the magnetic field for different values of ϵ in the fast magnetic Rossby mode for $n = 1$, $m = 1$ and $N = 50$.

Figure 4.18, it shows that the amplitudes for η are small compared with the velocity amplitude, when α or ϵ are large. It is very clear that large ϵ produces waves equatorially trapped, as it is shown in figure 4.18(a) and (c). Also, a strong magnetic field increases the equatorially trapping, see panels 4.18(b) and (d).

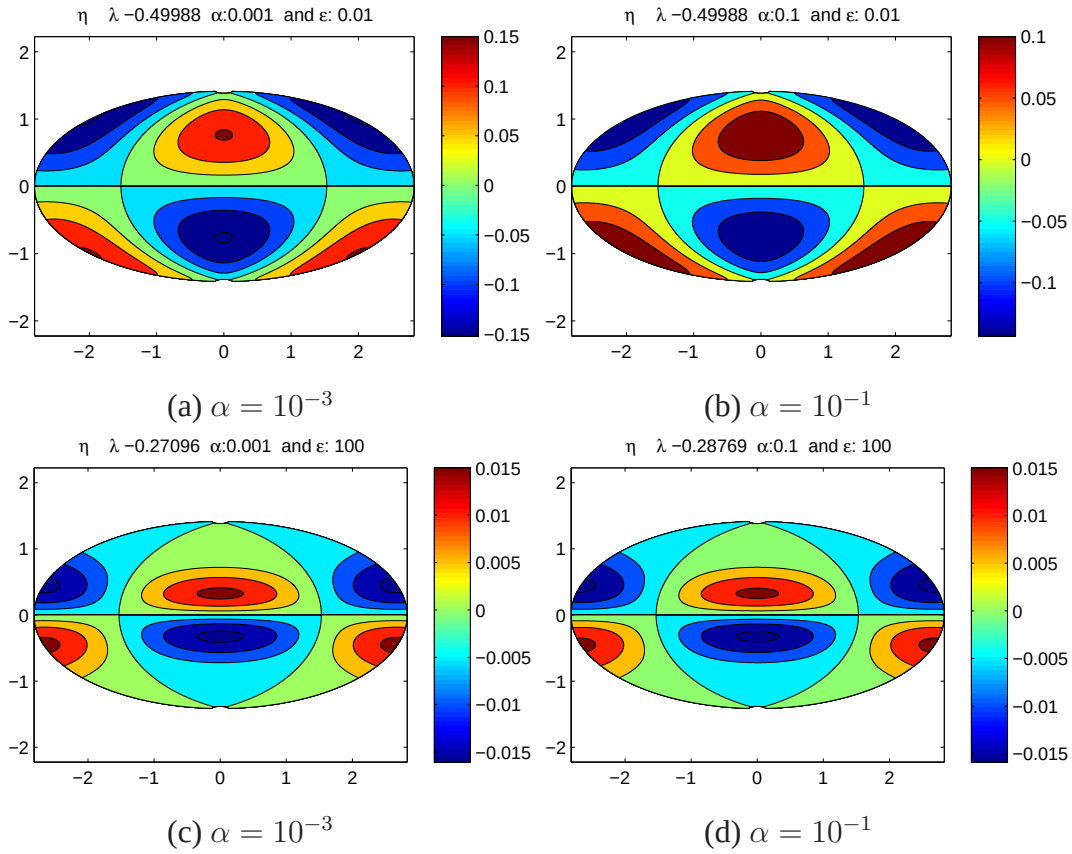

(a) $\alpha = 10^{-3}$ (b) $\alpha = 10^{-1}$

(c) $\alpha = 10^{-3}$ (d) $\alpha = 10^{-1}$

Figure 4.18: Numerical solution for the scaled height η for increasing ϵ (0.01 and 100) in the fast magnetic Rossby mode for $n = 1$, $m = 1$ and $N = 50$.

Figure 4.19 shows the second mode of the fast magnetic Rossby waves. In this case, as reflected in the figure, $\tilde{u}_\theta$ is antisymmetric with respect to the equator while $\tilde{u}_\phi$ is symmetric, opposite to the $n = 1$ case. In the figure we can note that when ϵ is large the waves become trapped at the equator. When α increases from 10^{-3} (panels 4.19(a) and (c)) to 10^{-1} (panels 4.19(b) and (d)), the behaviour remains similar but the amplitude of the waves are slightly different. For ϵ small, the amplitude decreases slightly but for ϵ large the amplitude increases notably for $\tilde{u}_\phi$ and decrease for $\tilde{u}_\theta$. According to Longuet-Higgins (1968), for the fast Rossby modes the ratio between kinetic energy and total energy is 0.5 when ϵ is large, i.e. kinetic energy are in the same proportion as potential

energy. Then the waves are more sensitive to the changes in the ϵ parameter. When ϵ is small, according to Longuet-Higgins (1968), the waves have mostly kinetic energy.

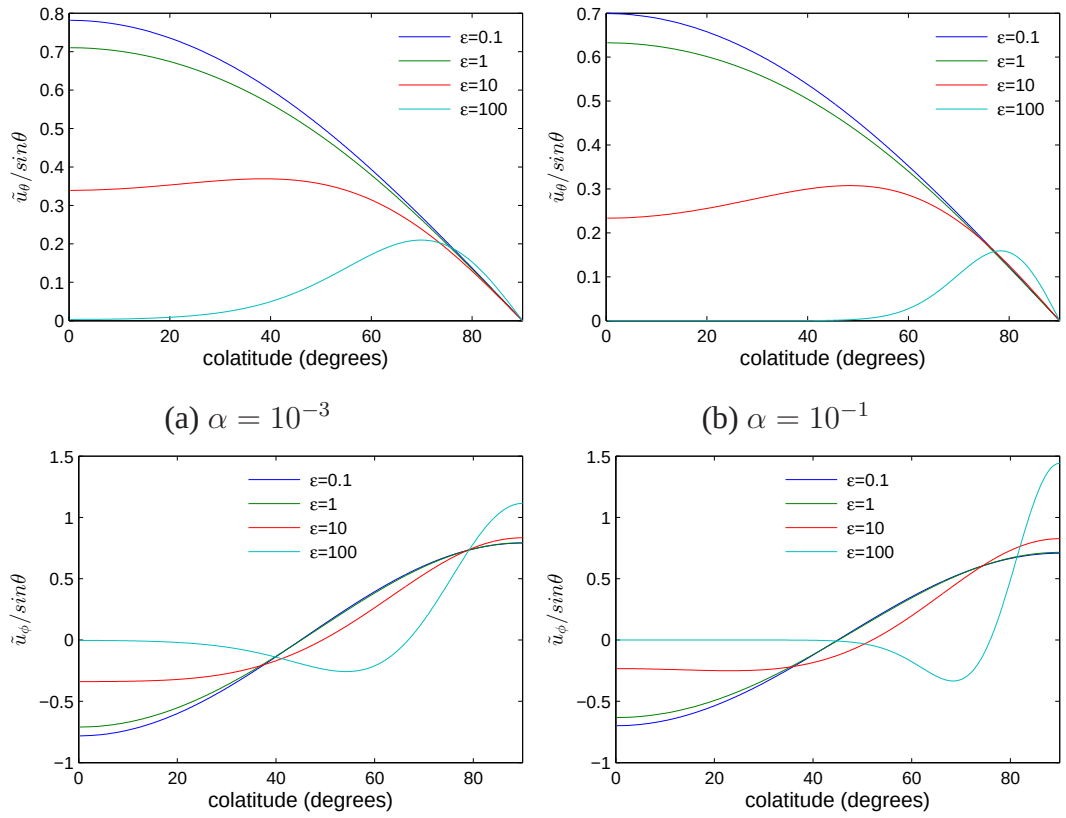

(a) $\alpha = 10^{-3}$ (b) $\alpha = 10^{-1}$

(c) $\alpha = 10^{-3}$ (d) $\alpha = 10^{-1}$

Figure 4.19: Numerical solution of the velocity for different values of ϵ in the fast magnetic Rossby mode for $n = 2$, $m = 1$ and $N = 50$.

The behaviour of the magnetic perturbations has no major changes when α increases from 10^{-3} to 10^{-1} but the amplitudes decrease considerably for stronger field. As the frequencies decrease the magnetic field becomes stronger, as shown in figure 4.20. For this mode $n = 2$, the azimuthal component of the magnetic field is higher than the latitudinal component.

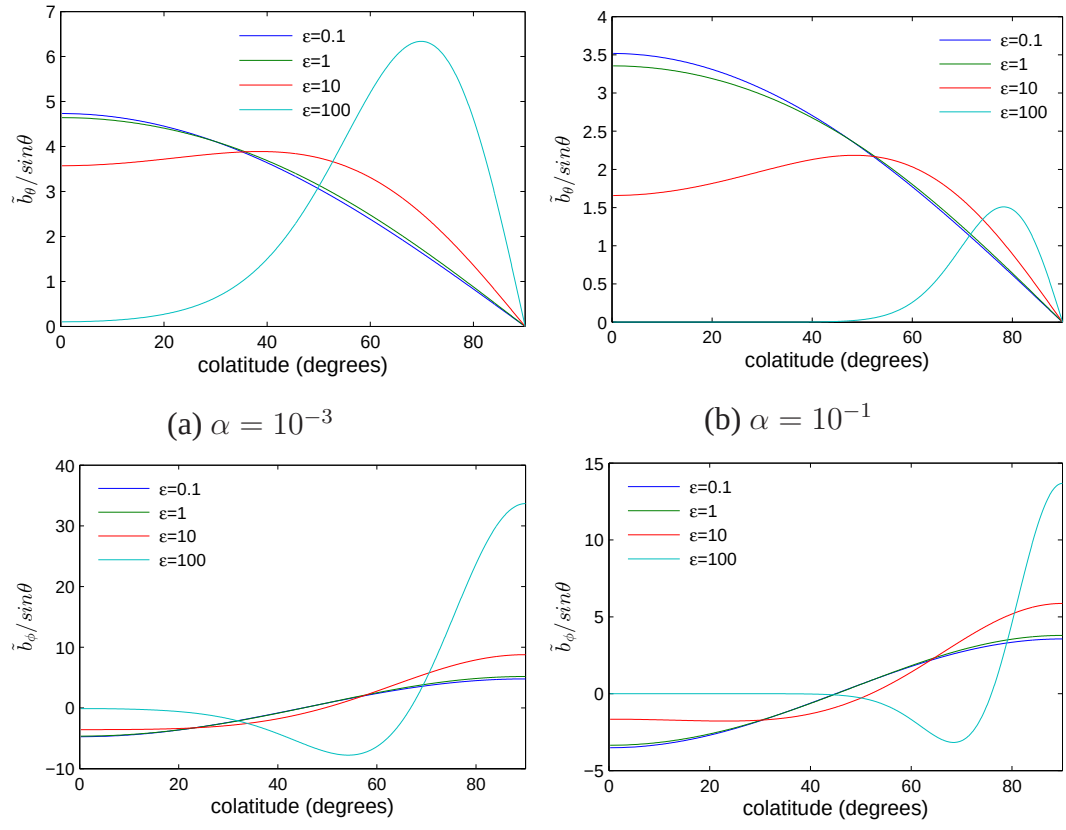

(a) $\alpha = 10^{-3}$

(b) $\alpha = 10^{-1}$

(c) $\alpha = 10^{-3}$

(d) $\alpha = 10^{-1}$

Figure 4.20: Numerical solution of the magnetic field for different values of ϵ in the fast magnetic Rossby mode for $n = 2$, $m = 1$ and $N = 50$.

Figure 4.21 shows the scaled height and two important facts for fast magnetic Rossby waves are clear:

- There is equatorial trapping when ϵ is large and α has a moderate value ~ 0.1.
- The height amplitude is very small compared with the velocities and decreases considerably when ϵ or α increase.

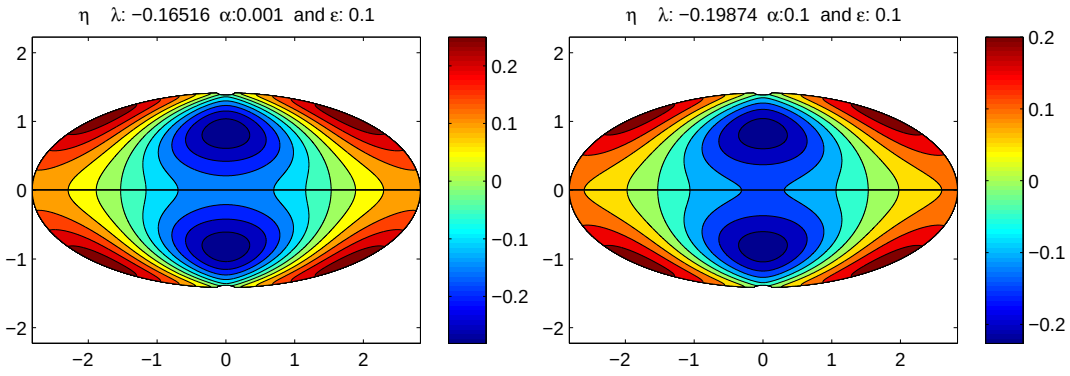

(a) $\alpha = 10^{-3}$ (b) $\alpha = 10^{-1}$

(c) $\alpha = 10^{-3}$ (a) $\alpha = 10^{-1}$

Figure 4.21: Numerical solution for the scaled height η for increasing ϵ (0.1 and 100) in the fast magnetic Rossby mode for $n = 2$, $m = 1$ and $N = 50$.

Table 4.9 is an example of the first fast mode $n = 2$, when $m = 2$. These waves have more nodes in longitude. In addition, when α is small solutions correspond to the Associated Legendre polynomials. These eigenvalues are always real. The values for large α can be predicted by the asymptotic theory for $m = 2$. The waves for large α are polar trapped.

Table 4.9: Eigenvalues fast magnetic Rossby modes for different values of α and ϵ, $n = 2$ $N = 50$ and $m = 2$: waves travelling westward.

α	10^{-3}	10^{-2}	10^{-1}	1	10^{1}	10^{2}	10^{3}
$\epsilon = 0.01$	-0.33331	-0.3341	-0.39997	-1.80799	-15.9209	-63.6549	-200.49622
$\epsilon = 0.1$	-0.33299	-0.33378	-0.39971	-1.80657	-11.5124	-36.0576	-111.97047
$\epsilon = 1$	-0.32991	-0.33071	-0.39714	-1.79058	-6.81047	-20.5035	****
$\epsilon = 10$	-0.30562	-0.30648	-0.37713	-1.58640	-4.08217	-11.7911	****
$\epsilon = 100$	-0.22998	-0.23115	-0.31886	-1.26152	-2.55842	****	****

4.2.2 Slow Magnetic Rossby Waves

Solving the eigenvalue problem, we found numerically that the smallest and positive frequencies correspond to slow magnetic Rossby waves, travelling to the east. We select the azimuthal wavenumbers $m = 1$ and $m = 2$ to illustrate clearly the properties of slow magnetic Rossby waves. The first mode corresponds to $n = 2$ in the formula (4.3), for $n = 1$, the value of λ is equal to zero.

Then, the table 4.10 shows the numerical results for the normalized frequency λ, for $n = 2$ and $m = 1$. For a weak magnetic field the eigenvalues do not change with the rotation parameter ϵ, except when α is 0.1 and ϵ is large. Before $\alpha = 0.5$, the waves are subalfvénic and after $\alpha = 0.5$, enter in a new regime: the modes grow and then become negative to coalesce with the corresponding second fast magnetic Rossby mode and an unstable mode branches off. Because the frequency changes its sign, there is a solution for $\lambda = 0$, corresponding to a stationary solution of the linear equations, it is possible that steady nonlinear solutions exist in the neighbourhood of this point.

Table 4.10: Eigenvalues for different values of α and ϵ, for $N = 50$ and $m = 1$. Slow magnetic Rossby Mode $n = 2$: Waves travelling eastward.

α	10^{-3}	10^{-2}	10^{-1}	1	10^{1}	10^{2}	10^{3}
$\epsilon = 0.01$	4×10^{-6}	0.00039904	0.033322	0.73319	4.7293	-0.482+92.7i	-0.498+992.9i
$\epsilon = 0.1$	4×10^{-6}	0.000399	0.033222	0.69392	-0.443+7.5i	-0.494+97.7i	-0.499+997.8i
$\epsilon = 1$	4×10^{-6}	0.000399	0.032244	0.2865461	-0.482 + 9.3i	-0.498 + 99.3i	-0.500 + 999.1i
$\epsilon = 10$	4×10^{-6}	0.000397	0.024642	-0.437+ 0.6i	-0.494 + 9.8i	-0.499 + 99.8i	-0.500 + 999.3i
$\epsilon = 100$	4×10^{-6}	0.00038	0.004171	-0.480 + 0.8i	-0.498 + 9.9i	-0.500 + 99.9i	-0.500+ 999.3i

In figure 4.22, the mode $n = 2$ has been plotted for a weak field ($\alpha = 10^{-3}$) and moderate field ($\alpha = 10^{-1}$). One striking feature of these waves is that they are not trapped at the equator. On the other hand, the panels 4.22(a) and (c) show that the rotation parameter does not have effects on this mode when the magnetic field is weak. Increasing the field, in panels 4.22(b) and (d), the rotation becomes important, and when ϵ increases the amplitude of the velocity decreases.

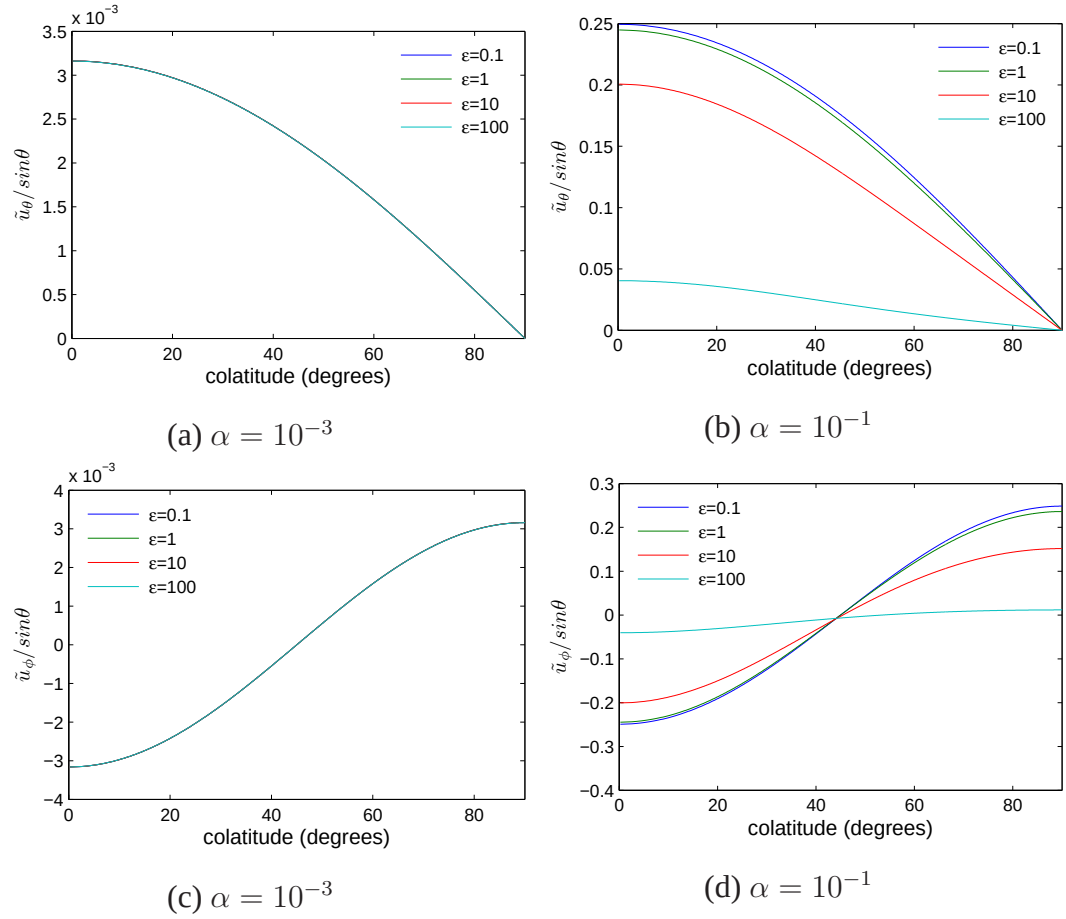

(a) $\alpha = 10^{-3}$

(b) $\alpha = 10^{-1}$

(c) $\alpha = 10^{-3}$

(d) $\alpha = 10^{-1}$

Figure 4.22: Numerical solution for the velocity for different values of ϵ in the slow magnetic Rossby mode for $n = 2$, $m = 1$ and $N = 50$. Note that in the left panel, all curves lie on top of each other.

Another major aspect of slow magnetic Rossby waves, is that the amplitude of the magnetic field is high with respect to the velocity, see figure 4.23. Due to the fact that the magnetic field is proportional to the velocity and inverse with the frequency, then if slow magnetic Rossby waves have the shortest frequencies, the magnetic perturbations will be the highest in amplitude. Also, we note in figure 4.23(b) and (d) that the amplitude of the field for a moderate value of $\alpha = 0.1$ increases with ϵ, unlike the velocity.

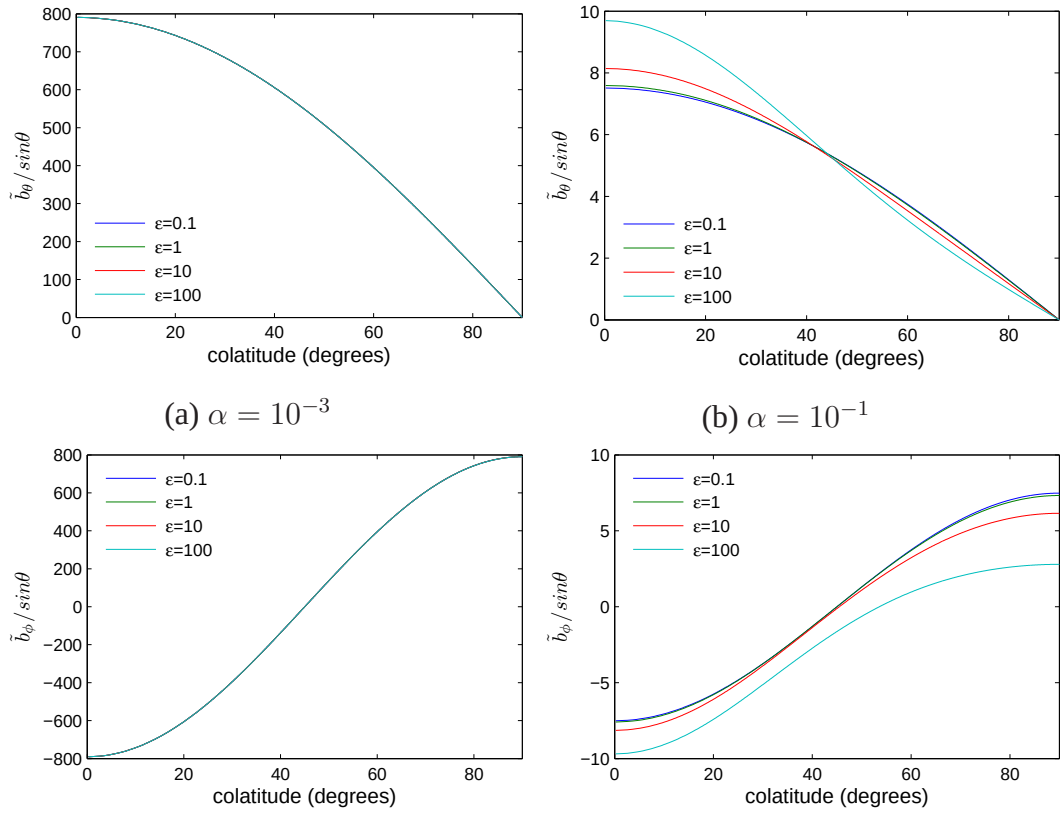

(a) $\alpha = 10^{-3}$ (b) $\alpha = 10^{-1}$

(c) $\alpha = 10^{-3}$ (d) $\alpha = 10^{-1}$

Figure 4.23: Numerical solution for the magnetic field for different values of ϵ in the slow magnetic Rossby mode for $n = 2$, $m = 1$ and $N = 50$. All curves at 10^{-3} lie on top of each other.

In figure 4.24, the scaled height is shown, for $n = 2$ slow magnetic Rossby waves. The eigenfunctions corresponds to the Legendre polynomials and are not trapped at the equator. We note that for a weak field, in panels 4.24(a) and (c) the height of the layer is very small compared to the magnitude of the velocities, increasing α to 0.1, the height also increase in two orders of magnitude.

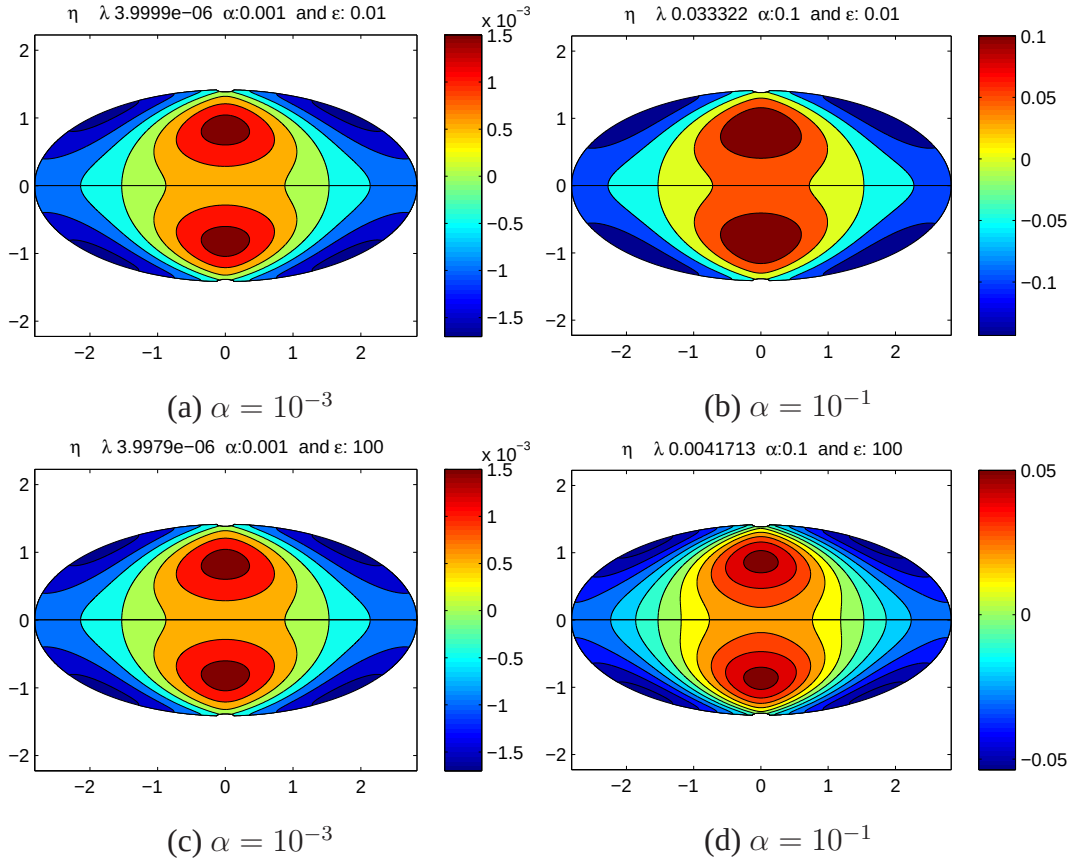

(a) $\alpha = 10^{-3}$ (b) $\alpha = 10^{-1}$

(c) $\alpha = 10^{-3}$ (d) $\alpha = 10^{-1}$

Figure 4.24: Numerical solution for the scaled height η for increasing ϵ (0.01 and 100) in the slow magnetic Rossby mode for $n = 2$, $m = 1$ and $N = 50$.

The next slow mode $n = 3$ for $m = 1$ satisfies the relation (4.3) when α is small. In the cases where $\alpha > 0.5$ the mode grows, after that becomes negative and then collides with the magnetic fast Rossby mode $n = 3$, as an unstable mode, see table 4.11.

Table 4.11: Eigenvalues λ for different values of α and ϵ, for $N = 50$ and $m = 1$. Slow magnetic Rossby wave $n = 3$: Waves travelling eastward.

α	10^{-3}	10^{-2}	10^{-1}	1	10^{1}	10^{2}	10^{3}
$\epsilon = 0.01$	9.999×10^{-6}	9.883×10^{-4}	0.05867	0.8701	8.010	-0.4747+62.6i	-0.4832+93.2i
$\epsilon = 0.1$	9.999×10^{-6}	9.882×10^{-4}	0.05854	0.8518	2.342	-0.4832+93.2i	-0.4994+997.8i
$\epsilon = 1$	9.999×10^{-6}	9.875×10^{-4}	0.05733	0.6902	-0.4467+7.7i	-0.4947 + 97.9i	-0.4988 + 997.0i
$\epsilon = 10$	9.998×10^{-6}	9.809×10^{-4}	0.04778	0.09633	-0.4832 + 9.3i	-0.4983 + 99.3i	-0.4988 + 997.5i
$\epsilon = 100$	9.991×10^{-6}	9.217×10^{-4}	0.02041	-0.4408+0.63 i	-0.4947 + 9.77 i	-0.4988 + 99.7i	-0.4988+ 997.6 i

Another example of slow magnetic Rossby waves is illustrated in figure 4.25. If the fluid is immersed in a weak field, the wave is not affected by rotation, when the field increases the rotation modify slightly the wave form and the frequency. The panels 4.25(b) and (d), show that these waves undergo polar trapping for $\alpha = 0.1$ and ϵ large. Also it is evident that in the panels 4.26(b) and (d), the wave undergoes polar trapping for ϵ large and $\alpha = 0.1$.

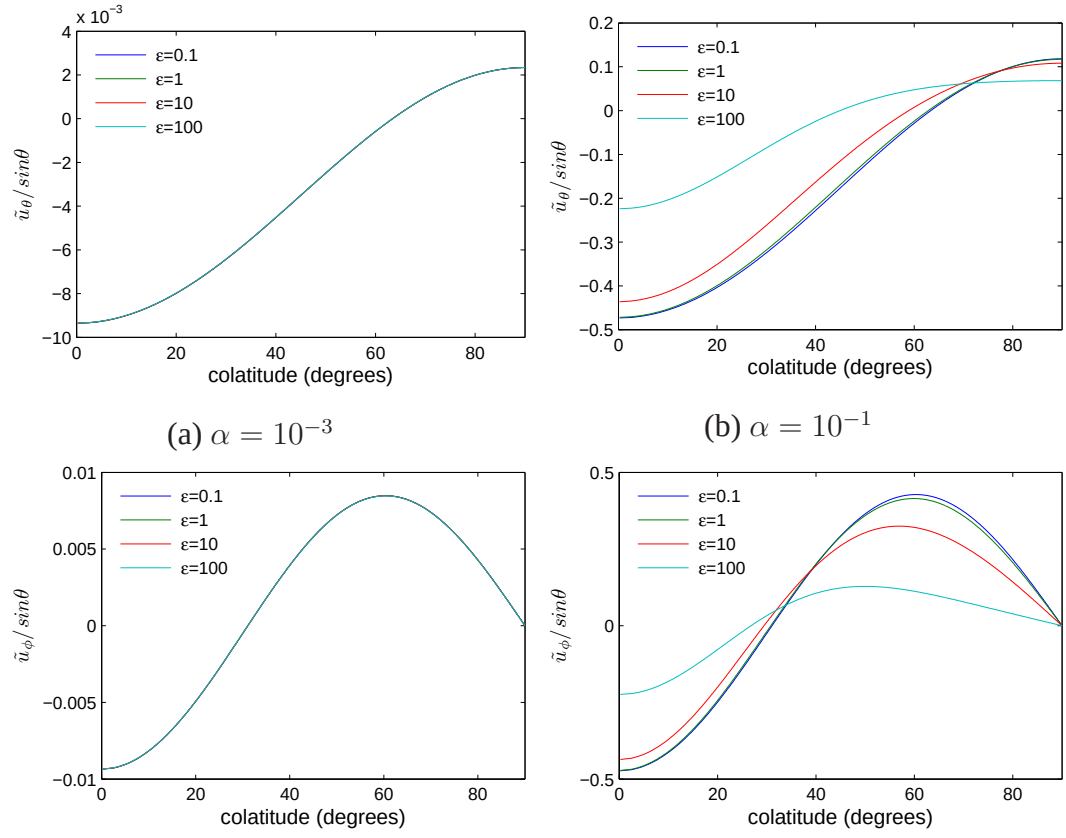

(a) $\alpha = 10^{-3}$ (b) $\alpha = 10^{-1}$

(c) $\alpha = 10^{-3}$ (d) $\alpha = 10^{-1}$

Figure 4.25: Numerical solution for the velocity for different values of ϵ in the slow magnetic Rossby mode for $n = 3$, $m = 1$ and $N = 50$. All curves at 10^{-3} lie on top of each other.

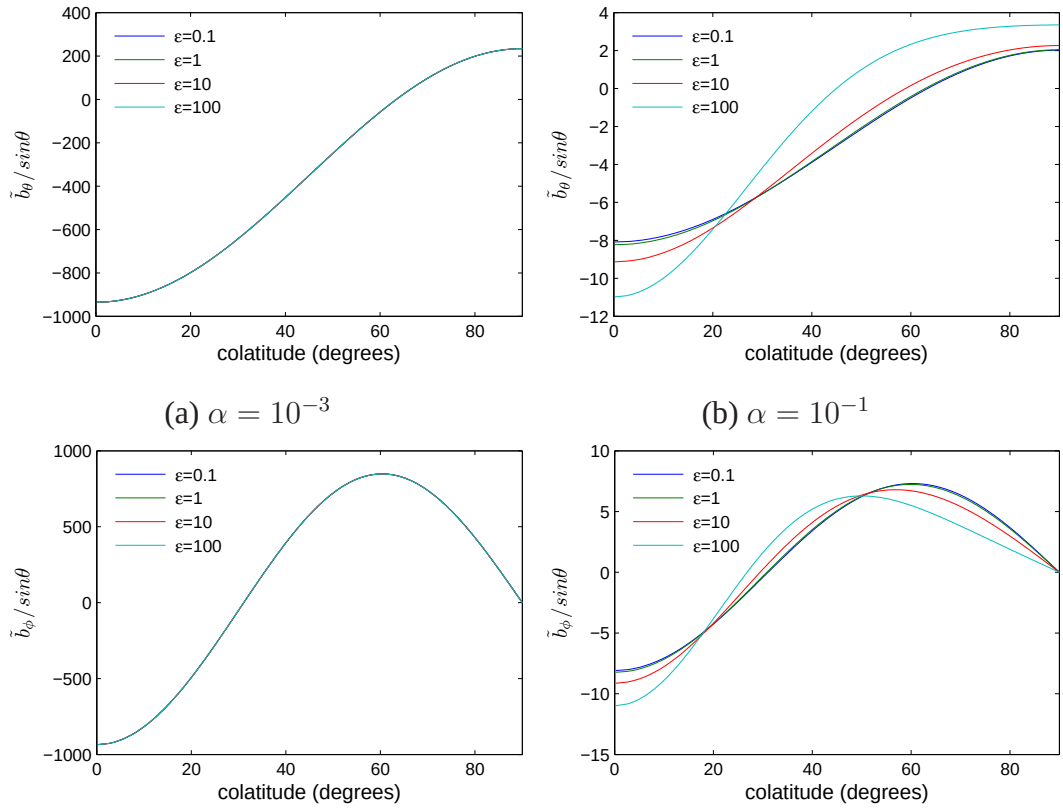

(a) $\alpha = 10^{-3}$ (b) $\alpha = 10^{-1}$

(c) $\alpha = 10^{-3}$ (d) $\alpha = 10^{-1}$

Figure 4.26: Numerical solution for the magnetic field for different values of ϵ in the slow magnetic Rossby mode for $n = 3$, $m = 1$ and $N = 50$. All curves at 10^{-3} lie on top of each other.

Figure 4.27 reveals that slow magnetic Rossby waves are not equatorially trapped, at large or small α or ϵ. In contrast, the perturbation moves poleward when α is 0.1 and ϵ is large.

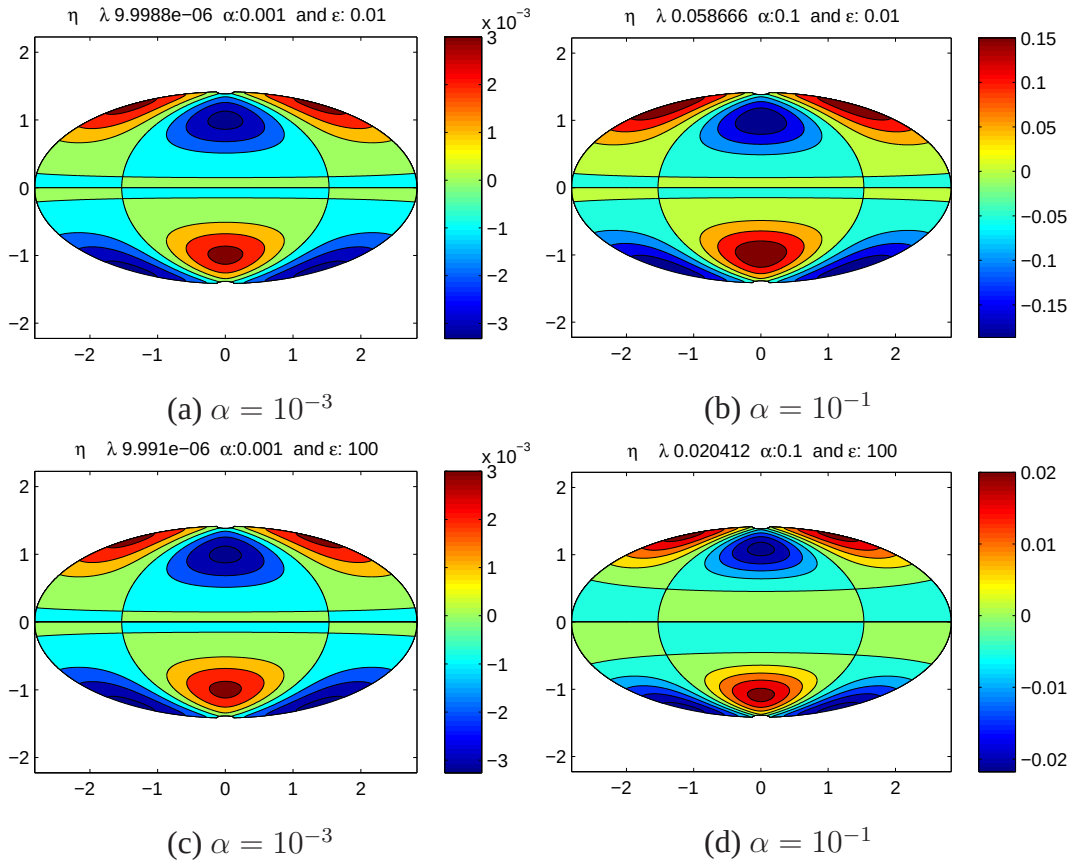

(a) $\alpha = 10^{-3}$ (b) $\alpha = 10^{-1}$

(c) $\alpha = 10^{-3}$ (d) $\alpha = 10^{-1}$

Figure 4.27: Numerical solution for the scaled height η for increasing ϵ (0.01 and 100) in the slow magnetic Rossby mode for $n = 3$, $m = 1$ and $N = 50$.

This is certainly true in the case, when $m = 2$, the eigenvalues are real and there is no instability, as shown in table 4.12 for all the range in ϵ or α. Another significant aspect of the value of λ for slow magnetic Rossby waves is that the frequency is in the subalfvénic regime $|\lambda| < m\alpha$. For small α, the values are given by the formula (4.3) for $n = 2$ and $m = 2$, since λ is directly proportional to m, it is clear that the values of this table are double that of the eigenvalues in table 4.10, where $n = 2$ and $m = 1$. The large α results are proportional to α.

Figure 4.28 demonstrates that for slow magnetic Rossby waves in a weak field the rotation does not have a significant effect on the oscillations. But for a moderate value

Table 4.12: Eigenvalues for different values of α and ϵ, $n = 2$, and $m = 2$, an eastward slow magnetic Rossby mode.

α	10^{-3}	10^{-2}	10^{-1}	1	10^{1}	10^{2}	10^{3}
$\epsilon = 0.01$	7.9998×10^{-6}	0.00079809	0.066664	1.4738	15.48	62.705	199.5
$\epsilon = 0.1$	7.9998×10^{-6}	0.00079808	0.066641	1.4649	10.677	35.073	111.97040
$\epsilon = 1$	7.9998×10^{-6}	0.00079804	0.066408	1.3557	5.8606	19.508	****
$\epsilon = 10$	7.9998×10^{-6}	0.00079764	0.064068	0.76454	3.098	10.758	****
$\epsilon = 100$	7.9994×10^{-6}	0.00079356	0.044464	0.31526	1.5634	****	****

of $\alpha = 0.1$, the waves are slightly shifted to the poles when ϵ is large. For the first mode $n = 2$, $m = 2$, the northward velocity is symmetric with respect to the equator, conversely, the azimuthal velocity is antisymmetric.

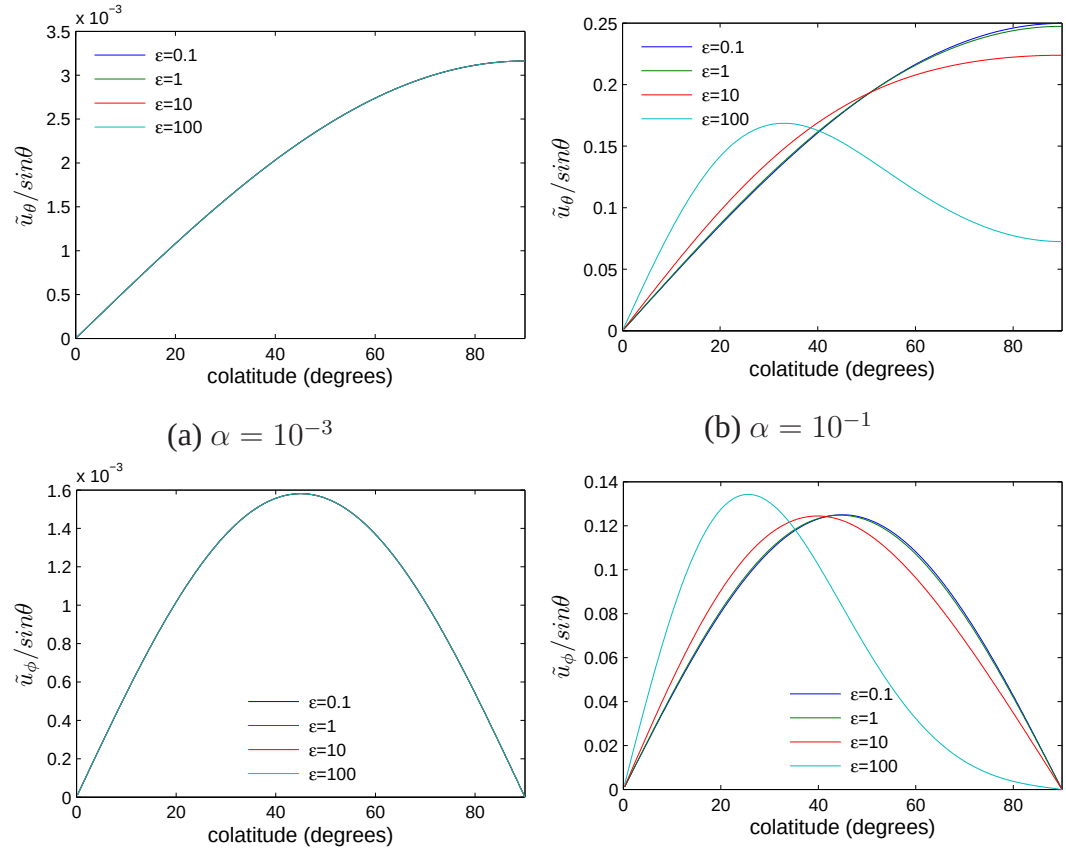

(a) $\alpha = 10^{-3}$ (b) $\alpha = 10^{-1}$

(c) $\alpha = 10^{-3}$ (d) $\alpha = 10^{-1}$

Figure 4.28: Numerical solution for different values of ϵ in the slow magnetic Rossby mode for $n = 2$, $m = 2$ and $N = 50$. All curves at 10^{-3} lie on top of each other.

Figure 4.29 for the scaled height η shows that for $m = 2$, there are more longitudinal nodes and for a weak field the solutions are not trapped at the equator, even though ϵ is large. Then for moderate magnetic fields, the polar trapping becomes evident.

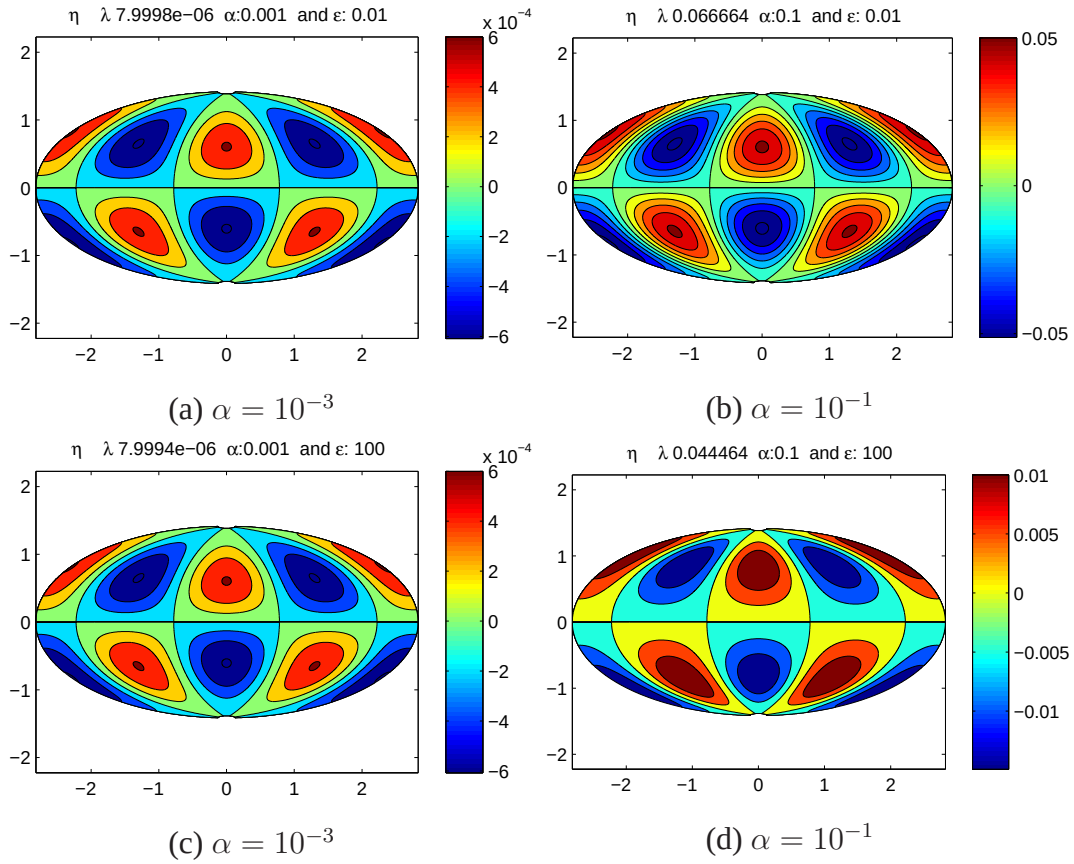

(a) $\alpha = 10^{-3}$ (b) $\alpha = 10^{-1}$

(c) $\alpha = 10^{-3}$ (d) $\alpha = 10^{-1}$

Figure 4.29: Numerical solution for the scaled height η for increasing ϵ (0.01 and 100) in the slow magnetic Rossby mode for $n = 2$, $m = 2$ and $N = 50$.

In table 4.13, the eigenvalues are tabulated for the second slow magnetic Rossby wave, $n = 3$, $m = 2$. The eigenvalues for small α can be calculated with the formula (4.3). All of these modes are real and for large α and small ϵ, the value of λ are proportional to α. All of these frequencies remain in the sufalvénic regime.

Table 4.13: Eigenvalues for different values of α and ϵ, $n = 3$, $N = 50$ and $m = 2$.Slow magnetic Rossby modes: Waves travelling eastward.

α	10^{-3}	10^{-2}	10^{-1}	1	10^{1}	10^{2}	10^{3}
$\epsilon = 0.01$	2×10^{-5}	0.001977	0.117341	1.741586	16.5706	62.70506	199.5012
$\epsilon = 0.1$	2×10^{-5}	0.001976	0.117174	1.716517	10.67918	35.07343	112.3185
$\epsilon = 1$	2×10^{-5}	0.001976	0.115525	1.463803	5.860625	19.5085	76.69158
$\epsilon = 10$	2×10^{-5}	0.001967	0.101004	0.764634	3.097991	10.79252	71.02618
$\epsilon = 100$	2×10^{-5}	0.001884	0.048614	0.31526	1.563428	7.2357	70.42379

In fact, for the second mode $n = 3$ and $m = 2$ the northward velocity is antisymmetric and the azimuthal velocity is symmetric, see figure 4.30. Again, the variation in the rotation parameter does not affect the oscillation for a weak field, but when the field is moderate and ϵ increases, the solutions are more concentrated at high latitudes.

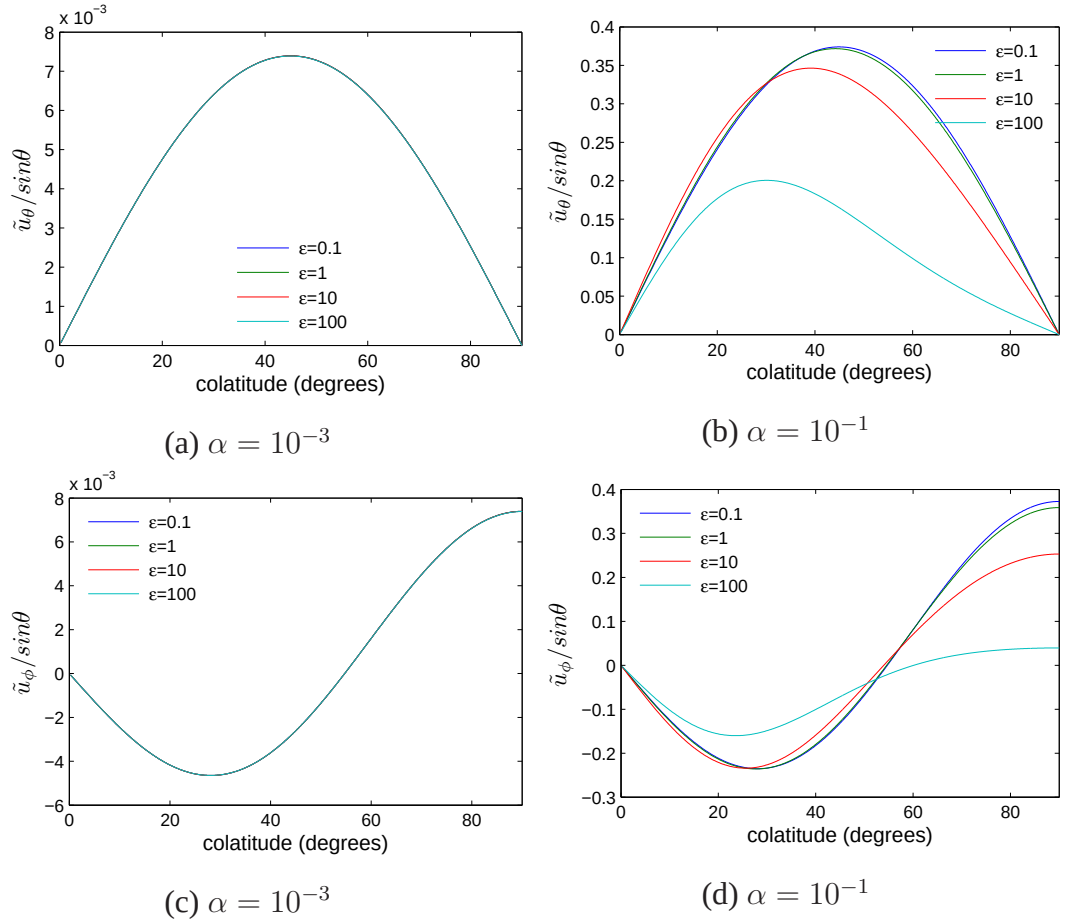

(a) $\alpha = 10^{-3}$

(b) $\alpha = 10^{-1}$

(c) $\alpha = 10^{-3}$

(d) $\alpha = 10^{-1}$

Figure 4.30: Numerical solution of the velocity for different values of ϵ in the slow magnetic Rossby mode for $n = 3$, $m = 2$ and $N = 50$. All curves at 10^{-3} lie on top of each other.

Figure 4.31 shows the effect of the rotation parameter on the waves. For small α, the effect is imperceptible, but for large ϵ, the wave is moved poleward. It is clear that here the slow magnetic Rossby waves are not equatorially trapped and are produced by the effect of the magnetic field.

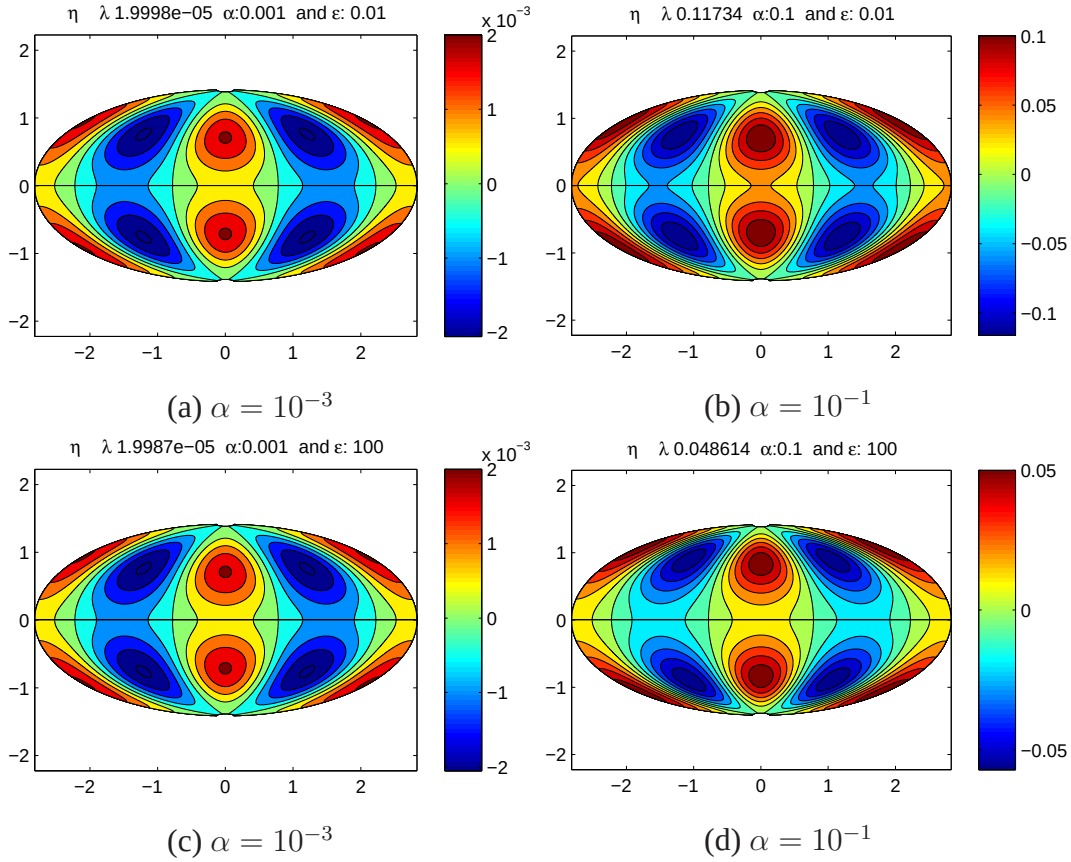

(a) $\alpha = 10^{-3}$ (b) $\alpha = 10^{-1}$

(c) $\alpha = 10^{-3}$ (d) $\alpha = 10^{-1}$

Figure 4.31: Numerical solution for the scaled height η for increasing ϵ (0.01 and 100) in the slow magnetic Rossby mode for $n = 3$, $m = 2$ and $N = 50$.

4.3 Anomalous Mode

In the numerical results a new mode was found in the presence of the magnetic field, propagating westward. It is a very slow wave which we call “anomalous”, this is the first slow magnetic Rossby mode. This mode collides with the first fast magnetic Rossby wave $n = 1$ and the wave becomes unstable, see chapter 5. This instability occurs only for $m = 1$. The normalized frequency is summarized in table 4.14, these numerical results show the frequency of the anomalous mode increases linearly with ϵ and α^4.

Table 4.14: Eigenvalues for different values of α and ϵ, $m = 1$, and $n = 1$, the anomalous westward slow magnetic Rossby mode.

α	10^{-3}	10^{-2}	10^{-1}	1	10^{1}	10^{2}	10^{3}
$\epsilon = 0.01$	****	-1.88×10^{-10}	-2.00×10^{-7}	-2.01×10^{-3}	-0.301+3.19i	-0.482 +92.7i	-0.498+992.9i
$\epsilon = 0.1$	-1.29×10^{-9}	-2.28×10^{-10}	-2.00×10^{-6}	-0.02053	-0.442+7.48i	-0.494+97.73i	-0.499+997.8i
$\epsilon = 1$	-7.47×10^{-11}	-2.34×10^{-9}	-2.00×10^{-5}	-0.294+ 0.1i	-0.482 + 9.3i	-0.498 + 99.3i	-0.500+ 999.1i
$\epsilon = 10$	-1.39×10^{-10}	-1.997×10^{-8}	-1.97×10^{-4}	-0.435+0.6i	-0.494+ 9.8i	-0.499 - 99.8i	-0.500 - 999.9i
$\epsilon = 100$	-4.41×10^{-11}	-2.00×10^{-7}	-0.00172	-0.480 + 0.8i	-0.498+ 9.9i	-0.500 + 99.9i	-0.500 + 999.3i

The velocity field shows a small amplitude that increases with ϵ, see figure 4.32. When the magnetic field increases, from 10^{-2} to 10^{-1}, the wave amplitude increases too by at least three orders of magnitude. The northward velocity is symmetric but the azimuthal velocity is antisymmetric. For ϵ and α small the solution corresponds to $\tilde{u}_\theta = \sin\theta$, this is clearly shown in the panel 4.32(a).

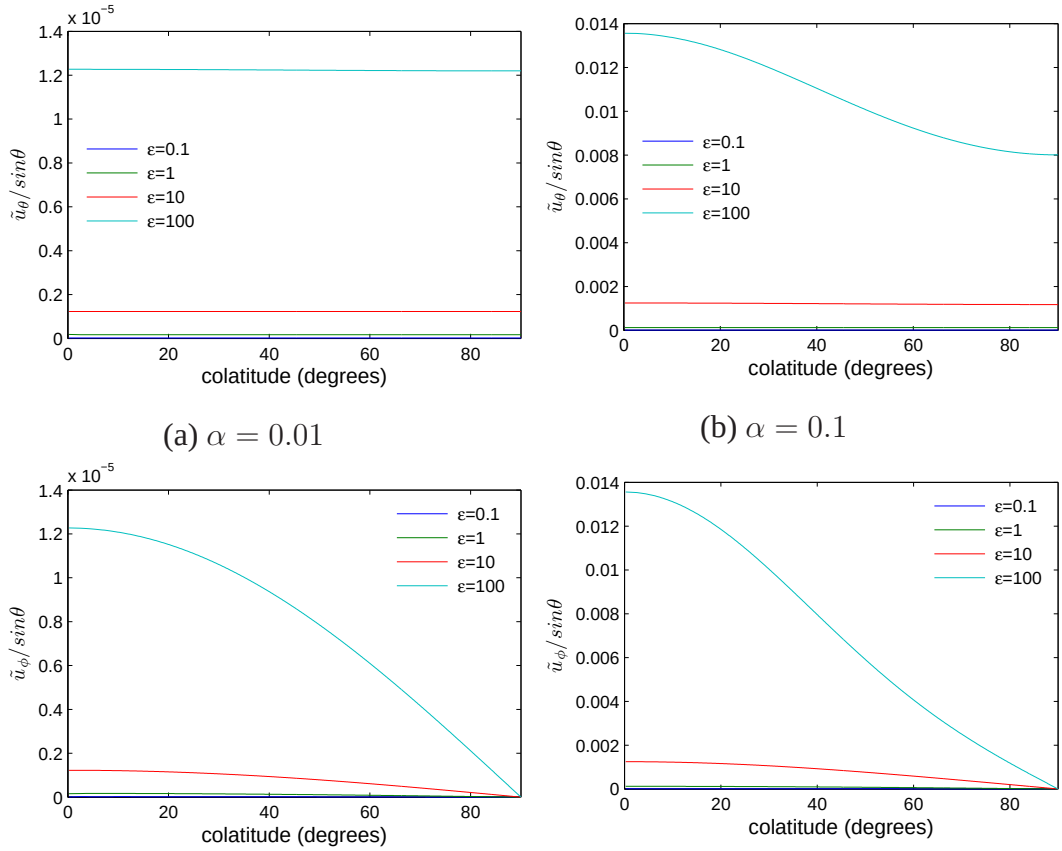

(a) $\alpha = 0.01$ (b) $\alpha = 0.1$

(c) $\alpha = 0.01$ (d) $\alpha = 0.1$

Figure 4.32: At the top, the northward velocity for the anomalous magnetic Rossby mode with $m = 1$ and $N = 50$. The azimuthal velocity at the bottom, with different values of ϵ.

The scaled height $\tilde{\eta}\epsilon^{1/2}$ is plotted in the figure 4.33, the amplitudes are small but it increases with α. In these plots, it is clear that this wave is not equatorially trapped.

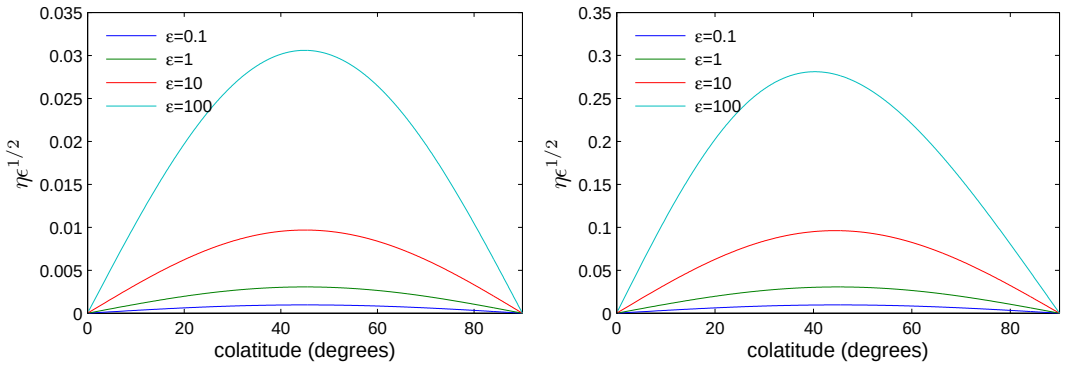

(a) $\alpha = 0.01$ (b) $\alpha = 0.1$

Figure 4.33: Scaled height $\eta\epsilon^{1/2}$ for the anomalous magnetic Rossby mode with $m = 1$ and $N = 50$, with different values of ϵ.

For the anomalous mode the magnetic field behaves differently from the slow magnetic Rossby modes ($n \geq 2$), as we can see in figure 4.34. The northward component of the field $\tilde{b}_\theta$ has a shift of $90°$ with respect to the velocity $\tilde{u}_\theta$ and the amplitudes are higher, so when α increases. This anomalous mode is analysed in more detail in section 5.5 below.

4.4 Kelvin Waves

Generally, our numerical results provide three types of frequencies: gravity waves, fast and slow magnetic Rossby waves. The high frequency gravity waves travelling to the east has a mode that behaves differently when ϵ increases and becomes a Kelvin wave, as the theory of Longuet-Higgins (1968) predicted. In the case of the fluid is immersed in a weak field, i.e, α parameter is small, the eigenvalues for the Kelvin mode can also be predicted by Longuet-Higgins (1968) theory and the formula (3.42), the numerical values obtained for λ with the Matlab code are in table 4.15.

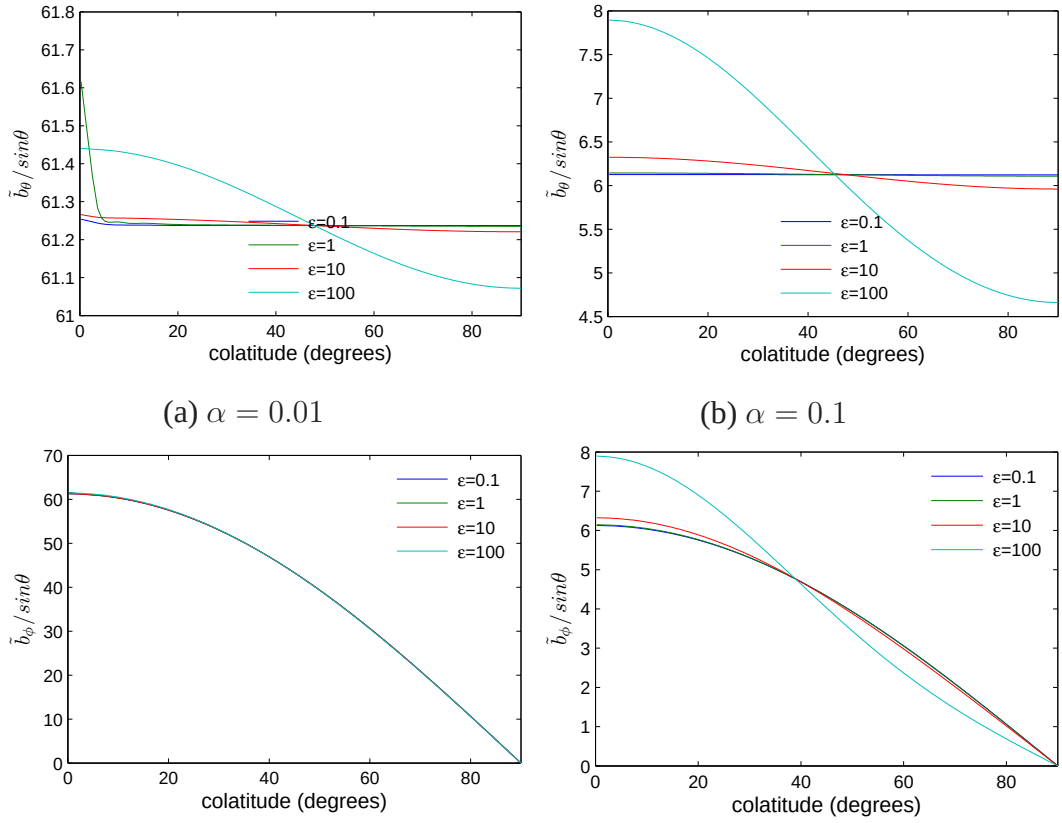

(a) $\alpha = 0.01$ (b) $\alpha = 0.1$

(c) $\alpha = 0.01$ (d) $\alpha = 0.1$

Figure 4.34: At the top, $\tilde{b}_\theta/\sin\theta$ for the anomalous magnetic Rossby mode with $m = 1$ and $N = 50$. The magnetic field $\tilde{b}_\phi/\sin\theta$ at the bottom, with different values of ϵ.

Table 4.15: Numerical results for eigenvalues λ that correspond to the Kelvin mode for $N = 50$ and $m = 1$. Waves travelling eastward.

α	10^{-3}	10^{-2}	10^{-1}	1	10^{1}	10^{2}	10^{3}
$\epsilon = 0.01$	13.9	13.9	13.9	13.9012	15.2263	100.5000	****
$\epsilon = 0.1$	4.2452	4.2452	4.2453	4.2649	10.4999	100.0500	****
$\epsilon = 1$	1.2307	1.2307	1.2323	1.4782	10.0050	****	****
$\epsilon = 10$	0.34457	0.34468	0.35618	1.0496	10.0050	****	****
$\epsilon = 100$	0.10263	0.10309	0.14257	1.005	****	****	****

When ϵ is large the waves are trapped at the equator and the Northward velocity becomes zero, as shown in figure 4.35, $\tilde{u}_\theta$ velocity is smaller compared with $\tilde{u}_\phi$. When we increase the magnetic field, the waves are more trapped, see figure 4.36, the Northward component of the magnetic field becomes zero.

The eigenvalues λ tends to $m\alpha$, when α and ϵ are large.

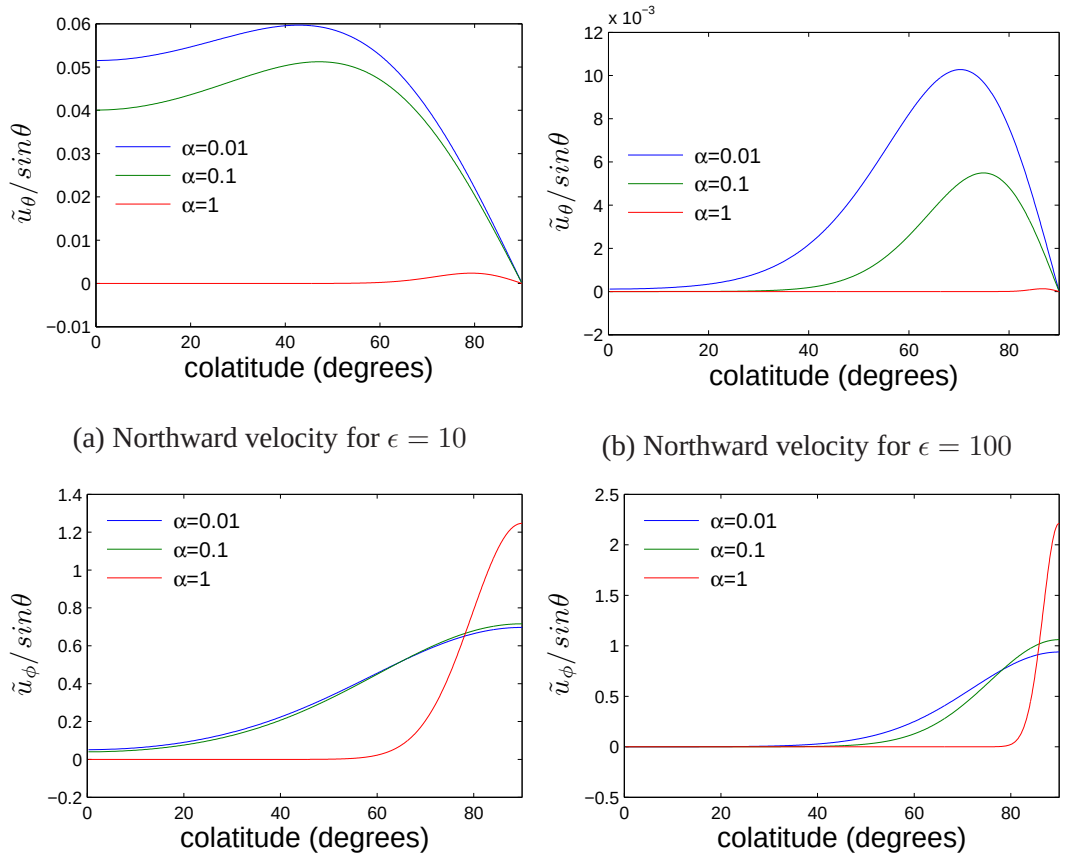

(a) Northward velocity for $\epsilon = 10$

(b) Northward velocity for $\epsilon = 100$

(c) Azimuthal velocity for $\epsilon = 10$

(d) Azimuthal velocity for $\epsilon = 100$

Figure 4.35: Numerical calculation of the northward and azimuthal velocities for different values of α for the Magneto Kelvin Mode with $m = 1$ and $N = 50$.

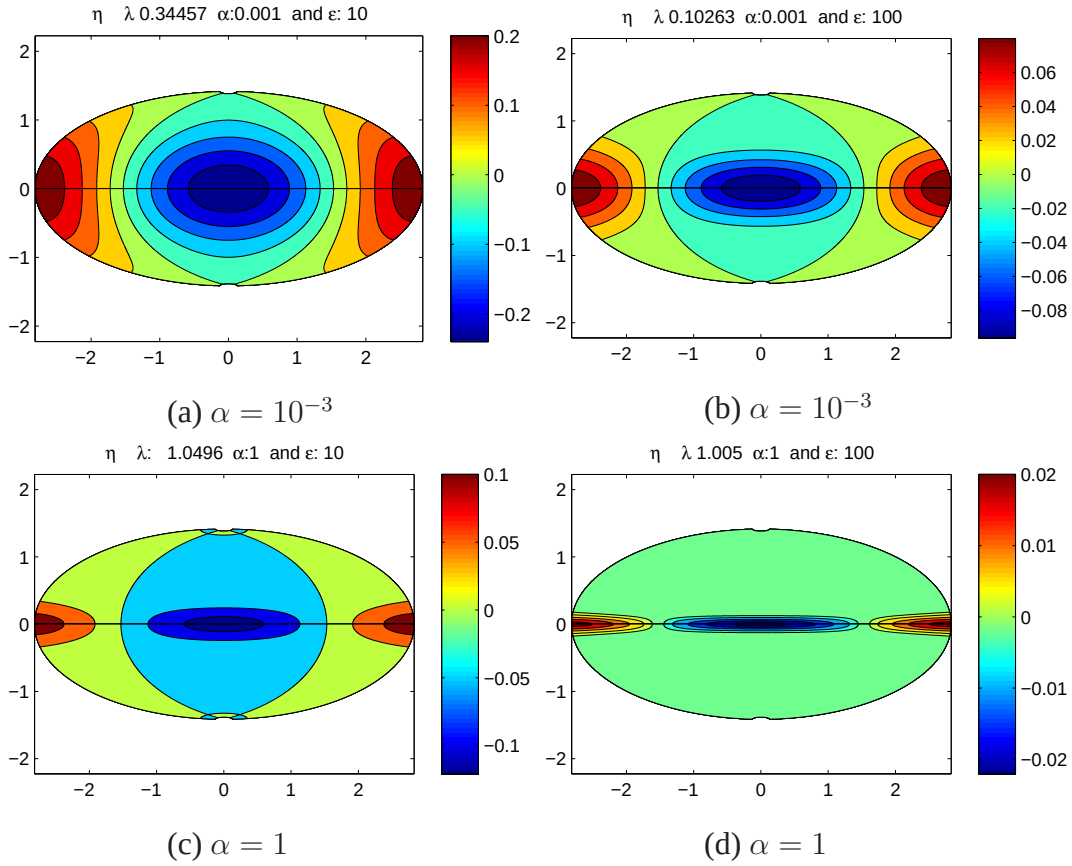

(a) $\alpha = 10^{-3}$ (b) $\alpha = 10^{-3}$

(c) $\alpha = 1$ (d) $\alpha = 1$

Figure 4.36: Numerical solution for the scaled height η with $\alpha = 10^{-3}$ in (a) and (b). Then, $\alpha = 1$ in (c) and (d), for magneto Kelvin mode travelling eastward with $m = 1$ and $N = 50$. In the first column $\epsilon = 10$ and $\epsilon = 100$ for the second one.

There is a new mode travelling to the west that has a frequency $\lambda \sim -m\alpha$ which appears for certain values of the magnetic parameter α, see table 4.16. This wave undergoes equatorial trapping and the velocity $\tilde{u}_\theta$ tends to zero when α or ϵ are large, as shown in figure 4.37, although, this Kelvin mode travelling westward is not always present when $\alpha > 100$. It seems possible that it cannot be resolved by the number of modes we include in our numerical scheme. This mode is considered further in section 5.6 below.

Table 4.16: Numerical results for eigenvalues λ that correspond to the Kelvin mode for $N = 50$ and $m = 1$. Waves travelling westward.

α	1	10^1	10^2
$\epsilon = 0.01$	****	-15.3966**	-100.5000
$\epsilon = 0.1$	****	-10.5013	****
$\epsilon = 1$	-1.6888**	-10.050	****
$\epsilon = 10$	-1.0516	-10.0050	****
$\epsilon = 100$	-1.0050	****	****

Values marked with ** correspond to the First mode($n = 1$) of MIG waves travelling westward.

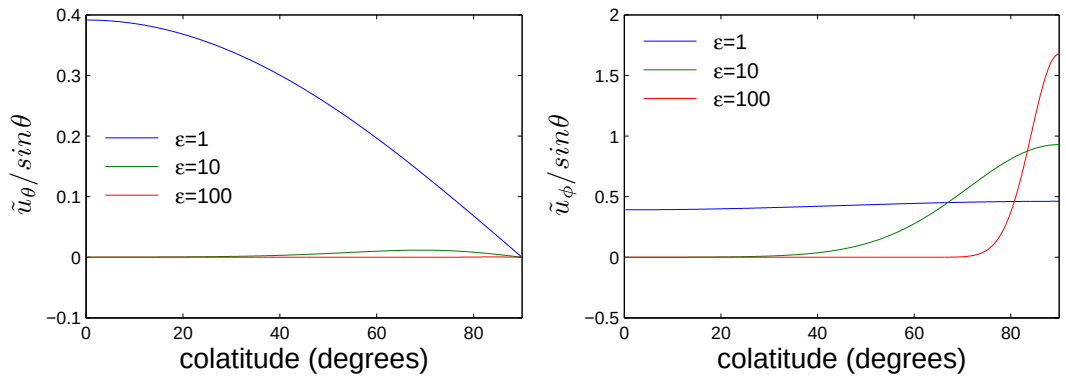

(a) Northward velocity

(b) Azimuthal velocity

Figure 4.37: Numerical solution for the velocity field with different values of ϵ for the Magneto Kelvin Mode travelling to the west with $\alpha = 1$, $m = 1$ and $N = 50$.

4.5 Summary

This chapter has reviewed the key aspects of the MHD waves for the shallow water system and the main results are summarized here. The analytical procedures and the asymptotic results for them are described in the next chapter.
As previously stated, MIG waves are always stable and the frequencies are superalfvénic, the waves are equatorially trapped for α or ϵ large. There are two exceptional Kelvin modes which are equatorially trapped also, and their motion is almost azimuthal.

The magnetic Rossby waves for $m = 1$, becomes unstable after $\alpha = 0.5$. The fast modes are equatorially trapped for α moderate and large values of ϵ. On the contrary, slow magnetic Rossby modes are not equatorially trapped. These modes always remain subalfvénic. A new anomalous slow mode travelling to the west is present. If $m \neq 1$ the magnetic Rossby waves are stable. For large ϵ and α their frequencies are subalfvénic and undergo polar trapping.

Chapter 5

Magnetohydrodynamics: Analytical Approach

In this chapter, we derive analytical expressions for the solutions valid in certain asymptotic regions of the parameter space, based on observations of the numerical results of chapter 4 to determine the behaviour and the values of the frequencies for each set of waves. In general these results are our original contribution to the solution of the problem. We start from the ordinary differential equation formula (2.64) for $\tilde{u}_\theta$, derived in chapter 2, i.e.

$$(1-\mu^2)\frac{\mathrm{d}^2\tilde{u}_\theta}{\mathrm{d}\mu^2}+\frac{2m^2}{[(\lambda^2-m^2\alpha^2)\epsilon(1-\mu^2)-m^2]}\mu\frac{\mathrm{d}\tilde{u}_\theta}{\mathrm{d}\mu}+\Big\{\epsilon(\lambda^2-m^2\alpha^2)$$
$$-\frac{m(\lambda+2m\alpha^2)}{(\lambda^2-m^2\alpha^2)}-\frac{\epsilon(\lambda+2m\alpha^2)^2\mu^2}{(\lambda^2-m^2\alpha^2)}-\frac{m^2}{(1-\mu^2)}-\frac{2\epsilon m(\lambda+2m\alpha^2)\mu^2}{[(\lambda^2-m^2\alpha^2)\epsilon(1-\mu^2)-m^2]}\Big\}\tilde{u}_\theta=0.$$

Based on observations from our numerical results, described in the previous chapter, we derive some asymptotic theories that can explain the behaviour of the waves in the limits when the parameters are large or small.

5.1 Asymptotic Theory for Magneto-Inertial Gravity Waves and Fast Magnetic Rossby Waves when $\epsilon\alpha^2 \gg 1$

The magneto-inertial gravity waves are trapped at the equator when ϵ is large for all values of the magnetic parameter, α, and the fast magnetic Rossby waves are equatorially trapped when ϵ is large and α has a moderate value around 0.1. This behaviour has been pointed out for hydrodynamic solutions by many authors (Matsuno, 1966, Longuet-Higgins, 1968). In general terms, equatorially trapped waves implies that the solution is confined to a region where $\mu = \cos\theta$ is small. Since μ is small and ϵ is large the factor $[\epsilon(\lambda^2 - m^2\alpha^2)(1-\mu^2) - m^2]$ tends to $\sim \epsilon(\lambda^2 - m^2\alpha^2)$. Then the equation (2.64) becomes:

$$\frac{d^2\tilde{u}_\theta}{d\mu^2} + \left\{(\lambda^2 - m^2\alpha^2)\epsilon - \frac{m(\lambda + 2m\alpha^2)}{(\lambda^2 - m^2\alpha^2)}\right\}\tilde{u}_\theta - \frac{\epsilon(\lambda + 2m\alpha^2)^2}{(\lambda^2 - m^2\alpha^2)}\mu^2\tilde{u}_\theta = 0. \qquad (5.1)$$

We introduce a scaling $\mu = \frac{1}{\sqrt{2}}\left[\frac{(\lambda^2 - m^2\alpha^2)}{\epsilon(\lambda+2m\alpha^2)^2}\right]^{1/4}\hat{\mu}$, and define a scale factor

$$s \equiv \sqrt{2}\left[\frac{\epsilon(\lambda + 2m\alpha^2)^2}{(\lambda^2 - m^2\alpha^2)}\right]^{1/4} \qquad \text{so} \qquad \hat{\mu} = s\mu.$$

Since the waves are equatorially trapped, the factor scale must be $s \gg 1$ for the asymptotic theory to be valid, if this condition is not satisfied the solution is discarded. For this scaling, the differential operator must be

$$\frac{d}{d\mu} = \sqrt{2}\left[\frac{\epsilon(\lambda + 2m\alpha^2)^2}{(\lambda^2 - m^2\alpha^2)}\right]^{1/4}\frac{d}{d\hat{\mu}},$$

and the rescaled equation becomes

$$\frac{d^2\tilde{u}_\theta}{d\hat{\mu}^2} + \frac{1}{2}\left[\frac{(\lambda^2 - m^2\alpha^2)}{\epsilon(\lambda + 2m\alpha^2)^2}\right]^{1/2}\left\{(\lambda^2 - m^2\alpha^2)\epsilon - \frac{m(\lambda + 2m\alpha^2)}{(\lambda^2 - m^2\alpha^2)}\right\}\tilde{u}_\theta - \frac{1}{4}\hat{\mu}^2\tilde{u}_\theta = 0. \qquad (5.2)$$

This equation corresponds to the standard Parabolic Cylinder Differential equation, where

$$\frac{1}{2}\left[\frac{(\lambda^2 - m^2\alpha^2)}{\epsilon(\lambda + 2m\alpha^2)^2}\right]^{1/2}\left\{(\lambda^2 - m^2\alpha^2)\epsilon - \frac{m(\lambda + 2m\alpha^2)}{(\lambda^2 - m^2\alpha^2)}\right\} = \nu + \frac{1}{2}, \qquad (5.3)$$

for $\nu = 0, 1, 2....$ The solutions of $\tilde{u}_\theta$ for this differential equation are given by $D_\nu(\hat{\mu})$ and $\mathcal{D}_{-\nu-1}(\hat{\mu}e^{i\pi/2})$, where $\mathcal{D}_\nu(\hat{\mu})$ is the parabolic cylinder function, defined by Abramowitz and Stegun (1964). The $\mathcal{D}_{-\nu-1}(\hat{\mu}e^{i\pi/2})$ solution goes to infinity at large $\hat{\mu}$ and so must be discarded. The first solutions of $D_\nu(\hat{\mu})$ are, for $\nu = 0$,

$$\tilde{u}_\theta = e^{-\frac{1}{4}s^2\mu^2}.$$

When $\nu = 1$, the solution will be

$$\tilde{u}_\theta = s\mu e^{-\frac{1}{4}s^2\mu^2},$$

and for $\nu = 2$, the function must be

$$\tilde{u}_\theta = (s^2\mu^2 - 1)e^{-\frac{1}{4}s^2\mu^2}.$$

The asymptotic solutions for $\nu = 0$ are plotted in the figure 5.1. For high values of α and ϵ the eigenfunctions become trapped at the equator.

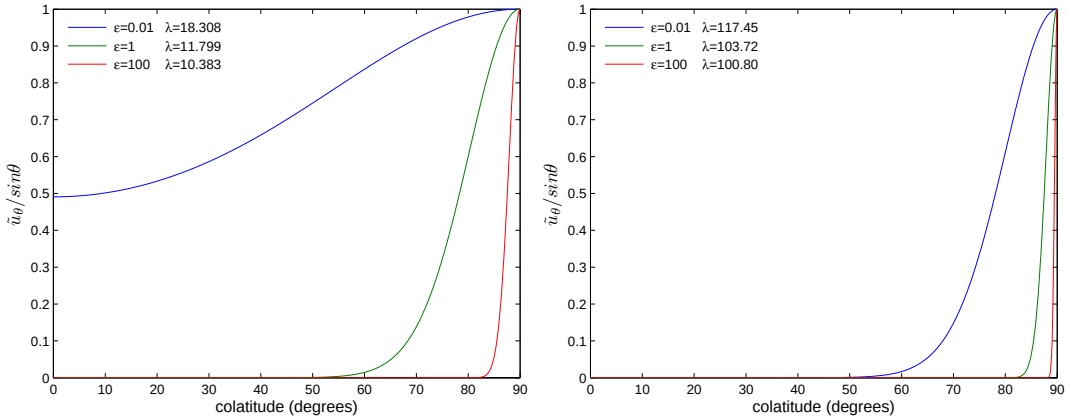

Figure 5.1: Asymptotic even solutions for equation (5.1) for different values of α, for $\nu = 0$ with $m = 1$. The first panel corresponds to $\alpha = 10$, and $\alpha = 100$ for the second one.

The eigenvalues calculated with the numerical solution of formula 5.3 agree with the numerical calculations made previously in chapter 4. When the eigenfunctions

are equatorially trapped, hence the factor scale must be much greater than 1. The eigenfunctions in figure 5.1 describe perfectly the equatorially trapped behaviour, for ϵ greater than 0.01 when $\alpha = 10$. In order to calculate these eigenfunctions, the truncation N must be very large. For example, if $\alpha = 10$ and $\epsilon = 100$, the scale factor is ~ 38.8. When $\alpha = 100$ and $\epsilon = 100$ the factor will be ~ 178.1. This means that we need a truncation number, N, which is 5 times larger than that when α is 10 in order to resolve the solutions. Our code with the method of the eigenvalues in Matlab is not able to compute this because the matrices are too large, but at large α or ϵ the asymptotic theory is very accurate.

5.1.1 Dispersion relation and eigenvalues

The dispersion relation of the waves gives λ as a function of ϵ, m and α, which are given parameters in our case. It can be found that expression (5.3) can be written as

$$\epsilon(\lambda^2 - m^2\alpha^2)^2 - m(\lambda + 2m\alpha^2) = (2\nu + 1)(\lambda + 2m\alpha^2)(\lambda^2 - m^2\alpha^2)^{1/2}\epsilon^{1/2}. \quad (5.4)$$

This expression must have $\lambda \sim \pm m\alpha$, as is shown in the numerical results, in the limit when $\epsilon\alpha^2 \gg 1$.

Let $\lambda = \delta + m\alpha$, and $\delta \ll m\alpha$. In this approximation, $(\lambda^2 - m^2\alpha^2) = (\lambda - m\alpha)(\lambda + m\alpha) = \delta(\delta + 2m\alpha) \sim 2m\alpha\delta$.

Since $\delta \ll m\alpha$, to leading order $(\alpha \gg 1)$, equation (5.4) becomes

$$\delta^2 - (2\nu + 1)\left(\frac{\alpha}{2m\epsilon}\right)^{1/2}\delta^{1/2} - \frac{1}{2\epsilon} = 0. \quad (5.5)$$

Neglecting the last term, because ϵ is large, we have

$$\delta^2 - (2\nu + 1)\left(\frac{\alpha}{2m\epsilon}\right)^{1/2}\delta^{1/2} = 0. \quad (5.6)$$

Therefore, the approximate solution for δ is

$$\delta = (2\nu + 1)^{2/3}\left(\frac{\alpha}{2m\epsilon}\right)^{1/3}. \quad (5.7)$$

These are a sequence of symmetric and antisymmetric solutions with respect to the equator. The dispersion relation for large ϵ becomes

$$\lambda = (2\nu+1)^{2/3}\left(\frac{\alpha}{2m\epsilon}\right)^{1/3} + m\alpha. \tag{5.8}$$

The solutions for waves travelling westward in this approximation must be the same as for eastward waves but with an opposite sign by taking $\lambda = -\delta - m\alpha$.
In order to obtain more accurate results for the eigenvalues with the formula (5.8), we have to improve our first order approximation by going to higher order.

Second order approximation for the solutions of equation (5.3)**: MIG waves travelling eastward**

Initially, we arrange equation (5.3), to be solved analytically for the case of large α and/or large ϵ

$$(\lambda^2 - m^2\alpha^2)^{1/2}\left\{(\lambda^2 - m^2\alpha^2)\epsilon - \frac{m(\lambda+2m\alpha^2)}{(\lambda^2-m^2\alpha^2)}\right\} = (2\nu+1)\epsilon^{1/2}(\lambda+2m\alpha^2). \tag{5.9}$$

Substitute $\lambda = m\alpha+\delta$, for eastward propagating waves, where δ is very small compared with $m\alpha$, motivated by the numerical results in chapter 4. The factors become

$$\lambda^2 - m^2\alpha^2 \sim 2m\alpha\delta\Big(1+\frac{\delta}{2m\alpha}\Big), \qquad \text{and} \qquad \lambda + 2m\alpha^2 \sim 2m\alpha^2\Big(1+\frac{1}{2\alpha}+\frac{\delta}{2m\alpha^2}\Big).$$

After a sequence of algebraic steps, the equation (5.9) turns into

$$\delta^2\left(1+\frac{3\delta}{4m\alpha}\right) - \frac{1}{2\epsilon}\left(1+\frac{1}{2\alpha}+\frac{\delta}{2m\alpha^2}\right)\left(1-\frac{\delta}{4m\alpha}\right) = \frac{(2\nu+1)\alpha^{1/2}}{(2m\epsilon)^{1/2}}\delta^{1/2}\left(1+\frac{1}{2\alpha}+\frac{\delta}{2m\alpha^2}\right). \tag{5.10}$$

Retaining the order $\mathcal{O}(1)$ terms of the expression (5.10), the second term and terms of order $\mathcal{O}(\alpha^{-1})$ are neglected. Hence, to first order in $\delta \sim \delta_0$, we have

$$\delta_0^2 = \frac{(2\nu+1)\alpha^{1/2}}{(2m\epsilon)^{1/2}}\delta_0^{1/2}. \tag{5.11}$$

In the first order approximation, an expression for δ is

$$\delta_0 = \frac{(2\nu+1)^{3/2}\alpha^{1/3}}{(2m\epsilon)^{1/3}}, \tag{5.12}$$

and so the δ term represents the deviation from the Alfvén speed which increases with α and decreases with ϵ. This is also the formula (5.7) obtained previously.

In a second order approximation for δ, we add a smaller amount δ_1 and neglect terms with $\mathcal{O}(\alpha^{-2})$,

$$\delta = \delta_0 + \delta_1 \qquad \text{and} \qquad \frac{\delta}{2m\alpha^2} \ll \frac{1}{2\alpha}.$$

Substituting $\delta = \delta_0 + \delta_1$ and $\delta^2 = \delta_0^2\left(1 + \frac{2\delta_1}{\delta_0}\right)$ into the equation (5.10), we obtain

$$\delta_0^2\left(1+\frac{2\delta_1}{\delta_0}\right)\left[1+\frac{3\delta_0}{4m\alpha}\left(1+\frac{\delta_1}{\delta_0}\right)\right] - \frac{1}{2\epsilon}\left(1+\frac{1}{2\alpha}\right)\left[1+\frac{\delta_0}{4m\alpha}\left(1+\frac{\delta_1}{\delta_0}\right)\right] = \delta_0^2\left(1+\frac{1}{2\alpha}\right)\left(1+\frac{\delta_1}{2\delta_0}\right). \tag{5.13}$$

Neglecting the terms $\mathcal{O}(\epsilon^{-1}\alpha^{-1})$, $\mathcal{O}(\delta_1\delta_0\alpha^{-1})$ and $\mathcal{O}(\delta_1\delta_0^2\alpha^{-1})$ or similar higher orders, equation (5.13) reduces to

$$\frac{3\delta_0^3}{m\alpha} + \frac{3}{2}\delta_0\delta_1 - \frac{1}{2\epsilon} = \frac{\delta^2}{2\alpha}. \tag{5.14}$$

Solving this equation for δ_1

$$\delta_1 = \frac{1}{3\epsilon\delta_0} + \frac{\delta_0}{3\alpha} - \frac{\delta_0^2}{2m\alpha}. \tag{5.15}$$

substituting δ_0 into the equation (5.15), the expression becomes

$$\delta_1 = \frac{(2m)^{1/3}}{3(2\nu+1)^{2/3}\epsilon^{2/3}\alpha^{1/3}} + \frac{(2\nu+1)^{2/3}}{3(2m\epsilon)^{1/3}\alpha^{2/3}} - \frac{(2\nu+1)^{4/3}}{2m\alpha^{1/3}(2m\epsilon)^{2/3}}. \tag{5.16}$$

When ϵ and α are large, the dispersion relation for magneto-inertial gravity waves propagating to the east is

$$\lambda = m\alpha + (2\nu+1)^{2/3}\left(\frac{\alpha}{2m\epsilon}\right)^{1/3} + \frac{(2m)^{1/3}}{3(2\nu+1)^{2/3}\epsilon^{2/3}\alpha^{1/3}}\left[1 - \frac{3(2\nu+1)^2}{4m^2}\right] + \frac{(2\nu+1)^{2/3}}{3(2m\epsilon)^{1/3}\alpha^{2/3}}. \tag{5.17}$$

which is accurate to $\mathcal{O}(\alpha^{-2/3})$. The value of λ is calculated with the formula (5.17) for $m = 1$ and $\nu = 0$ reported in the table 5.1; the results are in agreement with the numerical results of table 4.3 of chapter 4, except for the first value in the first row, because this solution is not equatorially trapped and does not satisfy the condition $\epsilon\alpha^2 >> 1$.

Table 5.1: Calculation of λ with the formula (5.17) for $\nu = 0$ and $m = 1$.

α	10^1	10^2	10^3
$\epsilon = 0.01$	19.2515	117.6441	1037.1
$\epsilon = 0.1$	14.0330	108.0685	1017.2
$\epsilon = 1$	11.8157	103.7189	1008.0
$\epsilon = 10$	10.8307	101.7205	1003.7
$\epsilon = 100$	10.3829	100.7974	1001.7

Second order approximation for the solutions of equation 5.3: MIG waves travelling westward

We follow the same mathematical steps as in the previous section. Equation (5.3) is solved analytically for $\epsilon\alpha^2 \gg 1$, when $\lambda = -m\alpha - \delta$, where δ is very small compared to $m\alpha$. This behaviour is also observed in westward propagating MIG waves, in chapter 4. Hence, the factors are

$$\lambda^2 - m^2\alpha^2 \sim 2m\alpha\delta\Big(1 + \frac{\delta}{2m\alpha}\Big), \qquad \text{and} \qquad \lambda + 2m\alpha^2 \sim 2m\alpha^2\Big(1 - \frac{1}{2\alpha} - \frac{\delta}{2m\alpha^2}\Big).$$

Substituting the expressions in the equation (5.9), we obtain

$$\delta^2\left(1+\frac{3\delta}{4m\alpha}\right)-\frac{1}{2\epsilon}\left(1-\frac{1}{2\alpha}-\frac{\delta}{2m\alpha^2}\right)\left(1-\frac{\delta}{4m\alpha}\right) = \frac{(2\nu+1)\alpha^{1/2}}{(2m\epsilon)^{1/2}}\delta^{1/2}\left(1-\frac{1}{2\alpha}-\frac{\delta}{2m\alpha^2}\right). \tag{5.18}$$

The first order approximation neglects the second term and terms of order $\mathcal{O}(\alpha^{-1})$ in the expression (5.18). Therefore, to first order in $\delta \sim \delta_0$, we have the same expression as for

eastward propagating MIG waves

$$\delta_0^2 = \frac{(2\nu+1)\alpha^{1/2}}{(2m\epsilon)^{1/2}}\delta_0^{1/2}. \tag{5.19}$$

The deviation from the Alfvén speed, δ, in the first order approximation is again

$$\delta_0 = \frac{(2\nu+1)^{3/2}\alpha^{1/3}}{(2m\epsilon)^{1/3}}. \tag{5.20}$$

Now, a second order approximation for δ is developed here, we add a smaller amount δ_1 and neglect terms with $\mathcal{O}(\alpha^{-2})$,

$$\delta = \delta_0 + \delta_1 \qquad \text{and} \qquad \frac{\delta}{2m\alpha^2} \ll \frac{1}{2\alpha}.$$

The second order equation for $\delta = \delta_0 + \delta_1$ and $\delta^2 = \delta_0^2\left(1 + \frac{2\delta_1}{\delta_0}\right)$ turns the equation (5.18) into

$$\delta_0^2\left(1+\frac{2\delta_1}{\delta_0}\right)\left[1+\frac{3\delta_0}{4m\alpha}+\frac{3\delta_1}{4m\alpha}\right]-\frac{1}{2\epsilon}\left(1-\frac{1}{2\alpha}\right)\left[1-\frac{\delta_0}{4m\alpha}-\frac{\delta_1}{4m\alpha}\right] = \delta_0^2\left(1-\frac{1}{2\alpha}\right)\left(1+\frac{\delta_1}{2\delta_0}\right). \tag{5.21}$$

The terms $\mathcal{O}(\epsilon^{-1}\alpha^{-1})$, $\mathcal{O}(\delta_1\delta_0\alpha^{-1})$ and $\mathcal{O}(\delta_1\delta_0^2\alpha^{-1})$ or similar higher orders will be neglected here and the equation (5.21) reduces to

$$\frac{3\delta_0^3}{4m\alpha} + \frac{3}{2}\delta_0\delta_1 - \frac{1}{2\epsilon} = -\frac{\delta_0^2}{2\alpha}. \tag{5.22}$$

Consequently, the expression for δ_1 is

$$\delta_1 = \frac{1}{3\epsilon\delta_0} - \frac{\delta_0}{3\alpha} - \frac{\delta_0^2}{2m\alpha}. \tag{5.23}$$

Substituting δ_0 into the equation (5.23), the expression becomes

$$\delta_1 = \frac{(2m)^{1/3}}{3(2\nu+1)^{2/3}\epsilon^{2/3}\alpha^{1/3}} - \frac{(2\nu+1)^{2/3}}{3(2m\epsilon)^{1/3}\alpha^{2/3}} - \frac{(2\nu+1)^{4/3}}{(2m)^{5/2}\epsilon^{2/3}\alpha^{1/3}}. \tag{5.24}$$

In the limit of large ϵ and α, the MIG waves are equatorially trapped and the dispersion relation for the westward Magneto-inertial gravity waves is

$$\lambda = -m\alpha-(2\nu+1)^{2/3}\left(\frac{\alpha}{2m\epsilon}\right)^{1/3}-\frac{(2m)^{1/3}}{3(2\nu+1)^{2/3}\epsilon^{2/3}\alpha^{1/3}}\left[1-\frac{3(2\nu+1)^2}{4m^2}\right]+\frac{(2\nu+1)^{2/3}}{3(2m\epsilon)^{1/3}\alpha^{2/3}}, \tag{5.25}$$

which is the analogous to the formula (5.17) for waves propagating eastward except that for the westward waves the last term is also positive, which gives a difference in the values between eastward and westward frequencies.

Table 5.2 shows a comparison between the results of the formula (5.25) and the numerical calculations in table 4.4 in chapter 4. The results are accurate and provide a good asymptotic formula when the code is not able to calculate the eigenvalues, except for the first value in the first row which does not satisfy the condition $\epsilon\alpha^2 \gg 1$ and the solution is not equatorially trapped.

Table 5.2: Calculation of λ with the formula (5.25) for $\nu = 0$ and $m = 1$.

α	10^1	10^2	10^3
$\epsilon = 0.01$	-18.7224	-117.5301	-1037.1
$\epsilon = 0.1$	-13.7874	-108.0155	-1017.1
$\epsilon = 1$	-11.7017	-103.6944	-1007.9
$\epsilon = 10$	-10.7777	-101.7091	-1003.7
$\epsilon = 100$	-10.3584	-100.7921	-1001.7

Second order approximation for the solutions of equation 5.3: Fast magnetic Rossby waves travelling westward.

The fast magnetic Rossby waves tend to be confined at the equator for large ϵ and also moderate values of α, as demonstrated by the numerical results in chapter 4. The values of α for equatorial trapping are between 0.1 and 0.5. After $\alpha = 0.5$, the frequency of the wave becomes subalfvénic and complex at certain point (as discussed in the next chapter). In the regime $\alpha < 0.5$, λ remains superalfvénic and $|\lambda| > m\alpha$, except when α is near 0.5, this behaviour will be discussed later in section 5.2. Since, the fast magnetic Rossby waves have these features, the factor $(\lambda^2 - m^2\alpha^2)$ is always positive and $m(\lambda + 2m\alpha^2)$

is always negative. Hence

$$(\lambda^2 - m^2\alpha^2)\epsilon \ll -\frac{m(\lambda + 2m\alpha^2)}{(\lambda^2 - m^2\alpha^2)}. \tag{5.26}$$

Then, the equation (5.3) reduces to

$$-\frac{1}{2}\left[\frac{(\lambda^2 - m^2\alpha^2)}{\epsilon(\lambda + 2m\alpha^2)^2}\right]^{1/2} \frac{m(\lambda + 2m\alpha^2)}{(\lambda^2 - m^2\alpha^2)} = \nu + \frac{1}{2}. \tag{5.27}$$

Simplifying the equation, the result is

$$\lambda^2 - m^2\alpha^2 = \frac{m^2}{(2\nu + 1)^2\epsilon}. \tag{5.28}$$

The quadratic (5.28) has two roots, only the negative root is valid, because the condition (5.26) must be satisfied. The dispersion relation for fast magnetic Rossby waves is therefore

$$\lambda = -m\alpha - \frac{m}{2\epsilon\alpha(2\nu + 1)^2}. \tag{5.29}$$

Using the formula (5.29), we obtain reasonable values of λ, when ϵ is large but the values for $\epsilon \leq 10$ are inaccurate, see table 5.3. This discrepancy can be attributed to the fact that for $\epsilon \leq 10$ the waves are not equatorially trapped and this theory does not apply in this case.

Table 5.3: Asymptotic solution for λ obtained with the equation (5.29) for $\nu = 1$ and the numerical calculation for $N = 50$. In both cases: $\alpha = 0.1$ and $m = 1$.

	Equation (5.29)	λ_{num}
$\epsilon = 1$	-0.655555	-0.1886
$\epsilon = 10$	-0.1555556	-0.1408
$\epsilon = 100$	-0.1055556	-0.1054

Numerical solutions for equation 5.4

In order to solve equation (5.4) numerically, we square both sides of this equation, and obtain an eighth order equation, for solving with MATLAB, finding the roots of the

polynomial. Then, the equation is

$$\begin{aligned}\epsilon^2\lambda^8 - 4m^2\alpha^2\epsilon^2\lambda^6 - 2m\epsilon\lambda^5 + [6m^4\alpha^4\epsilon - 4m^2\alpha^2\epsilon - (2\nu+1)^2\epsilon]\lambda^4 \\ +[4m^3\alpha^2\epsilon - 4(2\nu+1)^2 m\alpha^2\epsilon]\lambda^3 \\ +[m^2 - 4m^6\alpha^6\epsilon^2 + 8m^4\alpha^4\epsilon + (2\nu+1)^2 m^2\alpha^2\epsilon(1-4\alpha^2)]\lambda^2 \\ +[4m^3\alpha^2 - 2m^5\alpha^4\epsilon + 4(2\nu+1)^2 m^3\alpha^4\epsilon]\lambda^1 \\ +[m^8\alpha^8\epsilon^2 - 4m^6\alpha^6\epsilon + 4m^4\alpha^4 + 4(2\nu+1)^2 m^4\alpha^6\epsilon] = 0. \qquad (5.30)\end{aligned}$$

In table 5.4 the positive root of the equation (5.30) is reported, this is the second Magneto-inertial gravity mode ($n = 2$) for $m = 1$. We compare the results of this table for the asymptotic theory with the eigenvalues obtained with the eigenvalues code of Matlab, see table 4.3, there is good agreement between this asymptotic solution and the numerical method. Although there is a difference in the values of λ (underlined values) when $\alpha < 0.1$ and $\epsilon < 1$, this inconsistency may be due to that the scale factor is less than 1, see table 5.5, and also small $\epsilon\alpha^2 < 1$ then this theory is not applicable in this regime.

Table 5.4: Eigenvalues λ for different values of α and ϵ, as numerical results of solving equation (5.30) for $\nu = 0$ and $m = 1$. Asymptotic solution.

α	10^{-3}	10^{-2}	10^{-1}	1	10^{1}	10^{2}	10^{3}
$\epsilon = 0.01$	5.3549	5.355	5.3637	6.0784	18.308	117.45	1037.1
$\epsilon = 0.1$	2.6371	2.6372	2.6475	3.3806	13.896	108.05	1017.2
$\epsilon = 1$	1.3247	1.3249	1.3381	2.102	11.799	103.72	1007.9
$\epsilon = 10$	0.68056	0.68075	0.69917	1.5044	10.829	101.72	1003.7
$\epsilon = 100$	0.35771	0.358	0.38501	1.2303	10.383	100.8	1001.7

Table 5.5: Scale factor for different values of α and ϵ, of the first numerical solution of equation (5.30) for $\nu = 0$ and $m = 1$.

α	10^{-3}	10^{-2}	10^{-1}	1	10^{1}	10^{2}	10^{3}
$\epsilon = 0.01$	0.44721	0.44722	0.44809	0.51911	1.6873	8.0814	38.166
$\epsilon = 0.1$	0.79527	0.7953	0.79855	1.0265	3.7445	17.63	82.486
$\epsilon = 1$	1.4142	1.4143	1.4267	2.1065	8.2243	38.226	177.98
$\epsilon = 10$	2.5149	2.5154	2.5638	4.4406	17.914	82.612	383.71
$\epsilon = 100$	4.4722	4.4743	4.6676	9.4946	38.813	178.24	826.94

Figure 5.2 shows the scale factor for different values of the magnetic parameter α. In the limit of α small the scale factor is $\sqrt{2}\epsilon^{1/4}$ and for α large it is proportional to $(\epsilon\alpha^3)^{1/4}$.

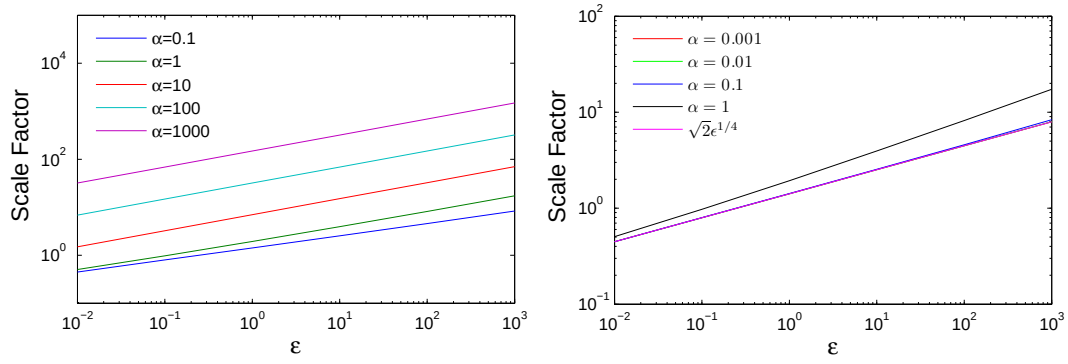

Figure 5.2: Plot of the scale factor of the first solution for different values of α, for $\nu = 0$ with $m = 1$. The first column corresponds to calculations for $\alpha = 0.1$ to $\alpha = 1000$, the second one shows the results for small values of α.

There are 8 solutions for equation (5.30) but just 4 solutions are valid. We take the solutions where $A = \nu + 1/2$

$$A = \frac{1}{2}\left[\frac{(\lambda^2 - m^2\alpha^2)}{\epsilon(\lambda + 2m\alpha^2)^2}\right]^{1/2}\left\{(\lambda^2 - m^2\alpha^2)\epsilon - \frac{m(\lambda + 2m\alpha^2)}{(\lambda^2 - m^2\alpha^2)}\right\}.$$

Three type of waves can be identified: MIG waves travelling eastward and westward and the fast magnetic Rossby wave travels to the west. Particularly, the fast magnetic Rossby mode will disappear when $\alpha > 0.1$, and our solutions reduce to two real roots, the table 5.6 illustrates this point clearly. When α greater than 1, this is evident from the numerical results (section 4.2) that magnetic Rossby waves experience confinement at the poles.

Table 5.6: Numerical solution of the eigenvalues λ solving equation (5.30) when $\epsilon = 100$ and $m = 1$.

α	0.1	10
	0.38501	10.383
$\nu = 0$	-0.26206	-10.358
	-0.15025	
	0.58571	10.768
$\nu = 1$	-0.53412	-10.717
	-0.10542	

Table 5.7: Eigenvalues λ calculated with the method described in section 2.4 with $\epsilon = 100$, $m = 1$ and $N = 50$.

α	0.1	10
	0.4042	10.383
$n = 2$	-0.2877	-10.358
	-0.1020	
	0.5959	10.769
$n = 3$	-0.5322	-10.717
	-0.1054	

In table 5.7 we compare the numerical solution of equation (5.30) with the eigenvalues obtained with our numerical method (section 2.4), the values in color blue are fast

magnetic Rossby modes. There is again agreement between this asymptotic solution and the eigenvalues numerical method if the value of the scale factor is $s \gg 1$.

5.2 Behaviour of Fast Magnetic Rossby Waves near $\alpha = 0.5$

As mentioned in chapter 4, there is a value of α that divides two different regimes where magnetic Rossby modes change from stable to unstable behaviour. So, the following is a mathematical description of the solutions when $\alpha = 0.5$. To determine the behaviour when α is near 0.5, we consider $\alpha = 1/2 + \hat{\alpha}$ where $|\hat{\alpha}| \ll 1$, i.e. very close to $\alpha = 1/2$ and $\lambda = -m/2 + \hat{\delta}$ when $|\hat{\delta}| \ll 1$. We also assume $\epsilon\hat{\alpha} \ll 1$ and $\epsilon\hat{\delta} \ll 1$. Then the factors of the equation (2.64) become

$$\lambda^2 - m^2\alpha^2 \sim -m^2\hat{\alpha} - m\hat{\delta} + \mathcal{O}(\hat{\alpha}^2),$$

$$\lambda + 2m\alpha^2 \sim \hat{\delta} + 2m\hat{\alpha} + \mathcal{O}(\hat{\alpha}^2),$$

$$(\lambda^2 - m^2\alpha^2)\epsilon(1-\mu^2) \ll m^2.$$

Because m is order 1, the differential equation (2.64) reduces to

$$(1-\mu^2)\frac{d^2\tilde{u}_\theta}{d\mu^2} - 2\mu\frac{d\tilde{u}_\theta}{d\mu} + \left\{\frac{(\hat{\delta} + 2m\hat{\alpha})}{(\hat{\delta} + m\hat{\alpha})} - \frac{m^2}{(1-\mu^2)} + \mathcal{O}(\hat{\alpha})\right\}\tilde{u}_\theta = 0. \tag{5.31}$$

This is the Associated Legendre differential equation, with solutions

$$\tilde{u}_\theta = P_n^m(\mu) \qquad \text{with} \qquad n(n+1) = \frac{(\hat{\delta} + 2m\hat{\alpha})}{(\hat{\delta} + m\hat{\alpha})}.$$

Hence,

$$\hat{\delta} = -\frac{m\hat{\alpha}[n(n+1) - 2]}{[n(n+1) - 1]}. \tag{5.32}$$

Therefore, near $\alpha = 0.5$, the dispersion relation for fast magnetic Rossby waves is:

$$\lambda = -\frac{m}{2} - \frac{m\hat{\alpha}[n(n+1) - 2]}{[n(n+1) - 1]}. \tag{5.33}$$

Note that, if $n = 1$, then $\hat{\delta} = 0$. In particular this case is singular, we need to go to higher order.

Let us now consider $n = 2$ and $m = 1$ which illustrates the behaviour clearly, so

$$\hat{\delta} = -\frac{4}{5}\hat{\alpha}.$$

Consequently, in the neighbourhood of $\alpha = 0.5$, the dispersion relation for fast magnetic Rossby waves is:

$$\lambda = -\frac{1}{2} - \frac{4}{5}(\frac{1}{2} - \alpha). \tag{5.34}$$

The numerical results for λ are reported in the table 5.8. If $\alpha = 0.498$ the formula (5.34) gives $\lambda = -0.4984$ and for $\alpha = 0.502$ then $\lambda = -0.5016$. These values are independent of ϵ. The asymptotic formula (5.34) agrees well with the numerical results, especially when ϵ is small, see table 5.8.

Table 5.8: Numerical results for eigenvalues λ with $n = 2$, $m = 1$ and $N = 50$.

α	0.498	0.502
$\epsilon = 0.01$	-0.4984001	-0.5016001
$\epsilon = 1$	-0.4983995	-0.5015995
$\epsilon = 100$	-0.4983422	-0.5015300

5.3 Asymptotic Theory for Stable Modes Trapped at the Pole $m \geq 3$

Let us now consider the behaviour of stable modes when the magnetic parameter, α, is large. The theory explains the limit case for the eigenvalues and analytic solutions for the eigenfunctions. Fast magnetic Rossby waves and slow magnetic Rossby waves are

expected to be unstable when $\alpha > 0.5$ and $m = 1$. If m is different from 1 the magnetic Rossby modes are stable and the values of the eigenvalues and the eigenfunctions can be predicted for this problem for $m \geq 3$. The case $m = 2$ is dealt with in section 5.4 below. In general, the magnetic Rossby waves are the result of balance between the Coriolis force and the magnetic tension and have a magnetic origin. They undergo polar trapping for large α and ϵ, and the waves become concentrated in a small region near the poles. The eigenfunction for a fast magnetic Rossby wave ($m = 3$) illustrates the polar trapping, in figure 5.3, waves are more trapped as ϵ and α increase. Heng and Spitkovsky (2009) have described this feature for magnetostrophic modes, in their formulation for shallow water model with a basic state for the magnetic field as a radial constant field.

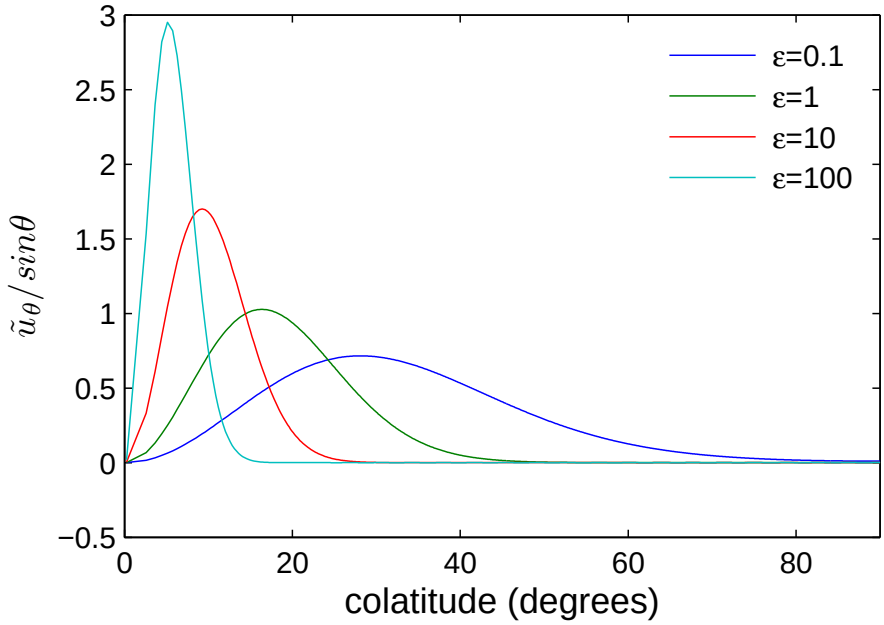

Figure 5.3: Numerical calculation of northward velocity for different values of epsilon in fast magnetic Rossby mode for $\alpha = 10$, $m = 3$ with $N = 50$.

As indicated previously when α is large the solutions are confined in a small gap at the poles where $\mu = \cos\theta$ tends to 1, then a new scaled variable and its differential operators

are defined by

$$\mu = 1 - \frac{\gamma_1}{\alpha}\hat{\mu}, \qquad \frac{d}{d\mu} = -\frac{\alpha}{\gamma_1}\frac{d}{d\hat{\mu}}, \qquad \frac{d^2}{d\mu^2} = \frac{\alpha^2}{\gamma_1^2}\frac{d^2}{d\hat{\mu}^2}, \qquad 1-\mu^2 = \frac{2\gamma_1}{\alpha}\hat{\mu} + ...$$

Substituting in the general differential equation (2.64) for the northward velocity $\tilde{u_\theta}$ we consider each term to find its leading order in the large parameter α. The differential equation (2.64) has seven terms, here named T_1, T_2,...and T_7 respectively. We note from the numerical solutions that λ is $\mathcal{O}(\alpha)$ for these trapped polar modes,

$$T_1 = (1-\mu^2)\tfrac{\partial^2 \tilde{u}_\theta}{\partial \mu^2} \sim 2\tfrac{\alpha}{\gamma_1}\hat{\mu}\tfrac{\partial^2 \tilde{u}_\theta}{\partial \hat{\mu}^2} \sim \mathcal{O}(\alpha),$$

$$T_2 = \tfrac{2m^2}{[(\lambda^2 - m^2\alpha^2)\epsilon(1-\mu^2)-m^2]}\mu\tfrac{\partial \tilde{u}_\theta}{\partial \mu} \sim \mathcal{O}(1),$$

$$T_3 = \epsilon(\lambda^2 - m^2\alpha^2)\tilde{u}_\theta \sim \mathcal{O}(\alpha^2),$$

$$T_4 = \tfrac{-m(\lambda+2m\alpha^2)}{(\lambda^2-m^2\alpha^2)}\tilde{u}_\theta \sim \mathcal{O}(1),$$

$$T_5 = -\tfrac{\epsilon(\lambda+2m\alpha^2)^2\mu^2}{(\lambda^2-m^2\alpha^2)}\tilde{u}_\theta \sim \mathcal{O}(\alpha^2),$$

$$T_6 = \tfrac{-m^2}{1-\mu^2}\tilde{u}_\theta \sim \mathcal{O}(\alpha),$$

$$T_7 = -\tfrac{2m\epsilon(\lambda+2m\alpha^2)\mu^2}{[(\lambda^2-m^2\alpha^2)\epsilon(1-\mu^2)-m^2]}\tilde{u}_\theta \sim \mathcal{O}(\alpha).$$

Terms T_3 and T_5 of order $\mathcal{O}(\alpha^2)$ are dominants. These terms cancel out at leading order to get a valid solution, so since $\mu^2 = 1 - \frac{2\gamma_1}{\alpha}\hat{\mu} + ...$, we obtain

$$\epsilon(\lambda^2 - m^2\alpha^2) = \frac{\epsilon(\lambda+2m\alpha^2)^2}{(\lambda^2-m^2\alpha^2)}, \tag{5.35}$$

which reduces to $\lambda^2 - m^2\alpha^2 = \pm(\lambda + 2m\alpha^2)$. Numerical results show that fast magnetic Rossby waves are subalfvénic when α is large, so we must choose the minus sign to get

$$\lambda = -\frac{1}{2} \pm \sqrt{\frac{1}{4} + m(m-2)\alpha^2}. \tag{5.36}$$

Here $\lambda \sim \pm\sqrt{m(m-2)}\alpha$ is the leading order part, and leads to the cancellation of terms $\mathcal{O}(\alpha^2)$: T_3 and T_5.

The differential equation for $\tilde{u}_\theta$ have terms of order $\mathcal{O}(\alpha)$. The terms T_2 and T_4 are $\mathcal{O}(1)$ only, and so can be neglected. We need to rethink the terms T_3 and T_5 to get the $\mathcal{O}(\alpha)$ part.

For eastward propagating waves let

$$\lambda = k + \sqrt{m(m-2)}\alpha.$$

Then

$$T_1 \sim 2\tfrac{\alpha}{\gamma_1}\hat{\mu}\tfrac{\partial^2\tilde{u}_\theta}{\partial\hat{\mu}^2} \sim \mathcal{O}(\alpha),$$

$$T_3 \sim \epsilon(-2m\alpha^2 + 2k\alpha\sqrt{m(m-2)} + k^2\alpha)\tilde{u}_\theta \sim \mathcal{O}(\alpha^2),$$

$$T_5 =\sim (2m\epsilon\alpha^2 + 2k\epsilon\alpha\sqrt{m(m-2)} + 2\epsilon\alpha\sqrt{m(m-2)} - 4m\epsilon\gamma_1\alpha\hat{\mu})\tilde{u}_\theta \sim \mathcal{O}(\alpha^2),$$

$$T_6 \sim -\tfrac{m^2\alpha}{2\gamma_1\hat{\mu}}\tilde{u}_\theta \sim \mathcal{O}(\alpha),$$

$$T_7 \sim \tfrac{m\alpha}{\gamma_1\hat{\mu}}\tilde{u}_\theta \sim \mathcal{O}(\alpha).$$

The terms $\mathcal{O}(\alpha^2)$ cancel as expected and only $\mathcal{O}(\alpha)$ terms remain and the equation (2.64) becomes

$$\frac{d^2\tilde{u_\theta}}{d\hat{\mu}^2} - 2m\epsilon\gamma_1^2\tilde{u_\theta} + \Big\{\frac{(2k+1)\epsilon\sqrt{m(m-2)}\gamma_1}{\hat{\mu}} + \frac{\frac{m}{2} - \frac{m^2}{4}}{\hat{\mu}^2}\Big\}\tilde{u_\theta} = 0. \tag{5.37}$$

As a result of this, we choose the value of the variable $\gamma_1 = 1/\sqrt{8m\epsilon}$, and it gives the Whittaker differential equation

$$\frac{d^2\tilde{u_\theta}}{d\hat{\mu}^2} + \Big\{-\frac{1}{4} + \frac{\kappa}{\hat{\mu}} + \frac{\frac{1}{4} - \left(\frac{m-1}{4}\right)^2}{\hat{\mu}^2}\Big\}\tilde{u_\theta} = 0, \tag{5.38}$$

where $\kappa = (1+2k)\sqrt{\frac{\epsilon(m-2)}{8}}$. In addition, the solutions are Whittaker functions (Abramowitz and Stegun, 1964)

$$\tilde{u_\theta}(\hat{\mu}) = e^{-\frac{\hat{\mu}}{2}}\hat{\mu}^{\frac{m}{2}}\left[c_1\mathcal{U}(\kappa+\frac{m}{2},m,\hat{\mu}) + c_2{\mathcal{L}_{\kappa-\frac{m}{2}}}^{m-1}(\hat{\mu})\right] \tag{5.39}$$

where $\mathcal{U}$ is the confluent hyper-geometric function of second kind and $\mathcal{L}$ is a generalized Laguerre polynomial. The solution $\mathcal{U}$ is singular as $\hat{\mu}$ tends to zero, so we choose $c_1 = 0$. So let

$$n = \kappa - \frac{m}{2} = (1+2k)\sqrt{\frac{\epsilon(m-2)}{8}} - \frac{m}{2}.$$

Then we have a set of solutions trapped at the poles, there are different modes depending on the poloidal wave number: n.

$$\tilde{u_\theta}(\hat{\mu}) = c_2 e^{-\frac{\hat{\mu}}{2}}\hat{\mu}^{\frac{m}{2}}{\mathcal{L}_n}^{m-1}(\hat{\mu}). \tag{5.40}$$

Consequently, the dispersion relation for magnetic Rossby waves trapped at the poles for $m \geq 3$ is

$$\lambda = \alpha\sqrt{m(m-2)} + \left(n+\frac{m}{2}\right)\sqrt{\frac{2}{\epsilon(m-2)}} - \frac{1}{2}, \qquad n = 0,1,2... \tag{5.41}$$

For instance, let $n = 0$, $\mathcal{L}(0,m-1,\hat{\mu}) = 1$ and $m = 3$, the corresponding solution is

$$\tilde{u_\theta}(\mu) = c_2(1-\mu)^{\frac{3}{2}}e^{-\sqrt{6\epsilon}\alpha(1-\mu)}. \tag{5.42}$$

The solution tends to zero when $\mu = 1$ at the poles and also vanishes at the equator ($\mu = 0$) if α or ϵ are large, as the theory requires.

Table 5.9: Comparison of eigenvalues λ calculated with the formula (5.41) and the numerical results for $m = 3$ and $N = 50$.

α	ϵ	λ_{cal}	λ_{num}
10	0.1	23.5287	22.4811
	100	17.0326	17.0414
100	0.1	179.4133	179.2968
	100	172.9172	173.0246
1000	0.1	1739.3	1738.4
	100	1731.8	1734.8

This solution is plotted in figure 5.4 for $\alpha = 10$ and different values of ϵ.
The theory works in the range where the scale factor for polar trapping, $1/(\sqrt{(8m\epsilon)}\alpha)$ is less than 1. If the values of α and ϵ are large the polar trapping is very large, and the fluid is strongly confined at the poles. This behaviour has been reproduced numerically in chapter 4. Some eigenvalues λ have been calculated with the formula (5.41) for $m = 3$, as shown in table 5.9, the results agree with the numerical method ($n = 3$, $m = 3$, $N = 50$).

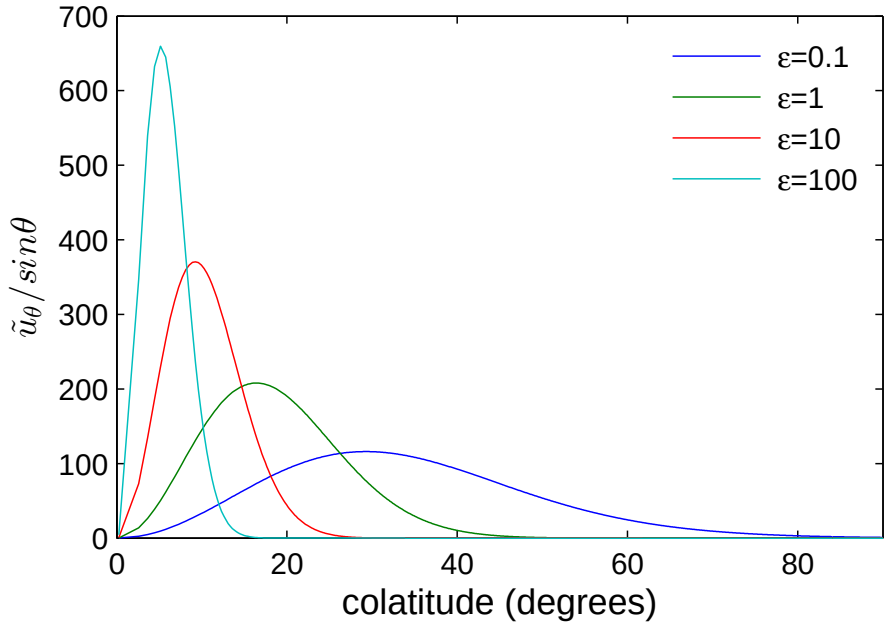

Figure 5.4: Northward velocity for different values of epsilon in with $\alpha = 10$ and $m = 3$, calculated using the formula (5.42)

For fast magnetic Rossby waves travelling westwards at large α, the dispersion relation is

$$\lambda = -\alpha\sqrt{m(m-2)} - k_-.$$

If the same procedure is applied to the equation (2.64), we obtain the Whittaker equation with a small difference with respect to the eastward waves

$$\frac{d^2\tilde{u_\theta}}{d\hat{\mu}^2} - 2m\epsilon\gamma_1^2\tilde{u_\theta} + \Big\{\frac{(2k_- - 1)\epsilon\sqrt{m(m-2)}\gamma_1}{\hat{\mu}} + \frac{\frac{m}{2} - \frac{m^2}{4}}{\hat{\mu}^2}\Big\}, \tilde{u_\theta} = 0. \qquad (5.43)$$

where the condition for k_- is

$$k_- = +\frac{1}{2} + \big(n + \frac{m}{2}\big)\sqrt{\frac{2}{\epsilon(m-2)}} \qquad n = 0, 1, 2, ...$$

The solutions will be a set of functions depending on the azimuthal and poloidal wave

numbers: m and k_- respectively. Then, the expression for λ is given by

$$\lambda = -\alpha\sqrt{m(m-2)} - \big(n + \frac{m}{2}\big)\sqrt{\frac{2}{\epsilon(m-2)}} - \frac{1}{2}, \tag{5.44}$$

so the magnitude of the frequency of the fast magnetic Rossby wave is one greater than the slow magnetic Rossby wave, although at large α the form of the waves become similar and also trapped at the poles.

From equation (5.44), we calculate the normalized frequency λ for $\alpha = 10$, 100 and 1000, with $\epsilon = 0.1$ and 100. Accordingly, the results compare well with our numerical results, as illustrated in table 5.10. We note that the difference in λ between eastward and westward magnetic Rossby waves is 1, see tables 5.9 and 5.10.

Table 5.10: Comparison of eigenvalues λ calculated with the formula (5.44) and the numerical results for $m = 3$ and $N = 50$.

α	ϵ	λ_{cal}	λ_{num}
10	0.1	-24.5287	-23.2768
	100	-18.0326	-18.0353
100	0.1	-180.4133	-180.2775
	100	-173.9172	-174.0744
1000	0.1	-1739.3	-1739.4
	100	-1732.8	-1735.8

The accuracy for λ improves when α and ϵ are large, except for the last row, where we suppose that the polar trapping is large and the code is not able to compute the eigenvalues when the truncation number is $N = 50$. It is possible that at high N the value could improve but also we know the limitations of our numerical calculations.

5.4 Asymptotic Theory for Stable Modes Trapped at the Pole $m = 2$

In the case of magnetic Rossby waves trapped at the poles for $m = 2$, the formula (5.41) cannot reproduce the frequencies, because of the factor $\alpha\sqrt{m(m-2)}$. Another new approximation is proposed here, motivated by the numerical results,

$$\lambda = \beta\alpha^{1/2} + \kappa, \tag{5.45}$$

where β and κ are constants to be determined. The numerical results have shown that these waves are confined at the poles when α is large, therefore the same scalings used for the previous sections are valid here

$$\mu = 1 - \frac{\gamma_1}{\alpha}\hat{\mu} \qquad \frac{d}{d\mu} = -\frac{\alpha}{\gamma_1}\frac{d}{d\hat{\mu}} \qquad \frac{d^2}{d\mu^2} = \frac{\alpha^2}{\gamma_1^2}\frac{d^2}{d\hat{\mu}^2}, \qquad 1-\mu^2 = \frac{2\gamma_1}{\alpha}\hat{\mu} + ...$$

Substituting (5.45) and the scaling in the differential equation (2.64), every term of the equation can be approximated as follows

$$T_1 = (1-\mu^2)\tfrac{\partial^2\tilde{u}_\theta}{\partial\mu^2} \sim 2\tfrac{\alpha}{\gamma_1}\hat{\mu}\tfrac{\partial^2\tilde{u}_\theta}{\partial\hat{\mu}^2} = \mathcal{O}(\alpha),$$

$$T_2 = \tfrac{2m^2}{[(\lambda^2-m^2\alpha^2)\epsilon(1-\mu^2)-m^2]}\mu\tfrac{\partial\tilde{u}_\theta}{\partial\mu} \sim \tfrac{1}{\gamma_1\epsilon\hat{\mu}}\tfrac{d\tilde{u}_\theta}{d\hat{\mu}} = \mathcal{O}(1),$$

$$T_3 = \epsilon(\lambda^2 - m^2\alpha^2)\tilde{u}_\theta \sim (-4\epsilon\alpha^2 + \beta^2\epsilon\alpha + 2\beta\kappa\epsilon\alpha^{1/2})\tilde{u}_\theta = \mathcal{O}(\alpha^2),$$

$$T_4 = \tfrac{-m(\lambda+2m\alpha^2)}{(\lambda^2-m^2\alpha^2)}\tilde{u}_\theta \sim 2\tilde{u}_\theta = \mathcal{O}(1),$$

$$T_5 = -\tfrac{\epsilon(\lambda+2m\alpha^2)^2\mu^2}{(\lambda^2-m^2\alpha^2)}\tilde{u}_\theta \sim [4\epsilon\alpha^2 + \beta^2\epsilon\alpha - 8\gamma_1\epsilon\alpha\hat{\mu} + 2(\kappa+1)\beta\epsilon\alpha^{1/2}]\tilde{u}_\theta = \mathcal{O}(\alpha^2),$$

$$T_6 = \tfrac{-m^2}{1-\mu^2}\tilde{u}_\theta \sim \tfrac{-2\alpha}{\gamma_1\hat{\mu}}\tilde{u}_\theta = \mathcal{O}(\alpha),$$

$$T_7 = -\tfrac{2m\epsilon(\lambda+2m\alpha^2)\mu^2}{[(\lambda^2-m^2\alpha^2)\epsilon(1-\mu^2)-m^2]}\tilde{u}_\theta \sim \tfrac{2\alpha}{\gamma_1\hat{\mu}}\tilde{u}_\theta = \mathcal{O}(\alpha).$$

We neglect terms of order $\mathcal{O}(1)$: T_2 and T_4. The terms T_6 and T_7 are cancelled. Then, the equation (2.64) becomes

$$\frac{d^2\tilde{u_\theta}}{d\hat{\mu}^2} + \Big\{\frac{\beta^2\epsilon\gamma_1}{\hat{\mu}} - 4\gamma_1^2\epsilon + \frac{(2\kappa+1)\gamma_1\beta\epsilon}{\hat{\mu}\alpha^{1/2}}\Big\}\tilde{u_\theta} = 0. \tag{5.46}$$

In order to eliminate the last term, we set $\kappa = -1/2$, and make the convenient choice $\gamma_1 = 1/4\epsilon^{1/2}$. Now the differential equation is the Whittaker equation (Abramowitz and Stegun, 1964), where

$$\beta^2 = \frac{4(n+1)}{\epsilon^{1/2}}.$$

So

$$\frac{d^2\tilde{u_\theta}}{d\hat{\mu}^2} + \Big\{-\frac{1}{4} + \frac{(n+1)}{\hat{\mu}}\Big\}\tilde{u_\theta} = 0. \tag{5.47}$$

There is a set of solutions corresponding to

$$\tilde{u_\theta} = \hat{\mu}e^{-\hat{\mu}/2}\mathcal{L}_n^1(\hat{\mu}). \tag{5.48}$$

where $\mathcal{L}_n^1(\hat{\mu})$ is the Generalized Laguerre function. For example, if $n = 0$ then $\mathcal{L}_0^1(\hat{\mu}) = 1$, therefore the lowest mode solution is

$$\tilde{u_\theta}(\mu) = 4\epsilon^{1/2}\alpha(1-\mu)e^{-2\epsilon^{1/2}\alpha(1-\mu)}.$$

This solution is confined at the pole because of the factor $e^{-2\epsilon^{1/2}\alpha(1-\mu)}$, which is maximum at the poles and at the equator tends to zero.

In general, the dispersion relation for the polar trapped magnetic Rossby waves for $m = 2$ is

$$\lambda_n = \pm\frac{2[(n+1)\alpha]^{1/2}}{\epsilon^{1/4}} - \frac{1}{2}. \tag{5.49}$$

The frequency of the magnetic Rossby waves increases with α and decreases with ϵ, as shown in the following tables. The results of the formula (5.49) are in table 5.11 and the numerical results for a truncation number of $N = 50$ are reported in table 5.12. Comparing these values is clear that there is a good agreement between the asymptotic theory and the numerics, although the value of λ for $\alpha = 10$ and $\epsilon = 0.01$ in the table

5.11 is not right, possibly because the mode here is not sufficiently trapped.

Table 5.11: Eigenvalues calculated with the formula (5.49).

α	10	100	1000
$\epsilon = 0.01$	19.5000	62.7456	199.5000
$\epsilon = 0.1$	10.7468	35.0656	111.9683
$\epsilon = 1$	5.8246	19.5000	62.7456
$\epsilon = 10$	3.0566	10.7468	35.0656
$\epsilon = 100$	1.5000	5.8246	19.5000

The asymptotic theory provides reasonable results when the numerical method is limited because the polar trapping of the functions.

Table 5.12: Numerical results for the lowest mode $n = 2$, $m = 2$ and $N = 50$.

α	10	100	1000
$\epsilon = 0.01$	15.48	62.705	199.5
$\epsilon = 0.1$	10.677	35.073	111.970
$\epsilon = 1$	5.8606	19.508	****
$\epsilon = 10$	3.098	10.758	****
$\epsilon = 100$	1.5634	****	****

5.4.1 Solutions near the poles

In order to find solutions near the poles the dispersion relation for magnetic Rossby modes can be approximated using the expression $\lambda = \beta\alpha^{1/2} + \kappa$, for $m = 2$ and a

new scaling

$$\mu = 1 - \frac{\gamma_2}{\alpha^2}\tilde{\mu}.$$

Therefore

$$\mu^2 = 1 - \frac{2\gamma_2}{\alpha^2}\tilde{\mu} + \frac{\gamma_2^2}{\alpha^4}\tilde{\mu}^2 \qquad \text{and} \qquad 1 - \mu^2 = \frac{2\gamma_2}{\alpha^2}\tilde{\mu}.$$

Then, the differential operators can be expressed as: $\frac{d}{d\mu} = -\frac{\alpha^2}{\gamma_2}\frac{d}{d\tilde{\mu}}$ and $\frac{d^2}{d\mu^2} = \frac{\alpha^4}{\gamma_2^2}\frac{d^2}{d\tilde{\mu}^2}$. Also the factor $(\lambda^2 - m^2\alpha^2)\epsilon(1-\mu^2) - m^2 \to -8\epsilon\gamma_2\left[\tilde{\mu} + \frac{1}{2\epsilon\gamma_2}\right]$. Substituting this scaling into equation (2.64), the terms will reduce to

$$T_1 = (1-\mu^2)\tfrac{\partial^2\tilde{u}_\theta}{\partial\mu^2} \sim 2\tfrac{\alpha^2}{\gamma_2}\tilde{\mu}\tfrac{\partial^2\tilde{u}_\theta}{\partial\tilde{\mu}^2} = \mathcal{O}(\alpha^2),$$

$$T_2 = \tfrac{2m^2}{[(\lambda^2-\alpha^2m^2)\epsilon(1-\mu^2)-m^2]}\mu\tfrac{\partial\tilde{u}_\theta}{\partial\mu} \sim \tfrac{\alpha^2}{\epsilon\gamma_2^2}\tfrac{1}{\left[\tilde{\mu}+\frac{1}{2\epsilon\gamma_2}\right]}\tfrac{d\tilde{u}_\theta}{d\tilde{\mu}} = \mathcal{O}(\alpha^2),$$

$$T_3\epsilon(\lambda^2 - \alpha^2m^2)\tilde{u}_\theta \sim -4\epsilon\alpha^2\tilde{u}_\theta = \mathcal{O}(\alpha^2),$$

$$T_4 = \tfrac{-m(\lambda+2m\alpha^2)}{(\lambda^2-\alpha^2m^2)}\tilde{u}_\theta \sim 2\tilde{u}_\theta = \mathcal{O}(1),$$

$$T_5 = -\tfrac{\epsilon(\lambda+2m\alpha^2)^2\mu^2}{(\lambda^2-\alpha^2m^2)}\tilde{u}_\theta \sim 4\epsilon\alpha^2\tilde{u}_\theta = \mathcal{O}(\alpha^2),$$

$$T_6 = \tfrac{-m^2}{1-\mu^2}\tilde{u}_\theta \sim -\tfrac{2\alpha^2}{\gamma_2\tilde{\mu}}\tilde{u}_\theta = \mathcal{O}(\alpha^2),$$

$$T_7 = \tfrac{-2m\epsilon(\lambda+2m\alpha^2)\mu^2}{[(\lambda^2-\alpha^2m^2)\epsilon(1-\mu^2)-m^2]}\tilde{u}_\theta \sim \tfrac{2\alpha^2}{\gamma_2\left[\tilde{\mu}+\frac{1}{2\epsilon\gamma_2}\right]}\tilde{u}_\theta = \mathcal{O}(\alpha^2).$$

When the terms balance at $\mathcal{O}(\alpha^2)$, the equation is

$$\tilde{\mu}\frac{d^2\tilde{u}_\theta}{d\tilde{\mu}^2} + \frac{1}{2\epsilon\gamma_2}\frac{1}{\left[\tilde{\mu}+\frac{1}{2\epsilon\gamma_2}\right]}\frac{d\tilde{u}_\theta}{d\tilde{\mu}} - \frac{1}{\tilde{\mu}}\tilde{u}_\theta + \frac{1}{\left[\tilde{\mu}+\frac{1}{2\epsilon\gamma_2}\right]}\tilde{u}_\theta = 0. \tag{5.50}$$

This equation has a very simple general solution. We let $2\epsilon\gamma_2 = 1$, i.e, choose $\gamma_2 = 1/2\epsilon$. Therefore

$$\tilde{\mu}\frac{d^2\tilde{u}_\theta}{d\tilde{\mu}^2} + \frac{1}{(1+\tilde{\mu})}\frac{d\tilde{u}_\theta}{d\tilde{\mu}} - \frac{1}{\tilde{\mu}}\tilde{u}_\theta + \frac{1}{(1+\tilde{\mu})}\tilde{u}_\theta = 0. \tag{5.51}$$

One valid solution for the previous equation is $\tilde{u}_\theta = \tilde{\mu}$, then near the poles, the velocity can be expressed by

$$\tilde{u}_\theta = 2\epsilon\alpha^2(1-\mu). \tag{5.52}$$

when $\mu \to 1$ the velocity tends to zero.

5.5 Asymptotic Theory for the Anomalous Mode in the Small α Regime

In the numerical results there is also a slow anomalous mode travelling to the west, that appears in the presence of the magnetic field. This mode collides with the first magnetic Rossby mode and the wave becomes unstable. This phenomenon occurs only for $m = 1$ and for the magnetic Rossby modes. This mode has been found numerically and the normalized frequency is summarized in table 4.14. We can note that the wave is very slow in the small α regime and the frequencies are very small. Therefore, in the equation (2.64) ϵ is $\mathcal{O}(1)$, α^2 is small, $m = 1$ and $\lambda = \hat{\lambda}\epsilon\alpha^4$. The factor $[(\lambda^2 - m^2\alpha^2)\epsilon(1-\mu^2) - m^2] \sim -[1 + \alpha^2\epsilon(1-\mu^2)]$, and using geometric series, and the fact that $\lambda^2 \ll \alpha^2$ the following fraction reduces to

$$\frac{1}{[(\lambda^2 - m^2\alpha^2)\epsilon(1-\mu^2) - m^2]} \sim -[1 - \alpha^2\epsilon(1-\mu^2)]$$

With these approximations the equation (2.64) for the northward velocity becomes

$$(1-\mu^2)\frac{\mathrm{d}^2\tilde{u}_\theta}{\mathrm{d}\mu^2} - 2[1-\alpha^2\epsilon(1-\mu^2)]\mu\frac{\mathrm{d}\tilde{u}_\theta}{\mathrm{d}\mu} + \Big\{\frac{\lambda}{\alpha^2} + 2 + 4\epsilon\alpha^2\mu^2 - \frac{1}{(1-\mu^2)} - \epsilon\alpha^2 + 4\epsilon\alpha^2\mu^2[1-\alpha^2\epsilon(1-\mu^2)]\Big\}\tilde{u}_\theta = 0. \tag{5.53}$$

Taking $\lambda = \hat{\lambda}\epsilon\alpha^4$, the equation (5.53) can be written as

$$(1-\mu^2)\frac{\mathrm{d}^2\tilde{u}_\theta}{\mathrm{d}\mu^2} - 2[1-\alpha^2\epsilon(1-\mu^2)]\mu\frac{\mathrm{d}\tilde{u}_\theta}{\mathrm{d}\mu} + \Big\{\hat{\lambda}\epsilon\alpha^2 + 2 + 8\epsilon\alpha^2\mu^2 - \frac{1}{(1-\mu^2)} - \epsilon\alpha^2 - 4\epsilon^2\alpha^4\mu^2(1-\mu^2)\Big\}\tilde{u}_\theta = 0. \quad (5.54)$$

Rearranging the terms of the differential equation, we have

$$(1-\mu^2)\frac{\mathrm{d}^2\tilde{u}_\theta}{\mathrm{d}\mu^2} - 2\mu\frac{\mathrm{d}\tilde{u}_\theta}{\mathrm{d}\mu} + 2\tilde{u}_\theta - \frac{\tilde{u}_\theta}{(1-\mu^2)} + \epsilon\alpha^2\Big\{2\mu(1-\mu^2)\frac{\partial\tilde{u}_\theta}{\partial\mu} + \big[\hat{\lambda} + 8\mu^2 - 1 - 4\epsilon\alpha^2\mu^2(1-\mu^2)\big]\tilde{u}_\theta\Big\} = 0. \quad (5.55)$$

We propose a sinusoidal solution for this differential equation

$$\tilde{u}_\theta = (1-\mu^2)^{1/2} + \epsilon\alpha^2 y. \quad (5.56)$$

Substituting the solution into the equation (5.55) and taking the solutions of order $\mathcal{O}(\epsilon\alpha^2)$

$$\epsilon\alpha^2\Big\{(1-\mu^2)\frac{\mathrm{d}^2y}{\mathrm{d}\mu^2} - 2\mu\frac{\mathrm{d}y}{\mathrm{d}\mu} - \frac{y}{(1-\mu^2)} + 2y\Big\} + \epsilon\alpha^2\Big\{2\mu(1-\mu^2)\frac{\mathrm{d}\tilde{u}_\theta}{\mathrm{d}\mu} + \big[\hat{\lambda} + 8\mu^2 - 1\big]\tilde{u}_\theta\Big\} = 0. \quad (5.57)$$

We take $\tilde{u}_\theta = (1-\mu^2)^{1/2}$ and $\frac{\mathrm{d}\tilde{u}_\theta}{\mathrm{d}\mu} = \frac{-\mu}{(1-\mu^2)^{1/2}}$ to maintain the order $\mathcal{O}(\epsilon\alpha^2)$ of the equation.

$$(1-\mu^2)\frac{d^2y}{d\mu^2} - 2\mu\frac{dy}{d\mu} - \frac{y}{(1-\mu^2)} + 2y = -\big[\hat{\lambda} + 6\mu^2 - 1\big](1-\mu^2)^{1/2}. \quad (5.58)$$

We try a power of $\sin\theta$ as solution for the differential equation

$$y = A(1-\mu^2)^{3/2}, \qquad \frac{dy}{d\mu} = -3A\mu(1-\mu^2)^{1/2}, \qquad \frac{d^2y}{d\mu^2} = 3A\frac{(2\mu^2-1)}{(1-\mu^2)^{1/2}}.$$

Substituting this expression into equation (5.58), we find an algebraic equation for powers of μ

$$-A(1-\mu^2)^2 + (9A+6)\mu^2(1-\mu^2) + (\hat{\lambda} - A - 1)(1-\mu^2) = 0. \quad (5.59)$$

We obtain $A = -3/5$, $\hat{\lambda} = -1/5$. Hence, the frequency of the anomalous mode will be

$$\lambda = -\frac{1}{5}\epsilon\alpha^4. \tag{5.60}$$

As has been shown, the wave has a magnetic origin and is influenced by the rotation. Undeniably, the formula (5.60) agrees with the results of table 4.14, and also the solution for the velocity agrees with figure 4.32(a) and (b). Finally, the solution for the Northward velocity is

$$\tilde{u}_\theta = (1-\mu^2)^{1/2} - \frac{3}{5}\epsilon\alpha^2(1-\mu^2)^{3/2}. \tag{5.61}$$

This demonstrates that the wave form is mostly sinusoidal. We notice that for small α, the wave form will not be affected by variations in the magnetic field or the rotation, because the second term will be small.

5.6 Kelvin Waves

In this section, we analyse the effect of the magnetic field on the Kelvin waves. We obtain an analytical formulation for the dispersion relation and also the eigenfunctions. For the non-magnetic case, Longuet-Higgins has studied the Kelvin waves. He found just one mode that travels to the east that corresponds to this kind of oscillation. He established the features of this mode as follows:

- For small parameter ϵ, the Kelvin mode correspond to the first gravity wave travelling eastward ($n - m = 0$), with dispersion relation

$$\lambda = \sqrt{\frac{n(n+1)}{\epsilon}}.$$

- When ϵ is large, the waves are equatorially trapped and the dispersion relation changes to

$$\lambda = \frac{m}{\sqrt{\epsilon}}.$$

- The northward velocity $\tilde{u_\theta}$ is small compared with the other quantities for large ϵ.

When a toroidal magnetic field is introduced in the system, the waves become modified by the magnetic field. Then, these wave becomes trapped at the equator for large α or ϵ, as shown in the numerical solutions for the eigenfunctions. From the numerical results, we note that increasing ϵ or α the northward velocity goes to zero faster, as a property of this magneto-Kelvin mode. The fluid reduces the movement to an azimuthal flow. The original set of equations, when $\tilde{u}_\theta = 0$ (Holton and Lindzen, 1968), is reduced to

$$(\lambda + 2m\alpha^2)\mu\tilde{u}_\phi + \lambda(1-\mu^2)\frac{\partial\tilde{\eta}}{\partial\mu} = 0, \tag{5.62a}$$

$$(\lambda^2 - m^2\alpha^2)\tilde{u}_\phi - \lambda m\tilde{\eta} = 0, \tag{5.62b}$$

$$\lambda\epsilon(1-\mu^2)\tilde{\eta} - m\tilde{u}_\phi = 0. \tag{5.62c}$$

Taking the derivative of equation (5.62b) and rearranging gives

$$\lambda m\frac{\mathrm{d}\tilde{\eta}}{\mathrm{d}\mu} = (\lambda^2 - m^2\alpha^2)\frac{\mathrm{d}\tilde{u}_\phi}{\mathrm{d}\mu}. \tag{5.63}$$

Substituting $\lambda m\partial\tilde{\eta}/\partial\mu$ into equation (5.62a), we obtain a first order differential equation:

$$(1-\mu^2)\frac{\mathrm{d}\tilde{u}_\phi}{\mathrm{d}\mu} + \frac{m(\lambda + 2m\alpha^2)}{(\lambda^2 - m^2\alpha^2)}\mu\tilde{u}_\phi = 0, \tag{5.64}$$

The analytic solution of this differential equation, can be calculated by direct integration, then, the expression will be

$$\tilde{u}_\phi = C_1(1-\mu^2)^{q/2}, \tag{5.65}$$

where C_1 is a constant associated with the normalization and the power q is related to the frequency, and it is expected to be positive in order to obtain finite solutions

$$q = \frac{m(\lambda + 2m\alpha^2)}{(\lambda^2 - m^2\alpha^2)}. \tag{5.66}$$

The exponential function for x near zero is

$$e^x = 1 + x + \frac{x^2}{2!} + \frac{x^3}{3!} + ...$$

Therefore, at the equator $\mu = \cos\theta$ tends to zero, the polynomial function $1 - \mu^2 + ... \sim e^{-\mu^2}$. As a consequence of this, the solution (5.65) can be expressed as

$$\tilde{u}_\phi = C_1 e^{-q\mu^2/2}. \tag{5.67}$$

Then a formula for $\tilde{\eta}$ can be found as

$$\tilde{\eta} = C_1 \frac{(\lambda^2 - m^2\alpha^2)}{\lambda m} e^{-q\mu^2/2}. \tag{5.68}$$

Substituting these expressions for $\tilde{\eta}$ and $\tilde{u}_\phi$ into the equation (5.62c), and taking the limit, when $1 - \mu^2 \sim 1$ for equatorially trapped waves, a dispersion relation is found

$$\lambda^2 - m^2\alpha^2 = \frac{m^2}{\epsilon}. \tag{5.69}$$

Then, we may define a dispersion relation for Magneto-Kelvin waves

$$\lambda = \pm m\sqrt{\frac{1}{\epsilon} + \alpha^2}. \tag{5.70}$$

As shown in the last equation, if $\alpha = 0$ the dispersion relation will coincide with Longuet-Higgins formula for Kelvin waves. Substituting λ into the expression for the power q, we will have

$$q = \epsilon\left(2\alpha^2 \pm \sqrt{\frac{1}{\epsilon} + \alpha^2}\right).$$

Longuet-Higgins neglected the negative answer for λ, but in this case we can consider the negative answer when q is greater than zero, which is possible for values of $\alpha > 0.5$ for large epsilon. For small values of ϵ this wave exists for $\alpha > 1/\sqrt{2}\epsilon^{1/4}$, approximately. Then, for α or ϵ very large, q will be very large and the function will be more trapped. Using this asymptotic theory we can predict the eigenvalues for the Magneto-Kelvin waves, from equation (5.70). The results are summarized in table 5.13. The results are very accurate compared with our numerical results reported in table 4.15.

Table 5.13: Eigenvalues calculated with the formula (5.69) from the asymptotic theory for large α, the values with the star* were calculated with the formula of Longuet-Higgins for gravity waves for small $\epsilon = 0.01$ and $\epsilon = 0.1$.

α	10^{-3}	10^{-2}	10^{-1}	1	10^{1}	10^{2}	10^{3}
$\epsilon = 0.01$	14.1421*	14.1421*	14.1421*	14.1421*	14.1421	100.49876	1000.0500
$\epsilon = 0.1$	4.4721*	4.4721*	4.4721*	4.4721*	10.4881	100.0500	1000.0050
$\epsilon = 1$	1.0000	1.0000	1.0050	1.4142	10.0499	100.0050	1000.0005
$\epsilon = 10$	0.3162	0.3164	0.3317	1.0488	10.0050	100.0005	1000.0000
$\epsilon = 100$	0.1000	0.1005	0.1414	1.0050	10.0005	100.0000	1000.0000

The westward Kelvin mode is produced by the magnetic field. The eigenfunctions for the northward velocity also tend to zero when α or ϵ grow. In table 5.14 the values of λ have been computed with the formula (5.70). The spaces with the dashed line were discarded because they correspond to solutions for q negative. The starred values are associated to high $q > 1900$ and the numerical solution could no longer computed with the code due to the high confinement at the equator, as expected.

Table 5.14: Propagating westward Kelvin wave. Eigenvalues λ calculated with the formula (5.70) for $m = 1$.

α	1	10^{1}	10^{2}
$\epsilon = 0.01$	- - -	-14.1421	-100.4988
$\epsilon = 0.1$	- - -	-10.4881	-100.0500*
$\epsilon = 1$	-1.4142	-10.0499	-100.0050*
$\epsilon = 10$	-1.0488	-10.0050*	-100.0005*
$\epsilon = 100$	-1.0050	-10.0005*	-100.0000*

5.7 Summary

In this chapter we found asymptotic expressions for the different kinds of waves when $\epsilon\alpha^2 \gg 1$. As discussed MIG waves solutions satisfy the parabolic cylinder differential equation with solutions

$$\tilde{u}_\theta = e^{-\frac{\hat{\mu}^2}{4}} H_\nu(\frac{\hat{\mu}}{\sqrt{2}}),$$

where H_ν are the Hermite polynomials. These functions represent equatorially trapped waves, with frequencies

$$\lambda = \pm m\alpha \pm (2\nu+1)^{2/3}\left(\frac{\alpha}{2m\epsilon}\right)^{1/3} \pm \frac{(2m)^{1/3}}{3(2\nu+1)^{2/3}\epsilon^{2/3}\alpha^{1/3}}\Big[1-\frac{3(2\nu+1)^2}{4m^2}\Big] + \frac{(2\nu+1)^{2/3}}{3(2m\epsilon)^{1/3}\alpha^{2/3}}.$$

With regard to the Kelvin mode, it takes the form of an exponential function

$$u_\phi = e^{-\frac{q}{2}\mu^2},$$

where q is a positive number, for waves concentrated at the equator with relation dispersion

$$\lambda = \pm m\sqrt{\frac{1}{\epsilon} + \alpha^2}.$$

There is a possibility that a Kelvin mode propagating westward can exist for certain values of ϵ and α.

Similarly fast magnetic Rossby waves satisfy the parabolic cylinder differential equation as MIG waves but when the parameter α has a moderate value where these waves are trapped at the equator, with frequencies

$$\lambda = -m\alpha - \frac{m}{2\epsilon\alpha(2\nu+1)^2}.$$

In the case when α is large and $m = 2$, magnetic Rossby waves (fast and slow) eigenfunctions correspond to the Whittaker functions

$$\tilde{u}_\theta = e^{-\frac{\hat{\mu}}{2}}\hat{\mu}\mathcal{L}^1_{n'}(\hat{\mu}),$$

where $\mathcal{L}_{n'}^{m-1}$ are the Generalized Laguerre polynomials.
Although if α is large and $m \geq 3$, the solutions for magnetic Rossby waves (fast and slow) are the Whittaker functions

$$\tilde{u}_\theta = e^{-\frac{\hat{\mu}}{2}} \hat{\mu}^{m/2} \mathcal{L}_{n'}^{m-1}(\hat{\mu}).$$

In addition, an asymptotic theory was developed in the case of small α for the anomalous slow magnetic Rossby wave traveling to the west with frequency $\lambda = -0.2\epsilon\alpha^4$, with sinusoidal solutions equal to

$$\tilde{u}_\theta = (1-\mu^2)^{1/2} - \frac{3}{5}\epsilon\alpha^2(1-\mu^2)^{3/2}.$$

A mathematical description for unstable magnetic Rossby waves (when $m = 1$) is provided in the next chapter.

Chapter 6

Instabilities

The most interesting aspect of the magnetic Rossby waves is the instability that occurs when $m = 1$. Unlike MIG and Kelvin waves, these magnetic Rossby modes become unstable due to the toroidal magnetic field intensity. In this chapter, the main numerical results for instability of magnetic Rossby waves are presented here, in section 6.1. Then, we propose a theory for the behaviour of unstable modes when the magnetic parameter, α, is large. The theory explains the limit case for the eigenvalues and finds analytic solutions for the eigenfunctions and the dispersion relation.

6.1 Numerical Results for Instabilities

Magnetic Rossby waves evolve into growing modes in the presence of the magnetic field. For $\alpha < 0.5$, fast and slow frequencies are real and have some properties which have been mentioned in previous chapters, these include that fast magnetic Rossby waves undergo equatorial trapping. Here the fast magnetic Rossby mode is in the superalfvénic regime $|\lambda| > m\alpha$.

For $\alpha > 0.5$, each fast magnetic Rossby frequency becomes subalfvénic, coalesces with its counterpart slow Rossby mode and a complex mode branches off. Figure 6.1

illustrates this behaviour for the fast magnetic Rossby mode $n = 2$. When $\alpha = 0.1$ the normalized frequency is real and the wave is trapped at the equator. For higher values of α, the mode is complex and it is polar trapped, for $\epsilon = 100$.

This instability is driven by the magnetic field, but it requires $\alpha > 0.5$ and $m = 1$. In

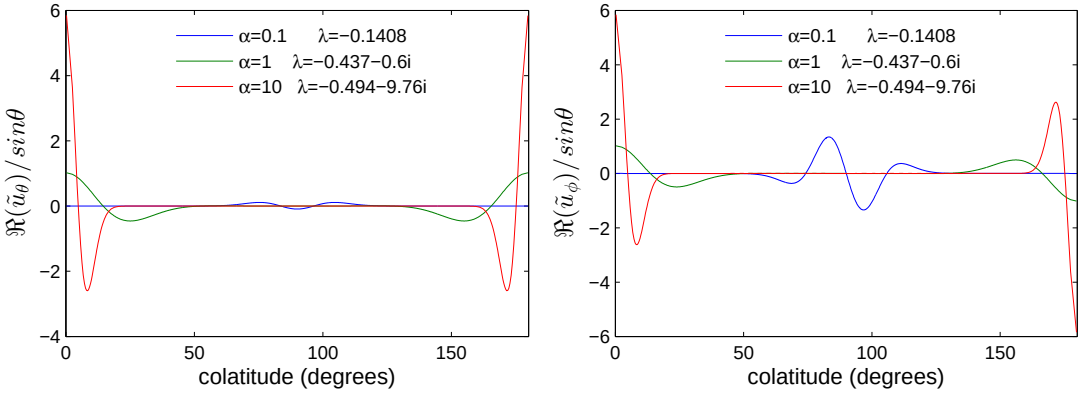

Figure 6.1: Real part of the northward velocity and azimuthal velocity for magnetic Rossby mode with $m = 1$, $\epsilon = 100$ with $N = 50$. The blue line corresponds to $\alpha = 0.1$ when the eigenvalue and eigenfunction are real and trapped at the equator for these values of the parameters α and ϵ. In green the values for $\alpha = 1$ and in red the values for $\alpha = 10$, where the eigenfunctions are trapped at the poles.

figure 6.2(a), the normalized frequency λ of these modes for $m = 1$, $m = 2$ and $m = 3$ is plotted against α. When $m = 1$ (in blue) the fast magnetic Rossby mode collides with an anomalous magnetic Rossby wave travelling westward and an unstable mode branches off, represented by the dashed line in blue. If $m \geq 2$ the frequencies remain always real as shown in the pink ($m = 2$) and the red ($m = 3$) curves. In all these cases the upper branches are slow magnetic Rossby waves and the lower are fast magnetic Rossby waves. Also, instability has been found by Malkus (1967), for a sphere of rotating fluid immersed in a toroidal field: $B_\phi = B_0 \sin\theta$. In this analysis in cylindrical coordinates (r, ϕ, z), the instability occurs when $m = 1$ and for a minimum value of the magnetic field intensity equivalent to our criteria $\alpha \geq 0.5$.

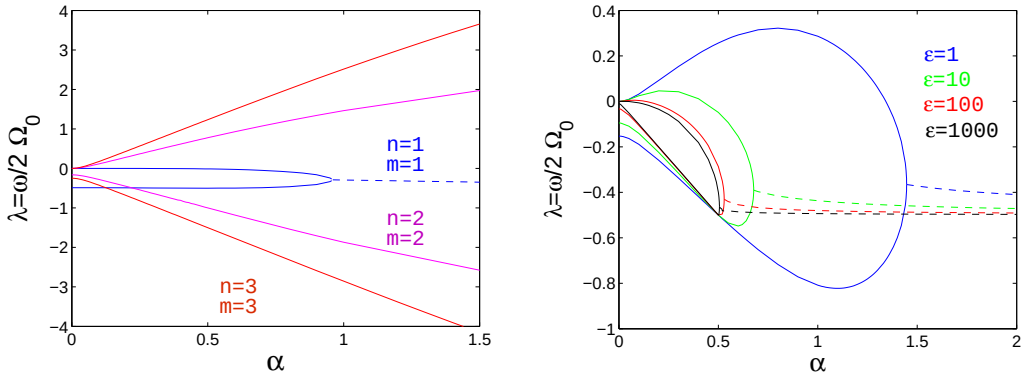

(a) $\epsilon = 1$ (b) $m = 1$

Figure 6.2: Dispersion relation for Magnetic Rossby Modes λ against α. Lower branches are fast magnetic Rossby waves and upper branches are slow magnetic Rossby waves. (a) For the blue curve: the lower branch is a fast magnetic Rossby wave with $m = 1$ which collides with an anomalous wave traveling westward and a complex eigenvalue branches off, the dashed line is the real part of the complex eigenvalue. The other lines represent fast magnetic Rossby waves and slow magnetic Rossby waves for $m = 2$ in pink and $m = 3$ in red, when $\epsilon = 1$. (b) Behaviour of unstable modes for different values of the parameter $\epsilon = 1, 10, 100, 1000$ when $m = 1$. The dashed lines are related to the real part of the complex eigenvalue.

The instability sets in near $\alpha = 0.5$ when ϵ is very large but onsets at larger values of α when ϵ is small, as shown in figure 6.2(b). The numerical calculations indicate that in the small ϵ regime the first fast magnetic Rossby mode ($n = 1$) becomes unstable slightly after $\alpha \sim \epsilon^{-1/4}$; in the case of the second fast magnetic Rossby mode ($n = 2$) instability starts near $\alpha \sim \sqrt{2}\epsilon^{-1/2}$ see figure 6.3.

This criterion has been found by Malkus (1967), and in the limit $\epsilon \to \infty$ his criterion reduces to ours. The limit $\epsilon \to \infty$ corresponds to the effect of gravity dropping out from our problem, which is equivalent to the buoyancy frequency being small compared to the

rotation frequency.

Sharif and Jones (2005) have found instabilities for $m = 1$, considering Ohmic diffusion in a homogeneous fluid for a spherical shell which implies a very large buoyancy frequency where $\epsilon \to 0$. They found instability when magnetic diffusion was added, but no instability in the absence of diffusion. In this case the magnetic field had a slightly more complicated basic state, but their results are consistent with ours, because with no magnetic diffusion and small ϵ our critical α for instability goes to infinity.

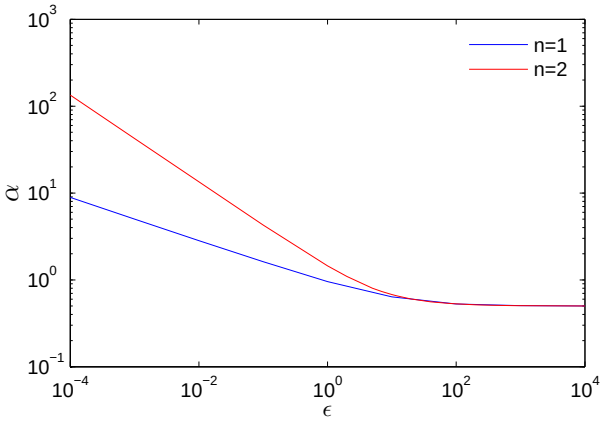

Figure 6.3: Values of α and ϵ for instability when $m = 1$ for the first and second fast magnetic Rossby mode. The modes are unstable for the values of the parameters above the lines.

Unstable and stable magnetic Rossby waves are polar trapped when α increases. This polar trapping has been also described by Cally (2003) in the context of a 3-D Boussinesq thin layer approximation for instabilities and it is called " Polar Kink Instability". As shown in figure 6.4 the eigenfunctions for $\tilde{u}_\theta$ become polar trapped for large values of α, waves are more localised when ϵ or α increase.

These numerical results are consistent with those observed in earlier studies. Tayler (1973) demonstrated that instability can occur in a non rotating star with a toroidal field

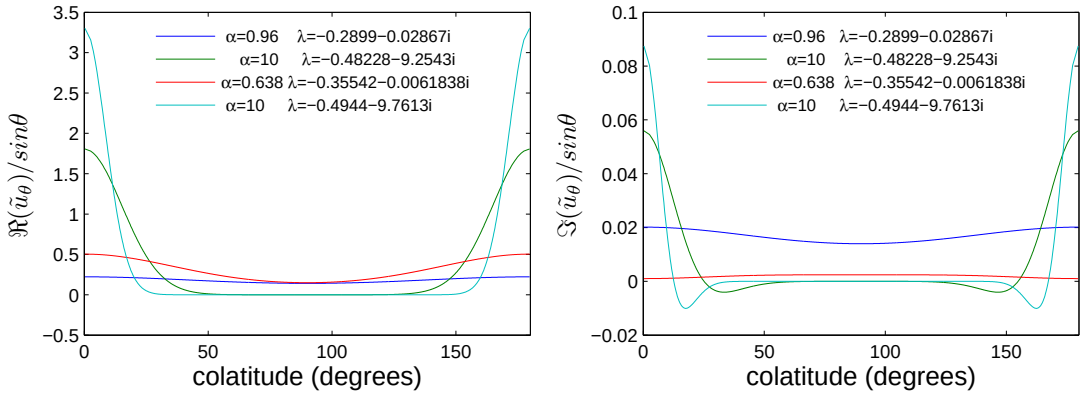

Figure 6.4: Real and Imaginary part of the northward velocity for Magnetic Rossby mode with $m = 1$ with $N = 50$. The blue line corresponds to $\alpha = 0.96$ and $\epsilon = 1$, the green curve is related to $\alpha = 10$ and $\epsilon = 1$, in red the values for $\alpha = 0.638$ and $\epsilon = 10$ and $\alpha = 10$ with $\epsilon = 10$ in cyan.

configuration. He states that the occurrence of the instability depends on the topology of the field and not on its intensity and derives its energy from horizontal interchanges. Later works by Tayler (1980) and Pitts and Tayler (1985) showed that current driven instabilities for a toroidal field can become unstable to non-axisymmetric disturbances, both also in cylindrical and spherical coordinates, see Spruit (1999). The current provides the energy for the instability, and the magnetic field is an energy source, then a strong magnetic field is required to set the instability. In current driven instabilities the role of the rotation rate is to mediate the rate at which energy can be extracted from the mean field. There are other classes of instabilities that emerge from the differential rotation and current, see Gilman and Fox (1997), Dikpati et al. (2003), Cally (2003), Cally et al. (2008), Hollerbach and Cally (2009). The *Joint instabilities* described there occur for relatively weak fields that may be present in stable layers of planets and stars, in differential rotating layers. Without differential rotation or magnetic field the system is linearly stable. In these cases the toroidal magnetic field extracts energy from the differential rotation, although some energy can be extracted from the current.

6.2 Asymptotic Theory for Unstable Modes Trapped at the Pole for $\alpha >> 10$

Polar trapping of unstable modes can be understood via asymptotic analysis. We assume $m = 1$, to analyse the instabilities as there is no instability for $m \neq 1$.

In order to identify the scaling for the problem, the northward velocity plots have been observed to determine how the confinement in the poles changes with the magnetic parameter α.

At the north pole $\mu = \cos\theta$ tends to 1, then a new scaled variable $\hat{\mu}$ and its differential operators are defined by

$$\mu = 1 - \frac{\gamma_1}{\alpha}\hat{\mu}, \qquad \frac{d}{d\mu} = -\frac{\alpha}{\gamma_1}\frac{d}{d\hat{\mu}}, \qquad \frac{d^2}{d\mu^2} = \frac{\alpha^2}{\gamma_1^2}\frac{d^2}{d\hat{\mu}^2}.$$

Then from the numerical calculations for the eigenvalues in tables 4.7, 4.8, 4.10, 4.11 and 4.14, we deduce that $\lambda = -1/2 + i(\alpha - k)$, where k and γ_1 must be calculated and are order $\mathcal{O}(1)$. The factors λ^2 and $(\lambda^2 - \alpha^2)$ will be reduced to

$$\lambda^2 \sim \frac{1}{4} - \alpha^2 - 2\alpha k - i\alpha + \mathcal{O}(1), \qquad \lambda^2 - \alpha^2 \sim -2\alpha^2.$$

Substituting into the general differential equation (2.64) for the northward velocity $\tilde{u}_\theta$ we reduce each term, which gives

$$T_1 = (1-\mu^2)\tfrac{\partial^2 \tilde{u}_\theta}{\partial \mu^2} \sim 2\hat{\mu}\tfrac{\alpha}{\gamma_1}\tfrac{\partial^2 \tilde{u}_\theta}{\partial \hat{\mu}^2} = \mathcal{O}(\alpha),$$

$$T_2 = \tfrac{2m^2}{[(\lambda^2-\alpha^2m^2)\epsilon(1-\mu^2)-m^2]}\mu\tfrac{\partial \tilde{u}_\theta}{\partial \mu} \sim \left(\tfrac{1}{2\gamma_1\epsilon\hat{\mu}} + \mathcal{O}(\alpha^{-1})\right)\tfrac{d\tilde{u}_\theta}{d\hat{\mu}} = \mathcal{O}(1),$$

$$T_3 = \epsilon(\lambda^2 - \alpha^2m^2)\tilde{u}_\theta \sim (-2\epsilon\alpha^2 + 2k\epsilon\alpha - i\epsilon\alpha + \mathcal{O}(1))\tilde{u}_\theta = \mathcal{O}(\alpha^2),$$

$$T_4 = \tfrac{-m(\lambda+2m\alpha^2)}{(\lambda^2-\alpha^2m^2)}\tilde{u}_\theta \sim -m^2\tilde{u}_\theta = \mathcal{O}(1),$$

$$T_5 = -\tfrac{\epsilon(\lambda+2m\alpha^2)^2\mu^2}{(\lambda^2-\alpha^2m^2)}\tilde{u}_\theta \sim (2\epsilon\alpha^2 + 2k\epsilon\alpha + i\epsilon\alpha - 4\gamma_1\epsilon\alpha\hat{\mu} + \mathcal{O}(1))\tilde{u}_\theta = \mathcal{O}(\alpha^2),$$

$$T_6 = \tfrac{-m^2}{1-\mu^2}\tilde{u}_\theta \sim \tfrac{-\alpha}{2\gamma_1\hat{\mu}}\tilde{u}_\theta = \mathcal{O}(\alpha),$$

$$T_7 = \tfrac{2m\epsilon(\lambda+2m\alpha^2)\mu^2}{[(\lambda^2-\alpha^2m^2)\epsilon(1-\mu^2)-m^2]}\tilde{u}_\theta \sim (\tfrac{\alpha}{\gamma_1\hat{\mu}} + \mathcal{O}(1))\tilde{u}_\theta = \mathcal{O}(\alpha).$$

Note that the sum of the terms T_3+T_5 have order α, therefore the terms T_1, T_3, T_5, T_6 and T_7 are retained. Then, the equation (2.64) reduces to a second order differential equation

$$\frac{d^2\tilde{u}_\theta}{d\hat{\mu}^2} - 2\gamma_1^2\epsilon\tilde{u}_\theta + \left\{\frac{2k\epsilon\gamma_1}{\hat{\mu}} + \frac{1}{4\hat{\mu}^2}\right\}\tilde{u}_\theta = 0. \tag{6.1}$$

Although the theory is directed to latitudes corresponding to the northern hemisphere, we know that the solutions are symmetric for both hemispheres and it is expected that the solutions for equation 6.1 vanish at the equator which allow that northern and southern solutions join across the equator. In addition, we choose the value of the variable $\gamma_1 = 1/\sqrt{8\epsilon}$.

The differential equation has the form of the Whittaker differential equation

$$\frac{d^2\tilde{u}_\theta}{d\hat{\mu}^2} - \frac{1}{4}\tilde{u}_\theta + \left\{\frac{k\sqrt{\epsilon}}{\sqrt{2}\hat{\mu}} + \frac{1}{4\hat{\mu}^2}\right\}\tilde{u}_\theta = 0. \tag{6.2}$$

The proposed solutions are $\tilde{u}_\theta = W(\hat{\mu})\hat{\mu}^{1/2}e^{-\frac{\hat{\mu}}{2}}$. Substituting into (6.2), the differential equation becomes

$$\hat{\mu}\frac{d^2W}{d\mu^2} + (1-\hat{\mu}^2)\frac{dW}{d\hat{\mu}} + \left(k\sqrt{\frac{\epsilon}{2}} - \frac{1}{2}\right)W = 0. \tag{6.3}$$

Taking $k\sqrt{\frac{\epsilon}{2}} = n' + \frac{1}{2}$, where n' is a natural number to have finite solutions. The resulting differential equation is the standard form of the Laguerre equation

$$\hat{\mu}\frac{d^2W}{d\mu^2} + (1-\hat{\mu})\frac{dW}{d\hat{\mu}} + n'W = 0, \tag{6.4}$$

and the solutions are the Laguerre polynomials $\mathcal{L}_{n'}$. The solutions are a set of functions depending of the poloidal wave number n'

$$\tilde{u}_\theta(\hat{\mu}) = \hat{\mu}^{\frac{1}{2}}e^{-\frac{\hat{\mu}}{2}}\mathcal{L}_{n'}. \tag{6.5}$$

For $n' = 0$, $\mathcal{L}_0 = 1$. Therefore, the corresponding solution is

$$\tilde{u}_\theta(\hat{\mu}) = e^{-\frac{\hat{\mu}}{2}}\hat{\mu}^{\frac{1}{2}}. \tag{6.6}$$

As expected form the numerical results, the expression for the frequency is increasing with α and decreasing with ϵ, as follows

$$\lambda = -1/2 + i(\alpha - 1/\sqrt{2\epsilon}). \tag{6.7}$$

The theory works in the range where the scale factor for polar trapping is less than 1

$$\frac{\gamma_1}{\alpha} = \frac{1}{\sqrt{8\epsilon}\alpha} \ll 1.$$

From equation (6.7), we calculate the normalized frequency for $\alpha = 10$, 100 and 1000, for different values of ϵ. Accordingly, the results are very accurate compared with our numerical results, as shown in tables 6.1-6.2 and 6.3-6.4. The numerical calculations show that the correspondence between the solutions is $n' = n-2$, where n is the poloidal wave number used for the solutions in chapter 4.

Table 6.1: Imaginary part of the eigenvalues calculated in the asymptotic theory with the formula (6.7). In this case $n' = 0$.

α	10	100	1000
$\epsilon = 0.01$	****	92.9289	992.9289
$\epsilon = 0.1$	7.7639	97.7639	997.7639
$\epsilon = 1$	9.2929	99.2929	999.2929
$\epsilon = 10$	9.7764	99.7764	999.7764
$\epsilon = 100$	9.9293	99.9293	999.9293

Table 6.2: Imaginary part of the eigenvalues, calculated numerically with the method described in section 2.4, for $n = 2$, $N = 50$ and $m = 1$.

α	10	100	1000
$\epsilon = 0.01$	****	92.7	992.9
$\epsilon = 0.1$	7.5	97.7	997.8
$\epsilon = 1$	9.3	99.3	999.1
$\epsilon = 10$	9.8	99.8	999.3
$\epsilon = 100$	9.9	99.9	999.3

Tables 6.3 and 6.4 illustrate that there is a difference between the values of λ when ϵ is small because this asymptotic formula is for waves confined at the poles. The numerical values for α and ϵ large are not accurate, due to the fact that the numerical method is not able to compute them in this regime with accuracy.

Table 6.3: Imaginary part of the eigenvalues calculated in the asymptotic theory. In this case $n' = 1$.

α	10	100	1000
$\epsilon = 0.01$	****	78.7868	978.7868
$\epsilon = 0.1$	****	93.2918	993.2918
$\epsilon = 1$	7.8787	97.8787	997.8787
$\epsilon = 10$	9.3292	99.3292	999.3292
$\epsilon = 100$	9.7879	99.7879	999.7879

Table 6.4: Imaginary part of the eigenvalues, calculated numerically with the method described in section 2.4, for $n = 3$, $N = 50$ and $m = 1$.

α	10	100	1000
$\epsilon = 0.01$	****	62.6	992.9
$\epsilon = 0.1$	****	93.2	997.8
$\epsilon = 1$	7.7	97.9	997.0
$\epsilon = 10$	9.3	99.3	997.5
$\epsilon = 100$	9.77	99.7	997.6

6.2.1 Solutions near the poles

Another possible scaling for approximating solutions with high polar trapping is described in this section. This scaling can be more useful for characterising the functions at the pole due to the fact that the term $(1 - \mu^2)$ tends to zero near the pole and the considerations of the last section are not valid in this case.

In the previous section 6.2, the factor related to the latitude is

$$1-\mu = 1-\cos\theta = 2\sin^2\left(\frac{\theta}{2}\right) = \frac{\gamma_1}{\alpha}\hat{\mu} = \frac{1}{\alpha\sqrt{8\epsilon}}\hat{\mu}.$$

If the solutions are near the north pole, θ is small, then, $\sin\theta/2 \sim \theta/2$, so

$$\frac{\theta^2}{2} = \frac{\hat{\mu}}{\alpha\sqrt{8\epsilon}} \quad \rightarrow \quad \hat{\mu} = \sqrt{2\epsilon}\alpha\theta^2.$$

For example, when $n' = 0$, the solution is

$$\tilde{u}_\theta = A\theta e^{-\sqrt{\frac{\epsilon}{2}}\alpha\theta^2}, \tag{6.8}$$

where A is a normalization constant. As a consequence of this $\tilde{u}_\theta$ is linearly proportional to θ near the pole. Calculating the first derivative

$$\frac{d\tilde{u}_\theta}{d\theta} = [1-\sqrt{2\epsilon}\alpha\theta^2]Ae^{-\sqrt{\frac{\epsilon}{2}}\alpha\theta^2}, \tag{6.9}$$

When the derivative is zero, the value of the function is maximum:

$$\frac{d\tilde{u}_\theta}{d\theta} = 0 \qquad \text{when} \quad 1-\sqrt{2\epsilon}\alpha\theta^2 = 0, \quad \text{for the} \quad n=0 \quad \text{mode.}$$

The maximum occurs at $\theta = \sqrt{1/(\alpha\sqrt{2\epsilon})}$, when θ is in radians.

The only unsatisfactory feature of this analysis is that to eliminate the second term T_2 we assume $(\lambda^2 - m^2\alpha^2)\epsilon(1-\mu^2) \gg m^2$, and that $(\lambda^2 - m^2\alpha^2)\epsilon(1-\mu^2)$ is $\mathcal{O}(\alpha)$. When $(1-\mu^2)$ is very small, close to the pole, this will not be true. To investigate this region, we need a second scaling:

$$\mu = 1 - \frac{\gamma_2}{\alpha^2}\tilde{\mu}.$$

Then, $\mu^2 = 1 - \frac{2\gamma_2}{\alpha^2}\tilde{\mu} + \frac{\gamma_2^2}{\alpha^4}\tilde{\mu}^2$. Therefore

$$1-\mu^2 = \frac{2\gamma_2}{\alpha^2}\tilde{\mu}.$$

The differential operators become $\frac{d}{d\mu} = -\frac{\alpha^2}{\gamma_2}\frac{d}{d\tilde{\mu}}$ and $\frac{d^2}{d\mu^2} = \frac{\alpha^4}{\gamma_2^2}\frac{d^2}{d\tilde{\mu}^2}$. Also the factor $(\lambda^2 - m^2\alpha^2)\epsilon(1-\mu^2) - 1 \rightarrow -1 - 4\gamma_2\epsilon\tilde{\mu}$. Substituting this scaling into equation (2.64), the terms reduce to

$$T_1 = (1-\mu^2)\tfrac{\partial^2 \tilde{u}_\theta}{\partial \mu^2} \sim 2\tfrac{\alpha^2}{\gamma_2}\tilde{\mu}\tfrac{\partial^2 \tilde{u}_\theta}{\partial \tilde{\mu}^2} = \mathcal{O}(\alpha^2),$$

$$T_2 = \tfrac{2}{[(\lambda^2-\alpha^2m^2)\epsilon(1-\mu^2)-m^2]}\mu\tfrac{\partial \tilde{u}_\theta}{\partial \mu} \sim \tfrac{2\alpha^2}{\gamma_2(1+4\epsilon\gamma_2\tilde{\mu})}\tfrac{d\tilde{u}_\theta}{d\tilde{\mu}} = \mathcal{O}(\alpha^2),$$

$$T_3 = \epsilon(\lambda^2-\alpha^2m^2)\tilde{u}_\theta \sim -2\epsilon\alpha^2\tilde{u}_\theta = \mathcal{O}(\alpha^2),$$

$$T_4 = \tfrac{-m(\lambda+2m\alpha^2)}{(\lambda^2-\alpha^2m^2)}\tilde{u}_\theta \sim \big[2+\tfrac{i}{2\alpha}-\tfrac{(2k+1)}{4\alpha^2}\big]\tilde{u}_\theta = \mathcal{O}(1),$$

$$T_5 = -\tfrac{\epsilon(\lambda+2m\alpha^2)^2\mu^2}{(\lambda^2-\alpha^2m^2)}\tilde{u}_\theta \sim 2\epsilon\alpha^2\tilde{u}_\theta = \mathcal{O}(\alpha^2),$$

$$T_6 = \tfrac{-1}{1-\mu^2}\tilde{u}_\theta \sim \tfrac{-\alpha^2}{2\gamma_2\tilde{\mu}}\tilde{u}_\theta = \mathcal{O}(\alpha^2),$$

$$T_7 = \tfrac{-2m\epsilon(\lambda+2m\alpha^2)\mu^2}{[(\lambda^2-\alpha^2m^2)\epsilon(1-\mu^2)-m^2]}\tilde{u}_\theta \sim \tfrac{4\epsilon\alpha^2}{1+4\epsilon\gamma_2\tilde{\mu}}\tilde{u}_\theta = \mathcal{O}(\alpha^2).$$

When the terms balance at $\mathcal{O}(\alpha^2)$, the equation is

$$\tilde{\mu}\frac{d^2\tilde{u}_\theta}{d\tilde{\mu}^2} + \frac{1}{(1+4\gamma_2\epsilon\tilde{\mu})}\frac{d\tilde{u}_\theta}{d\tilde{\mu}} - \frac{1}{4\tilde{\mu}}\tilde{u}_\theta + \frac{2\epsilon\gamma_2}{(1+4\epsilon\gamma_2\tilde{\mu})}\tilde{u}_\theta = 0. \tag{6.10}$$

This equation has a very simple general solution. We let $4\epsilon\gamma_2 = 1$, i.e, choose $\gamma_2 = 1/4\epsilon$. Then

$$\tilde{\mu}\frac{d^2\tilde{u}_\theta}{d\tilde{\mu}^2} + \frac{1}{(1+\tilde{\mu})}\frac{d\tilde{u}_\theta}{d\tilde{\mu}} - \frac{1}{4\tilde{\mu}}\tilde{u}_\theta + \frac{1}{2(1+\tilde{\mu})}\tilde{u}_\theta = 0. \tag{6.11}$$

The general solution is

$$\tilde{u}_\theta = C_1\tilde{\mu}^{1/2} + C_2\big(\frac{\tilde{\mu}ln\tilde{\mu}-1}{\sqrt{\tilde{\mu}}}\big), \tag{6.12}$$

which can be verified by direct substitution. Now, because $\tilde{u}_\theta \to 0$ as $\tilde{\mu} \to 0$, $C_2 = 0$. This matches with the Laguerre polynomial solutions, e.g. when $n' = 0$, $\tilde{u}_\theta \sim \tilde{\mu}^{1/2}e^{-\tilde{\mu}/2}$, and $e^{-\tilde{\mu}/2} \to 1$, as $\tilde{\mu} \to 0$. So as $\tilde{\mu} \to \infty$ it matches to $\tilde{u}_\theta$ as $\hat{\mu} \to 0$. This means that we have a leading order solution valid for all μ near the pole.

For this work, the third and fifth terms of the equation (2.64) have to cancel at leading

order in the previous scaling where μ now set to be 1, this requires

$$(\lambda^2 - \alpha^2 m^2)^2 - (\lambda + 2m\alpha^2)^2 = 0.$$

For this quadratic equation, two solutions exist

$$(\lambda^2 - \alpha^2 m^2) = \pm(\lambda + 2m\alpha^2). \tag{6.13}$$

If we take the negative sign, we find complex eigenvalues

$$\lambda = -\frac{1}{2} \pm \frac{\sqrt{1 + 4\alpha^2 m(m-2)}}{2}. \tag{6.14}$$

If $m = 1$ instability can be possible, as reflected in the numerical results, with $m = 2$ or bigger, λ is purely real, so a growing mode of this type cannot occur. When α is large $\lambda = -\frac{1}{2} \pm \alpha i$, as expected. Note that taking the plus sign in equation (6.13), λ is again real. The formula (6.14) seems to be consistent with other research which found a similar result for the frequencies of the solutions in 3D Boussinesq thin layer approximation where "polar kink" instabilities are mentioned (Cally, 2003).

6.3 Transport of Angular Momentum

There is a special interest to study angular momentum transport in the tachocline (Zahn et al., 1996, Hughes et al., 2007, Dikpati et al., 2003). We consider here how do the unstable waves could change the angular momentum in the system and propose an example.

An equation for the conservation of angular momentum can be obtained multiplying the ϕ-component of the Navier-Stokes equation by the radius of rotation, $R_\perp = R_0 \sin\theta$ and average over longitude and time, denoted here by $\langle\rangle$, see e.g. Miesch and Hindman (2011). These quantities are associated with the Reynolds and magnetic stresses (Gastine et al., 2013). According to Gilman and Dikpati (2002), the tilt in the plot 6.5 implies that

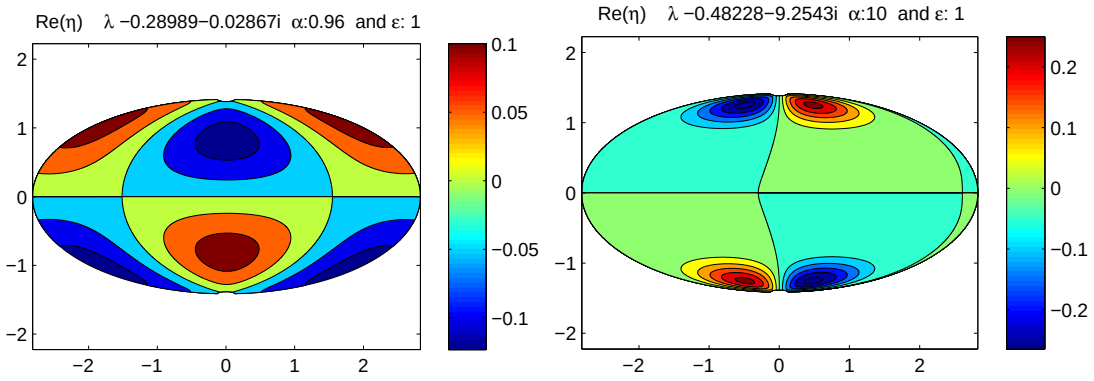

Figure 6.5: Contour plots of the scaled height for Magnetic Rossby mode with $m = 1$, $\epsilon = 1$ with $N = 50$. For weak magnetic fields, $\alpha = 0.96$ (left) the wave are not trapped, then waves are polar trapped when alpha is very large: $\alpha = 10$ (right).

angular momentum is transported towards the poles, as we show in this section. Because the average for linear terms is zero, the nonlinear terms are taken into account in this derivation. We start from the original nonlinear equation (2.25b), and its ϕ-component, as follows

$$\frac{\partial u_\phi}{\partial t} + 2\Omega_0 \cos\theta u_\theta + \frac{1}{R_0}\Big[u_\theta \frac{\partial u_\phi}{\partial \theta} + \frac{u_\phi}{\sin\theta}\frac{\partial u_\phi}{\partial \phi} + u_\theta u_\phi \cot\theta\Big] = -\frac{g}{R_0 \sin\theta}\frac{\partial h}{\partial \phi} \quad (6.15)$$
$$+\frac{1}{\mu_0 \rho R_0}\Big[2B_0 b_\theta \cos\theta + b_\theta \frac{\partial b_\phi}{\partial \theta} + B_0 \frac{\partial b_\phi}{\partial \phi} + \frac{b_\phi}{\sin\theta}\frac{\partial b_\phi}{\partial \phi} + b_\theta b_\phi \cot\theta\Big].$$

Multiplying the equation (6.15) by the radius of rotation, $R_\perp = R_0 \sin\theta$, the equation becomes

$$\frac{\partial}{\partial t}(R_\perp u_\phi) + 2R_\perp \Omega_0 \cos\theta u_\theta + \frac{1}{R_0}\Big[u_\theta \frac{\partial}{\partial \theta}(R_\perp u_\phi) + R_0 u_\phi \frac{\partial u_\phi}{\partial \phi}\Big] = -g\frac{\partial h}{\partial \phi} \quad (6.16)$$
$$+\frac{\sin\theta}{\mu_0 \rho}\Big[2B_0 b_\theta \cos\theta + b_\theta \frac{\partial b_\phi}{\partial \theta} + B_0 \frac{\partial b_\phi}{\partial \phi} + \frac{b_\phi}{\sin\theta}\frac{\partial b_\phi}{\partial \phi} + b_\theta b_\phi \cot\theta\Big].$$

Each quantity can be expressed by:

$$u_\theta = \frac{1}{2}[\hat{u}_\theta e^{i(\omega t - m\phi)} + \hat{u}^*_\theta e^{-i(\omega^* t - m\phi)}],$$

where the star means complex conjugate and $\hat{u}_\theta$ is the amplitude of the function depending on θ.

Averaging the equation (6.16) in time and longitude, the linear terms are zero due to the periodicity of the solutions, then the expression takes the form

$$\frac{\partial}{\partial t}\langle R_\perp u_\phi\rangle = -\frac{1}{R_0}\langle u_\theta \frac{\partial}{\partial\theta}(R_\perp u_\phi)\rangle + \frac{\sin\theta}{\mu_0\rho}\Big[\langle b_\theta \frac{\partial b_\phi}{\partial\theta}\rangle + \langle b_\theta b_\phi\rangle\cot\theta\Big]. \tag{6.17}$$

The first term on the right hand side of this equation is the **Reynolds stress** and the second term is related to **the magnetic stress** (Gilman and Fox, 1997). From the definition of angular momentum per unit volume

$$\mathbb{L} = \rho R_\perp u_\phi,$$

the angular momentum variation is given by

$$\frac{\partial}{\partial t}\langle\mathbb{L}\rangle = -\rho\Big[\langle u_\theta \sin\theta\frac{\partial u_\phi}{\partial\theta}\rangle + \langle u_\theta u_\phi\rangle\cos\theta\Big] + \frac{\sin\theta}{\mu_0}\Big[\langle b_\theta\frac{\partial b_\phi}{\partial\theta}\rangle + \langle b_\theta b_\phi\rangle\cot\theta\Big]. \tag{6.18}$$

Using the relations (2.27d) and (2.27e) between the velocity and the magnetic field, we obtain

$$\frac{\partial}{\partial t}\langle\mathbb{L}\rangle = -\rho\Big[\langle u_\theta \sin\theta\frac{\partial u_\phi}{\partial\theta}\rangle + \langle u_\theta u_\phi\rangle\cos\theta\Big] + \frac{\rho m^2\alpha^2}{|\lambda|^2}\Big[\langle u_\theta \sin\theta\frac{\partial u_\phi}{\partial\theta}\rangle + \langle u_\theta u_\phi\rangle\cos\theta\Big]. \tag{6.19}$$

Calculating the averages, we have

$$\langle u_\theta u_\phi\rangle = \frac{1}{4\tau\omega_i}(1-e^{-2\omega_i\tau})(\hat{u}_\theta\hat{u}_\phi^* + \hat{u}_\theta^*\hat{u}_\phi),$$

where the complex frequency of the wave can be expressed by $\omega = \omega_r + i\omega_i$ and $\tau = 2\pi/\omega_r$ is the period of the wave.

$$\frac{d}{dt}\langle\mathbb{L}\rangle = \rho\frac{(1-e^{-2\omega_i\tau})}{4\tau\omega_i R_0}\Big(\frac{m^2\alpha^2}{|\lambda|^2}-1\Big)\Big\{\hat{u}_\theta\sin\theta\frac{\partial\hat{u}_\phi^*}{\partial\theta} + \hat{u}_\theta^*\sin\theta\frac{\partial\hat{u}_\phi}{\partial\theta} + [\hat{u}_\theta\hat{u}_\phi^* + \hat{u}_\theta^*\hat{u}_\phi]\cot\theta\Big\}. \tag{6.20}$$

We change the variable θ for $\mu = \cos\theta$, and the differential operator D defined before in chapter 2. Therefore the formula (6.20) becomes

$$\frac{d}{dt}\langle \mathbb{L} \rangle = \rho \frac{(1-e^{-2\omega_i \tau})}{4\tau\omega_i R_0}\Big(\frac{m^2\alpha^2}{|\lambda|^2} - 1\Big)\Big\{ - \hat{u}_\theta D\hat{u}_\phi^* - \hat{u}_\theta^* D\hat{u}_\phi + (\hat{u}_\theta\hat{u}_\phi^* + \hat{u}_\theta^*\hat{u}_\phi)\mu \Big\}. \quad (6.21)$$

In the context of α and ϵ large, we have an asymptotic theory explained in detail in section 6.2. In this approximation the expression for the northward velocity , for the mode $n = 0$, can be calculated with the equation (6.6)

$$\tilde{u}_\theta(\mu) = (8\epsilon)^{1/4}\alpha^{1/2}e^{-\sqrt{2\epsilon}\alpha(1-\mu)}(1-\mu)^{\frac{1}{2}}, \qquad \text{and} \qquad \frac{\partial \tilde{u}_\theta}{\partial \mu} = \sqrt{2\epsilon}\alpha\tilde{u}_\theta.$$

The relation between the $\hat{u}_\theta$ and $\tilde{u}_\theta$ is in section 2.4

$$\hat{u}_\theta = \frac{2i\Omega_0 R_0}{\sin\theta}\tilde{u}_\theta.$$

Then $\hat{u}_\theta = -\hat{u}_\theta^*$, and the variable $\tilde{u}_\phi$ in this approximation tends to

$$\tilde{u}_\phi = -\frac{(\lambda + 2m\alpha^2)}{(\lambda^2 - m^2\alpha^2)}\mu\hat{u}_\theta,$$

and its derivative is approximated by

$$\frac{\partial \tilde{u}_\phi}{\partial \mu} = -\frac{(\lambda + 2m\alpha^2)}{(\lambda^2 - m^2\alpha^2)}(1 + \sqrt{2\epsilon}\alpha\mu)\tilde{u}_\theta.$$

Substituting the results into the equation (6.21), we obtain

$$\frac{d}{dt}\langle \mathbb{L} \rangle = \rho \frac{(1-e^{-2\omega_i \tau})}{8\tau\omega_i R_0}\Big(\frac{m^2\alpha^2}{|\lambda|^2} - 1\Big)\Big[\frac{(\lambda + 2m\alpha^2)}{(\lambda^2 - m^2\alpha^2)} + \frac{(\lambda^* + 2m\alpha^2)}{(\lambda^{*2} - m^2\alpha^2)}\Big][1 - 2\mu^2 + \sqrt{2\epsilon}\alpha\mu(1-\mu^2)]|\hat{u}_\theta|^2. \quad (6.22)$$

In the limit of large α, $(\lambda^2 - m^2\alpha^2) \sim -2\alpha^2 + i\alpha$, and $(\lambda + 2m\alpha^2) \sim 2k\alpha + i\alpha$, therefore the factor reduces to

$$\Big[\frac{(\lambda + 2m\alpha^2)}{(\lambda^2 - m^2\alpha^2)} + \frac{(\lambda^* + 2m\alpha^2)}{(\lambda^{*2} - m^2\alpha^2)}\Big] \sim -\frac{(8k\alpha - 2)}{(4\alpha^2 + 1)}, \quad (6.23)$$

where k is an integer greater than zero defined in section 6.2. In conclusion the angular momentum equation is

$$\frac{d}{dt}\langle \mathbb{L} \rangle = -\rho \frac{(1-e^{-2\omega_i \tau})}{8\tau\omega_i R_0}\Big(\frac{m^2\alpha^2}{|\lambda|^2}-1\Big)\frac{(8k\alpha-2)}{(4\alpha^2+1)}[1-2\mu^2+\sqrt{2\epsilon}\alpha\mu(1-\mu^2)]|\hat{u}_\theta|^2. \tag{6.24}$$

Substituting the expression for $\hat{u}_\theta$ and $m=1$, we have the formula

$$\frac{d}{dt}\langle \mathbb{L} \rangle = -\rho(2\epsilon)^{1/2}\alpha \frac{(1-e^{-2\omega_i \tau})}{2\tau\omega_i R_0}\Big(\frac{\alpha^2}{|\lambda|^2}-1\Big)\frac{(4k\alpha-1)}{(4\alpha^2+1)} \tag{6.25}$$

$$[1-2\mu^2+\sqrt{2\epsilon}\alpha\mu(1-\mu^2)]\frac{4\Omega_0^2 R_0^2 e^{-2\sqrt{2\epsilon}\alpha(1-\mu)}}{(1+\mu)}.$$

There is an angular momentum change which depends on latitude. It is likely that this instabilities for magnetic Rossby waves transport angular momentum in the system.

6.4 Summary

This chapter has reviewed the key aspects of instability for magnetic Rossby waves. As shown instability requires two conditions $m=1$ and $\alpha > 0.5$. These unstable modes arise when the frequencies of fast and slow Rossby waves converge towards the same value. In particular when α is large the complex frequencies tends to

$$\lambda = -1/2 + i(\alpha - 1/\sqrt{2\epsilon})$$

and the eigenfunctions for polar trapped waves are

$$\tilde{u}_\theta(\mu) = (1-\mu)^{\frac{1}{2}} e^{-\sqrt{2\epsilon}\alpha(1-\mu)} \mathcal{L}_{n'}\sqrt{8\epsilon}\alpha(1-\mu),$$

where $\mathcal{L}_{n'}$ are the Laguerre polynomials, however we found an expression for solutions near the pole.

It is has been reported that instabilities could be a mechanism for angular momentum transport which might build the rotation profile in the sun.

Chapter 7

Antisymmetric Magnetic Field

7.1 New Antisymmetric Field

In this chapter, we study the development of MHD waves for an antisymmetric field configuration: $B_\phi = B_0 \cos\theta \sin\theta$. The polarity of the basic state of the field is now positive in the northern hemisphere and negative in the southern. This is one of the most striking features of the geomagnetic field. Then we expect that the results could be more related to the geophysical and planetary observations. In addition, the main features of the basic state of the magnetic field, $B_0 \cos\theta \sin\theta$ are that the field is zero at the equator and the maximum in amplitude is at a latitude of $45°$.

Zaqarashvili et al. (2009) carried out a investigation for shallow water MHD using this field configuration. They solved the problem in two special cases for $\alpha^2 \ll 1$. The solutions correspond to Poincaré gravity waves and slow and fast magnetic Rossby waves, with the particularity there is a single slow mode traveling eastward instead of a set of solutions. The first case is for $\epsilon \ll 1$ where the eigenfunctions corresponds to the spherical wave functions $\mathcal{S}_{mn}(\epsilon_1, \mu)$ for $\epsilon_1 = \epsilon_1(\epsilon)$. Then the other case for $\epsilon \gg 1$, where the solutions are confined to the equator.

Again the basic state is chosen for a fluid in rest, the magnetic field is a toroidal field

$B_\phi = B_0 \cos\theta \sin\theta$ and a height field constant H_0 which maybe maintained by imposing and external stress to balance the magnetic stress.

Taking the new magnetic field expression, the MHD Shallow Water model changes to this set of equations

$$\frac{\partial u_\theta}{\partial t} - 2\Omega_0 cos\theta u_\phi + \frac{g}{R_0}\frac{\partial h}{\partial \theta} - \frac{B_0 \cos\theta}{\mu_0 \rho R_0}\frac{\partial b_\theta}{\partial \phi} + \frac{2B_0 \cos^2\theta}{\mu_0 \rho R_0} b_\phi = 0, \tag{7.1a}$$

$$\frac{\partial u_\phi}{\partial t} + 2\Omega_0 \cos\theta u_\theta + \frac{g}{R_0 \sin\theta}\frac{\partial h}{\partial \phi} + (1 - 3\cos^2\theta)\frac{B_0}{\mu_0 \rho R_0} b_\theta - \frac{B_0}{\mu_0 \rho R_0}\cos\theta \frac{\partial b_\phi}{\partial \phi} = 0, \tag{7.1b}$$

$$\frac{\partial h}{\partial t} + \frac{H_0}{R_0 \sin\theta}\frac{\partial}{\partial \theta}(\sin\theta u_\theta) + \frac{H_0}{R_0 \sin\theta}\frac{\partial u_\phi}{\partial \phi} = 0, \tag{7.1c}$$

$$\frac{\partial b_\theta}{\partial t} - \frac{B_0}{R_0}\cos\theta \frac{\partial u_\theta}{\partial \phi} = 0, \tag{7.1d}$$

$$\frac{\partial b_\phi}{\partial t} - \frac{B_0}{R_0}\sin^2\theta u_\theta - \frac{B_0}{R_0}\cos\theta \frac{\partial u_\phi}{\partial \phi} = 0. \tag{7.1e}$$

Performing a Fourier analysis in the form $e^{i(m\phi - \omega t)}$, we know that each derivative with respect to ϕ or t, can be substituted by

$$\frac{\partial}{\partial \phi} = im \qquad \text{and} \qquad \frac{\partial}{\partial t} = -i\omega,$$

Then, the equations will be

$$-\omega i u_\theta - 2\Omega_0 cos\theta u_\phi + \frac{g}{R_0}\frac{\partial h}{\partial \theta} - \frac{mB_0 \cos\theta}{\mu_0 \rho R_0} i b_\theta + \frac{2B_0 \cos^2\theta}{\mu_0 \rho R_0} b_\phi = 0, \tag{7.2a}$$

$$\omega u_\phi + 2\Omega_0 \cos\theta i u_\theta - \frac{mg}{R_0 \sin\theta} h + (1 - 3\cos^2\theta)\frac{B_0}{\mu_0 \rho R_0} i b_\theta - \frac{mB_0}{\mu_0 \rho R_0}\cos\theta b_\phi = 0, \tag{7.2b}$$

$$\omega h + \frac{H_0}{R_0 \sin\theta}\frac{\partial}{\partial \theta}(\sin\theta i u_\theta) - \frac{mH_0}{R_0 \sin\theta} u_\phi = 0, \tag{7.2c}$$

$$\omega b_\theta + \frac{mB_0}{R_0}\cos\theta u_\theta = 0, \tag{7.2d}$$

$$\omega b_\phi - \frac{B_0}{R_0}\sin^2\theta i u_\theta + \frac{mB_0}{R_0}\cos\theta u_\phi = 0. \tag{7.2e}$$

These are the non-dimensional parameters and variables

$$\lambda = \frac{\omega}{2\Omega_0}, \qquad \alpha^2 = \frac{B_0^2}{\rho \mu_0 4\Omega^2 R_0^2}, \qquad \epsilon = \frac{4\Omega^2 R_0^2}{g H_0}.$$

$$\tilde{u}_\theta = \frac{\sin\theta i u_\theta}{2\Omega_0 R_0}, \qquad \tilde{u}_\phi = \frac{\sin\theta u_\phi}{2\Omega_0 R_0}, \qquad \eta = \frac{gh}{4\Omega_0^2 R_0^2}, \qquad \tilde{b}_\theta = \frac{\sin\theta i b_\theta}{B_0}, \qquad \tilde{b}_\phi = \frac{\sin\theta b_\phi}{B_0}.$$

Changing to the dimensionless variables and parameters, the system of equations becomes

$$\lambda i\tilde{u}_\theta + \mu\tilde{u}_\phi + (1-\mu^2)\frac{d\eta}{d\mu} + m\alpha^2\mu\tilde{b}_\theta - 2\alpha^2\mu^2\tilde{b}_\phi = 0, \tag{7.3a}$$

$$\lambda\tilde{u}_\phi + \mu\tilde{u}_\theta - m\eta + \alpha^2(1-3\mu^2)\tilde{b}_\theta - m\alpha^2\mu\tilde{b}_\phi = 0, \tag{7.3b}$$

$$\epsilon\lambda(1-\mu^2)\eta - (1-\mu^2)\frac{d\tilde{u}_\theta}{d\mu} - m\tilde{u}_\phi = 0, \tag{7.3c}$$

$$\lambda\tilde{b}_\theta + m\mu\tilde{u}_\theta = 0, \tag{7.3d}$$

$$\lambda\tilde{b}_\phi - (1-\mu^2)\tilde{u}_\theta + m\mu\tilde{u}_\phi = 0, \tag{7.3e}$$

which we shall solve using a similar technique to previously.

7.1.1 Eigenvalues Method for Solving the System of Equations

As before, the solutions proposed are expansions of Associated Legendre polynomials. Each expansion must have $n \geq m$ because the polynomials are not defined for $n < m$,

$$\tilde{u}_\theta = \sum_{n=m}^{\infty} A_n^m P_n^m(\mu), \qquad \tilde{b}_\theta = \sum_{n=m}^{\infty} B_n^m P_n^m(\mu),$$

$$\tilde{u}_\phi = \sum_{n=m}^{\infty} C_n^m P_n^m(\mu), \qquad \tilde{b}_\phi = \sum_{n=m}^{\infty} D_n^m P_n^m(\mu), \qquad \eta = \sum_{n=m}^{\infty} E_n^m P_n^m(\mu).$$

We substitute these solutions into the equations (7.3a), (7.3b), (7.3c), (7.3d) and (7.3e), and use the recurrence relations for Associated Legendre polynomials,

$$\mu P_n^m = p_n P_{n-1}^m + q_n P_{n+1}^m,$$

$$DP_n^m = (n+1)p_n P_{n-1}^m - nq_n P_{n+1}^m.$$

$$\mu^2 P_n^m = p_n p_{n-1} P_{n-2}^m + q_n q_{n+1} P_{n+2}^m + [p_n q_{n-1} + p_{n+1} q_n] P_n^m,$$

where, $q_n = (n-m+1)/(2n+1)$ and $p_n = (n+m)/(2n+1)$. In each of (7.3) we must set the coefficient of $P_n^m(\mu)$ to zero, to obtain a set of equations. Then, we have a

system of equations which is a matrix equation in the form $\lambda \mathbf{B}\vec{v} = \mathbf{A}\vec{v}$. The eigenvectors $\vec{v}$ are the coefficients of the Legendre expansions and the values of λ are the eigenvalues. These take the form

$$\begin{aligned}
\lambda A_n^m &= -2\alpha^2 q_{n-2}q_{n-1}D_{n-2}^m - (n-1)q_{n-1}E_{n-1}^m - m\alpha^2 q_{n-1}B_{n-1}^m + q_{n-1}C_{n-1}^m \\
&- 2\alpha^2(p_n q_{n-1} + p_{n+1}q_n)D_n^m - m\alpha^2 p_{n+1}B_{n+1}^m + p_{n+1}C_{n+1}^m \\
&+ (n+2)p_{n+1}E_{n+1}^m - 2\alpha^2 p_{n+2}p_{n+1}D_{n+2}^m, \qquad (7.4)
\end{aligned}$$

$$\begin{aligned}
\lambda C_n^m &= -3\alpha^2 q_{n-2}q_{n-1}B_{n-2}^m + q_{n-1}A_{n-1}^m - m\alpha^2 q_{n-1}D_{n-1}^m \\
&+ \alpha^2[1 - 3(p_n q_{n-1} + p_{n+1}q_n)]B_n^m + mE_n^m + p_{n+1}A_{n+1}^m \\
&- 3\alpha^2 p_{n+2}p_{n+1}B_{n+2}^m - m\alpha^2 p_{n+1}D_{n+1}^m, \qquad (7.5)
\end{aligned}$$

$$\begin{aligned}
&\lambda\{\epsilon[1 - p_n q_{n-1} - q_n p_{n+1}]E_n^m - \epsilon p_{n+2}p_{n+1}E_{n+2}^m - \epsilon q_{n-1}q_{n-2}E_{n-2}^m\} \\
&\qquad = (n-1)q_{n-1}A_{n-1}^m + mC_n^m - (n+2)p_{n+1}A_{n+1}^m, \qquad (7.6)
\end{aligned}$$

$$\lambda B_n^m = -mq_{n-1}A_{n-1}^m - mp_{n+1}A_{n+1}^m, \qquad (7.7)$$

$$\begin{aligned}
\lambda D_n^m &= q_{n-2}q_{n-1}A_{n-2}^m - mq_{n-1}C_{n-1}^s - [1 - (p_n q_{n-1} + p_{n+1}q_n)]A_n^m \\
&- mp_{n+1}C_{n+1}^m + p_{n+2}p_{n+1}A_{n+2}^m. \qquad (7.8)
\end{aligned}$$

The coefficients A_n^m, D_n^m, B_{n+1}^m, C_{n+1}^m, E_{n+1}^m form an independent set of equations, and the coefficients A_{n+1}^m, D_{n+1}^m, B_n^m, C_n^m, E_n^m form another independent set of equations of different symmetry. We solve each set separately using a MATLAB eigenvalue and eigenvector solver, designed to solve the system of equations $\mathbf{A}\tilde{\mathbf{v}} = \lambda\mathbf{B}\tilde{\mathbf{v}}$.

7.1.2 First System of Equations

The first system of equation is related to the coefficients A_n^m, D_n^m, B_{n+1}^m, C_{n+1}^m, E_{n+1}^m where the solutions for $\tilde{u}_\theta$ and $\tilde{b}_\phi$ are symmetric with respect to the equator and the

eigenfunctions for $\tilde{b}_\theta$, $\tilde{u}_\phi$ and η are antisymmetric. The set of equations is

$$\begin{aligned}\lambda D_n^m &= q_{n-2}q_{n-1}A_{n-2}^m - mq_{n-1}C_{n-1}^s - [1-(p_nq_{n-1}+p_{n+1}q_n)]A_n^m \\ &- mp_{n+1}C_{n+1}^m + p_{n+2}p_{n+1}A_{n+2}^m, \end{aligned} \tag{7.9}$$

$$\begin{aligned}\lambda C_{n+1}^m &= -3\alpha^2 q_{n-1}q_nB_{n-1}^m + q_nA_n^m - m\alpha^2 q_nD_n^m \\ &+ \alpha^2[1-3(p_{n+1}q_n+p_{n+2}q_{n+1})]B_{n+1}^m + mE_{n+1}^m + p_{n+2}A_{n+2}^m \\ &- 3\alpha^2 p_{n+3}p_{n+2}B_{n+3}^m - m\alpha^2 p_{n+2}D_{n+2}^m, \end{aligned} \tag{7.10}$$

$$\begin{aligned}\lambda\{\epsilon[1-p_{n+1}q_n-q_{n+1}p_{n+2}]E_{n+1}^m - \epsilon p_{n+3}p_{n+2}E_{n+3}^m - \epsilon q_nq_{n-1}E_{n-1}^m\} \\ = nq_nA_n^m + mC_{n+1}^m - (n+3)p_{n+2}A_{n+2}^m, \end{aligned} \tag{7.11}$$

$$\lambda B_{n+1}^m = -mq_nA_n^m - mp_{n+2}A_{n+2}^m, \tag{7.12}$$

$$\begin{aligned}\lambda A_n^m &= -2\alpha^2 q_{n-2}q_{n-1}D_{n-2}^m - (n-1)q_{n-1}E_{n-1}^m - m\alpha^2 q_{n-1}B_{n-1}^m + q_{n-1}C_{n-1}^m \\ &- 2\alpha^2(p_nq_{n-1}+p_{n+1}q_n)D_n^m - m\alpha^2 p_{n+1}B_{n+1}^m + p_{n+1}C_{n+1}^m \\ &+ (n+2)p_{n+1}E_{n+1}^m - 2\alpha^2 p_{n+2}p_{n+1}D_{n+2}^m, \end{aligned} \tag{7.13}$$

where $n = m, m+2, m+4, m+6, ...$

7.1.3 Second System of Equations

On the other hand, the second system of equation is obtained when rearrange the equations for the other parity with coefficients: A_{n+1}^m, D_{n+1}^m, C_n^m, B_n^m, E_n^m.... The eigenfunctions $\tilde{b}_\phi$ and $\tilde{u}_\theta$ are antisymmetric with respect to the equator and the solutions for $\tilde{b}_\theta$, $\tilde{u}_\phi$ and η are symmetric.

$$\begin{aligned}\lambda D_{n+1}^m &= q_{n-1}q_nA_{n-1}^m - mq_nC_n^m - [1-(p_{n+1}q_n+p_{n+2}q_{n+1})]A_{n+1}^m \\ &- mp_{n+2}C_{n+2}^m + p_{n+3}p_{n+2}A_{n+3}^m, \end{aligned} \tag{7.14}$$

$$\begin{aligned}\lambda C_n^m &= -3\alpha^2 q_{n-2}q_{n-1}B_{n-2}^m + q_{n-1}A_{n-1}^m - m\alpha^2 q_{n-1}D_{n-1}^m \\ &+ \alpha^2[1-3(p_nq_{n-1}+p_{n+1}q_n)]B_n^m + mE_n^m + p_{n+1}A_{n+1}^m \\ &- 3\alpha^2 p_{n+2}p_{n+1}B_{n+2}^m - m\alpha^2 p_{n+1}D_{n+1}^m, \end{aligned} \tag{7.15}$$

$$\begin{aligned}&\lambda\{\epsilon[1-p_nq_{n-1}-q_np_{n+1}]E_n^m - \epsilon p_{n+2}p_{n+1}E_{n+2}^m - \epsilon q_{n-2}q_{n-1}E_{n-2}^m\} \\ &\qquad = (n-1)q_{n-1}A_{n-1}^m + mC_n^m - (n+2)p_{n+1}A_{n+1}^m, \end{aligned} \tag{7.16}$$

$$\lambda B_n^m = -mq_{n-1}A_{n-1}^m - mp_{n+1}A_{n+1}^m, \tag{7.17}$$

$$\begin{aligned}\lambda A_{n+1}^m &= -2\alpha^2 q_{n-1}q_n D_{n-1}^m - nq_nE_n^m - m\alpha^2 q_nB_n^m + q_nC_n^m \\ &- 2\alpha^2(p_{n+1}q_n + p_{n+2}q_{n+1})D_{n+1}^m - m\alpha^2 p_{n+2}B_{n+2}^m + p_{n+2}C_{n+2}^m \\ &+ (n+3)p_{n+2}E_{n+2}^m - 2\alpha^2 p_{n+3}p_{n+2}D_{n+3}^m, \end{aligned} \tag{7.18}$$

for $n = m, m+2, m+4, m+6, ...$

7.1.4 Ordinary Differential Equation Formulation

In this section, we find a differential equation for the northward velocity $\tilde{u}_\theta$. From equation (7.3d) and (7.3e), the components of the magnetic field are

$$\tilde{b}_\theta = -\frac{m\mu}{\lambda}\tilde{u}_\theta, \qquad \text{and} \qquad \tilde{b}_\phi = \frac{(1-\mu^2)}{\lambda}\tilde{u}_\theta - \frac{m\mu}{\lambda}\tilde{u}_\phi.$$

We substitute $\tilde{b}_\theta$ and $\tilde{b}_\phi$, in equations (7.3a) and (7.3b), and obtain

$$[\lambda^2 - 2\alpha^2\mu^2(1-\mu^2) - m^2\alpha^2\mu^2]\tilde{u}_\theta + (\lambda + 2m\alpha^2\mu^2)\mu\tilde{u}_\phi + \lambda(1-\mu^2)\frac{d\eta}{d\mu} = 0, \tag{7.19}$$

$$(\lambda^2 - m^2\alpha^2\mu^2)\tilde{u}_\phi + (\lambda + 2m\alpha^2\mu^2)\mu\tilde{u}_\theta - m\lambda\eta = 0. \tag{7.20}$$

From equation (7.3c) we have the relation

$$\tilde{u}_\phi = \frac{1}{m}\big[\epsilon\lambda(1-\mu^2)\eta - (1-\mu^2)\frac{d\tilde{u}_\theta}{d\mu}\big]. \tag{7.21}$$

Substituting $\tilde{u}_\phi$ into equations (7.19) and (7.20)

$$m[\lambda^2 - 2\alpha^2\mu^2(1-\mu^2) - m^2\alpha^2\mu^2]\tilde{u}_\theta - (\lambda + 2m\alpha^2\mu^2)(1-\mu^2)\mu\frac{d\tilde{u}_\theta}{d\mu}$$
$$+\epsilon\lambda(\lambda + 2m\alpha^2\mu^2)(1-\mu^2)\mu\eta + m\lambda(1-\mu^2)\frac{d\eta}{d\mu} = 0, \qquad (7.22)$$

$$\lambda[\epsilon(\lambda^2 - m^2\alpha^2\mu^2)(1-\mu^2) - m^2]\eta + m(\lambda + 2m\alpha^2\mu^2)\mu\tilde{u}_\theta - (\lambda^2 - m^2\alpha^2\mu^2)(1-\mu^2)\frac{d\tilde{u}_\theta}{d\mu} = 0. \qquad (7.23)$$

Isolating η in equation (7.23), the expression becomes

$$\eta = \frac{1}{\lambda[\epsilon(\lambda^2 - m^2\alpha^2\mu^2)(1-\mu^2) - m^2]}\left[(\lambda^2 - m^2\alpha^2\mu^2)(1-\mu^2)\frac{d\tilde{u}_\theta}{d\mu} - m(\lambda + 2m\alpha^2\mu^2)\mu\tilde{u}_\theta\right]. \qquad (7.24)$$

and so

$$\frac{d\eta}{d\mu} = \frac{1}{\lambda[\epsilon(\lambda^2 - m^2\alpha^2\mu^2)(1-\mu^2) - m^2]}\Big\{2\epsilon\lambda[\lambda^2 + m^2\alpha^2(1-2\mu^2)]\mu\eta$$
$$-m(\lambda + 6m\alpha^2\mu^2)\tilde{u}_\theta$$
$$-[\lambda(m+2\lambda) + 2m^2\alpha^2(1-2\mu^2)]\mu\frac{d\tilde{u}_\theta}{d\mu} + (\lambda^2 - m^2\alpha^2\mu^2)(1-\mu^2)\frac{d^2\tilde{u}_\theta}{d\mu^2}\Big\}. \qquad (7.25)$$

Substituting η and its derivative into equation (7.22), the resulting expression gives

$$(1-\mu^2)\frac{d^2\tilde{u}_\theta}{d\mu^2} + \frac{2m^2[\lambda^2 + m^2\alpha^2(1-2\mu^2)]}{(\lambda^2 - m^2\alpha^2\mu^2)[\epsilon(\lambda^2 - m^2\alpha^2\mu^2)(1-\mu^2) - m^2]}\mu\frac{d\tilde{u}_\theta}{d\mu}$$
$$+\Bigg\{\left[\frac{1}{1-\mu^2} - \frac{2\alpha^2\mu^2}{(\lambda^2 - m^2\alpha^2\mu^2)}\right][\epsilon(\lambda^2 - m^2\alpha^2\mu^2)(1-\mu^2) - m^2]$$
$$-\frac{[m(\lambda + 6m\alpha^2\mu^2) + \epsilon(\lambda + 2m\alpha^2\mu^2)^2\mu^2]}{(\lambda^2 - m^2\alpha^2\mu^2)}$$
$$-\frac{2\epsilon m(\lambda + 2m\alpha^2\mu^2)[\lambda^2 + m^2\alpha^2(1-2\mu^2)]\mu^2}{(\lambda^2 - m^2\alpha^2\mu^2)[\epsilon(\lambda^2 - m^2\alpha^2\mu^2)(1-\mu^2) - m^2]}\Bigg\}\tilde{u}_\theta = 0. \qquad (7.26)$$

The problem is mathematically more complicated than the symmetric field and the simplification of the equations is more difficult. New factors have been introduced, for instance $(\lambda^2 - m^2\alpha^2\mu^2)$; this produces an Alfvén speed or frequencies dependent on the

latitude. Arregui and Ballester (2011) has shown that if the Alfvén speed varies with latitude then, the modes form a continuous set.

There is the possibility of $\lambda^2 = m^2\alpha^2\mu^2$ and this leads to singularities in the equation and critical layers when $\mu^2 = \lambda^2/m^2\alpha^2$. The behaviour of the critical layer is a nonlinear problem and dissipative effects become important (Maslowe, 1986), but this case is beyond the scope of this thesis.

7.1.5 Normalization Constant

Through the original set of equations, we will try to find an expression for the energy of the system and use this as a normalization constant for the eigenfunctions. Starting from the equations for the MHD Shallow water model we will derive these expressions.

Multiplying equation (7.1a) by u_θ and (7.1b) by u_ϕ

$$\frac{\partial}{\partial t}(\frac{1}{2}u_\theta^2) - 2\Omega_0\cos\theta u_\theta u_\phi + \frac{g}{R_0}u_\theta\frac{\partial h}{\partial\theta} - \frac{B_0\cos\theta}{\mu_0\rho R_0}u_\theta\frac{\partial b_\theta}{\partial\phi} + \frac{2B_0\cos^2\theta}{\mu_0\rho R_0}u_\theta b_\phi = 0, \quad (7.27)$$

$$\frac{\partial}{\partial t}(\frac{1}{2}u_\phi^2) + 2\Omega_0\cos\theta u_\phi u_\theta + \frac{g}{R_0\sin\theta}u_\phi\frac{\partial h}{\partial\phi} + (1-3\cos^2\theta)\frac{B_0}{\mu_0\rho R_0}u_\phi b_\theta - \frac{B_0}{\mu_0\rho R_0}\cos\theta u_\phi\frac{\partial b_\phi}{\partial\phi} = 0 \quad (7.28)$$

Adding equations (7.27) and (7.28), we have

$$\frac{\partial}{\partial t}(\frac{1}{2}u_\theta^2 + \frac{1}{2}u_\phi^2) + \frac{g}{R_0}u_\theta\frac{\partial h}{\partial\theta} + \frac{g}{R_0\sin\theta}u_\phi\frac{\partial h}{\partial\phi} - \frac{B_0\cos\theta}{\mu_0\rho R_0}\big(u_\theta\frac{\partial b_\theta}{\partial\phi} + u_\phi\frac{\partial b_\phi}{\partial\phi}\big) + (1-3\cos^2\theta)\frac{B_0}{\mu_0\rho R_0}u_\phi b_\theta + \frac{2B_0\cos^2\theta}{\mu_0\rho R_0}u_\theta b_\phi = 0. \quad (7.29)$$

Multiply equations (7.1d) by $\frac{H_0 b_\theta}{\rho\mu_0}$ and (7.1e) by $\frac{H_0 b_\phi}{\rho\mu_0}$, the equations are

$$\frac{\partial}{\partial t}\big(\frac{H_0}{2\rho\mu_0}b_\theta^2\big) - \frac{B_0H_0}{\rho\mu_0R_0}\cos\theta b_\theta\frac{\partial u_\theta}{\partial\phi} = 0, \quad (7.30)$$

$$\frac{\partial}{\partial t}\big(\frac{H_0}{2\rho\mu_0}b_\phi^2\big) - \frac{B_0H_0}{\rho\mu_0R_0}\sin^2\theta b_\phi u_\theta - \frac{B_0H_0}{\rho\mu_0R_0}\cos\theta b_\phi\frac{\partial u_\phi}{\partial\phi} = 0. \quad (7.31)$$

Multiplying the equation (7.29) by H_0 and adding to equations (7.30) and (7.31), we obtain

$$\frac{\partial}{\partial t}\left[\frac{H_0}{2}(u_\theta^2+u_\phi^2+\frac{b_\theta^2}{\rho\mu_0}+\frac{b_\phi^2}{\rho\mu_0})+\frac{1}{2}gh^2\right]$$
$$+\frac{gH_0}{R_0}u_\theta\frac{\partial h}{\partial\theta}+\frac{gH_0}{R_0\sin\theta}u_\phi\frac{\partial h}{\partial\phi}+\frac{gH_0}{R_0\sin\theta}h\frac{\partial}{\partial\theta}(\sin\theta u_\theta)+\frac{gH_0}{R_0\sin\theta}h\frac{\partial u_\phi}{\partial\phi}$$
$$-\frac{H_0B_0}{\rho\mu_0R_0}\cos\theta\frac{\partial}{\partial\phi}\big(u_\theta b_\theta+u_\phi b_\phi\big)+(1-3\cos^2\theta)\frac{B_0H_0}{\rho\mu_0R_0}(u_\phi b_\theta-u_\theta b_\phi)=0. \quad (7.32)$$

The last equation can be expressed using differential operators

$$\frac{\partial}{\partial t}\left[\frac{H_0}{2}(u_\theta^2+u_\phi^2+\frac{b_\theta^2}{\rho\mu_0}+\frac{b_\phi^2}{\rho\mu_0})+\frac{1}{2}gh^2\right]-\frac{H_0B_0}{\rho\mu_0R_0}\cos\theta\frac{\partial}{\partial\phi}(\vec{u}\cdot\vec{b})$$
$$+gH_0\nabla\cdot(h\vec{u})+\frac{B_0H_0}{\rho\mu_0R_0}(1-3\cos^2\theta)(u_\phi b_\theta-u_\theta b_\phi)=0. \quad (7.33)$$

Performing a Fourier analysis, in the form $e^{i(m\phi-\omega t)}$, for the equations (7.1d) and (7.1e) where the frequency ω is real. Then evaluating the term $u_\phi b_\theta - u_\theta b_\phi$, we have

$$u_\phi b_\theta-u_\theta b_\phi=\frac{B_0}{\omega^2R_0}\sin^2\theta\frac{\partial}{\partial t}\left(\frac{1}{2}u_\theta^2\right).$$

Substituting this factor in the equation (7.33) , we obtain

$$\frac{\partial}{\partial t}\left[\frac{H_0}{2}(u_\theta^2+u_\phi^2+\frac{b_\theta^2}{\rho\mu_0}+\frac{b_\phi^2}{\rho\mu_0})+\frac{1}{2}gh^2+\frac{B_0^2H_0}{\rho\mu_0\omega^2R_0^2}(1-3\cos^2\theta)\sin^2\theta\left(\frac{1}{2}u_\theta^2\right)\right]$$
$$-\frac{H_0B_0}{\rho\mu_0R_0}\cos\theta\frac{\partial}{\partial\phi}(\vec{u}\cdot\vec{b})+gH_0\nabla\cdot(h\vec{u})=0. \quad (7.34)$$

Integrating this formula over an area, yields

$$\int\int\frac{\partial}{\partial t}\left[\frac{H_0}{2}(u_\theta^2+u_\phi^2+\frac{b_\theta^2}{\rho\mu_0}+\frac{b_\phi^2}{\rho\mu_0})+\frac{1}{2}gh^2+\frac{B_0^2H_0}{\rho\mu_0\omega^2R_0^2}(1-3\cos^2\theta)\sin^2\theta\left(\frac{1}{2}u_\theta^2\right)\right]dS$$
$$-\int\int\frac{H_0B_0}{\rho\mu_0R_0}\cos\theta\frac{\partial}{\partial\phi}(\vec{u}\cdot\vec{b})dS+\int\int gH_0\nabla\cdot(h\vec{u})dS=0. \quad (7.35)$$

The second and third integral are zero and the third one, because the eigenfunctions are periodic in ϕ.

Then, equation (7.35) becomes

$$\frac{\partial}{\partial t}\int\int\left\{\frac{H_0}{2}(u_\theta^2+u_\phi^2+\frac{b_\theta^2}{\rho\mu_0}+\frac{b_\phi^2}{\rho\mu_0})+\frac{1}{2}gh^2\right.$$
$$\left.+\frac{B_0^2H_0}{\rho\mu_0\omega^2R_0^2}(1-3\cos^2\theta)\sin^2\theta\left(\frac{1}{2}u_\theta^2\right)dS\right\}=0. \tag{7.36}$$

The equation for the conservation of energy has an extra term, compared to equation (2.47) due to the magnetic field configuration. Changing variables to the non dimensional quantities

$$\frac{\partial}{\partial t}\int\int 2\Omega_0^2R_0^2H_0\left\{\frac{1}{\sin^2\theta}[\tilde{u}_\theta^2+\tilde{u}_\phi^2+\alpha^2(\tilde{b}_\theta^2+\tilde{b}_\phi^2)]+\epsilon\eta^2+\frac{\alpha^2}{\lambda^2}(1-3\cos^2\theta)\tilde{u}_\theta^2\right\}dS=0. \tag{7.37}$$

Defining the energy per mass of the system as a constant in time as it follows

$$E=\int_0^\pi 4\pi\Omega_0^2R_0^4H_0\left\{\frac{1}{\sin^2\theta}[\tilde{u}_\theta^2+\tilde{u}_\phi^2+\alpha^2(\tilde{b}_\theta^2+\tilde{b}_\phi^2)]+\epsilon\eta^2+\frac{\alpha^2}{\lambda^2}(1-3\cos^2\theta)\tilde{u}_\theta^2\right\}\sin\theta d\theta. \tag{7.38}$$

Let $E=4\pi\Omega_0^2R_0^4H_0$, to normalize the last equation. Then

$$\int_0^\pi\left\{\frac{1}{\sin^2\theta}[\tilde{u}_\theta^2+\tilde{u}_\phi^2+\alpha^2(\tilde{b}_\theta^2+\tilde{b}_\phi^2)]+\epsilon\eta^2+\frac{\alpha^2}{\lambda^2}(1-3\cos^2\theta)\tilde{u}_\theta^2\right\}\sin\theta d\theta=1. \tag{7.39}$$

Let γ a normalization constant for the eigenfunctions and substitute them into the equation (7.39)

$$\tilde{u}_\theta=\gamma\sum_{n=m}^{\infty}A_n^mP_n^m(\mu)\quad e^{im\phi-i\omega t},\qquad \tilde{b}_\theta=\gamma\sum_{n=m}^{\infty}B_n^mP_n^m(\mu)\quad e^{im\phi-i\omega t},$$

$$\tilde{u}_\phi=\gamma\sum_{n=m}^{\infty}C_n^mP_n^m(\mu)\quad e^{im\phi-i\omega t},\qquad \tilde{b}_\phi=\gamma\sum_{n=m}^{\infty}D_n^mP_n^m(\mu)\quad e^{im\phi-i\omega t},$$

$$\eta=\gamma\sum_{n=m}^{\infty}E_n^mP_n^m(\mu)\quad e^{im\phi-i\omega t}.$$

We use again this important result

$$u_\theta u_\theta^* = \frac{\gamma^2}{2}\sum_{n=m}^{N}\sum_{k=m}^{N} A_n^m A_k^{m*} P_n^m(\mu) P_k^m(\mu),$$

where the star means complex conjugate. After some algebra we obtain for $\mu = \cos\theta$

$$\gamma^2 \sum_{n=m}^{\infty}\sum_{k=m}^{\infty}\int_{-1}^{1}\left\{\frac{(A_n^m A_k^{m*} + C_n^m C_k^{m*})}{1-\mu^2} + \frac{\alpha^2(B_n^m B_k^{m*} + D_n^m D_k^{m*})}{(1-\mu^2)}\right.$$

$$\left. -\frac{3\alpha^3}{\lambda^2} A_n^m A_k^{m*}\mu^2 + \left[\epsilon E_n^m E_k^{m*} + \frac{\alpha^2}{\lambda^2} A_n^m A_k^{m*}\right]\right\} P_n^m(\mu) P_k^m(\mu) \quad d\mu = 1. \qquad (7.40)$$

Some integrals have to be evaluated in this equation

$$\begin{aligned}\frac{1}{\gamma^2} = \sum_{n=m}^{\infty}\sum_{k=m}^{\infty}\left[(A_n^m A_k^{m*} + C_n^m C_k^{m*}) + \alpha^2(B_n^m B_k^{m*} + D_n^m D_k^{m*})\right]\int_{-1}^{1}\frac{P_n^m(\mu)P_k^m(\mu)}{(1-\mu^2)} \quad d\mu \\ - \sum_{n=m}^{\infty}\sum_{k=m}^{\infty}\frac{3\alpha^2}{\lambda^2} A_n^m A_k^{m*}\int_{-1}^{1}\mu^2 P_n^m(\mu)P_k^m(\mu) \quad d\mu \\ + \sum_{n=m}^{\infty}\sum_{k=m}^{\infty}\left[\epsilon E_n^m E_k^{m*} + \frac{\alpha^2}{\lambda^2} A_n^m A_k^{m*}\right]\int_{-1}^{1} P_n^m(\mu)P_k^m(\mu) \quad d\mu = 1.\end{aligned} \qquad (7.41)$$

In order to calculate the normalization constant γ, we have to evaluate the integrals with the Legendre polynomials (Abramowitz and Stegun, 1964),

$$\int_{-1}^{1} P_n^m(\mu)P_k^m(\mu) \quad d\mu = \frac{2(n+m)\,!}{(2n+1)(n-m)\,!}\delta_{nk}, \qquad (7.42)$$

$$I_{nk}^m = \int_{-1}^{1}\frac{P_n^m(\mu)P_k^m(\mu)}{(1-\mu^2)} \quad d\mu =$$

$$\begin{cases} \frac{(n+m)\,!}{m(n-m)\,!} & \text{if} \quad n<k \quad \text{when } n \text{ and } k \text{ have the same parity,} \\ \frac{(k+m)\,!}{m(k-m)\,!} & \text{if} \quad k<n \quad \text{when } n \text{ and } k \text{ have the same parity,} \\ 0, & \text{if } n \text{ and } k \text{ have different parity,} \end{cases} \qquad (7.43)$$

$$\int_{-1}^{1} \mu^2 P_n^m(\mu) P_k^m(\mu) \quad d\mu = \frac{(n+m)(n+m-1)}{(2n+1)(2n-1)} \frac{2(n+m-2)\,!}{(2n-3)(n-m-2)\,!} \delta_{n-2,k}$$
$$+ \Big[\frac{(n-m)(n+m)}{(2n+1)(2n-1)} + \frac{(n-m+1)(n+m+1)}{(2n+3)(2n+1)} \Big] \frac{2(n+m)\,!}{(2n+1)(n-m)\,!} \delta_{n,k}$$
$$+ \frac{(n-m+1)(n-m+2)}{(2n+3)(2n+1)} \frac{2(n+m+2)\,!}{(2n+5)(n-m+2)\,!} \delta_{n+2,k}. \quad (7.44)$$

7.2 Numerical results

Turning now to the numerical solutions of the MHD Shallow water equations for an antisymmetric field, a summary of the main findings is presented here. Our main results may be classified depending on their dispersion relation into MIG waves, fast magnetic Rossby waves and an anomalous slow mode travelling westward. We found a notable difference in our results between the symmetric and the antisymmetric field. The slow magnetic Rossby waves disappear from the solutions in the antisymmetric calculation. A possible explanation is that these waves are a result of a balance between the Coriolis force and the magnetic field, but in this case the magnetic field is zero at the equator. Now there is just one slow mode.

7.2.1 Small α Regime

When α is small, the behaviour of the waves is comparable with that found in chapter 4, as expected. Comparing the tables for the eigenvalues, it can be seen that there is a slight difference between the eigenvalues when α is 0.1. In general the eigenvalues follow the results of Longuet-Higgins (1968). By contrast, the set of slow magnetic Rossby waves are not present in the numerical result. There is only one slow mode travelling to the west.

Fast Magnetic Rossby Waves

The fast magnetic Rossby waves are travelling to the west, and for large values of ϵ or moderate values of α, these waves are equatorially trapped. In tables 7.1, 7.2 and 7.3, the values for the normalized frequency are shown, for $m = 1$ and poloidal wavenumbers $n = 1, 2, 3$ respectively. When ϵ and α are small, the fast Rossby wave has frequency (equation (3.18))

$$\lambda \approx -\frac{m}{n(n+1)}. \tag{7.45}$$

When ϵ is large, according to Longuet-Higgins (1968), the fast magnetic Rossby waves have the following dispersion relation for $\mu \geq 1$

$$\lambda \approx -\frac{m}{\epsilon^{1/2}(2\nu+1)}. \tag{7.46}$$

This formula correspond to the equation (4.4). The eigenvalues for the first fast magnetic Rossby mode, $n = 1$, are reported in table 7.1. For small ϵ the values agree with the formula (7.45) for $n = 1$. For ϵ large (10 and 100) these values correspond to the first MIG wave, the negative root in equation (4.2), with $\nu = 0$. This is the **magnetic mixed Rossby-gravity** mode.

Table 7.1: Eigenvalues λ for different values of α and ϵ. Magneto mixed Rossby-gravity mode, $n = 1$, $m = 1$ and $N = 50$: Waves travelling westward.

α	10^{-3}	10^{-2}	10^{-1}
$\epsilon = 0.01$	-0.49988750	-0.4998751	-0.4999
$\epsilon = 0.1$	-0.4987547	-0.4987552	-0.4988
$\epsilon = 1$	-0.4879711	-0.4879751	-0.4884
$\epsilon = 10$	-0.4139875	-0.4140077	-0.4160
$\epsilon = 100$	-0.2710	-0.2710	-0.273323

The velocity field for the magnetic mixed Rossby-gravity wave for this antisymmetric field has the same solutions as for the symmetric problem. As illustrated in figure 7.1,

the waves are equatorially trapped for large ϵ and there is no significant variation when α increases from 10^{-3} to 10^{-1}.

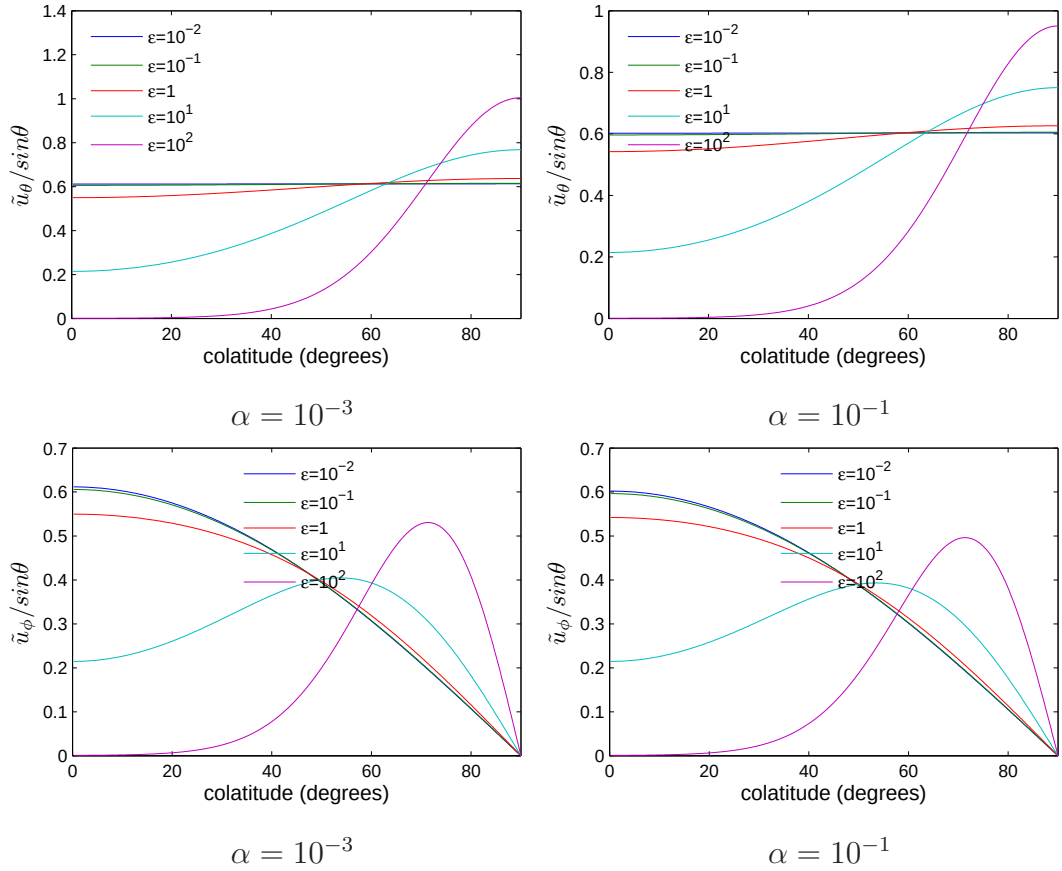

Figure 7.1: Numerical solution for the velocity with different values of ϵ in magnetic mixed Rossby-gravity mode travelling westward for $n = 1$, $m = 1$ and $N = 50$. The first row corresponds to $\tilde{u}_\theta/\sin\theta$ and $\tilde{u}_\phi/\sin\theta$ for the second one. The parameter α is increasing in each column (10^{-3} and 10^{-1}).

Figure 7.2 shows the equatorial trapping for large values of ϵ. When ϵ is small, the solutions correspond to the Legendre polynomials. In these plots there is no difference when α is increases.

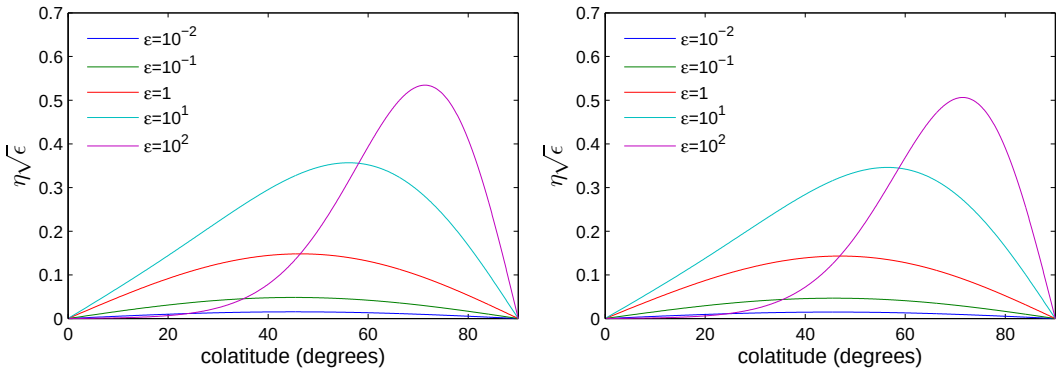

$\alpha = 10^{-3}$ $\alpha = 10^{-1}$

Figure 7.2: Numerical solution for the scaled height $\eta\sqrt{\epsilon}$ with different values of ϵ in magnetic mixed Rossby-gravity mode travelling westward for $n = 1$, $m = 1$ and $N = 50$. The first column corresponds to $\alpha = 10^{-3}$ and the second one to $\alpha = 10^{-1}$.

Figure 7.3 shows the magnetic field components are equatorially trapped waves when the rotation is fast. Also, as expected, the amplitudes of the field are higher than the amplitudes of the velocity, because the magnetic field is proportional to $\sim \lambda^{-1}$, from equations (7.3d) and (7.3e). In contrast to the symmetric field case, the behaviour of the magnetic field will change in this case; now it is not directly proportional to the velocity, as shown in equation (7.3e).

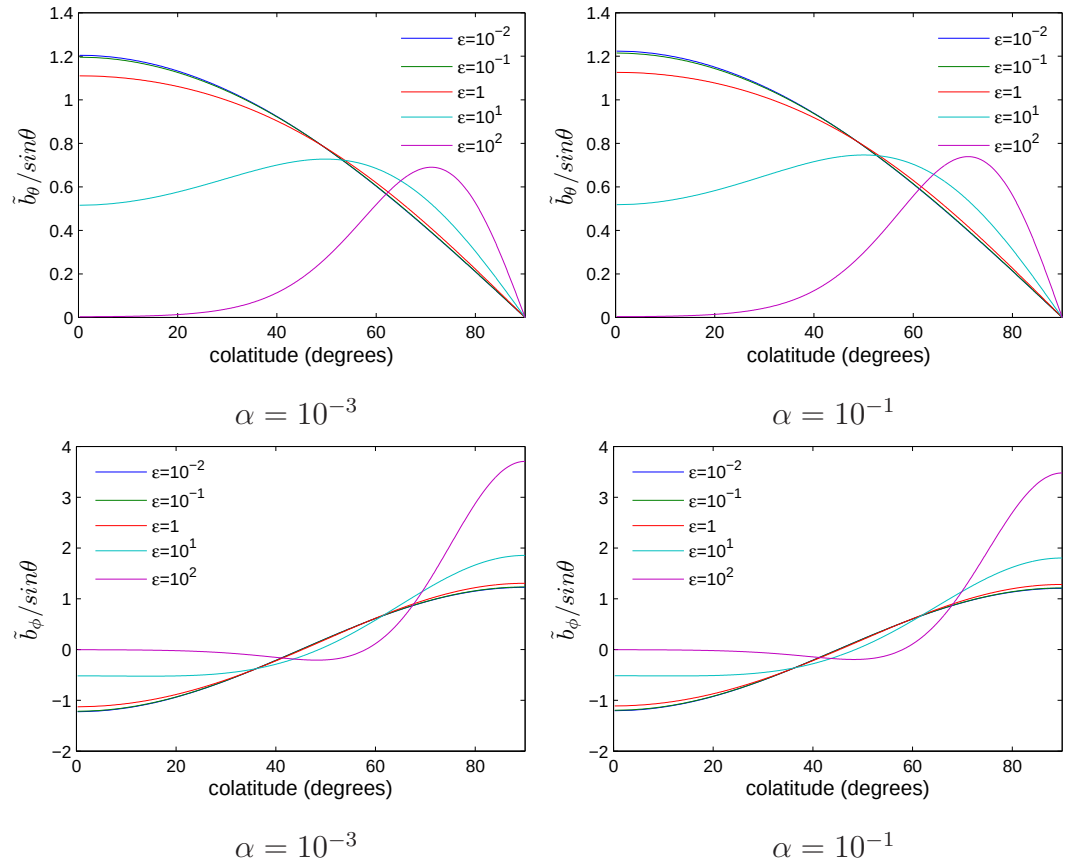

Figure 7.3: Numerical solution for the magnetic field with different values of ϵ in magnetic mixed Rossby-gravity mode travelling westward for $n = 1$, $m = 1$ and $N = 50$. The first row corresponds to $\tilde{b}_\theta/\sin\theta$ and $\tilde{b}_\phi/\sin\theta$ for the second one. The parameter α is increasing in each column (10^{-3} and 10^{-1}).

Table 7.2 corresponds to the eigenvalues for $n = 2$ in the formula (7.45), with ϵ small. However, these results tend to deviate from the expected value when α increases to 0.1 whereas for the symmetric case the values are more accurate as α increases. In the large ϵ region the values correspond to $\nu = 1$ in the expression (7.46) and an instability starts near $\alpha = 0.1$. Note that for the antisymmetric field, instability can occur for α smaller than 0.5, which was a lower bound for the symmetric field.

Table 7.2: Eigenvalues λ for different values of α and ϵ. Fast magnetic Rossby mode, $n = 2$, $m = 1$ and $N = 50$: Waves travelling westward.

α	10^{-3}	10^{-2}	10^{-1}
$\epsilon = 0.01$	-0.16651	-0.16657	-0.17258
$\epsilon = 0.1$	-0.16515	-0.16521	-0.17129
$\epsilon = 1$	-0.15297	-0.15303	-0.15973
$\epsilon = 10$	-0.09495	-0.09502	-0.10338
$\epsilon = 100$	-0.03308	-0.03315	$-0.03749 \pm 3.75 \times 10^{-4}i$

Table 7.3 gives the results for $n = 3$ when ϵ is small which corresponds to the eigenvalue for $\nu = 2$ when ϵ is large. The eigenvalues deviate from the formula (7.45) when α tends to 0.1. In chapter 4, it has been demonstrated that for fast magnetic Rossby waves the wave number follows $\nu = n - m$, where n is the poloidal wave number for small ϵ and ν is its counterpart for large ϵ theory (Longuet-Higgins, 1968).

Table 7.3: Eigenvalues λ for different values of α and ϵ. Fast magnetic Rossby modes $n = 3$, $m = 1$ and $N = 50$: Waves travelling westward.

α	10^{-3}	10^{-2}	10^{-1}
$\epsilon = 0.01$	-0.0832992	-0.0836288	-0.1140
$\epsilon = 0.1$	-0.0829632	-0.0832929	-0.1137
$\epsilon = 1$	-0.0797535	-0.080839	-0.1109
$\epsilon = 10$	-0.0580295	-0.0583440	-0.0998
$\epsilon = 100$	-0.0207079	-0.0209418	$-0.09883 + 0.129372i$

Magneto-Inertial Gravity Waves

The magneto-inertial gravity waves are the highest frequency modes. In general for large ϵ or large α these waves are equatorially trapped. Also these oscillations produce higher amplitudes in the variable η which is the scaled height. Longuet-Higgins (1968) notes that when the rotation parameter is low the potential energy and the kinetic energy are in the same proportion, but if the rotation parameter increases the kinetic energy is three times higher than the potential energy.

The first mode $n = 1$ of MIG waves travelling eastwards is reported in table 7.4. The eigenvalues for ϵ small can be calculated with the expression (equation (4.1))

$$\lambda = \pm\sqrt{\frac{n(n+1)}{\epsilon}}, \tag{7.47}$$

and when ϵ is large the eigenvalues can be calculated with the dispersion relation for the Kelvin mode.

Table 7.4: Eigenvalues λ for different values of α and ϵ. Magneto-inertial gravity waves $n = 1$, $m = 1$ and $N = 50$: Waves travelling eastward.

α	10^{-3}	10^{-2}	10^{-1}
$\epsilon = 0.01$	13.8996	13.8996	13.8995
$\epsilon = 0.1$	4.24517	4.24517	4.26646
$\epsilon = 1$	1.23068	1.23068	1.23068
$\epsilon = 10$	0.3445680	0.3445785	0.3456434
$\epsilon = 100$	0.1026271	0.1026485	0.1047540

There is a wave for $n = 1$ of similar frequency travelling to the west but when ϵ is large the wave turns into the $\nu = 1$ mode in the relation dispersion (4.2), see table 7.5. As expected, the frequencies for westward waves are greater than the eastward ones.

Table 7.5: Eigenvalues λ for different values of α and ϵ. Magneto-inertial gravity waves, $n = 1$, $m = 1$ and $N = 50$: Waves travelling westward.

α	10^{-3}	10^{-2}	10^{-1}
$\epsilon = 0.01$	-14.3997	-14.3997	-14.3997
$\epsilon = 0.1$	-4.74640	-4.74639	-4.26701
$\epsilon = 1$	-1.74147	-1.74146	-1.74085
$\epsilon = 10$	-0.8818762	-0.8818721	-0.881443
$\epsilon = 100$	-0.5283587	-0.5283814	-0.5306403

Next, the mode $n = 2$ for waves travelling eastward is reported in table 7.6. When ϵ is large, this corresponds to the mode $\nu = 0$ for the formula (4.2). We notice that with increasing α the variation in the value of λ is not significant.

Table 7.6: Eigenvalues λ for different values of α and ϵ. Magneto-inertial gravity waves, $n = 2$, $m = 1$ and $N = 50$: Waves travelling eastward.

α	10^{-3}	10^{-2}	10^{-1}
$\epsilon = 0.01$	24.4188	24.4188	24.4188
$\epsilon = 0.1$	7.6851	7.6851	7.6852
$\epsilon = 1$	2.4316	2.4316	2.4321
$\epsilon = 10$	0.8459042	0.8459314	0.8486
$\epsilon = 100$	0.3796	0.3797	0.3830271

The eigenfunctions for the mode $n = 2$, travelling to the east are trapped at the equator when ϵ is large, as shown in figure 7.4. For small ϵ, the eigenfunctions are the Legendre polynomials. The increase in α does not produce a significant change in the eigenvalues or eigenfunctions.

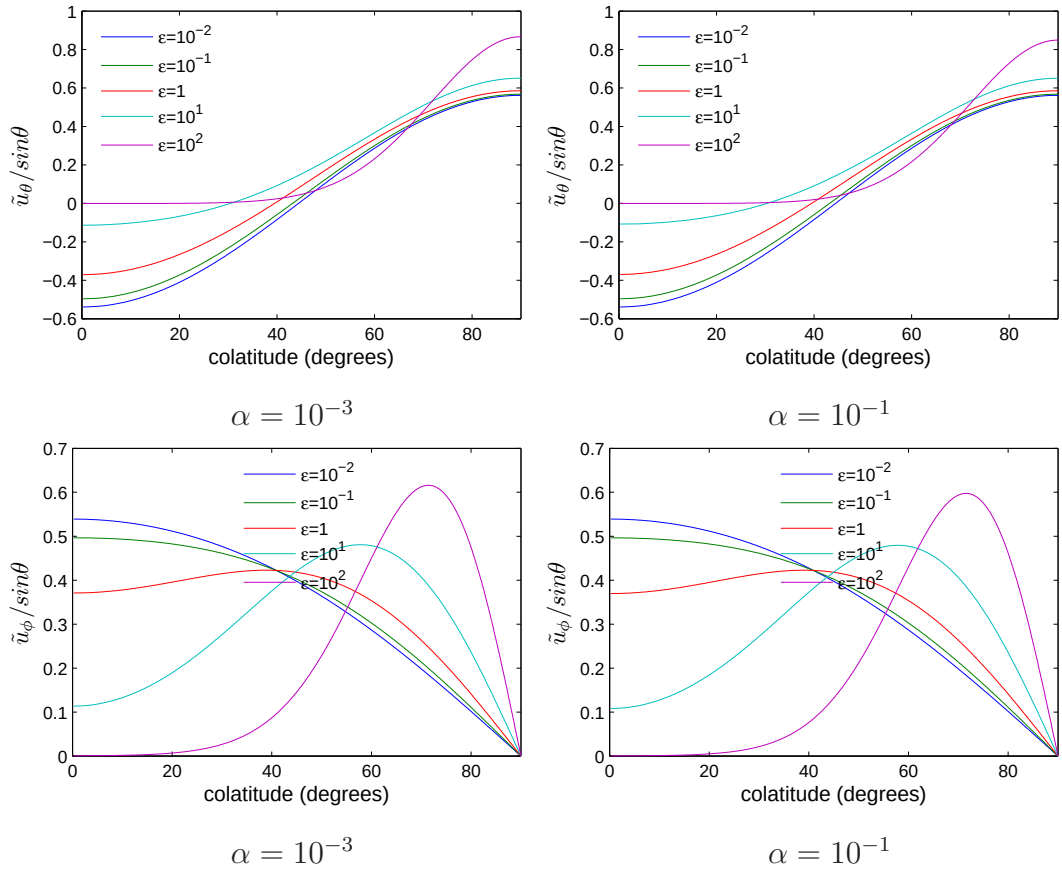

Figure 7.4: Numerical solution of the velocity with different values of ϵ in magneto-inertial gravity wave travelling eastward for the second mode with $n = 2$, $m = 1$ and $N = 50$. The first row corresponds to $\tilde{u}_\theta/\sin\theta$ and $\tilde{u}_\phi/\sin\theta$ for the second one. The parameter α is increasing in each column (10^{-3} and 10^{-1}).

Figures 7.4 and 7.5 show that MIG waves travelling eastward are equatorially trapped when ϵ is large. In the small ϵ regime the waves are Legendre functions. When α increases to 0.1, the eigenfunctions are not significantly changed from their hydrodynamic counterparts.

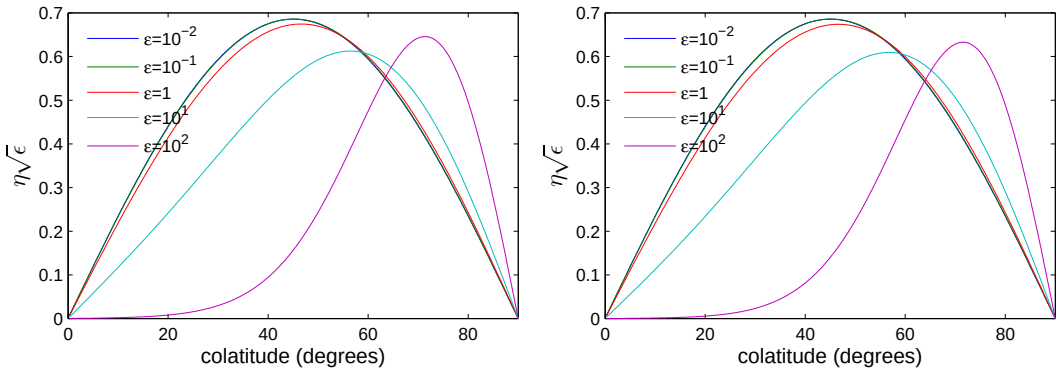

$\alpha = 10^{-3}$ $\alpha = 10^{-1}$

Figure 7.5: Numerical solution of the scaled height $\eta\sqrt{\epsilon}$ with different values of ϵ in magneto inertial gravity wave travelling eastward for the second mode $n = 2$, $m = 1$ with $N = 50$. The first column corresponds to $\alpha = 10^{-3}$ and $\alpha = 10^{-1}$ the second one.

The features of the magnetic field are shown in figure 7.6. The ϕ component is symmetric with respect to the equator whereas the θ component is antisymmetric, for the $n = 2$ mode, opposite to the respective components of the velocity. The waves are equatorially trapped for large ϵ and there is little variation when α is equal to 0.1.

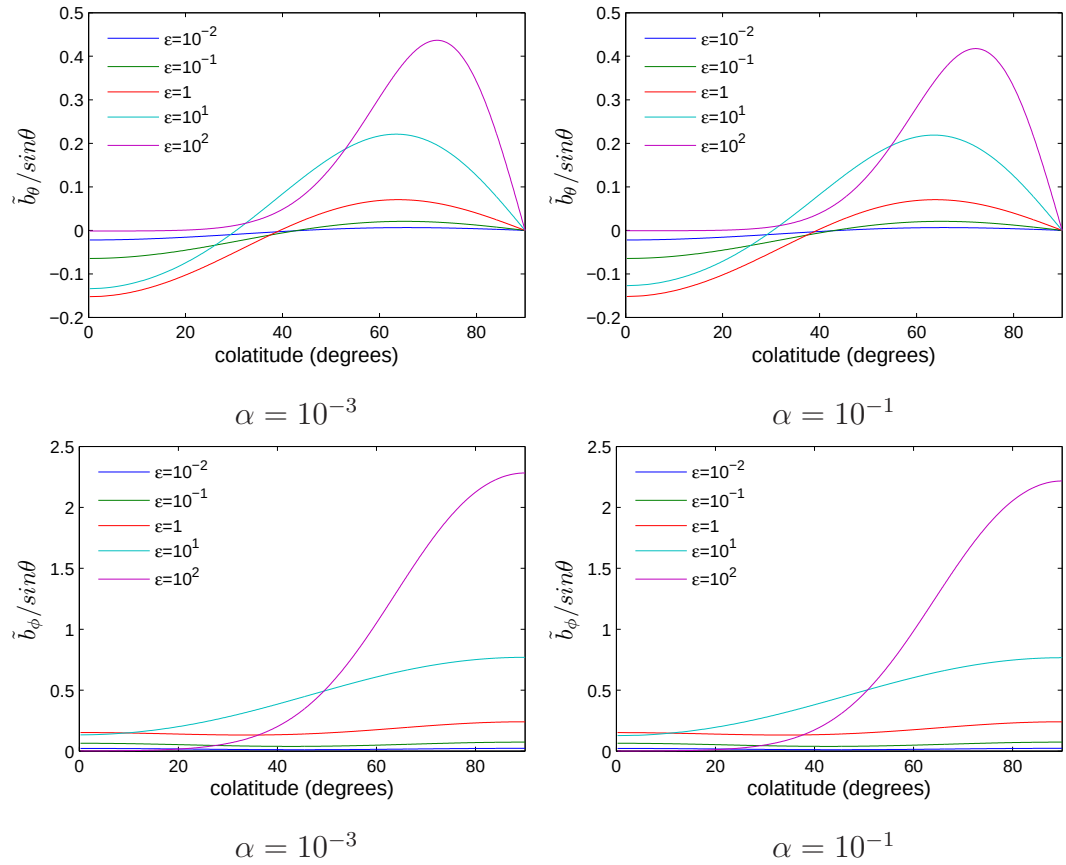

Figure 7.6: Numerical solution of the magnetic field with different values of ϵ in magneto-inertial gravity wave travelling eastward for the second mode with $n = 2$,$m = 1$ and $N = 50$. The first row corresponds to $\tilde{b}_\theta/\sin\theta$ and $\tilde{b}_\phi/\sin\theta$ for the second one. The parameter α is increasing in each column (10^{-3} and 10^{-1}).

As tables 7.6 and 7.7 very clearly demonstrate, westward waves propagate slightly faster than eastward ones; when ϵ is large the eigenvalues correspond to the $\nu = 1$ mode for the formula (4.2). The presence of the magnetic field does not modify considerably the eigenvalues or eigenfunctions in this weak field regime ($\alpha = 10^{-3} \quad \rightarrow \quad 0.1$).

Table 7.7: Eigenvalues λ for different values of α and ϵ. Magneto-inertial gravity waves, $n = 2$, $m = 1$ and $N = 50$: Waves travelling westward.

α	10^{-3}	10^{-2}	10^{-1}
$\epsilon = 0.01$	-24.5857	-24.5857	-24.5857
$\epsilon = 0.1$	-7.8533	-7.8533	-7.8533
$\epsilon = 1$	-2.6129	-2.6129	-2.6125
$\epsilon = 10$	-1.1119	-1.1118	-1.1097
$\epsilon = 100$	-0.6784	-0.6785	-0.6801381

Figure 7.7 illustrates the velocity field components for the $n = 2$ westward MIG wave. In the case when ϵ is small, the amplitude of the velocity increases with ϵ for westward waves in contrast to the eastward waves. Then, for ϵ large, the waves are equatorially trapped and the solution correspond to $\nu = 3$ in the large ϵ theory. There is no significant difference between a weak field and a moderate field for this mode.

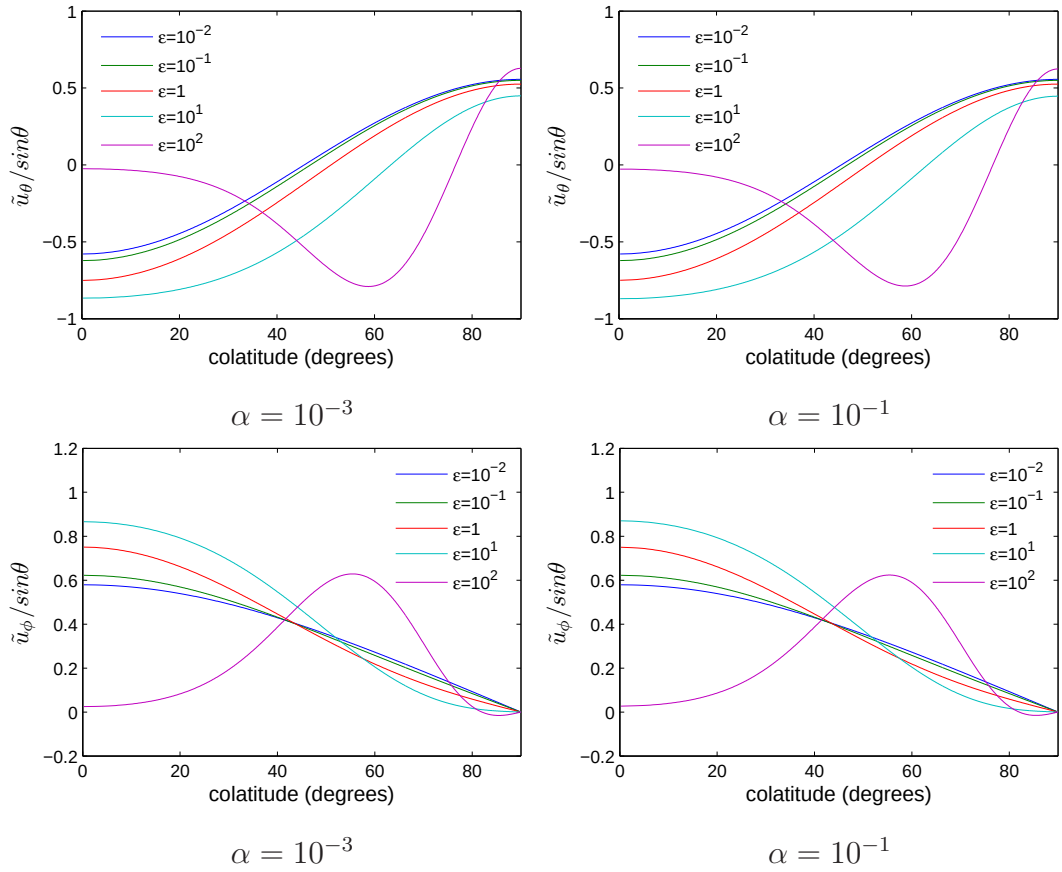

Figure 7.7: Numerical solution of the velocity with different values of ϵ in magneto-inertial gravity wave travelling westward for the second mode $n = 2$, $m = 1$ with $N = 50$. The first row corresponds to $\tilde{u}_\theta/\sin\theta$ and $\tilde{u}_\phi/\sin\theta$ for the second one. The parameter α is increasing in each column (10^{-3} and 10^{-1}).

In figure 7.8 the scaled height is plotted for the mode $n = 2$. The waves are equatorially trapped for large ϵ and the influence of the magnetic field, weak or moderate, does not change the shape of the waves. In the small ϵ case, there is little difference between waves propagating to the east or west for this variable η.

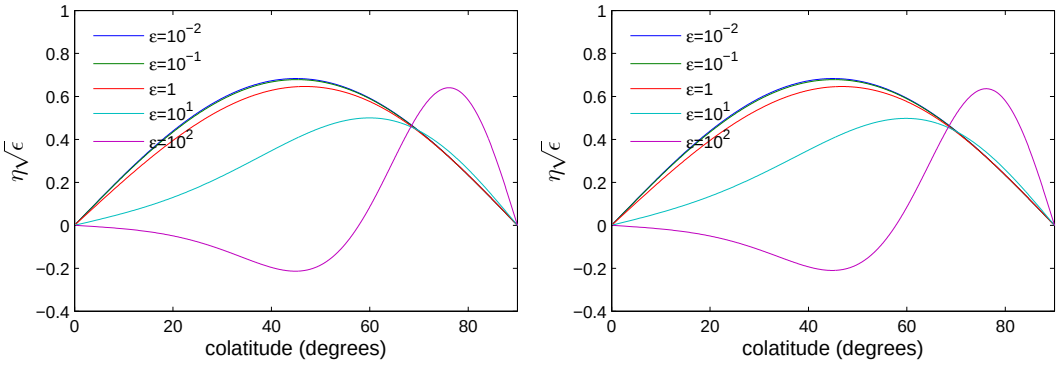

$\alpha = 10^{-3}$ $\alpha = 10^{-1}$

Figure 7.8: Numerical solution of the scaled height $\eta\sqrt{\epsilon}$ with different values of ϵ in magneto-inertial gravity wave travelling westward for the second mode with $n = 2$, $m = 1$ and $N = 50$. The first column corresponds to $\alpha = 10^{-3}$ and $\alpha = 10^{-1}$ the second one.

The magnetic field components for the $n = 2$ westward propagating mode are represented in figure 7.9. The θ component is antisymmetric whereas the ϕ component of the field is symmetric with respect to the equator, in contrast to the velocity components. The waves are equatorially trapped for large ϵ and there is little difference between the eigenfunctions when the magnetic parameter increases from 10^{-3} to 0.1. On the other hand, the wave forms of the westward components of the magnetic field are completely different to the eastward field.

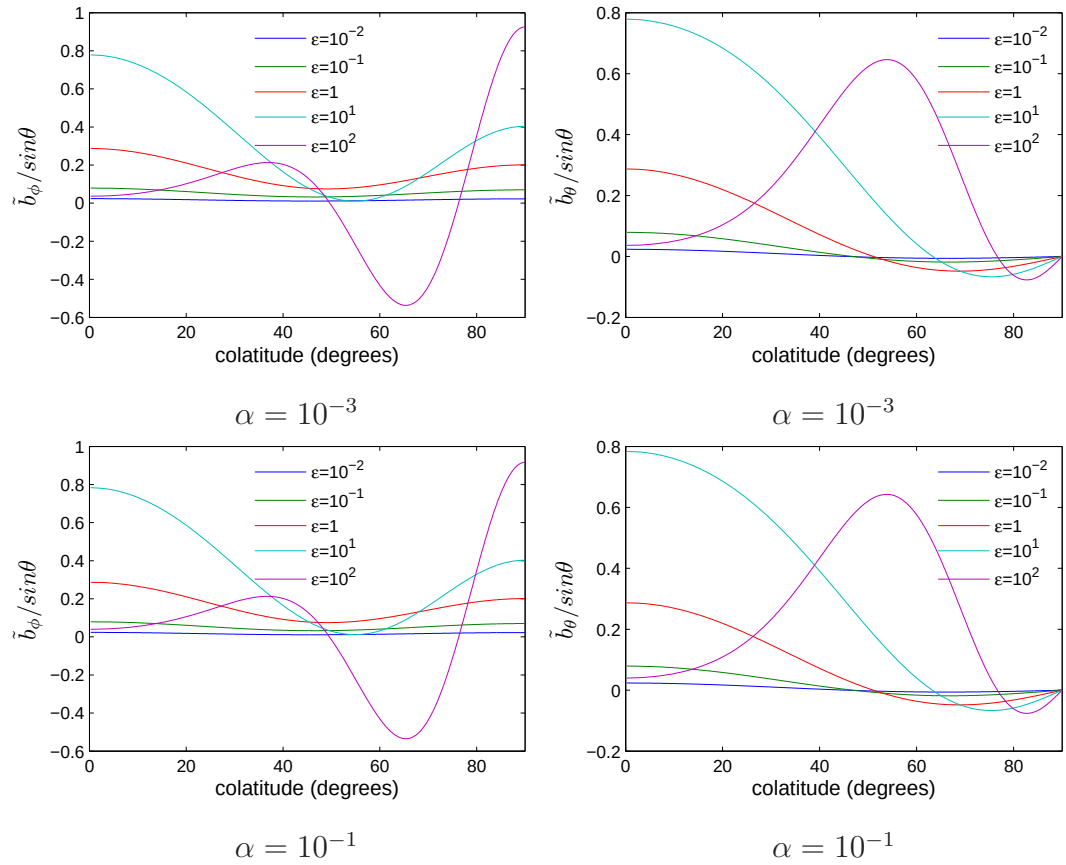

Figure 7.9: Numerical solution of the magnetic field with different values of ϵ in magneto-inertial gravity wave travelling westward for the second mode with $n = 2$, $m = 1$ and $N = 50$. The first row corresponds to $\tilde{b}_\theta/\sin\theta$ and $\tilde{b}_\phi/\sin\theta$ for the second one. The parameter α is increasing in each column (10^{-3} and 10^{-1}).

The eigenvalues for the eastward mode $n = 3$ are reported in table 7.8 and the values are consistent with the formula (7.47) with accuracy for small ϵ. This corresponds to the hydrodynamic formula for gravity waves. If ϵ is large, they turn into the mode $\nu = 1$ of the formula (4.2). When α increases, the values of λ do not change significantly. These waves are equatorially trapped for the field intensities of $\alpha \sim 0.1$ and large ϵ.

Table 7.8: Eigenvalues λ for different values of α and ϵ. Magneto-inertial gravity waves, $n = 3$, $m = 1$ and $N = 50$: Waves travelling eastward.

α	10^{-3}	10^{-2}	10^{-1}
$\epsilon = 0.01$	34.6055	34.6055	34.6056
$\epsilon = 0.1$	10.9321	10.9321	10.9324
$\epsilon = 1$	3.4819	3.4819	3.4829
$\epsilon = 10$	1.216644	1.2167	1.2210
$\epsilon = 100$	0.5750407	0.5751020	0.5810703

Table 7.9 presents a summary of frequencies for the westward propagating MIG waves with $n = 3$. In the small ϵ regime the values reproduce the formula (7.47) for hydrodynamic gravity waves. In our numerical results, the waves travelling to the west are slightly faster than the eastward ones. When ϵ is large the waves are equatorially trapped and the eigenvalues turn into the mode $\nu = 2$ of the dispersion relation (4.2). Increasing the magnetic field does not change the eigenfunctions or eigenvalues, in the small α range.

Table 7.9: Eigenvalues λ for different values of α and ϵ. Magneto-inertial gravity waves, $n = 3$, $m = 1$ and $N = 50$: Waves travelling westward.

α	10^{-3}	10^{-2}	10^{-1}
$\epsilon = 0.01$	-34.6889	-34.6889	-34.6889
$\epsilon = 0.1$	-11.0158	-11.0158	-11.0160
$\epsilon = 1$	-3.5690	-3.5690	-3.5692
$\epsilon = 10$	-1.3400	-1.3400	-1.3384
$\epsilon = 100$	-0.7913028	-0.7913090	-0.7919053

Anomalous Mode

The new anomalous mode was found in the presence of the magnetic field, propagating westward with a very low frequency. This is the first slow magnetic Rossby mode which collides with the first fast magnetic Rossby wave $n = 1$ and the wave becomes unstable, only for $m = 1$. The normalized frequency is summarized in table 7.10, from these numerical results, the frequency of the wave can be approximated by $\lambda = -\frac{4\sqrt{2}}{100}\epsilon\alpha^4$.

Table 7.10: Eigenvalues for different values of α and ϵ, $n = 1$, $m = 1$ and $N = 50$, the anomalous westward slow magnetic Rossby mode.

α	10^{-3}	10^{-2}	10^{-1}
$\epsilon = 0.01$	****	****	-5.5851×10^{-8}
$\epsilon = 0.1$	****	****	-5.6038×10^{-7}
$\epsilon = 1$	****	****	-5.6079×10^{-6}
$\epsilon = 10$	****	-5.6048×10^{-9}	-5.6465×10^{-5}
$\epsilon = 100$	-6.5908×10^{-11}	-5.6071×10^{-8}	-5.9988×10^{-4}

Figure 7.10 shows the northward velocity for the anomalous mode, which can be approximated by $\tilde{u}_\theta \sim \sin\theta$ and the northward component of the magnetic field perturbation. Also the eigenfunction for $\tilde{u}_\theta$ is symmetric whereas $\tilde{b}_\theta$ is antisymmetric.

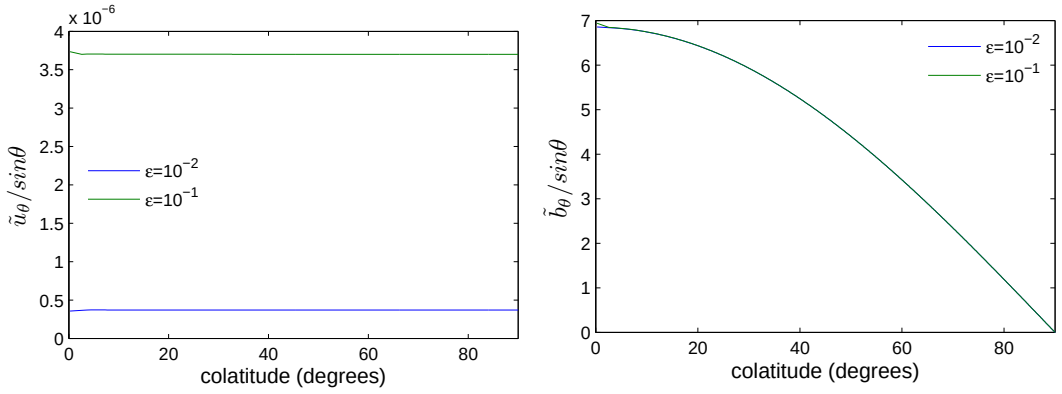

Northward velocity $\tilde{u}_\theta/\sin\theta$ Magnetic field $\tilde{b}_\theta/\sin\theta$

Figure 7.10: Numerical solution of the velocity and the magnetic field for the anomalous slow mode travelling westward with $\alpha = 0.1$, $m = 1$ and $N = 80$.

Numerical results indicate that if $\epsilon\alpha^2$ becomes near 1 the numerical method is not able to compute the eigenfunctions at the poles and for very small frequencies the eigenvalues are not accurate.

7.2.2 Large α Regime

Magnetic Rossby waves

The fast magnetic Rossby waves can become unstable after $\alpha \sim 0.1$ and two modes coalesce and turn into a complex mode. The unstable modes remain complex for certain range of ϵ and then suddenly split apart again, to give two real eigenvalues. This coalescence and separation continues as ϵ is increased. Figure 7.11(a) illustrates this point clearly. These results therefore need to be calculated with caution because the eigenvalues coalesce with different modes depending on the value of ϵ or α.

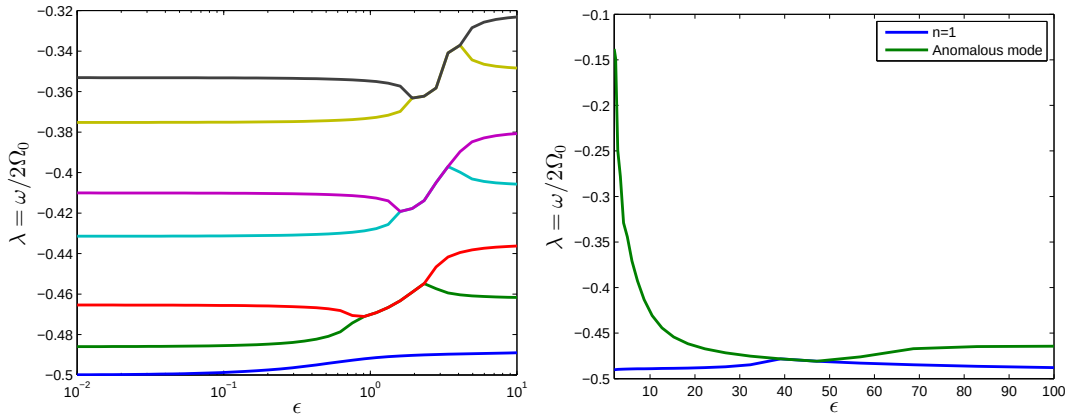

(a) (b)

Figure 7.11: Dispersion relation for fast magnetic Rossby waves for $\alpha = 1$, $m = 1$ with $N = 50$. When two modes coalesce they become complex and we plot only the real part of λ.(a) The $n = 1$ mode in blue, $n = 3$ in green, $n = 5$ in red and so on. (b) The mode $n = 1$ coalesces with the anomalous mode.

These numerical results would seem to suggest that there is no instability for $m \neq 1$. We looked extensively at $m = 2$ and $m = 3$ modes, but we never found any numerical evidence for unstable modes in the antisymmetric field case.

The eigenvalues for the fast magnetic Rossby mode $n = 1$ are reported in table 7.11. The first fast mode coalesces with an anomalous mode and when α increases $\lambda \to -0.5 + m\alpha i$. Even though the behaviour for the other modes with the same parity is different, they become complex at certain value of α then develop into real again, and so on, see figure 7.11(b). The complete plot of this web is not shown here.

The fast magnetic Rossby waves undergo polar trapping when the magnetic field is strong or the rotation is fast.

Table 7.11: Eigenvalues λ for different values of α and ϵ. Fast magnetic Rossby mode, $n = 1$, $m = 1$ and $N = 50$: Waves travelling westward.

α	1	10^1	10^2	10^3
$\epsilon = 0.01$	-0.4998720	-0.2740+1.6404i	-0.4886020+87.4544i	-0.49897+987.72i
$\epsilon = 0.1$	-0.4987279	-0.4441+5.8565i	-0.4967+96.0964i	-0.49962+996.03i
$\epsilon = 1$	-0.4916683	-0.4886+8.7318i	-0.4990+98.7711i	-0.49965+997.71i
$\epsilon = 10$	-0.4929	-0.4967+9.5969i	-0.4996+99.6013i	-0.49964+997.86i
$\epsilon = 100$	-0.4878+0.7248i	-0.4990+9.8646i	-0.4996+99.7693i	-0.49964+997.87i

The second fast magnetic Rossby mode $n = 2$ coalesces with the mode $n = 4$ and become complex after $\alpha = 1$. For large α, the real part of λ tends to -0.5 and the imaginary part tends to $m\alpha$. These waves are confined at the poles for large α and ϵ.

Table 7.12: Eigenvalues λ for different values of α and ϵ. Fast magnetic Rossby mode, $n = 2$, $m = 1$ and $N = 50$: Waves travelling westward.

α	1	10^1	10^2	10^3
$\epsilon = 0.01$	-0.17610	-0.05521+0.594i	-0.48860+87.45i	-0.49897+963.20i
$\epsilon = 0.1$	-0.17596	-0.44598+5.838i	-0.49667+96.10i	-0.49968+996.12i
$\epsilon = 1$	-0.03308+0.0298i	-0.45212+6.213i	-0.49897 + 98.77i	-0.49982 + 998.55i
$\epsilon = 10$	-0.43153+0.0373i	-0.49667+9.597i	-0.49962+99.60i	-0.49982 + 998.87i
$\epsilon = 100$	-0.48785+0.7248i	-0.49897+9.865i	-0.49982 + 99.85i	-0.49982+ 998.90i

Magneto-inertial gravity waves

The highest frequencies correspond to MIG waves. As shown in chapter 4 these waves have superalfvénic frequencies ($|\lambda| > m\alpha$) and are stable in the symmetric field case. For large α, for a given ϵ, the velocity becomes subalfvénic and the modes seem to disappear.

In table 7.13 the possible eigenvalues are summarized for the mode $n = 2$ travelling eastward and the result for the mode $n = 2$ travelling westward are reported in table 7.14. The spaces with stars reflect that the eigenvalues are not reliable.

Table 7.13: Eigenvalues λ for different values of α and ϵ. Magneto-inertial gravity waves, $n = 2$, $m = 1$ and $N = 50$: Waves travelling eastward.

α	1	10^1
$\epsilon = 0.01$	24.4200	24.6383
$\epsilon = 0.1$	7.6926	****
$\epsilon = 1$	2.4909	****
$\epsilon = 10$	1.0337	****

Table 7.14: Eigenvalues λ for different values of α and ϵ. Magneto-inertial gravity waves, $n = 2$, $m = 1$ and $N = 50$: Waves travelling westward.

α	1	10^1
$\epsilon = 0.01$	-24.5858	-24.7021
$\epsilon = 0.1$	-7.8504	****
$\epsilon = 1$	-2.5763	****

Figure 7.12 shows the scaled height against colatitude; the waves are equatorially trapped when ϵ increases for $\alpha = 1$, but for large values of α, and even for $\alpha = 1$ when ϵ is large, the mode disappears. The eigenfunctions cannot be calculated beyond this point.

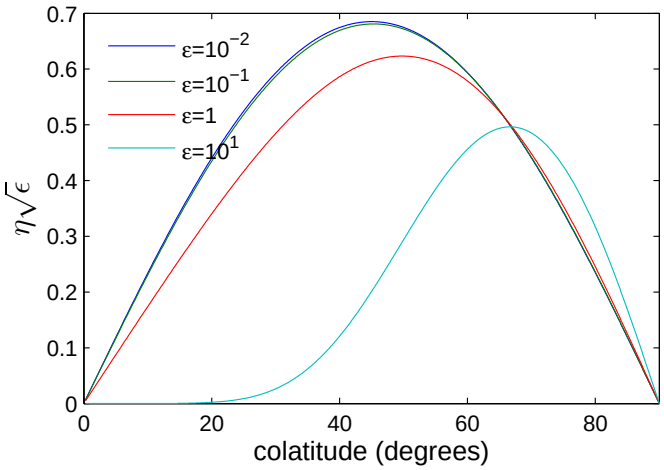

Figure 7.12: Numerical solution for the scaled height: $\eta\sqrt{\epsilon}$. Second mode $n = 2$ for magneto-inertial gravity waves travelling eastward with $\alpha = 1$, $m = 1$ and $N = 50$.

There is a value of the parameter α after which the frequency of the MIG waves becomes subalfvénic: $|\lambda| < m\alpha$. When α goes beyond that point the eigenfunctions present a problem near $\mu = \pm 1$ because the factor $\lambda^2 - m^2\alpha^2\mu^2$, which appears in equation (7.26), becomes zero near there. This means the equation becomes singular. The modes could not be found beyond this critical particular value of α, suggesting that a critical layer occurs.

The critical point occurs for a certain value of α, as shown in table 7.15 for the westward and eastward second MIG mode.

Table 7.15: Value of α after which the wave speed become subalfvénic. For the second magneto-inertial gravity waves: $n = 2$, $m = 1$ and $N = 50$. Waves travelling westward and eastward.

	Westward	Eastward
$\epsilon = 0.01$	28.6	28.7
$\epsilon = 0.1$	8.9	9
$\epsilon = 1$	2.7	2.9
$\epsilon = 10$	0.9	1.0
$\epsilon = 100$	0.8	0.4

The critical point increases when ϵ is small, and the difference between eastward and westward modes is evident when ϵ is large. For small ϵ and $n = 2$, $m = 1$ with $N = 50$. The numerics suggest that the critical value of α is given approximately by

$$\alpha_{crit} = \frac{2\sqrt{2}}{\sqrt{\epsilon}}. \tag{7.48}$$

Note in table 7.15 that there is little difference between eastward and westward propagating waves. For large values of ϵ the critical value tends to

$$\alpha_{crit} = \pm\frac{\sqrt{2\nu+1}}{\epsilon^{1/4}} + \frac{1}{(4\nu+2)\epsilon^{1/2}}. \tag{7.49}$$

In both cases the α value tends to be proportional to the frequency of the gravitational waves for small or large ϵ, we call this value λ_g.

In our numerical results at the critical point $\lambda = m\alpha$ where α is proportional to the frequency of the gravity waves. Then as $\lambda \to \lambda_g$, there is a critical point near the poles ($\mu = \pm 1$).

Also equation (7.26) has a singularity because the factor $(\lambda^2 - m^2\alpha^2\mu^2)$ tends to zero for the critical point $\mu = \pm 1$ when $\lambda = m\alpha$ for MIG waves.

The findings from these numerical results suggest that there is a critical layer because

there are no waves after a critical point. A critical layer could be defined as a region below a critical point with a considerable change of the momentum, also it might absorb the waves. The absorption of waves is evident in gravity waves (Bühler, 2014).
The critical layer is a non-linear problem that is beyond of the purpose of this thesis, but it is another possible area of future research. Several methods currently exist for studying how the waves interact with the critical layer; one common answer is to set complex frequencies as $\lambda = \lambda_r + i\lambda_i$ (Bühler, 2014) or consider viscosity (Wahlén, 2009). Also in the literature there are other methods (Aasen and Varholm, 2016).

7.3 Analytical Approaches

7.3.1 Cartesian Coordinates Approximation

In this section, we develop an approximation for a weak antisymmetric magnetic field, similarly to the method of Zaqarashvili et al. (2007), in order to enumerate the types of waves that we can find.

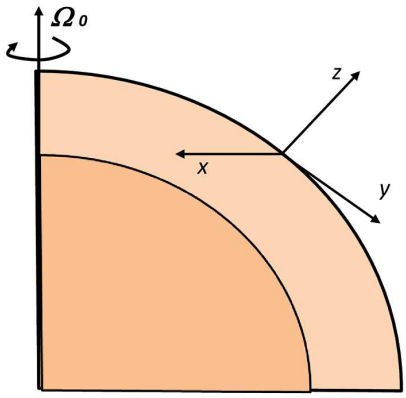

Figure 7.13: Tangent plane geometry.

In Cartesian coordinates there is an analogous antisymmetric field for the shallow water system, when the basic state of the magnetic field is $B_x = B_0 y$ and the height is H_0, a constant. In a tangent plane to a surface of a sphere, the coordinate x is in the azimuthal direction, the y coordinate points to the south and z is the vertical (Vallis, 2006), see figure 7.13.
The shallow water equations in this context are

linearised to

$$\frac{\partial u_x}{\partial t} - f u_y = \frac{B_0}{\rho\mu_0} b_y + \frac{B_0}{\rho\mu_0} y \frac{\partial b_x}{\partial x} - g\frac{\partial h}{\partial x}, \tag{7.50a}$$

$$\frac{\partial u_y}{\partial t} + f u_x = \frac{B_0}{\rho\mu_0} y \frac{\partial b_y}{\partial x} - g\frac{\partial h}{\partial y}, \tag{7.50b}$$

$$\frac{\partial h}{\partial t} + H_0\Big(\frac{\partial u_x}{\partial x} + \frac{\partial u_y}{\partial y}\Big) = 0, \tag{7.50c}$$

$$\frac{\partial b_x}{\partial t} = -B_0 u_y + B_0 y \frac{\partial u_x}{\partial x}, \tag{7.50d}$$

$$\frac{\partial b_y}{\partial t} = B_0 y \frac{\partial u_y}{\partial x}, \tag{7.50e}$$

where $f = f(y)$ is the Coriolis parameter. Differentiating (7.50a) and (7.50b) with respect to t, we have

$$\frac{\partial^2 u_x}{\partial t^2} - f\frac{\partial u_y}{\partial t} = \frac{B_0}{\rho\mu_0}\frac{\partial b_y}{\partial t} + \frac{B_0}{\rho\mu_0} y \frac{\partial^2 b_x}{\partial x \partial t} - g\frac{\partial^2 h}{\partial x \partial t}, \tag{7.51}$$

$$\frac{\partial^2 u_y}{\partial t^2} + f\frac{\partial u_x}{\partial t} = \frac{B_0}{\rho\mu_0} y \frac{\partial^2 b_y}{\partial x \partial t} - g\frac{\partial^2 h}{\partial y \partial t}. \tag{7.52}$$

Substituting $\frac{\partial b_x}{\partial t}$, $\frac{\partial b_y}{\partial t}$ and $\frac{\partial h}{\partial t}$ into equations (7.51) and (7.52)

$$\frac{\partial^2 u_x}{\partial t^2} - f\frac{\partial u_y}{\partial t} = (C_0^2 + v_A^2 y^2)\frac{\partial^2 u_x}{\partial x^2} + C_0^2 \frac{\partial^2 u_y}{\partial x \partial y}, \tag{7.53}$$

$$\frac{\partial^2 u_y}{\partial t^2} + f\frac{\partial u_x}{\partial t} = v_A^2 y^2 \frac{\partial^2 u_y}{\partial x^2} + C_0^2 \frac{\partial^2 u_x}{\partial x \partial y} + C_0^2 \frac{\partial^2 u_y}{\partial y^2}, \tag{7.54}$$

where $v_A^2 = B_0^2/\rho\mu_0$ is the Alfvén speed and $C_0^2 = gH_0$ is the velocity of the gravity waves. We perform a Fourier analysis in the form: $e^{i(k_x x - \omega t)}$, then the equations become

$$(k_x^2 C_0^2 + k_x^2 v_A^2 y^2 - \omega^2)u_x + if\omega u_y - ik_x C_0^2 \frac{\mathrm{d}u_y}{\mathrm{d}y} = 0, \tag{7.55}$$

$$if\omega u_x + (\omega^2 - k_x^2 v_A^2 y^2)u_y + ik_x C_0^2 \frac{\mathrm{d}u_x}{\mathrm{d}y} + C_0^2 \frac{\mathrm{d}^2 u_y}{\mathrm{d}y^2} = 0. \tag{7.56}$$

From equation (7.55)

$$u_x = \frac{i}{(k_x^2 C_0^2 + k_x^2 v_A^2 y^2 - \omega^2)}\Big[k_x C_0^2 \frac{\mathrm{d}u_y}{\mathrm{d}y} - f\omega u_y\Big]. \tag{7.57}$$

In this case, we use the β-plane approximation for the Coriolis parameter, where $f = f_0 + \beta y$, where $\beta = 2\Omega_0/R_0 \cos\Theta_0$ and $f_0 = 2\Omega_0 \sin\Theta_0$ (Vallis, 2006). We differentiate the equation (7.55), then

$$\frac{\mathrm{d}u_x}{\mathrm{d}y} = \frac{1}{(k_x^2 C_0^2 + k_x^2 v_A^2 y^2 - \omega^2)}\Big[ik_x C_0^2 \frac{\mathrm{d}^2 u_y}{\mathrm{d}y^2} - i\beta\omega u_y - if_0\omega\frac{\mathrm{d}u_y}{\mathrm{d}y} - 2k_x^2 v_A^2 y u_x\Big]. \quad (7.58)$$

Next, we substitute u_x and its derivative into the equation (7.56)

$$(k_x^2 v_A^2 y^2 - \omega^2)\frac{\mathrm{d}^2 u_y}{\mathrm{d}y^2} + \frac{2k_x^4 C_0^2 v_A^2}{(k_x^2 C_0^2 + k_x^2 v_A^2 y^2 - \omega^2)} y \frac{\mathrm{d}u_y}{\mathrm{d}y}$$
$$+\Big\{k_x\beta\omega + \frac{(f_0+\beta y)^2\omega^2}{C_0^2} - \frac{(k_x^2 C_0^2 + k_x^2 v_A^2 y^2 - \omega^2)}{C_0^2}(k_x^2 v_A^2 y^2 - \omega^2) - \frac{2k_x^3 v_A^2 \omega (f_0+\beta y) y}{(k_x^2 C_0^2 + k_x^2 v_A^2 y^2 - \omega^2)}\Big\}u_y = 0. \quad (7.59)$$

The following part of this section moves on to describe some approximations to the solution of the above equation. Also it could be demonstrated that some complex fast magnetic Rossby mode are present in the system.

Limit when $v_A^2 \ll C_0^2$

In the case where the magnetic field is weak and we consider waves away from the equator ($\beta y \ll f_0$), equation (7.59) simplifies to

$$-\omega^2\frac{\mathrm{d}^2 u_y}{\mathrm{d}y^2} + \Big\{k_x\beta\omega + k_x^2\omega^2 - \frac{\omega^4}{C_0^2} + \frac{f_0^2\omega^2}{C_0^2}\Big\}u_y = 0. \quad (7.60)$$

We propose solutions of the form $u_y \sim e^{ik_y y}$, hence

$$\omega^3 - \Big[f_0^2 + C_0^2(k_x^2 + k_y^2)\Big]\omega - \beta k_x C_0^2 = 0. \quad (7.61)$$

For large frequencies, the last term in the equation (7.61) is neglected, and the solutions are the Poincaré-inertia gravity waves as in Zaqarashvili et al. (2007)

$$\omega^2 = f_0^2 + C_0^2(k_x^2 + k_y^2). \quad (7.62)$$

For small frequencies the first term of the equation (7.61) is ignored. In this case the solutions correspond to fast magnetic Rossby waves

$$\omega = -\frac{k_x \beta}{k_x^2 + k_y^2 + \left(\frac{f_0}{C_0}\right)^2}. \tag{7.63}$$

Low frequency limit

When the magnetic field is weak $v_A \ll 1$, and the frequencies are low $\omega^2 \ll 1$, then the factor $k_x^2 C_0^2 + k_x^2 v_A^2 y^2 - \omega^2 \to k_x^2 C_0^2$. Substituting this approximation into (7.59) the expression reduces to

$$(k_x^2 v_A^2 y^2 - \omega^2)\frac{\mathrm{d}^2 u_y}{\mathrm{d}y^2} + 2k_x^2 v_A^2 y \frac{\mathrm{d}u_y}{\mathrm{d}y}$$

$$+\Big\{\frac{(f_0+\beta y)^2\omega^2}{C_0^2} + \beta k_x \omega - \frac{-2k_x v_A^2 (f_0+\beta y)\omega}{C_0^2} y - k_x^2(k_x^2 v_A^2 y^2 - \omega^2)\Big\}u_y = 0. \tag{7.64}$$

The frequencies for slow magnetic Rossby waves are expected to be

$$\omega = \frac{k_x v_A^2}{\beta}\hat{\omega}, \tag{7.65}$$

where $\hat{\omega} \sim \mathcal{O}(1)$. Now assume $v_A^2/\beta^2 \ll 1$ and $(f_0 + \beta y)^2 \sim k_x^2 C_0^2$, to get

$$y^2 \frac{\mathrm{d}^2 u_y}{\mathrm{d}y^2} + 2y\frac{\mathrm{d}u_y}{\mathrm{d}y} + \Big\{\hat{\omega} - k_x^2 y^2\Big\}u_y = 0. \tag{7.66}$$

Substituting $u_y = u y^{-1/2}$ the differential equation is now the modified Bessel equation

$$y^2 \frac{\mathrm{d}^2 u}{\mathrm{d}\hat{y}^2} + 2y\frac{\mathrm{d}u}{\mathrm{d}y} - \Big\{k_x^2 y^2 + \big(\frac{1}{4} - \hat{\omega}\big)\Big\}u_y = 0. \tag{7.67}$$

with solutions

$$u_y = A\frac{I_\nu(k_x y)}{y^{1/2}} + B\frac{K_\nu(k_x y)}{y^{1/2}}, \tag{7.68}$$

where ν is an integer number for defined solutions and $\nu^2 = 1/4 - \hat{\omega}$. The frequencies of the waves are given by

$$\omega = \frac{k_x v_A^2}{\beta}\Big(\frac{1}{4} - \nu^2\Big). \tag{7.69}$$

These are not wave like solutions, diverge when $y \to \infty$. The equation (7.64) is valid provided y is large compared to the very small $\hat{\omega}^2 v_A^2/\beta^2$. These findings cannot be extrapolated to values of y, close to the equator there is a different equation to solve.

Low frequency limit: near the equator

A new scaling is used for the case when the waves are equatorially trapped

$$y = \frac{\hat{\omega} v_A}{\beta}\hat{y}. \tag{7.70}$$

Also $\hat{\omega}^2 v_A^2/\beta^2 \ll 1$ then $y \to 0$. Then the differential equation becomes

$$(1-\hat{y}^2)\frac{\partial^2 u_y}{\partial \hat{y}^2} - 2\hat{y}\frac{\partial u_y}{\partial \hat{y}} - \hat{\omega}^2 u_y = 0. \tag{7.71}$$

This is the Legendre differential equation with solutions $u_y = P_n(\hat{y})$ and frequencies equal to

$$\omega = -\frac{k_x v_A^2}{\beta} n(n+1). \tag{7.72}$$

This solution corresponds to magnetic Rossby waves travelling westward and is valid in the limit $y \sim 0$ but diverges for other values of y. This conclusion proves that slow magnetic Rossby waves are not present in the system. Zaqarashvili et al. (2015) have mentioned that slow magnetic Rossby waves could explain the Rieger-type periodicity in the solar tachocline for a toroidal magnetic field $B_\phi = B_0 \sin\theta\cos\theta$. However, our results have demonstrated that the slow magnetic Rossby waves are absent for this field configuration. To get valid wave-like solutions for slow magnetic Rossby waves, additional physics, such as magnetic or vicous diffusion is required. The analysis sheds light on why it was not possible to find slow magnetic Rossby waves in a diffusion-less model with $B_\phi = B_0 \cos\theta\sin\theta$.

7.3.2 The Axisymmetric Case, $m = 0$

In the case of a symmetric magnetic field analysed in chapters 2-6, when $m = 0$ the system of equations reduces to the axisymmetric case for the non-magnetic problem, which has been solved and extensively studied by Longuet-Higgins (1968). In contrast, the presence of an antisymmetric magnetic field $B_\phi = B_0 \cos\theta \sin\theta$ leads to a new case when $m = 0$, which is the interest of this section.

The system of equations (7.3a)-(7.3e) for $m = 0$ is

$$\lambda\tilde{u}_\theta + \mu\tilde{u}_\phi + (1-\mu^2)\frac{d\eta}{d\mu} - 2\alpha^2\mu^2\tilde{b}_\phi = 0, \tag{7.73a}$$

$$\lambda\tilde{u}_\phi + \mu\tilde{u}_\theta + \alpha^2(1-3\mu^2)\tilde{b}_\theta = 0, \tag{7.73b}$$

$$\epsilon\lambda\eta - \frac{d\tilde{u}_\theta}{d\mu} = 0, \tag{7.73c}$$

$$\lambda\tilde{b}_\theta = 0, \tag{7.73d}$$

$$\lambda\tilde{b}_\phi - (1-\mu^2)\tilde{u}_\theta = 0. \tag{7.73e}$$

In the axisymmetric case, the northward component of the magnetic field is zero. Substituting (7.73d) and (7.73e) into the first three equations, we have

$$[\lambda^2 - 2\alpha^2\mu^2(1-\mu^2)]\tilde{u}_\theta + \lambda\mu\tilde{u}_\phi + \lambda(1-\mu^2)\frac{d\eta}{d\mu} = 0, \tag{7.74}$$

$$\lambda\tilde{u}_\phi = -\mu\tilde{u}_\theta, \tag{7.75}$$

$$\epsilon\lambda\eta - \frac{d\tilde{u}_\theta}{d\mu} = 0. \tag{7.76}$$

Substituting $\tilde{u}_\phi$ into equation (7.74), we obtain

$$[\lambda^2 - 2\alpha^2\mu^2(1-\mu^2) - \mu^2]\tilde{u}_\theta + \lambda(1-\mu^2)\frac{d\eta}{d\mu} = 0. \tag{7.77}$$

Differentiating this expression, we have

$$\lambda(1-\mu^2)\frac{d^2\eta}{d\mu^2} - 2\lambda\mu\frac{d\eta}{d\mu} + [\lambda^2 - 2\alpha^2\mu^2(1-\mu^2) - \mu^2]\frac{d\tilde{u}_\theta}{d\mu}$$
$$-2\mu(1 - 2\alpha^2\mu^2 + 2\alpha^2(1-\mu^2))\tilde{u}_\theta = 0. \tag{7.78}$$

Substituting $\tilde{u}_\theta$ from equation (7.77) and its derivative (equation (7.76)) into (7.78), an equation for the scaled height, η is

$$(1-\mu^2)\frac{d^2\eta}{d\mu^2} + \Big\{\frac{[\lambda^2 - 1 - 2\alpha^2(1-\mu^2)^2]}{[\lambda^2 - \mu^2 - 2\alpha^2\mu^2(1-\mu^2)]}\Big\}\mu\frac{d\eta}{d\mu} + \epsilon[\lambda^2 - \mu^2 - 2\alpha^2\mu^2(1-\mu^2)]\eta = 0. \tag{7.79}$$

This second order differential equation will be solved in the case where ϵ is small.

Small ϵ regime

In the case when ϵ is small, the gravity waves have large frequencies, and the equation (7.79) reduces to

$$(1-\mu^2)\frac{d^2\eta}{d\mu^2} - 2\mu\frac{d\eta}{d\mu} + \epsilon\lambda^2\eta = 0, \tag{7.80}$$

which is the Legendre differential equation with solutions

$$\eta = P_n(\mu), \qquad \text{and} \qquad \lambda = \pm\sqrt{\frac{n(n+1)}{\epsilon}}. \tag{7.81}$$

These are the gravity modes, found by Longuet-Higgins (1968), where P_n are the Legendre polynomials.

Large ϵ regime

When ϵ is large, the numerical results for the non-axisymmetric case show that some waves are equatorially trapped, then $\mu \to 0$. Therefore the terms $1-\mu^2 \sim 1$ and $\mu^4 \sim 0$. Hence the equation (7.79) becomes

$$\frac{d^2\tilde{u}_\theta}{d\mu^2} + \epsilon[\lambda^2 - (1+2\alpha^2)\mu^2]\tilde{u}_\theta = 0. \tag{7.82}$$

Let us define a new scale: $\chi = (1+2\alpha^2)^{1/4}\epsilon^{1/4}\mu$. In this scaling the differential equation is

$$\frac{d^2\tilde{u}_\theta}{d\chi^2} + \Big[\frac{\epsilon^{1/2}\lambda^2}{(1+2\alpha^2)^{1/2}} - \chi^2\Big]\tilde{u}_\theta = 0. \tag{7.83}$$

This is the parabolic cylinder differential equation, with solutions

$$\tilde{u}_\theta = Ce^{-\frac{1}{2}(1+2\alpha^2)^{1/2}\epsilon^{1/2}\mu^2} H_\nu((1+2\alpha^2)^{1/4}\epsilon^{1/4}\mu) \tag{7.84}$$

for $\nu = 0, 1, 2, ...$ and H_ν are the Hermite polynomials. The dispersion relation for these set of solutions is

$$\lambda = \pm(2\nu+1)^{1/2}\frac{(2\alpha^2+1)^{1/4}}{\epsilon^{1/4}}. \tag{7.85}$$

These are gravity waves with positive and negative frequencies. In this approximation there is no difference between positive or negative frequencies. We note that if α is equal zero the frequency λ tends to the first order approximation for the frequency of gravity waves in the hydrodynamic case (equation (3.33)). The effect of the magnetic field is to increase the frequency of the waves and enhance the equatorial trapping.

7.3.3 Kelvin Wave

One important feature of a Kelvin wave is that the flow is constrained to travel towards the east or west, and the northward velocity becomes zero when we increase the parameters α or ϵ. Using the fact that $\tilde{u}_\theta \to 0$, the system of equations (7.3a)-(7.3e) simplifies to

$$\mu\tilde{u}_\phi + (1-\mu^2)\frac{d\eta}{d\mu} - 2\alpha^2\mu^2\tilde{b}_\phi = 0, \tag{7.86a}$$

$$\lambda\tilde{u}_\phi - m\eta + m\alpha^2\mu\tilde{b}_\phi = 0, \tag{7.86b}$$

$$\epsilon\lambda(1-\mu^2)\eta - m\tilde{u}_\phi = 0, \tag{7.86c}$$

$$\tilde{b}_\theta = 0, \tag{7.86d}$$

$$\lambda\tilde{b}_\phi = -m\mu\tilde{u}_\phi. \tag{7.86e}$$

Substituting $\tilde{b}_\phi$ into the equations (7.86a) and (7.86b), we obtain

$$(\lambda + 2m\alpha^2\mu^2)\mu\tilde{u}_\phi + \lambda(1-\mu^2)\frac{d\eta}{d\mu} = 0, \tag{7.87}$$

$$(\lambda^2 - m^2\alpha^2\mu^2)\tilde{u}_\phi - m\lambda\eta = 0, \tag{7.88}$$

$$\epsilon\lambda(1-\mu^2)\eta - m\tilde{u}_\phi = 0. \tag{7.89}$$

The equations (7.87) and (7.89) lead to a first order differential equation

$$m\frac{d\eta}{d\mu} + \epsilon(\lambda + 2m\alpha^2\mu^2)\mu\eta = 0. \tag{7.90}$$

The solution is obtained by simple integration

$$\eta = e^{-\frac{\epsilon}{2m}\mu^2(\lambda+m\alpha^2\mu^2)}. \tag{7.91}$$

This wave is trapped at the equator for large ϵ or α as it is expected, and the dispersion relation is approximately

$$\lambda \sim \pm\frac{m}{\sqrt{\epsilon}},$$

which is the same expression found by Longuet-Higgins (1968). However, a negative frequency is still possible if the factor $\sqrt{\epsilon}\alpha^2\mu^2 \geq 1$. There is a possibility that a negative Kelvin wave is present.

7.4 Summary

The numerical results and theory reported here appear to support the assumption that the waves arising by the antisymmetric magnetic field are classified in four types: MIG waves, a Kelvin mode, fast magnetic Rossby waves and an anomalous slow mode. In the small α regime the MIG waves behave as expected from the Longuet-Higgins (1968) paper and the fast magnetic Rossby modes also follow the Rossby wave formula of Longuet-Higgins (1968).

To summarise, the oscillations have the same features to the properties of the waves arise by the symmetric field problem in chapter 4 except for the onset of instability is not $\alpha = 0.5$. Now the value of α which separates the regimes is in the interval of $]0.1, 1]$.

According to Zaqarashvili et al. (2009), the solution for this MHD shallow water model with the toroidal field $B_\phi = B_0 \sin\theta\cos\theta$, in the limit of small α and ϵ, includes two sets of waves: magnetic Poincaré waves (surface gravity waves) and magnetic Rossby waves (fast and slow). They found a sequence of fast magnetic Rossby waves but a single slow mode $\lambda \approx m\alpha^2$ travelling to the east. However, their formula for the eigenfunctions $\tilde{u}_\theta$ is singular at $\mu = \alpha$, so their solutions suffer from the same problems that in the low frequency limit in section 7.3.1. An important fact is that in our results there is one single mode travelling westward for slow magnetic Rossby waves, not a sequence of modes depending on a wave number.

In the other limit ($\epsilon \gg 1$ but $\alpha^2 \ll 1$), they found equatorially trapped waves for large ϵ and moderate α and mentioned the Poincaré waves and fast and slow magnetic Rossby waves. This discrepancy could be attributed to the fact that in the context of moderate or large α, the slow magnetic Rossby solution does not satisfy the condition $\sqrt{\epsilon}\alpha^2 \ll 1$.

There are a number of similarities between their results and ours. MIG waves are equatorially trapped for large α and ϵ and fast magnetic Rossby waves are confined at the equator when ϵ is large and α has a moderate value. On the other hand, the slow magnetic Rossby waves are not equatorially trapped for any value of α and ϵ.

When α is large the magnetic Rossby waves are unstable and the MIG waves could be absorbed by a possible critical layer.

Chapter 8

Conclusions

In the present research, the aim was to study solutions for the MHD shallow water system of equations with a basic state of a toroidal magnetic field in the form $B_\phi = B_0 \sin\theta$ for chapters 4, 5 and 6, and the antisymmetric form $B_\phi = B_0 \sin\theta\cos\theta$ in chapter 7. We suppose that the basic state height is maintained to be constant (H_0) by an external stress. The solutions are evaluated in a whole range for the parameters $\epsilon = 4\Omega_0^2 R_0^2/gH_0$ and $\alpha^2 = B_0^2/\rho\mu_0 4\Omega_0^2 R_0^2$, in order to apply the results to geophysical and astrophysical context. The numerical method was based on the Longuet-Higgins (1968) paper and analytical solutions were developed for limiting cases.

These cases is not a realistic representation of the complicated scenario in planets and stars, where the magnetic field has a complicated configurations and zonal flows. Also, the thermal wind shears may be important and isosurfaces of pressure may not be spherical. To keep the model treatable this study did not include diffusion or differential rotation. The diffusion may be particularly important when the model is applied to the stably stratified layer of the Earth's core. The absence of differential rotation in the problem limits the interpretation of solutions that can be related to the solar tachocline or other stars. But the simpler the mathematical model the more accurate it is likely to be.

Symmetric Magnetic Field: $B_\phi = B_0 \sin\theta$

The solutions can be classify in four types: MIG waves travelling eastward and westward, fast magnetic Rossby waves travel to the west, slow magnetic Rossby waves propagating eastward with an anomalous mode travels to the west and an exceptional solution which exists for large ϵ: the Kelvin wave travels to the east, though in the presence of an intense magnetic field there is a Kelvin mode travelling westward.

The solutions are presented as a discrete set of antisymmetric and symmetric oscillations depending of the poloidal and azimuthal wave numbers, except in the case of the Kelvin wave which is a single mode.

Magneto Inertial Gravity Waves

The Magneto Inertial Gravity (MIG) waves propagates eastward and westward. The normalized frequency remains superalfvénic $|\lambda| > m\alpha$ and the modes are always **stable**. There are no instabilities for these modes.

- **Small α regime:** The normalized frequency λ is proportional to $\epsilon^{-1/2}$ for small values of ϵ and the eigenfunctions are the Associated Legendre polynomials $P_n^m(\mu)$. When ϵ is large $\lambda \sim \epsilon^{-1/4}$, here MIG waves are equatorially trapped and the eigenfunctions correspond to the parabolic cylinder functions

$$\tilde{u}_\theta = Ce^{-\frac{1}{2}\epsilon^{1/2}\mu^2} H_\nu(\epsilon^{1/4}\mu),$$

  where H_ν are the Hermite polynomials.

- **Large α regime:** When α is large the behaviour of these waves is controlled mainly by the magnetic field and $|\lambda|$ tends to the Alfvén frequency $m\alpha + \delta$, where the small deviation δ depends on $\alpha^{1/3}\epsilon^{-1/3}$. These waves are **equatorially trapped** for large ϵ and/or α and the asymptotic form of the equation for the northward

velocity has a set of solutions corresponding to parabolic cylinder functions

$$\tilde{u}_\theta = e^{-\frac{1}{4}s^2\mu^2} H_\nu(\frac{s\mu}{\sqrt{2}}).$$

Kelvin Wave

The first mode of MIG waves travelling to the east becomes a Kelvin wave when α and ϵ are increased. The northward velocity goes to zero and the flow reduces to being purely in the azimuthal direction.

- The frequency for the Kelvin wave goes $\lambda \sim \alpha + 1/(2\epsilon\alpha^2)$. These waves are **equatorially trapped** with eigenfunctions

$$\tilde{u}_\phi = e^{-\frac{q\mu^2}{2}}.$$

- If the magnetic field is strong enough for a given value of ϵ, there is a Kelvin mode travelling to the west which is also trapped at the equator, and exists owing to the magnetic field.

Magnetic Rossby Waves: Small α regime

- The fast magnetic Rossby waves propagate westward and the discrete set of frequencies are in the superalfénic regime ($|\lambda| > m\alpha$). There is almost no effect of the magnetic field, the frequency λ is independent of ϵ as for the hydrodynamic Rossby waves, for ϵ is small, and the eigenfunctions correspond to the Associated Legendre polynomials.

- For ϵ large the magnetic mixed Rossby gravity mode ($n = 1$) tends to $\lambda \sim \epsilon^{-1/4}$. Then the other modes behave like $\lambda \sim \epsilon^{-1/2}$. The eigenfunctions corresponds to the parabolic cylinder functions and the waves are **equatorially trapped** for large values of ϵ and moderate values of α.

- The slow magnetic Rossby waves are produced via a balance between the magnetic field and the Coriolis force: when $\alpha = 0$ these modes are absent. The waves are a set of discrete very small subalfvénic frequencies which tends to $\lambda \sim \alpha^2$ in the small α regime with eigenfunctions defined by the Associated Legendre polynomials. This result is very sensitive to the magnitude of the magnetic field, whereas the other waves are just slightly affected by the magnetic field, in the weak field regime. These oscillations are **not equatorially trapped**. On the contrary, for some values of m the waves can be **confined at the poles** even when α is not large.

- One anomalous slow wave travels to the west which corresponds to a sinusoidal oscillation with a dispersion relation of $\lambda = -0.2\epsilon\alpha^4$ for $m = 1$.

Magnetic Rossby Waves:Large α regime.

- For sufficiency large magnetic field ($\alpha > 0.5$) and $m = 1$, the waves enter in a new regime, fast magnetic Rossby waves become subalfvénic and the first mode $n = 1$, the magnetic mixed Rossby gravity mode collides with the anomalous slow magnetic Rossby mode and becomes complex. The second mode collides with the $n = 2$ slow magnetic Rossby wave, and so on.

- Near the transition point ($\alpha \sim 0.5$), the fast magnetic Rossby eigenfunctions correspond to the associated Legendre polynomials $\tilde{u}_\theta = P_n^m(\mu)$. In this region, the frequency is calculated by $\lambda = -m/2 + \hat{\delta}(\alpha, n, m)$ with a high accuracy where $\hat{\delta} \ll 1$.

- As α or ϵ increases, the complex frequency tends to $\lambda = -1/2 + i(\alpha - 1/\sqrt{2\epsilon})$ and the eigenfunctions are $\tilde{u}_\theta \sim (1-\mu)^{1/2} e^{-\sqrt{2\epsilon}\alpha(1-\mu)} \mathcal{L}_{n'}$ where $\mathcal{L}_{n'}$ are the Laguerre polynomials. In addition, the modes undergo **polar trapping** in this regime and angular momentum is transferred toward the poles.

- This is a current driven instability that has previously been studied by Tayler (1973, 1980), Pitts and Tayler (1985) for stars containing a toroidal field and Malkus (1967) and others in the geophysical context. Also in stars and planets the presence of the differential rotation may lead to joint instabilities (Gilman and Fox, 1997), but field strengths at onset are lower for those joint instabilities than those in current driven instabilities. In addition, the configuration of the basic state of the magnetic field determines the stability of the field.

- The frequencies of the magnetic Rossby modes for $m \neq 1$ are real and have the same behaviour as the $m = 1$ case when α is small. These waves are always **stable**. In the case of α large, the frequency tends to be linear with α: however, for the case $m = 2$, the eigenvalues satisfy the equation $\lambda = -1/2 \pm 2[(n+1)\alpha]^{1/2}\epsilon^{-1/4}$ and the eigenfunctions follows $\tilde{u}_\theta \sim (1-\mu)e^{-2\sqrt{\epsilon}\alpha(1-\mu)}\mathcal{L}_n^1$. Lastly, the magnetic Rossby waves for $m \geq 3$ has frequencies $\lambda \sim \pm\alpha\sqrt{m(m-2)}$ and the eigenfunctions are $\tilde{u}_\theta \sim (1-\mu)^{m/2}e^{-2\sqrt{2m\epsilon}\alpha(1-\mu)}\mathcal{L}_n^{m-1}$. All cases correspond to waves **trapped at the poles**, and the formulas can describe the eigenfunctions and eigenvalues with high accuracy.

Antisymmetric magnetic field: $B_\phi = B_0 \sin\theta\cos\theta$

In this case, when the basic state is an antisymmetric field,the north and south hemisphere will have the opposite polarity, and the field at the equator will be zero. This will lead to many consequences for the waves that are arising in this context.

Since the problem is now more difficult to solve, we approximate some solutions and make some comparison with the analogous Cartesian problem to have an idea about what waves we can find.

We found three kinds of oscillations: MIG waves travelling eastward and westward, fast magnetic Rossby waves propagating to the west and one anomalous mode that travels to

the west. We stress that the set of slow magnetic Rossby waves propagating eastward are absent in this field configuration.

Small α regime

- The behaviour of MIG and fast magnetic Rossby waves remains similar to the symmetric case. The main change here is that the instability value of α has changed to lie in an interval $\sim]0.1, 1]$, and we note that the instability can start before $\alpha = 0.5$.
- From the numerical calculations, we note that there is an anomalous mode travelling to the west, with a frequency estimated to be $\lambda = -4\sqrt{2}/100\epsilon\alpha^4$.

Large α regime

- The numerical evidence shows that the MIG waves become subalfvénic for certain value or α which depend on ϵ, exactly when the frequency tends to be similar to the frequency of a hydrodynamic gravity wave. After this critical point the waves disappear. A likely explanation of the suppression of MIG waves is related to the existence of a critical layer which absorbs the waves. Also MIG waves are equatorially trapped for large α or ϵ.
- The fast magnetic Rossby waves start to become subalfvénic when α increases. We did not define exactly where the instability point lies here. But the fast magnetic Rossby waves coalesce with each other in a small range of α and then become real again and later collides with a different mode and become complex again, and so on, weaving a net where instability appears and disappears. The first fast magnetic Rossby wave coalesces with the anomalous slow magnetic Rossby wave.

- Analytically we found a Kelvin wave travelling eastward which is equatorially trapped and the frequency depends on the rotation: $\lambda \sim \epsilon^{-1/2}$, similar to the symmetric problem.

- Also, the axisymmetric case ($m = 0$) was solved analytically and the result shows gravity waves in the limit of small ϵ with positive and negative frequencies. For large ϵ these waves are equatorially trapped and large values of α enhanced the equatorial trapping. In the symmetric case, the problem reduces to the hydrodynamic case for $m = 0$ and was solved by Longuet-Higgins (1968). He found a set of gravity waves depending on the poloidal wave number n with positive frequencies.

This section has reviewed the key aspects of the waves that are solutions of the proposed problem. The following part of the conclusions moves on to describe in greater detail the possible applications for these results in the geophysical and astrophysical context.

Implications

The Stably Stratified Layer at the Earth's Core

Considering the existence of a stably stratified layer at the CMB, we can use the values of the parameters calculated in the introduction of this work (table 1.1) to obtain the solutions for the MHD shallow water equations for a toroidal field $B_0 \sin\theta$. Then, we have four kinds of waves: the MIG waves, fast and slow magnetic Rossby waves and the Kelvin wave. We will present some first modes, for $\alpha = 4 \times 10^{-4}$ $(B \sim 0.02T)$, $\epsilon = 0.08$, $m = 1$, and $N = 50$. None of the waves are trapped at the equator and instability is not possible with this value of α.

- For these values, the numerical calculation for highest frequencies corresponding to MIG waves have a maximum period of 2.8 days for the first mode, 1.6 days

for the second one and the following oscillations with decreasing frequencies. The electromagnetic effect of MIG modes can not reach the surface of the Earth because the screening of the mantle.

- The fast magnetic Rossby waves have periods from 27 days to 1.55 years for the westward propagating waves. Due to the screening of the mantle these waves have little chance of reaching the Earth's surface. In observational studies, Jackson and Finlay (2007) show some flux spots traveling westwards on the surface of Earth's core with a period hundreds of years ($100 \sim 1000$ years) and wavenumbers ($m = 8$ and $n = 11$) which are confined in the equatorial region. These results suggest that fast magnetic Rossby waves could not be related to this kind of secular variation for these values of the parameters.

- In the case of the lowest frequencies which are capable to travel through the mantle with periods from 2135 ($n = 2$), 854 ($n = 3$), 474 ($n = 4$), 305 ($n = 5$), 213 ($n = 6$),... years and travels to the east ($m = 1$). It could be possible that the measurements of the geomagnetic field can reveal some features similar to these oscillations.

- The anomalous mode propagates to the east and has a long period of $\sim 10^{12}$ years, even greater than the age of the Earth 4.5×10^9 years. In this context the presence of this wave has no physical meaning.

If we take $\epsilon = 2.7$ from table 1.1, the results will change but with the same conclusions. The MIG waves will have periods of few hours, the periods of fast modes will be around 1 day to several days and the slow magnetic Rossby wave periods will not change, as the formula does not depend on ϵ.
If the magnetic field in this stratified layer is weaker: $\alpha = 1.7 \times 10^{-6}$, $(B \sim 10^{-4}T)$, the slow magnetic Rossby modes could have periods of millions of years.
These results must be approached with some caution in geomagnetic problems. It would

be a better approximation if a more realistic basic state magnetic field with a radial component were used, but this work provides important insights into the properties of the MHD waves. The difficulty with including a radial magnetic field is that waves can travel along field lines and hence out of the shallow layer. This would possibly drain wave energy out of the stable layer. This means that a more complicated problem in which the stable shallow layer is coupled to the deep interior of the outer core would have to be studied.

The Solar Tachocline

The present study raises the possibility that these oscillations can be produced in the solar tachocline and could affect the "magnetic weather" called solar activity (Spiegel, 1994). A possible estimation for the parameters is $\alpha = 0.2$ and $\epsilon = 0.04$. Our numerical results, for $m = 1$ and $N = 50$, can give us a good illustration of possible oscillations arising in this layer. It is important to note that the waves are manifested as a single mode of oscillation or sometimes as a superposition of waves.

- The highest frequencies corresponding to MIG waves travelling eastward or westward could have approximated periods of 2.1 days for the first mode, 1.1 days for the second, 18.7 hours for the third one and so on. These results are comparable with some gravity waves (g-modes) produced below the convection zone.

- The fast magnetic Rossby waves should have frequencies from 26 days for the first mode of a sequence of modes, to ~ 67 days. Even though α has a moderate value the waves are not equatorially trapped in this case (for the configuration $B_0 \sin\theta$).

- The anomalous slow magnetic Rossby mode should have a period of ~ 2885 years.

- The slow magnetic Rossby waves are a set of oscillations where the first mode could have a period around 136 days, the next modes decrease in period to the value

of ~ 92 days. It is important to bear in mind the uncertainty of these responses. Lobzin et al. (2012) has found 156 days periodicities in the occurrence rate of coronal type III solar radio burst in a similar time scale than these waves.

If we take $\epsilon = 0.03$ from table 1.1, the periods for the waves will remain similar.
Observations in solar magnetic activity (McIntosh et al., 2017) have revealed patterns travelling westward with phase speeds of $3.25 \pm 2.25 m/s$ and $2.65 \pm 1.60 m/s$ in the north and south hemispheres and eastward group speeds of $24.4 \pm 15.3 m/s$ in the southern hemisphere and $23.8 \pm 20.8 m/s$ in the northern hemisphere. They believe that this is a kind of slow magnetic Rossby wave travelling to the east (west for the context of solar observations) due to the rotation and the toroidal magnetic field of the tachocline. We could infer using the dispersion relation for these modes for a weak field (equation 2.72) and some simple formulas of movement in a circle

$$v_{ph} = \frac{2\pi R_0}{mT}, \qquad \text{and} \qquad \lambda = \frac{\omega}{2\Omega_0} = \frac{\pi}{T\Omega_0},$$

a relation between the magnetic parameter and the phase velocity of these waves

$$\alpha^2 = \frac{v_{ph}}{2\Omega_0 R_0 [n(n+1) - 2]}$$

for a given poloidal wave number, n. Then, our calculations suggest that the value of α could be around 1.1×10^{-2} ($n = 3$) to 2.8×10^{-3} ($n = 12$). Hence our estimations of the solar magnetic field for the tachocline could be around $0.5T \sim 0.1T$ ($\sim 10^3 G$). However, these magnetic Rossby waves have the feature of that the phase speed and group speed in the azimuthal direction are the same, as shown in section 2.6.1. This fact does not fit with the observations, maybe due to that this model is very simple and does not take into account differential rotation.

Due to the uncertainty of the values for α in the solar tachocline, we cannot provide a good estimation for the periods for the slow magnetic Rossby waves. In the case of a weak field: $\alpha = 2.32 \times 10^{-3}$, the slow magnetic Rossby waves could have periods of

1713, 685, 380, 245, 171,... years, for $n = 1, 2, 3, 4, 5$,.... Zaqarashvili et al. (2015) has obtained similar results and has associated these waves with Rieger type periodicities.

However, the fast magnetic Rossby waves and MIG waves maintain their frequencies in almost with the same value if α varies from $\sim 10^{-3}$ to $\sim 10^{-1}$, as it is shown in the tables of chapter 4.

According to these data, we can infer that the magnetic field in the tachocline could be weak $\sim 0.1T(10^3G)$, in order to have slow waves with periods of decades.

Oláh et al. (2009) have studied the magnetic activity of 15 solar-type stars (G-K) with rotation rates from ~ 0.02 to ~ 0.95 times the rotation rate of the Sun. They found multiples cycles in the stars with lengths from ~ 2.5 to ~ 14 years but not in this order. Even though the authors suggested that these periodicities are due to a dynamo (Gilman, 1969), it is possible that slow magnetic Rossby waves could be associated with the cycles. Considering some appropriated values of the parameters α and ϵ for these stars similar to the Sun, the slow oscillations can have periods of years. Although, we have to be cautious for the direct application of our results to stars, as Pitts and Tayler (1985) had stated in similar research that the results "obtained are suggestive rather than rigorous". The antisymmetric field configuration presents similar values for the perodicities. There is no significant differences from the symmetric case in this range of values for the parameters α and ϵ, neither in the solar tachocline nor the Earth's core stratified layer.

Future Work

More research is needed to better understand the solutions for the antisymmetric problem $B_\phi = B_0 \sin\theta\cos\theta$, particularly for large values of the magnetic parameter α. The critical layer could be more studied and the windows of instability for magnetic Rossby waves have to be described in detail. Introducing diffusion might be helpful here.

Also, the analysis could include diffusion or differential rotation in order to estimate the

effect of it on the behaviour of the waves, and in this form try to reproduce with accuracy the conditions of the stratified layers present in the nature.

Final Considerations

This research makes several noteworthy contributions to the study of MHD waves in rotating fluids and provides evidence with respect to new modes which are excited in the system. Despite the limitations of the model, this study offers a deep insight into the dynamics of the waves and how the rotation and the magnetic field affect them. We expect that this systematic investigation can complement the earlier studies.

Bibliography

A. Aasen and K. Varholm. Traveling gravity water waves with critical layers. *Journal of Mathematical Fluid Mechanics*, pages 1–27, 2016.

M. Abramowitz and I. A. Stegun. *Handbook of mathematical functions: with formulas, graphs, and mathematical tables*, volume 55. Courier Corporation, 1964.

I. Arregui and J. L. Ballester. Damping mechanisms for oscillations in solar prominences. *Space Science Reviews*, 158(2-4):169–204, 2011.

M. I. Bergman. Magnetic Rossby waves in a stably stratified layer near the surface of the earth's outer core. *Geophysical & Astrophysical Fluid Dynamics*, 68(1-4):151–176, 1993.

S. I. Braginsky. Magnetic Rossby waves in the stratified ocean of the core, and topographic core-mantle coupling. *Earth, Planets and Space*, 50(8):641–649, 1998.

O. Bühler. *Waves and mean flows*. Cambridge University Press, 2014.

P. S. Cally. Three-dimensional magneto-shear instabilities in the solar tachocline. *Monthly Notices of the Royal Astronomical Society*, 339:957–972, March 2003.

P. S. Cally, M. Dikpati, and P. A. Gilman. Three-dimensional magneto-shear instabilities in the solar tachocline - ii. Axisymmetric case. *Monthly Notices of the Royal Astronomical Society*, 391:891–900, December 2008.

S. Chandrasekhar. *Hydrodynamic and hydromagnetic stability*. Courier Corporation, 2013.

P. Charbonneau, J. Christensen-Dalsgaard, R. Henning, R. M. Larsen, J. Schou, M. J Thompson, and S. Tomczyk. Helioseismic constraints on the structure of the solar tachocline. *The Astrophysical Journal*, 527(1):445, 1999.

B. Cushman-Roisin and J. Beckers. *Introduction to geophysical fluid dynamics: Physical and numerical aspects*, volume 101. Academic Press, 2011.

M. Dikpati and P. A. Gilman. Prolateness of the solar tachocline inferred from latitudinal force balance in a magnetohydrodynamic shallow-water model. *The Astrophysical Journal*, 552:348–353, May 2001.

M. Dikpati, P. A. Gilman, and M. Rempel. Stability analysis of tachocline latitudinal differential rotation and coexisting toroidal band using a shallow-water model. *The Astrophysical Journal*, 596(1):680, 2003.

A. M. Dziewonski and D. L. Anderson. Preliminary reference earth model. *Physics of the Earth and Planetary Interiors*, 25(4):297–356, 1981.

C. C. Finlay, M. Dumberry, A. Chulliat, and M. A. Pais. Short timescale core dynamics: Theory and observations. *Space Science Reviews*, 155(1-4):177–218, 2010.

C. M. Fowler. *The solid earth: An introduction to global geophysics*. Cambridge University Press, 1990.

T. Gastine, J. Wicht, and J. M. Aurnou. Zonal flow regimes in rotating anelastic spherical shells: An application to giant planets. *Icarus*, 225(1):156–172, 2013.

A. E. Gill. *Atmosphere-ocean dynamics*, volume 30. Academic Press, 1982.

P. A. Gilman. A Rossby-wave dynamo for the sun, I. *Solar Physics*, 8(2):316–330, 1969.

P. A. Gilman. Magnetohydrodynamic shallow water equations for the solar tachocline. *The Astrophysical Journal Letters*, 544(1):L79, 2000.

P. A. Gilman and M. Dikpati. Analysis of instability of latitudinal differential rotation and toroidal field in the solar tachocline using a magnetohydrodynamic shallow-water model. i. Instability for broad toroidal field profiles. *The Astrophysical Journal*, 576 (2):1031, 2002.

P. A. Gilman and P. A. Fox. Joint instability of latitudinal differential rotation and toroidal magnetic fields below the solar convection zone. *The Astrophysical Journal*, 484(1): 439, 1997.

D. Gubbins and E. Herrero-Bervera. *Encyclopedia of geomagnetism and paleomagnetism*. Springer Science & Business Media, 2007.

E. Hecht and A. Zajac. Optics. *Addison-Wesley, Reading, Mass*, 19872, 1974.

G. Helffrich and S. Kaneshima. Outer-core compositional stratification from observed core wave speed profiles. *Nature*, 468(7325):807–810, 2010.

K. Heng and A. Spitkovsky. Magnetohydrodynamic shallow water waves: Linear analysis. *The Astrophysical Journal*, 703(2):1819, 2009.

C. O Hines. Gravity waves in the atmosphere. *Nature*, 239:73–78, 1972.

R. Hollerbach and P. S. Cally. Nonlinear evolution of axisymmetric twisted flux tubes in the solar tachocline. *Solar Physics*, 260:251–260, 2009.

J. R. Holton and R. S. Lindzen. A note on Kelvin waves in the atmosphere. *Monthly Weather Review*, 96:385–386, 1968.

K. Hori, C. A Jones, and R. J Teed. Slow magnetic Rossby waves in the earth's core. *Geophysical Research Letters*, 42(16):6622–6629, 2015.

D. W. Hughes, R. Rosner, and N. O. Weiss. *The solar tachocline*. Cambridge University Press, 2007.

S. Hunter. *An examination of keystroke dynamics for continuous user authentication*. PhD thesis, University of Leeds, 2015.

A. Jackson. Intense equatorial flux spots on the surface of the earth's core. *Nature*, 424 (6950):760–763, 2003.

A. Jackson and C. C. Finlay. Geomagnetic secular variation and its applications to the core. *Treatise on Geophysics*, 5:147–193, 2007.

C. A. Jones. Planetary magnetic fields and fluid dynamos. *Annual Review of Fluid Mechanics*, 43:583–614, 2011.

S. Karato. *The dynamic structure of the deep earth: An interdisciplinary approach*. Princeton University Press, 2003.

L. Kaufman. Some thoughts on the QZ algorithm for solving the generalized eigenvalue problem. *ACM Transactions on Mathematical Software (TOMS)*, 3(1):65–75, 1977.

G. N. Kiladis, M. C. Wheeler, P. T. Haertel, K. H. Straub, and P. E. Roundy. Convectively coupled equatorial waves. *Reviews of Geophysics*, 47(2):1–42, 2009.

L. E. Kinsler, A. R. Frey, A. B. Coppens, and J. V. Sanders. Fundamentals of acoustics. *Fundamentals of Acoustics, 4th Edition, by Lawrence E. Kinsler, Austin R. Frey, Alan B. Coppens, James V. Sanders, pp. 560. ISBN 0-471-84789-5. Wiley-VCH, December 1999.*, page 560, 1999.

J. Lighthill. *Waves in fluids*. Cambridge University Press, 2001.

V. V. Lobzin, I. H. Cairns, and P. A. Robinson. Rieger-type periodicity in the occurrence of solar type III radio bursts. *The Astrophysical Journal Letters*, 754(2):L28, 2012.

M. S. Longuet-Higgins. The eigenfunctions of Laplace's tidal equations over a sphere. *Philosophical Transactions of the Royal Society of London A: Mathematical, Physical and Engineering Sciences*, 262(1132):511–607, 1968.

L. H. Ma. Gleissberg cycle of solar activity over the last 7000years. *New Astronomy*, 14 (1):1–3, 2009.

J. Mak, S. D. Griffiths, and D. W. Hughes. Shear flow instabilities in shallow-water magnetohydrodynamics. *Journal of Fluid Mechanics*, 788:767–796, 2016.

W. Malkus. Hydromagnetic planetary waves. *Journal of Fluid Mechanics*, 28(04):793–802, 1967.

S. A. Maslowe. Critical layers in shear flows. *Annual review of fluid mechanics*, 18(1): 405–432, 1986.

T. Matsuno. Quasi-geostrophic motions in the equatorial area. *J. Meteor. Soc. Japan*, 44 (1):25–43, 1966.

S. W. McIntosh, W. J. Cramer, M. Pichardo, and R. J. Leamon. The detection of Rossby-Like waves on the Sun. *Nature Astronomy*, 2017.

P. Melchior. *The physics of the earth's core: An introduction*. Elsevier, 2013.

M. S. Miesch. Large-scale dynamics of the convection zone and tachocline. *Living Reviews in Solar Physics*, 2(1):1–139, 2005.

M. S. Miesch and B. W. Hindman. Gyroscopic pumping in the solar near-surface shear layer. *The Astrophysical Journal*, 743(1):79, 2011.

C. B. Moler and G. W. Stewart. An algorithm for generalized matrix eigenvalue problems. *SIAM Journal on Numerical Analysis*, 10(2):241–256, 1973.

C. J. Nappo. *An introduction to atmospheric gravity waves*. Academic Press, 2013.

K. Oláh, Z. Kolláth, T. Granzer, K. G. Strassmeier, A. F. Lanza, S. Järvinen, H. Korhonen, S. L Baliunas, W. Soon, S. Messina, et al. Multiple and changing cycles of active stars-II. results. *Astronomy & Astrophysics*, 501(2):703–713, 2009.

J. Pedlosky. *Geophysical fluid dynamics*. Springer Science & Business Media, 2013.

P. R. Pinet. *Essential Invitation to Oceanography*. Jones & Bartlett Publishers, 2012.

E. Pitts and R. J. Tayler. The adiabatic stability of stars containing magnetic fields. IV - The influence of rotation. *Monthly Notices of the Royal Astronomical Society*, 216: 139–154, September 1985.

F. Q. Rashid, C. A. Jones, and S. M. Tobias. Hydrodynamic instabilities in the solar tachocline. *Astronomy & Astrophysics*, 488:819–827, September 2008.

J. R. Reitz, F. J. Milford, and R. W. Christy. *Foundations of electromagnetic theory*. Addison-Wesley Publishing Company, 2008.

M. Rempel, M. Schüssler, and G. Tóth. Storage of magnetic flux at the bottom of the solar convection zone. *Astronomy & Astrophysics*, 363:789–799, November 2000.

K. F. Riley, M. P. Hobson, and S. J. Bence. *Mathematical methods for physics and engineering: a comprehensive guide*. Cambridge University Press, 2006.

G. Rüdiger and R. Hollerbach. *The magnetic universe: geophysical and astrophysical dynamo theory*. John Wiley & Sons, 2006.

D. A. Schecter, J. F. Boyd, and P. A. Gilman. shallow-water magnetohydrodynamic waves in the solar tachocline. *The Astrophysical Journal Letters*, 551(2):L185, 2001.

J. Schou, H. M. Antia, S. Basu, R. S. Bogart, R. I. Bush, S. M. Chitre, J. Christensen-Dalsgaard, M. P. Di Mauro, W. A. Dziembowski, A. Eff-Darwich, et al. Helioseismic studies of differential rotation in the solar envelope by the solar oscillations

investigation using the Michelson Doppler imager. *The Astrophysical Journal*, 505 (1):390, 1998.

B. W. Sharif and C. A. Jones. Rotational and magnetic instability in the diffusive tachocline. *Geophysical and Astrophysical Fluid Dynamics*, 99(6):493–511, 2005.

E. A. Spiegel. The chaotic solar cycle. In *Lectures on solar and planetary dynamos*, page 245, 1994.

H. C. Spruit. Differential rotation and magnetic fields in stellar interiors. *Astronomy & Astrophysics*, 349:189–202, September 1999.

R. J. Tayler. The adiabatic stability of stars containing magnetic fields-I.Toroidal fields. *Monthly Notices of the Royal Astronomical Society*, 161:365, 1973.

R. J. Tayler. The adiabatic stability of stars containing magnetic fields. IV - Mixed poloidal and toroidal fields. *Monthly Notices of the Royal Astronomical Society*, 191: 151–163, April 1980.

M. J. Thompson. *An introduction to astrophysical fluid dynamics*. Imperial College Press, 2006.

S. M. Tobias. The solar tachocline: Formation, stability and its role in the solar dynamo. In *Fluid Dynamics and Dynamos in Astrophysics and Geophysics*, volume 1, page 193. CRC Press Boca Raton, Florida, 2005.

D. J. Tritton. *Physical fluid dynamics*. Springer Science & Business Media, 2012.

G. K. Vallis. *Atmospheric and oceanic fluid dynamics: Fundamentals and large-scale circulation*. Cambridge University Press, 2006.

E. Wahlén. Steady water waves with a critical layer. *Journal of Differential Equations*, 246(6):2468–2483, 2009.

J. M. Wallace and V. E. Kousky. Observational evidence of Kelvin waves in the tropical stratosphere. *Journal of the Atmospheric Sciences*, 25(5):900–907, 1968.

G. B. Whitham. *Linear and nonlinear waves*, volume 42. John Wiley & Sons, 2011.

M. Yanai, T. Maruyama, T. Nitta, and Y. Hayashi. Power spectra of large-scale disturbances over the tropical pacific. *Journal of the Meteorological Society of Japan. Ser. II*, 46(4):308–323, 1968.

J. P. Zahn, S. Talon, and J. Matias. Angular momentum transport by internal waves in the solar interior. *arXiv preprint astro-ph/9611189*, 1996.

T. V. Zaqarashvili, R. Oliver, J. L. Ballester, and B. M. Shergelashvili. Rossby waves in shallow water magnetohydrodynamics. *Astronomy & Astrophysics*, 470(3):815–820, 2007.

T. V. Zaqarashvili, R. Oliver, and J. L. Ballester. Global shallow water magnetohydrodynamic waves in the solar tachocline. *The Astrophysical Journal Letters*, 691(1):L41, 2009.

T. V. Zaqarashvili, M. Carbonell, R. Oliver, and J. L. Ballester. Magnetic Rossby waves in the solar tachocline and Rieger-type periodicities. *The Astrophysical Journal*, 709 (2):749, 2010a.

T. V. Zaqarashvili, M. Carbonell, R. Oliver, and J. L. Ballester. Quasi-biennial oscillations in the solar tachocline caused by magnetic Rossby wave instabilities. *The Astrophysical Journal Letters*, 724(1):L95, 2010b.

T. V. Zaqarashvili, R. Oliver, A. Hanslmeier, M. Carbonell, J. L. Ballester, T. Gachechiladze, and I. G. Usoskin. Long-term variation in the sun's activity caused by magnetic Rossby waves in the tachocline. *The Astrophysical Journal Letters*, 805 (2):L14, 2015.